Appendix I

Hydrodynamic and Salinity Modeling Study

Note: The Section 508 amendment of the Rehabilitation Act of 1973 requires that the information in Federal documents be accessible to individuals with disabilities. The USACE has made every effort to ensure that the information in this appendix is accessible. However, this appendix is not fully compliant with Section 508, and readers with disabilities are encouraged to contact Mr. Jayson Hudson at the USACE at (409) 766-3108 or at SWG201900067@usace.army.mil if they would like access to the information.

Environmental Impact Assessment for Channel Deepening, Port of Corpus Christi

Hydrodynamic and Salinity Modeling Study

May 25, 2023 | 13242.102.R3.Rev0

Baird.
Innovation Engineered.

baird.com

Environmental Impact Assessment for Channel Deepening, Port of Corpus Christi

Hydrodynamic and Salinity Modeling Study

Prepared for: Prepared by:

Freese & Nichols
10431 Morado Circle Suite 300
Austin, Texas 78759

W.F. Baird & Associates Ltd.

For further information, please contact
Qimiao Lu at +61 2 8278 7266
qlu@baird.com
www.baird.com

13242.102.R3.Rev0

Z:\Shared With Me\QMS\2023\Reports_2023\13242.102.R3.Rev0_PCCA_EIS_HD_Sal_Modeling.docx

Revision	Date	Status	Comments	Prepared	Reviewed	Approved
RevA	2022-01-25	Draft	Draft for Review	QL	LAW/RBN	LAW
RevB	2022-03-14	Draft	Draft for Review	QL	LAW	LAW
Rev0	2023-05-25	Final		QL	LAW	LAW

Executive Summary

W.F. Baird & Associates Ltd. (Baird) was retained by Freese & Nichols, Inc. (FNI) to perform the third-party environmental impact study (EIS) for the Corpus Christi Ship Channel Deepening Project (CDP). The project is the proposed deepening of the offshore channel, entrance channel, and seaward most portion of the Corpus Christi Ship Channel to a nominal depth of 75 ft. The main objectives of this modeling study are to assess the impacts of the CDP on tides, currents, and salinity on the surrounding bays using a three-dimensional (3D) hydrodynamic and salinity model, mainly focused on Corpus Christi Bay, Nueces Bay, and Redfish Bay. It also provides the hydrodynamic information for all other EIS and/or Sec. 408 required assessments and for navigation simulation.

Corpus Christi Bay connects to several subtropical bays, such as Nueces Bay to northwest, Aransas Bay and Copano Bay on the northeast side, and Baffin Bay on the southwest side. It is separated from the GOM by the longshore barrier islands, such as Mustang Island, Padre Island, and San Jose Island. These bays are connected to the GOM by a narrow entrance channel, Aransas Pass, where the navigation channel will be deepened in the CDP. There is a secondary pass, Packery Channel.

The tides in the GOM are primarily diurnal or mixed diurnal-semidiurnal with the tide range of about 0.7 m. The tidal exchange between the GOM and these bays is mainly through Aransas Pass, resulting in strong currents in the pass. The peak current speed in the pass reaches approximately 1.5 m/s. Beside tides, the water levels in the bays are also driven by the seasonal variation of water level in the GOM which likely results from sustained seasonal winds and the other related oceanographic circulation. Tropical storms (or hurricanes) periodically cause large fluctuations in water level in the bays.

Salinity in the bays is mainly driven by tide currents and river inflows and influenced by many physical processes. The saltwater carried by tidal currents from the GOM is the origin of salinity in the bays. Evaporation in dry season becomes important to drive salinity in shallow water areas to higher levels and sometimes even higher than in the GOM. The freshwater from the rivers and rainfalls results in significant decline of salinity in Nueces Bay.

A three-dimensional numerical model was developed to simulate hydrodynamics and salinity for this impact assessment. The model domain extends to offshore about 50 km into the Gulf of Mexico to the -50 m (NAVD88) contour, about 50 km north to Interstate Highway 37 including Nueces River Delta, and about 100 km along the GIWW. The two narrow connecting channels, Aransas Pass and Packery Channel, were included.

Three simulation periods were selected for the model calibration and validation, based on the data availability and driving force conditions. Each period has three-month duration which is sufficiently long to cover the full variation of tides. Each period represents the selected scenario of river inflow conditions, wind conditions, and salinity mixing in the Corpus Christi Bay. Model calibration shows that the model predicts water level, current speed and direction, and salinity reasonably well. The overall prediction error root mean square error (RMSE) is less than 0.07 m for water levels, less than 0.25 m/s for current speed, and 5 PSU for salinity, respectively.

The impact of the CDP was assessed by comparing the model results between Future With Project (FWP, i.e., this CDP) with Future Without Project (FWOP) which is currently in construction. The navigation channel in the FWOP is being dredged from the Port of Corpus Christi to the GOM to -54 ft MLLW, including Humble Basin and the Turning Basin. The FWP is the proposed project to dredge the Corpus Christi navigation channel to -

75 ft MLLW from approximately Light #1 near Port Aransas to the GOM. These two project scenarios were simulated by using the developed 3D model in these three selected periods.

The changes in water level caused by the FWP were evaluated. The model predicted that the FWP cause the drop of mean water level less than 1 cm, the rise of high tide less than 2 cm, and the drop of low tide less than 4 cm in Corpus Christi Bay. The FWP unlikely cause any risks of flooding and navigations. The tide range will increase about 1 to 2 cm in Corpus Christi Bay and Redfish Bay after the FWP is constructed. The largest increase in tide range occurs in the navigation channel from Point Mustang to the inner basin. There is no significant change in tidal range in Aransas Pass and the outer channel. The impact of FWP on current speed was also analyzed by comparing the model results predicted in the FWP scenario with the model results predicted in the FWOP scenario. Overall, the impact of FWP on the current speed is limited to the proposed dredge areas and the navigation channel extending about 15 km to Ingleside from the proposed dredge area near Port Aransas. There is no significant impact on currents in Corpus Christi Bay, Redfish Bay, and Nueces Bay. Deepening the navigation channel in Aransas Pass will result in the increase of conveyance capacity in the pass. As a result, tidal exchange between the bays and the GOM increases by about 8% The impact of FWP on salinity was assessed by comparing the salinity predicted in the FWP scenario with that predicted in the FWOP scenario in time and 3D space. The average change in salinity caused by FWP is less than 1 PSU. The range of salinity change was also calculated as the maximum salinity change minus the minimum salinity change, which represent the disturbing in salinity caused by the FWP. Figure E.1 shows the range of salinity change which is less than ±3 PSU in the proposed dredge area and the connected navigation channels.

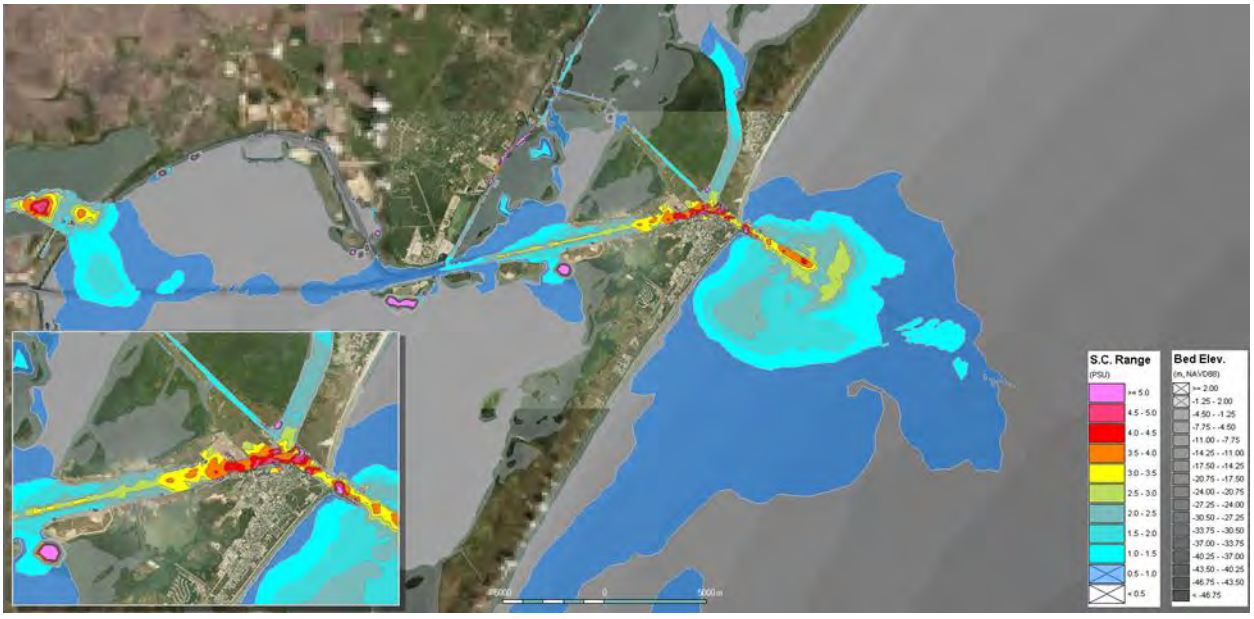

Figure E.1: Range of salinity change (maximum change minus minimum change) caused by FWP in Period 2.

Table of Contents

Tables

Figures

1. Introduction

W.F. Baird & Associates Ltd. (Baird) was retained by Freese & Nichols, Inc. (FNI) to perform the third-party environmental impact study (EIS) for the Corpus Christi Ship Channel Deepening Project (CDP). The project is the proposed deepening of the offshore channel, entrance channel, and seaward most portion of the Corpus Christi Ship Channel to a nominal depth of 75 ft. Baird has provided consulting services for the past 11 months on the project to FNI as part of the 3rd Party EIS contract with the Port of Corpus Christi Authority (PCCA). The work has been coordinated by the US Army Corps of Engineers (USACE) Galveston District Regulatory Branch. The main purpose of this hydrodynamic and salinity modeling study is to provide a direct response to the data gaps identified in the PCCA CDP Recommended Actions Plan developed by FNI on 30 September 2020 (Freese and Nichols, Inc., 2020).

The objectives for this modeling study are:

- To assess the impacts of deepening the navigation channels to Port of Corpus Christi (PCC) on tides (tidal prism and datum) on the surrounding bays, mainly focused on Corpus Christi Bay, Nueces Bay, and Redfish Bay including effects of wind driven changes to Gulf of Mexico (GOM) water levels.
- To access the impacts of deepening the navigation channel on tidal currents and Gulf wide circulation driven currents in the entrance channel, navigation channels (in the bays and jetty channel), and surrounding bays including assessment of offshore currents.
- To provide the base hydrodynamic model for all other EIS and/or Sec. 408 required assessments, for example, salinity model, sediment transport model, and water quality modeling (if required).
- To provide the necessary inputs for navigation simulation including offshore currents, three-dimensionality of currents, and current changes within the jetty channel and turning basin.
- To access the impacts of channel deepening on the salinity in the bays, particularly under high inflow events, using a three-dimensional physics-based model including the effects of varying offshore boundary conditions.

This report documents the data collected and used for the study, the model development, and the assessment on the impacts of CDP on hydrodynamics and salinity. The report consists of:

Section 1. Introduction (this section);

Section 2. Data collection and analysis – to document all data used in this study, including data sources, data gaps, data processing, and the understandings of physical processes from the data analysis;

Section 3. Hydrodynamic and salinity model development – to document the setup, calibration, validation, and uncertainties of the hydrodynamic and salinity model;

Section 4. Impact assessment – to document the modeling assessment of the impacts of channel deepening on hydrodynamics and salinity;

Section 5. Conclusions and uncertainty – to document the conclusions made from this study. The evaluation of uncertainties is also provided; and

Section 6. References.

2. Data Collection and Analysis

2.1 Data Collection

The collected data used in this modeling study includes the shorelines, topographic data and bathymetry, watershed and runoff, hydrological and meteorological information in the bays, the Intracoastal Waterway, and the Gulf of Mexico. Many of the datasets were collected from the publicly accessible data servers as detailed below.

2.1.1 Geospatial Data

Several geospatial datasets were acquired in support of the numerical modeling study. Elevation datasets were downloaded to cover the model domain and navigation channel boundaries in the study area.

2.1.1.1 Elevation Data

Four elevation datasets were acquired for use in the model grid, listed in hierarchical order within the model domain below. Figure 2.1 shows the spatial coverage within the model domain of each elevation source.

- United States Army Corps of Engineers (USACE), Galveston District, Sea Bar Channel Survey, 2018/07/17;
- Cooperative Institute for Research in Environmental Sciences (CIRES), Continuously Updated Digital Elevation Model (CUDEM) - 1/9 Arc-Second Resolution Bathymetric-Topographic Tiles (v2020);
- NOAA National Geophysical Data Center, 2007, Corpus Christi, Texas 1/3 arc-second MHW Coastal Digital Elevation Model;
- NOAA National Geophysical Data Center, 2001, U.S. Coastal Relief Model Vol.5 - Western Gulf of Mexico.

All elevations were converted to the North American Vertical Datum of 1988 (NAVD 88) at Port Aransas. The horizontal coordinate system of Universal Transverse Mercator 14-North (UTM-14N) was used for all bathymetry data.

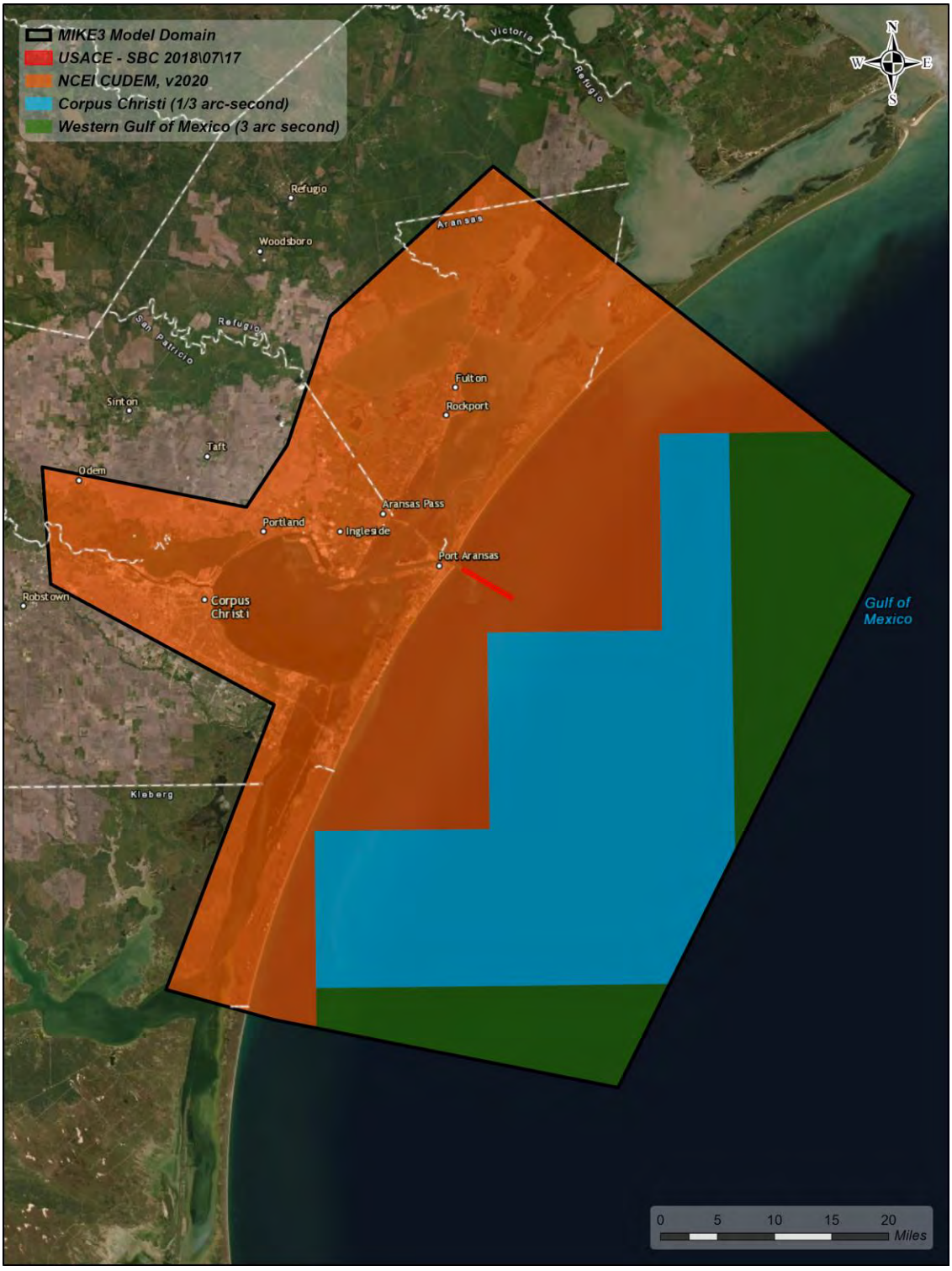

Figure 2.1: Bathymetry data collected for this modeling study

2.1.1.2 Navigation Channel Data

The extents of the navigation channels within the study area were downloaded from the USACE Geospatial National Channel Framework (NCF) portal. The data included channel areas, reaches, and lines.

2.1.2 Meteorological Data

2.1.2.1 Winds

Wind data was collected from in-situ observation stations in the Corpus Christi area (see locations in Figure 2.2). These stations, listed in Table 2.1, are operated by the National Oceanic and Atmospheric Administration (NOAA) with hourly data available online (https://tidesandcurrents.noaa.gov). Wind speed and direction was collected from January 2018 to June 2021 in hourly increments. Observed wind speeds were converted to wind speeds at 10 m above the ground using the log law:

$$u_2 = u_1 * \left(\frac{ln\frac{z_2}{z_0}}{ln\frac{z_1}{z_0}} \right)$$

where u_2 is the wind speed at the desired elevation, u_1 is the observed wind speed at the station elevation, z_2 is the desired elevation (10 m), z_1 is the station instrument elevation and z_0 is the roughness length coefficient. Figure 2.3 displays an example 10 m wind speed plot for Bob Hall Pier.

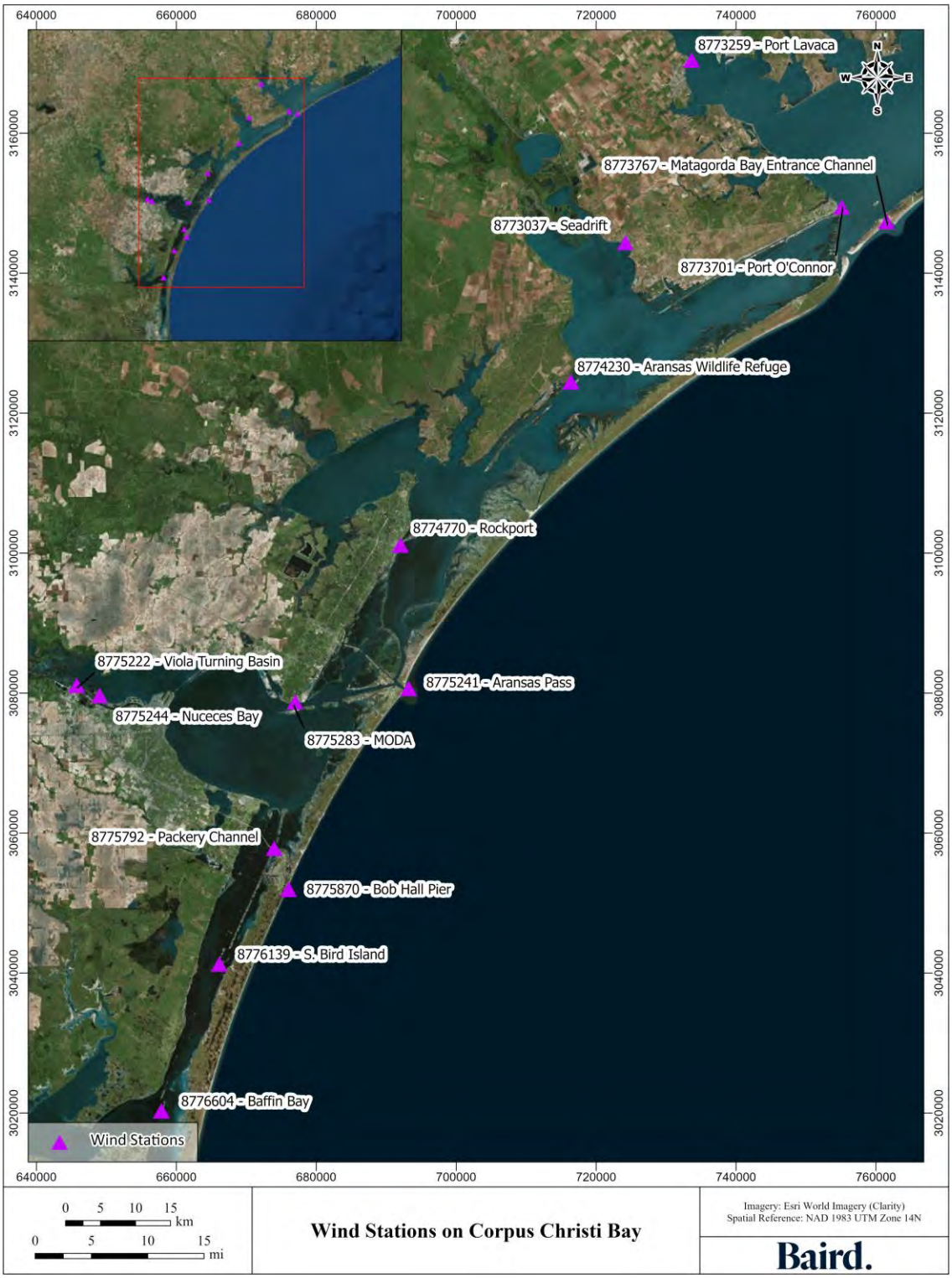

Figure 2.2: Locations of NOAA wind stations collected for this modeling study

Table 2.1: Summary of Wind Data Available from NOAA

Station Name	Station ID	Start Date	End Date
Matagorda Bay Entrance Channel	8773767	2016-06-18	Present
Port O'Connor	8773701	2004-06-24	Present
Port Lavaca	8773259	2007-06-06	Present
Seadrift	8773037	2004-04-06	Present
Aransas Wildlife Refuge	8774230	2014-03-28	Present
Rockport	8774770	2007-07-31	Present
Viola Turning Basin	8775222	2021-01-07	Present
Aransas Pass	8775241	2016-09-21	Present
Nueces Bay	8775244	2011-03-20	Present
MODA	8775283	1992-10-29	Present
Packery Channel	8775792	2007-06-06	Present
Bob Hall Pier	8775870	1995-06-19	2021-12-22
South Bird Island	8776139	2004-04-06	Present
Baffin Bay	8776604	2004-04-09	Present

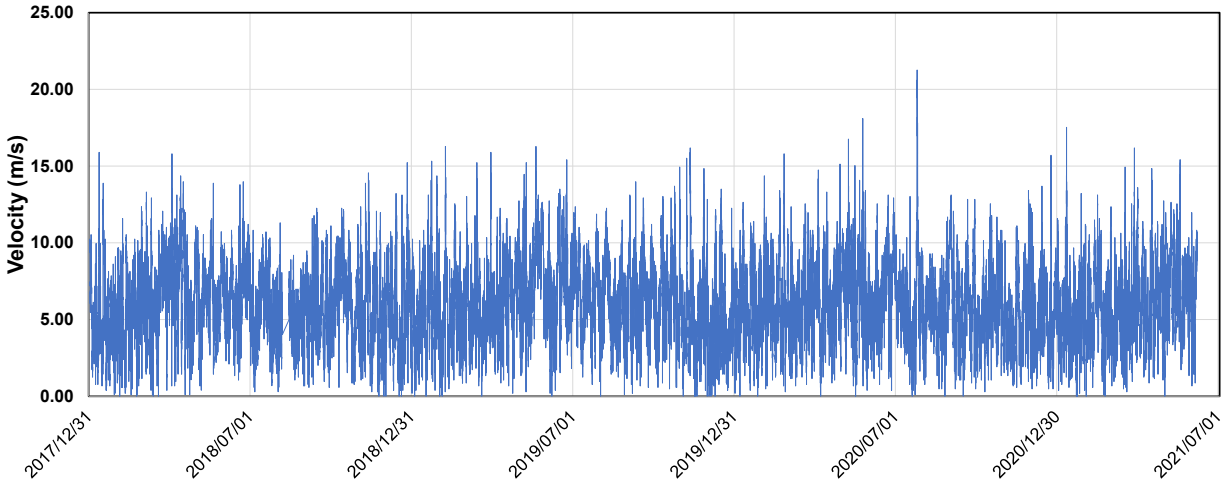

Figure 2.3: Wind speed measured at Bob Hall Pier which was corrected to an elevation of 10 m above the ground

2.1.2.2 Air Temperature

Air temperature data was collected from the National Centers for Environmental Information (NCEI), an agency under NOAA. The in-situ data (Figure 2.4) was collected via observations stations (https://gis.ncdc.noaa.gov/maps/ncei/summaries/daily), listed in Table 2.2. Observed air temperature data from the Corpus Christi airport were used to initially calculate evaporation rates utilizing methods outlined by Linacre

(1977). The sub-hourly temporal frequency provided by the Corpus Christi airport was favorably compared to the daily evaporation data sets provided by the Choke Canyon Dam and Mathis stations. However, upon further analysis, it was determined that the calculated evaporation rates, utilizing air temperature data from the Corpus Christi airport, underpredicted evaporation in the summer seasons. Therefore, it was decided that direct measurements of daily evaporation rates from Mathis were preferable compared to the calculated data sets. No additional air temperature data was utilized for modeling.

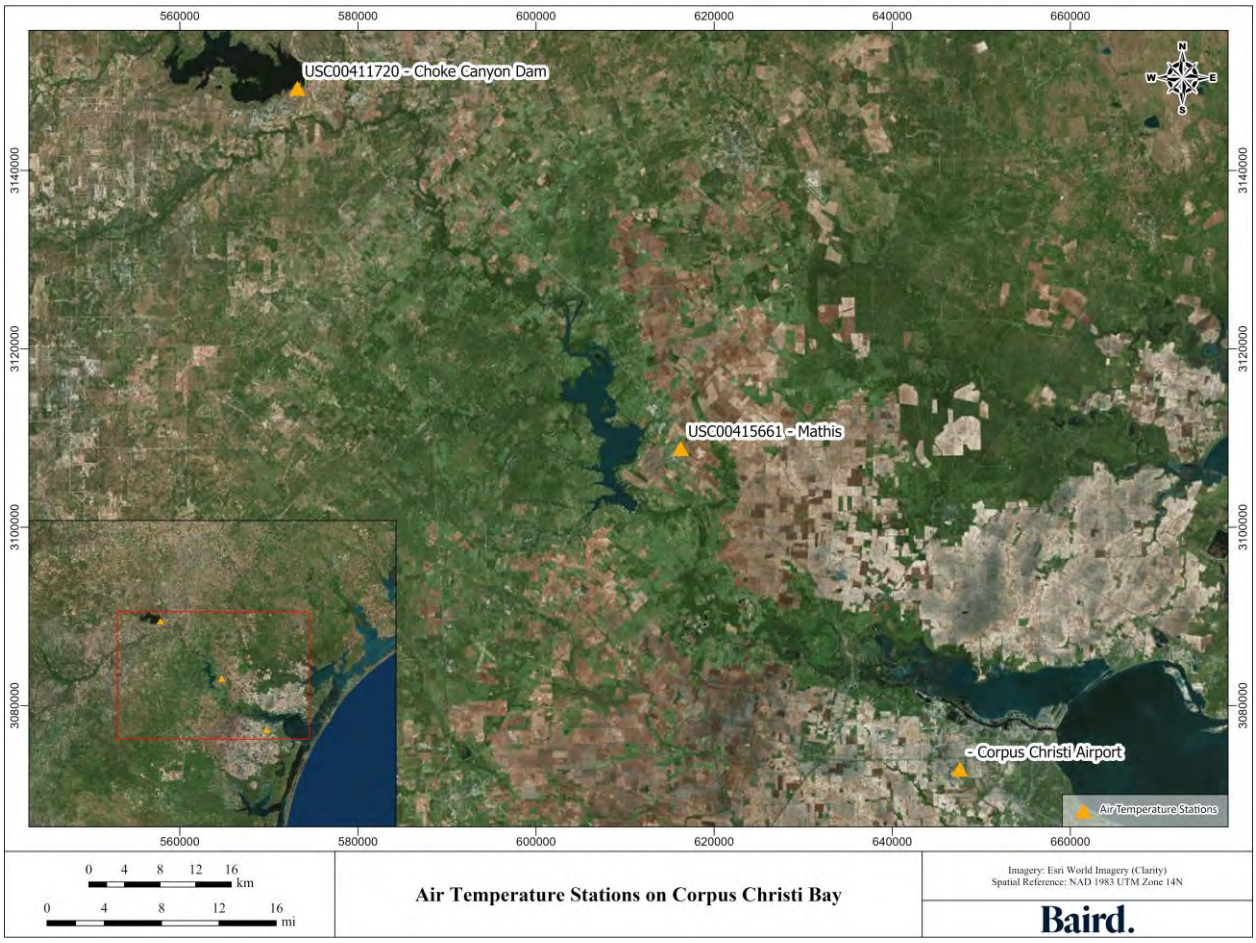

Figure 2.4: Location of NOAA Temperature Stations

Table 2.2:Summary Temperature Data Available from NOAA

Station Name	Station ID	Start Date	End Date
Mathis	USC00415661	1964-07-01	Present
Corpus Christi Airport	-	1946-08-01	Present
Choke Canyon Dam	USC00411720	1983-10-01	Present

2.1.2.3 Precipitation

Precipitation data was initially collected using the NCEI stations Mathis and Choke Canyon Dam with hourly sampling frequency. However, inconsistencies were discovered with the hourly data when compared to the same station's daily data. Additionally, daily precipitation data obtained from NOAA stations Rockport and Port Aransas depicted larger amount of precipitation when compared to the NCEI stations. Therefore, it was decided that the two NOAA stations with daily precipitation observations would be utilized. All four stations are shown in Figure 2.5 and listed in Table 2.3. Data was collected from January 2018 to June 2021 (https://tidesandcurrents.noaa.gov). The precipitation rates for Rockport and Port Aransas are shown in Figure 2.6.

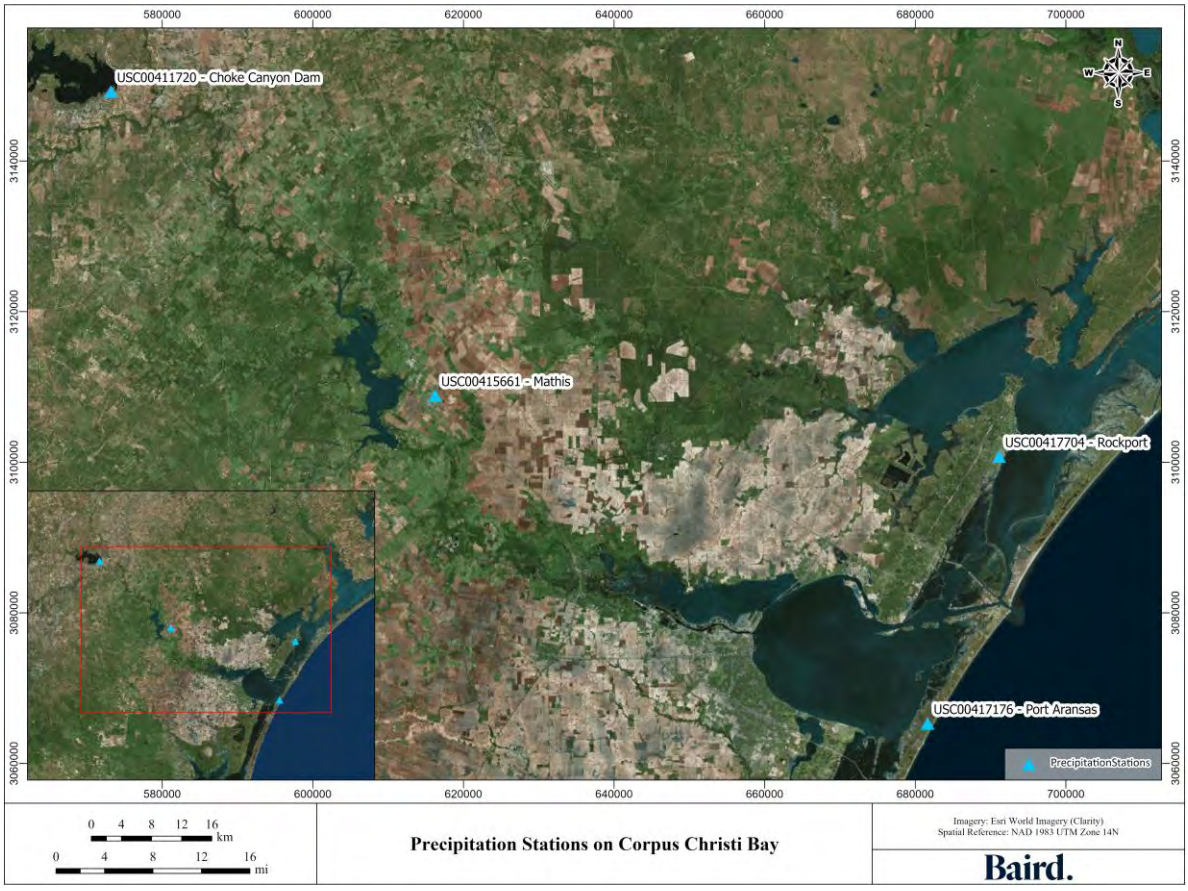

Figure 2.5: Location of NOAA Precipitation Stations

Table 2.3: Summary of precipitation data available from NOAA

Name	Station ID	Start Date	End Date
Mathis	USC00415661	1964-07-01	Present
Port Aransas	USC00417176	2007-11-18	Present
Choke Canyon Dam	USC00411720	1983-10-01	Present
Rockport	USC00417704	1959-01-01	Present

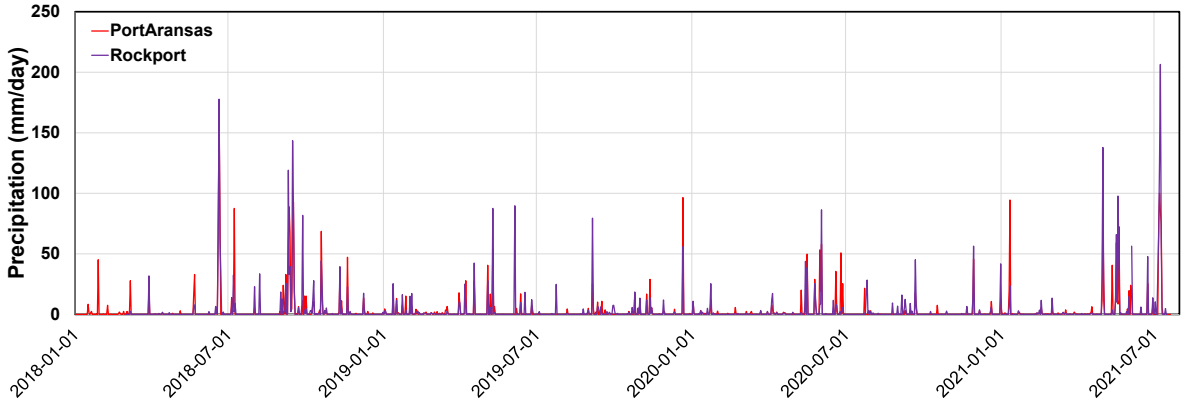

Figure 2.6: Daily precipitation rates

2.1.2.4 Evaporation

As previously mentioned in Section 2.1.2.2, daily evaporation rates were collected from two stations: Choke Canyon Dam and Mathis (Figure 2.5 and Table 2.3) from January 2018 to June 2021. Data from Mathis station was primarily used; however, data from Choke Canyon station was substituted if data from Mathis was unavailable. Evaporation rates for the two stations are shown in Figure 2.7.

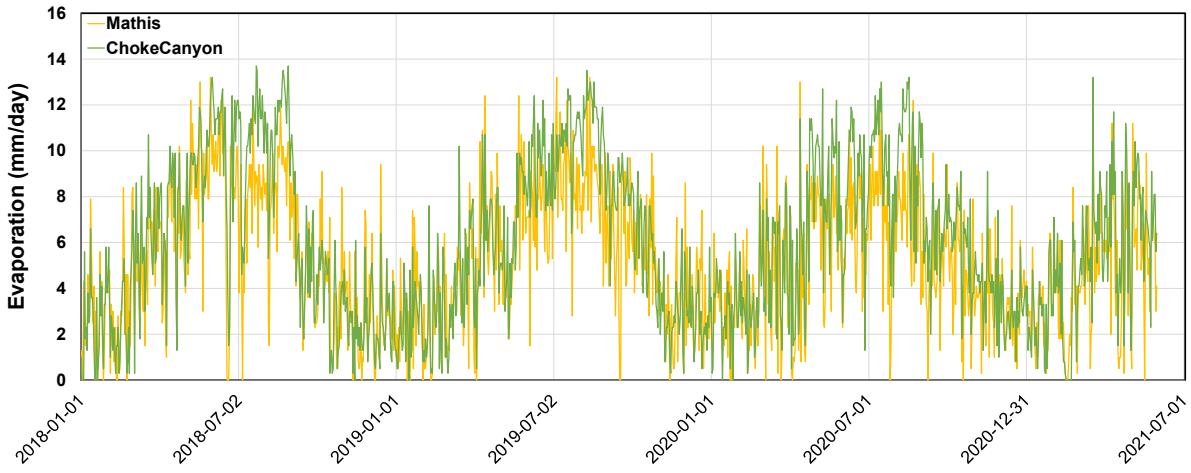

Figure 2.7: Daily evaporation rates measured at Mathis and Choke Canyon Dam

2.1.3 River Flows and Runoffs

2.1.3.1 Watersheds

Watershed boundaries and data were obtained from the United States Geological Survey (USGS) Watershed Boundary Dataset (WBD, https://apps.nationalmap.gov/downloader/#/). The watersheds surrounding Corpus Christi Bay are Nueces, South Corpus Christi Bay, and North Corpus Christi Bay watershed. The entirety of Nueces watershed (HUC6 121101) was used, while only specific catchments of the South and North Corpus Christi Bay watersheds were isolated, which are those surrounding Corpus Christi Bay and Oso Creek. The catchments of interest are illustrated in Figure 2.8, where the blue represents those directly draining into

Corpus Christi Bay or partially into Oso Bay, orange represents those contributing to the Nueces River flow, and purple represents those contributing to the Oso Creek flow.

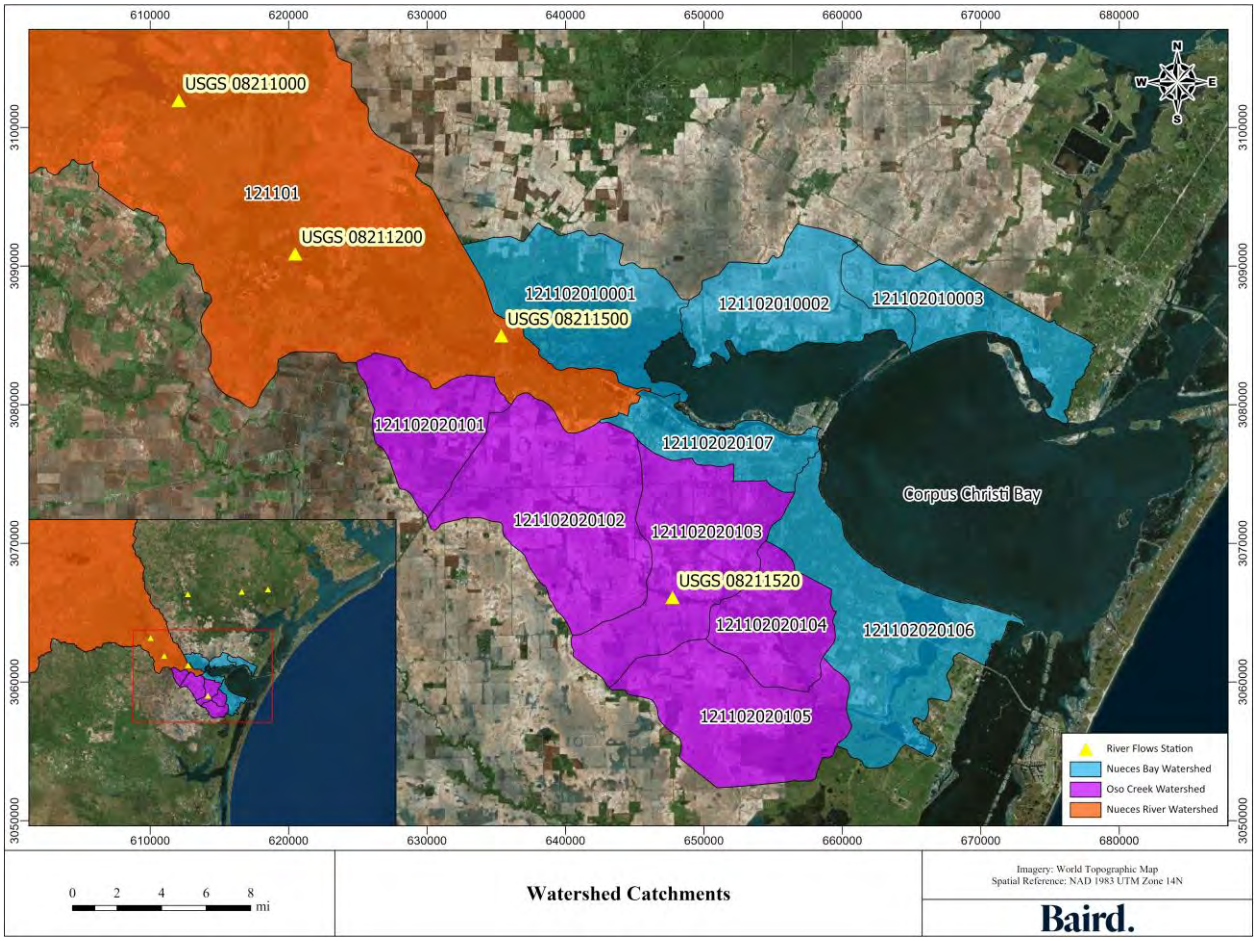

Figure 2.8: Watershed catchments for Nueces River, Oso Creek, and direct drainage

For the sub catchments of the South and North Corpus Christi Bay watersheds, present at HUC 12 (see below table), the areas were clipped and reviewed from the WBD using QGIS, an open-source geographic information system. The individual areas for each sub catchment are summarized in Table 2.4 and discussed in the following sections.

Table 2.4: North and South Corpus Christi Bay Watershed Sub catchment areas

HUC12	Area (Km^2)	Drained to
121102010001	114.96	Nueces Bay
121102010002	91.20	Nueces Bay
121102010003	74.28	Corpus Christi Bay
121102020101	67.66	Oso Creek
121102020102	156.88	Oso Creek

HUC12	Area (Km^2)	Drained to
121102020103	120.67	Oso Creek
121102020105	61.84	Oso Creek
121102020106	110.66	Oso Bay & Corpus Christi Bay
121102020107	49.71	Corpus Christi Bay

2.1.3.2 River Flows

River flows draining into Corpus Christi Bay and Aransas Bay were retrieved from seven USGS gages (https://maps.waterdata.usgs.gov/mapper/index.html). Nueces River, in which there are three gages, drains to Nueces Bay. There is one gage in Oso Creek which empties into Oso Bay. The remaining stations drain into Copano Bay. The data availability for each gage is summarized in Table 2.5. Figure 2.9 shows the location for each gage.

Table 2.5: Summary of river flow gages from USGS

Gage Name	Gage ID	Start Date	End Date
Nueces River nr Mathis	08211000	1987-09-01	Present
Nueces River at Bluntzer	08211200	1992-04-01	Present
Nueces River at Calallen	08211500	1989-10-02	Present
Oso Creek at Corpus Christi	08211520	1995-10-01	Present
Aransas River nr Skidmore	08189700	1964-03-27	Present
Mission River at Refugio	08189500	1939-07-01	Present
Copano Creek nr Refugio	08189200	1970-06-17	Present

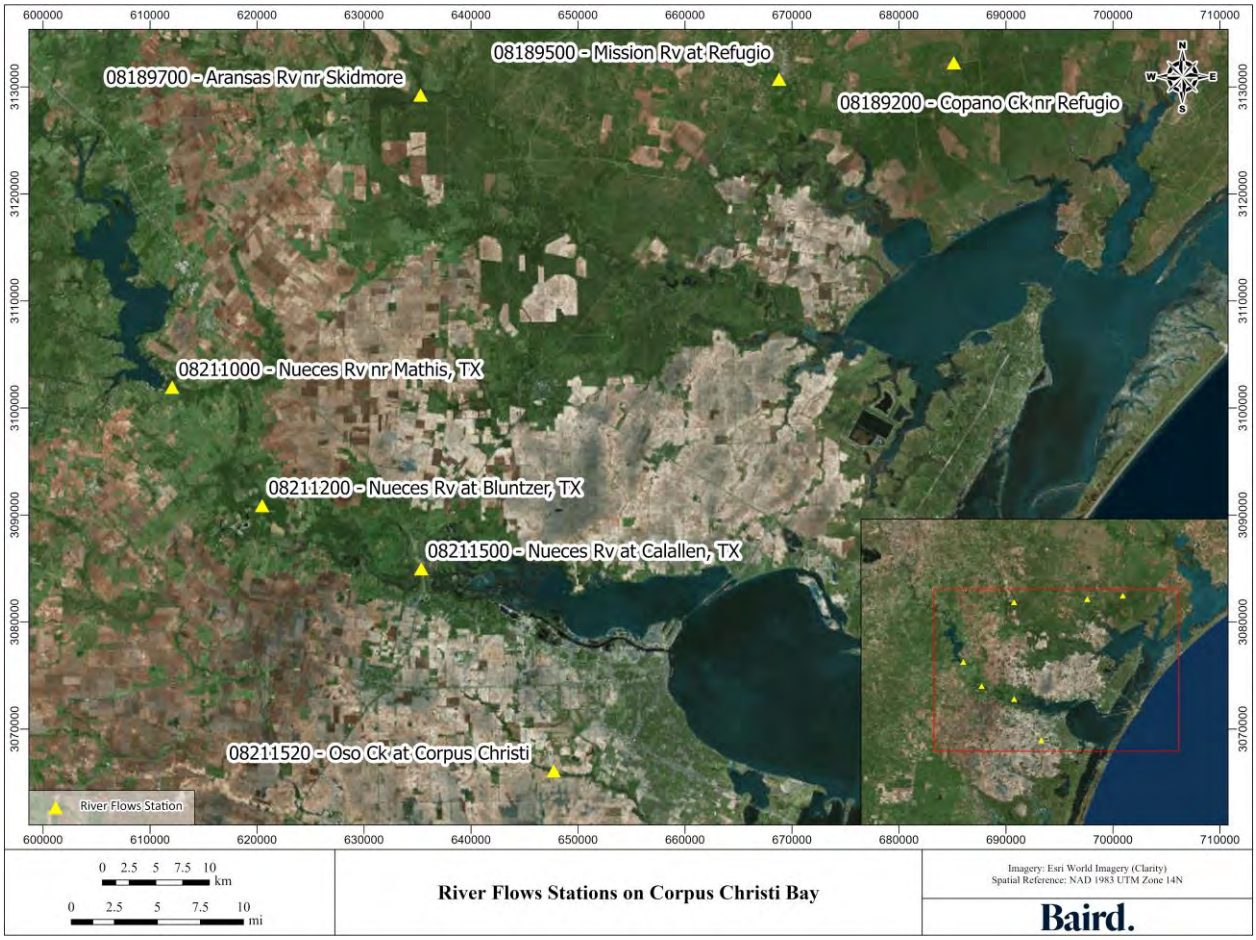

Figure 2.9: Location of USGS gages

A sample of the gaged flow is illustrated in Figure 2.10 from the period of August 2018 to the end of February 2019 for flows draining into Nueces Bay. Figure 2.11 displays a sample of the gage flows draining into Copano Bay. The upstream gages (08211000 and 08211200) were used to fill the data gaps at the most downstream gage in Nueces River.

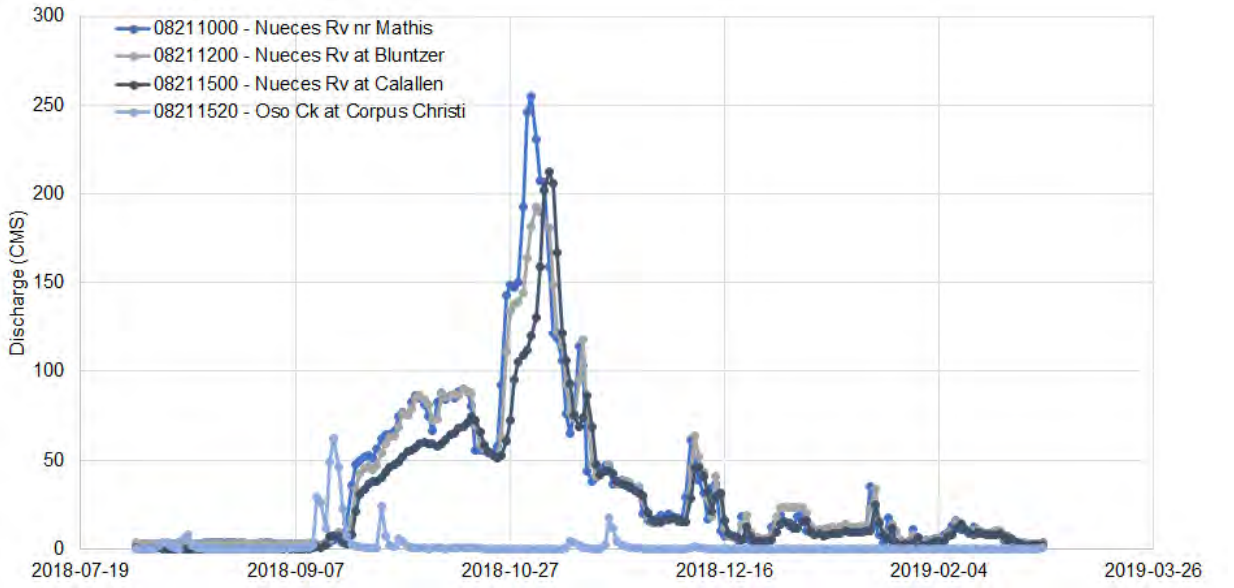

Figure 2.10: USGS River flows into Corpus Christi Bay

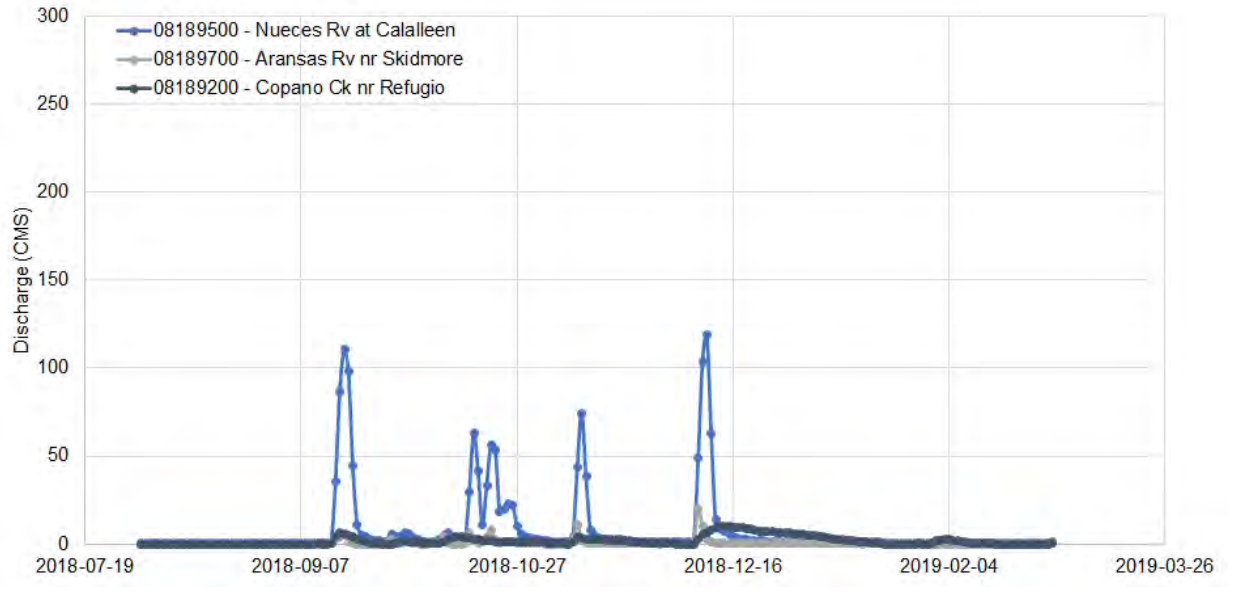

Figure 2.11: USGS River flows into Aransas Bay

It was concluded that the inflow from the Nueces River would be the combination of the gaged flows at 08211500 and the discharge from the Allison Waste Water Treatment Plant, which is estimated using return values obtained by the Texas Water Development Board (TWDB), discussed in Section 2.1.3.3. Oso Creek was determined to have unaccounted inflows from the surrounding watershed and was adjusted using a scale factor, which was estimated using the sub catchment areas. Figure 2.12 displays the final discharge estimates for Nueces River and Oso Creek after adjustments.

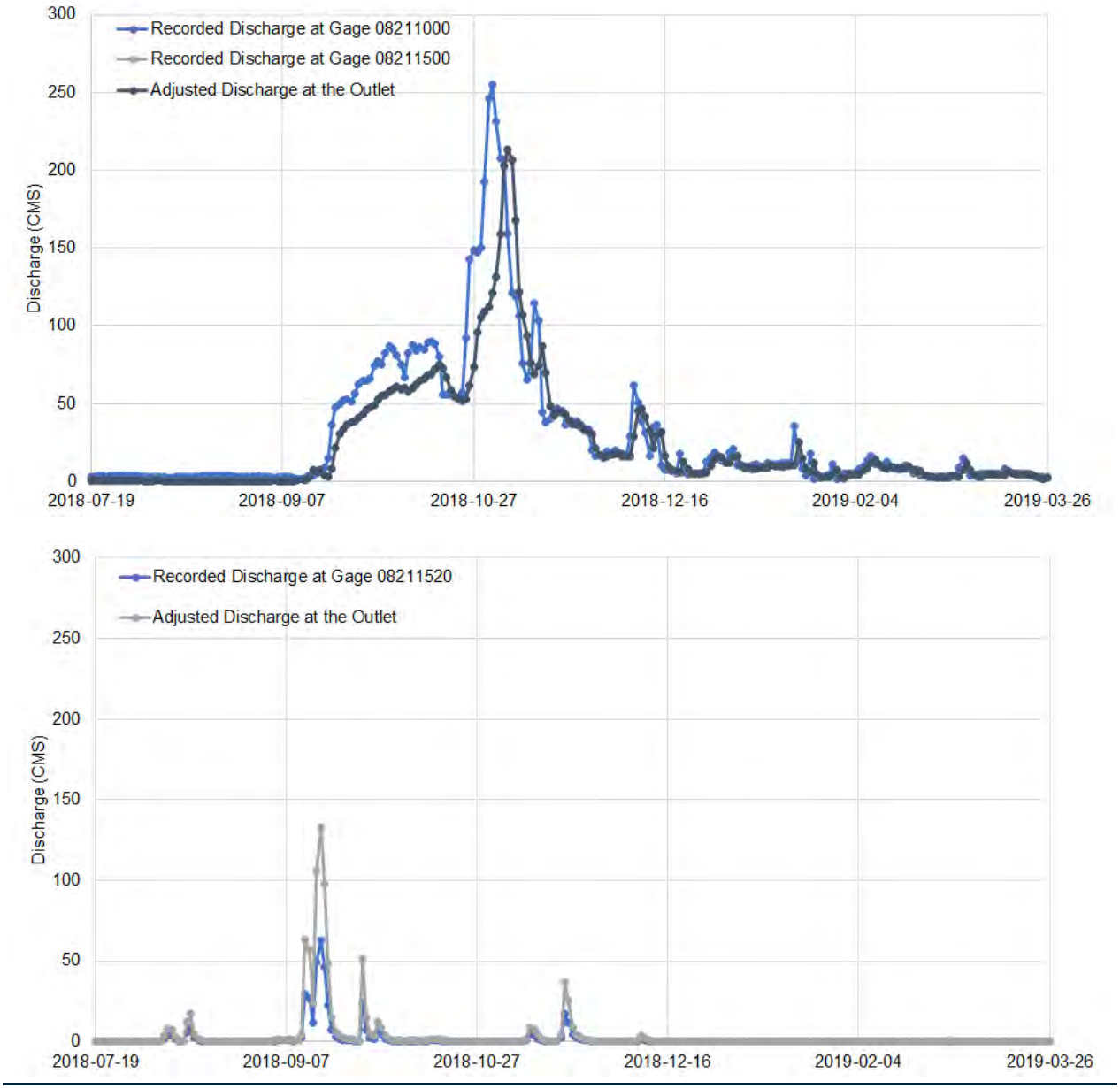

Figure 2.12: Adjusted discharge for Nueces River (top) and Oso Creek (bottom)

2.1.3.3 Runoffs from Ungagged Watershed

In addition to river flows, ungaged flows were estimated for the sub catchments draining directly into Corpus Christi Bay, which were identified in Section 2.1.3.1. To estimate the flows for the sub catchments, runoff data modeled with the Texas Rainfall-Runoff Model (TxRR) (Perales, *et al*, 2000) was obtained from the Texas Water Development Board (TWDB, https://waterdatafortexas.org/coastal/hydrology/corpus_christi). Data was available from 1940 to the end of 2019. Precipitation data used in the TxRR model was also provided for the period of 1900 to the end of 2019 and returns (from water usage facilities), and diversions were provided for

the period from 2000 to 2019. The modeled precipitation was comparable to precipitation retrieved from NOAA.

A report released by the TWDB in 2011 (Schoenbaechler, *et al*, 2011) documents the procedures involved with estimating the inflows and provides an overview of the associated catchments, shown in Figure 2.13, which was used to relate the TWDB data to the watersheds highlighted in Section 2.1.3.1. TWDB modeled the total freshwater inflows as a combination of the gaged inflows, ungaged inflows, return flows, modified precipitation, diversions, and evaporation. By relating the areas of Figure 2.8 to those in Figure 2.13, the discharges for the five highlighted catchments are estimated. A brief description of how each catchment's runoff flows are estimated are that:

- HUC 121102010001 is estimated as the total runoff from TWDB's watershed #21010 and #22012 combined with the flow at USGS 08211000, and removing the percentage of flows in the at gage 08211500 after adjustments.
- HUC 121102010002 and 121102010003 make up the total area of TWDB's watershed #20005, and thus are each a portion of the modeled runoff according to their areas.
- HUC 121102020107 is directly linked with TWBD's watershed #22013, and thus is recorded as having the same runoff.
- HUC 121102020106 is associated with TWBD's watershed #22014 and #22015. The runoff for HUC 121102020106 is the sum of the runoff of both TWBD watersheds.

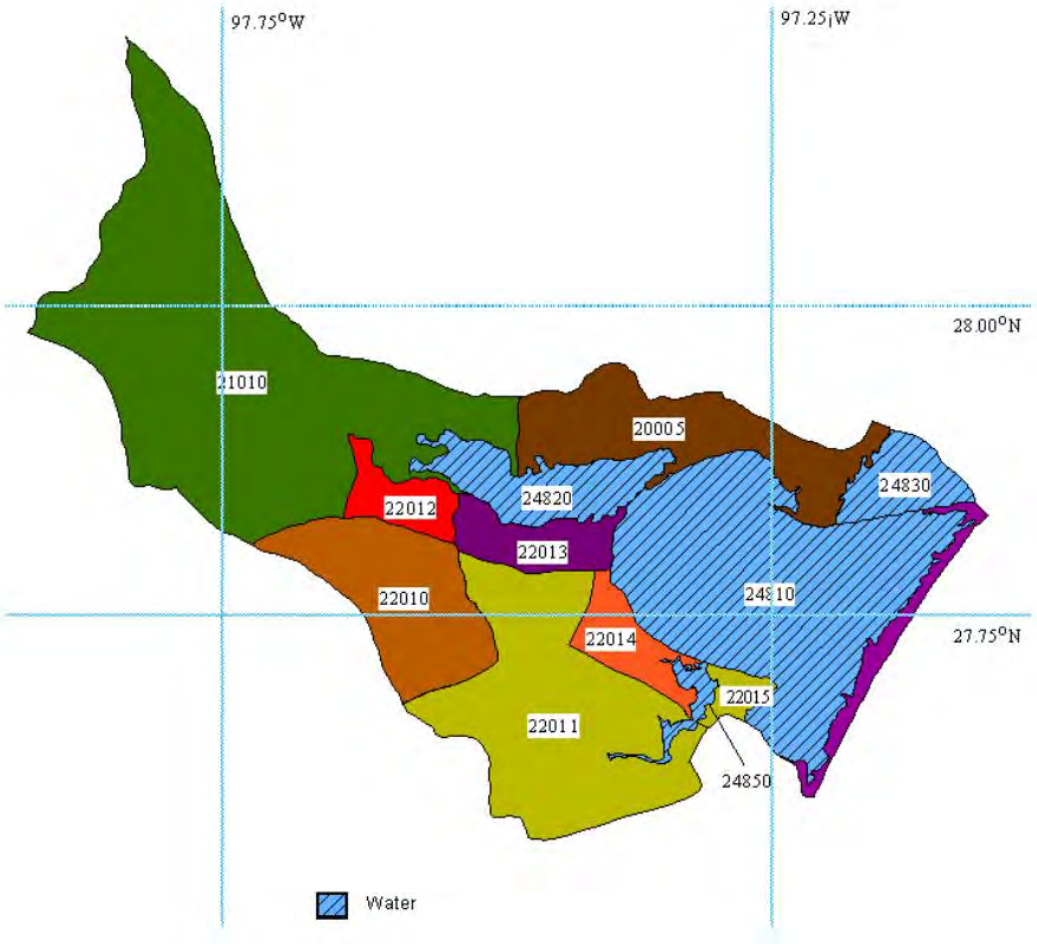

Figure 2.13: Ungaged watershed delineation (Schoenbaechler, *et al*, 2011)

2.1.4 Hydrological Data

2.1.4.1 Water Levels

Water levels from 10 stations in Corpus Christi's Bay and Aransas Bay were obtained from NOAA Tides & Currents database (https://tidesandcurrents.noaa.gov/map/index.html). Data availability at the stations is summarized in Table 2.6, and the locations are illustrated in Figure 2.14. Data gaps exist for four stations during the period of interest: Aransas Wildlife Refuge, Rockport, USS Lexington, and South Bird Island. Of these stations, Rockport has the greatest number of data gaps, representing approximately 14% of the available data. The other three stations have data gaps representing less than 2% of the available data for the period of interest.

Table 2.6: Summary of hourly data available from NOAA stations

Station Name	Station ID	Start Date	End Date
Aransas Wildlife Refuge	8774230	2012-11-01	Present
Rockport	8774770	1937-03-01	Present
Aransas Pass	8775241	2016-12-20	Present
Port Aransas	8775237	2002-06-26	Present
Nueces Bay	8775244	2012-01-01	2012-12-31
USS Lexington	8775296	2012-01-01	Present
Packery Channel	8775792	1996-01-01	Present
Bob Hall Pier	8775870	1983-11-30	Present
South Bird Island	8776139	2012-10-01	Present
Baffin Bay	8776604	2012-10-01	Present

Figure 2.14: Location of NOAA water level stations

2.1.4.2 Currents

Currents data was obtained for 12 stations, available from NOAA's Center for Operational Oceanographic Products and Services online database (https://tidesandcurrents.noaa.gov/) and the National Data Buoy Center (NDBC, https://www.ndbc.noaa.gov/). The availability of the 12 stations is listed in Table 2.7, and their locations are shown in Figure 2.15. The data was processed to fill gaps through interpolation and relation to nearby stations. All stations possess long gaps in their data, with Station TABS-D having the longest record of measurements available.

Table 2.7: Summary of currents data available from NOAA and NDBC

Station Name	Station ID	Start Date	End Date
AP Buoy	CC0101	2018-01-31	2019-07-23
Aransas Pass LB6	CC0201	2019-07-12	Present
Port Aransas, Channel View	CC0301	2018-10-31	Present
MODA Currents	CC0401	2018-03-27	Present
UTMSI Fisheries and Marine Lab	CC0601	2021-04-23	Present
Texas Automated Buoy System Buoy D	42048	2010-03-01	Present
Corpus Christi Channel (moved)	STX1804	2018-12-01	2019-01-31
La Quinta Channel	STX1803	2018-12-01	2019-01-31
ICW - CC Bay Light 51	STX1806	2018-12-01	2019-01-31
ICW - CC Bay Southern Ent	STX1807	2018-12-01	2019-02-01
Lydia Ann Channel, S end	STX1801	2018-12-1	2019-01-30
Murray Shoal	STX1802	2018-12-01	2019-01-30

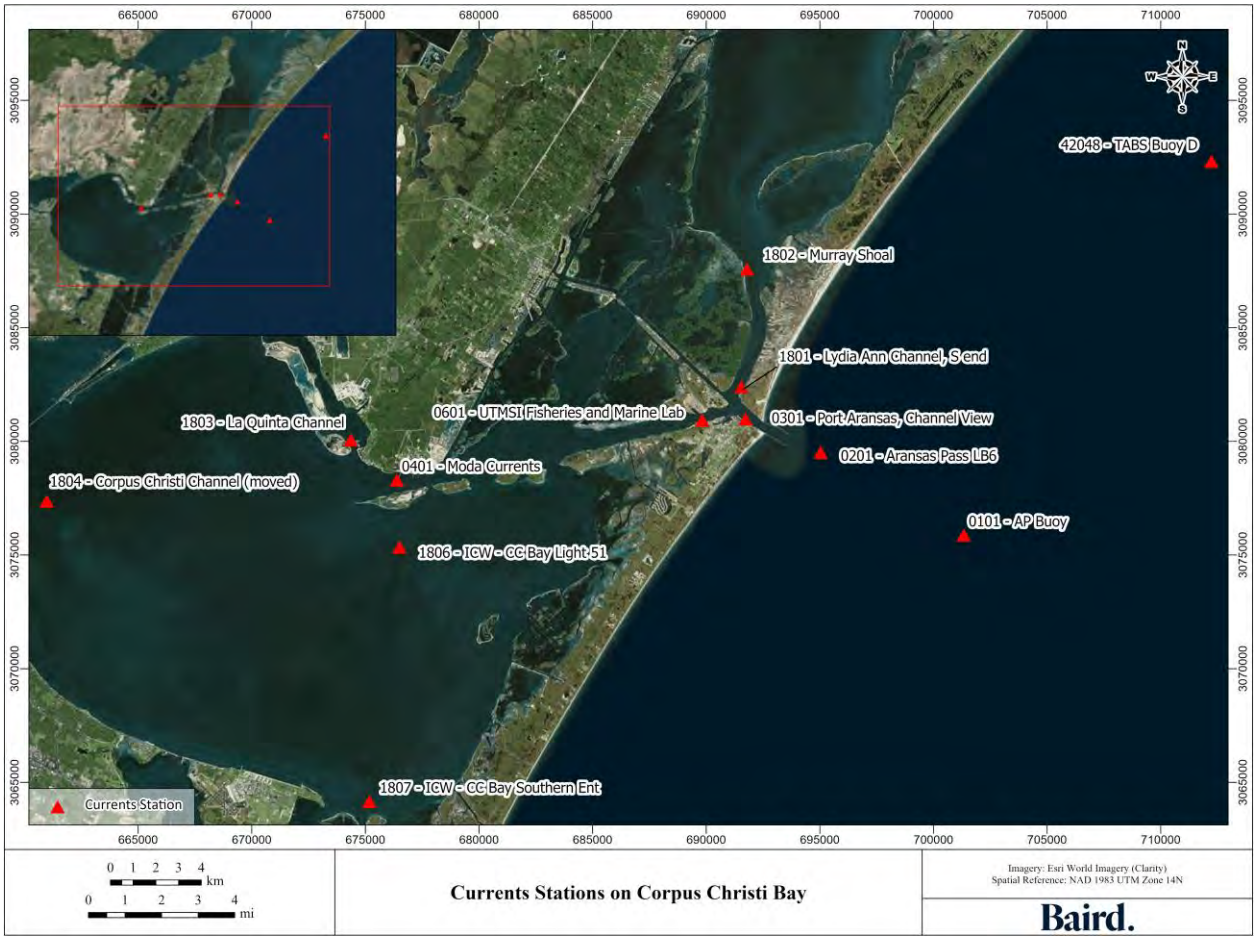

Figure 2.15: Currents monitoring locations by NOAA and NDBC

2.1.4.3 Salinity

Salinity data is available for six long term stations in and near Corpus Christi Bay. Salinity data was obtained from two sources: the Texas A&M University CBI (http://cbi.tamucc.edu) and the TWDB (https://www.waterdatafortexas.org/coastal). Outliers were manually removed from the salinity dataset prepared for the model. The data availability is presented in Table 2.8. Data processing involved removing outliers and filling in gaps through interpolation or relation to a nearby, similar station if large gaps were present, such as for MANER4, INPT and TABSD. Station further north, CHKN and GBRA#1, were used to fill in gaps for MANER4, and TABSW was used for the gaps in TABSD. Final adjustments were made through visual inspection to remove any persisting outliers.

Table 2.8: Summary of salinity data available from Texas A&M University CBI and TWDB

Station Names	Station ID	Start Date	End Date
National Park Service – Bird Island	171-NPSBI	2008-06-02	Present
MANNER Station #4 (Aransas Bay)	148-MANER4	2007-06-21	Present
SALT 01	072-SALT01	1991-12-04	Present
SALT 03	074-SALT03	1991-12-04	Present
SALT 05	076-SALT05	1995-08-18	Present
Nueces Delta 3	043-NUDE3	2009-05-19	Present
Indian Point Pier	INPT	2017-05-15	2019-05-06
Texas Automated Buoy System Buoy D	TABSD	2010-10-15	Present

In addition to the available salinity data retrieved from the Texas A&M University CBI and the TWDB, salinity measurements were obtained from two other sources: the observed salinity from Islam, Bonner, Edge, and Page (2014), and those provided by AECOM. The observed salinity measurements from Islam, Bonner, Edge, and Page consisted of three stations, known as Platform 1, Platform 2 and Platform 3, during the period of July 7 to August 10, 2007. AECOM provided nine measurement sets recorded on September 18, 2018. The AECOM stations, along with their cast times and number of measurements, are summarized in Table 2.9.

All salinity stations are displayed in Figure 2.16.

Table 2.9: Summary of salinity data available from AECOM

Name	Station ID	Start Cast	End Cast	Number of Measurements
AECOM 01	A01	9:47 CST	9:58 CST	45
AECOM 02	A02	10:16 CST	10:29 CST	55
AECOM 03	A03	10:42 CST	10:52 CST	42
AECOM 04	A04	11:08 CST	11:20 CST	55
AECOM 05	A05	11:33 CST	11:43 CST	52
AECOM 06	A06	11:53 CST	12:04 CST	52
AECOM 07	A07	12:28 CST	12:33 CST	14
AECOM 08	A08	12:46 CST	12:52 CST	16
AECOM 09	A09	13:11 CST	13:14 CST	11

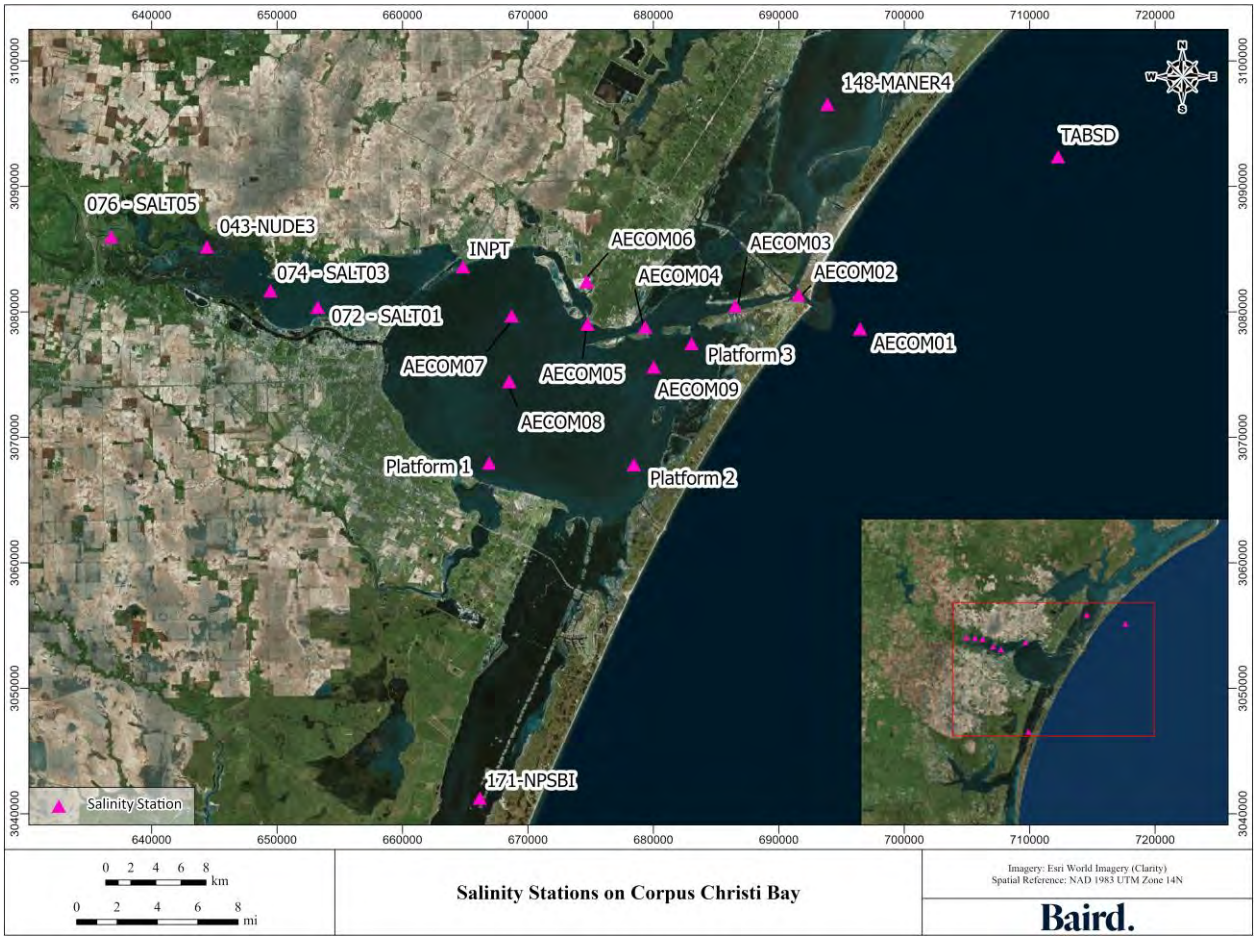

Figure 2.16: Salinity monitoring locations by the Texas A&M University CBI and TWDB

2.1.4.4 HYCOM Model

The HYCOM (Hybrid Coordinate Ocean Model) is an ocean circulation model with primitive equations that combines three types of vertical coordinates (z, sigma and isopycnal). For horizontal coordinates, HYCOM works with orthogonal rectilinear and curvilinear meshes. HYCOM efficiently solves the diapycnal diffusion, which is the interaction between layers of different densities. Also, it solves the dynamics in the stratified subsurface part of the ocean and its adjustment with the mixing layer.

The oceanic model calculates 541×385 cells in the horizontal at 1/25 degrees (~2.2 miles) in both easting and southern directions, and 27 hybrid layers (z, sigma and isopycnal coordinates) in the vertical, detailing on the surface and zone of the mixed layer with z-coordinates. From this model, the surface elevation and fluxes at the model boundary conditions were extracted.

From this source, the surface elevation and fluxes at the model offshore boundary conditions (see details in Section 3) were extracted. Figure 2.17 shows the HYCOM model nodes as black dots, the offshore boundary of the mesh as yellow dots, the northeast offshore boundary with purple lines, the southwest offshore boundary as orange dots, and the mesh elements used with blue lines. At the offshore boundary (yellow) the surface

elevation was extracted from the HYCOM nodes using linear interpolation, while velocities were extracted at the northeast and southwest offshore boundary.

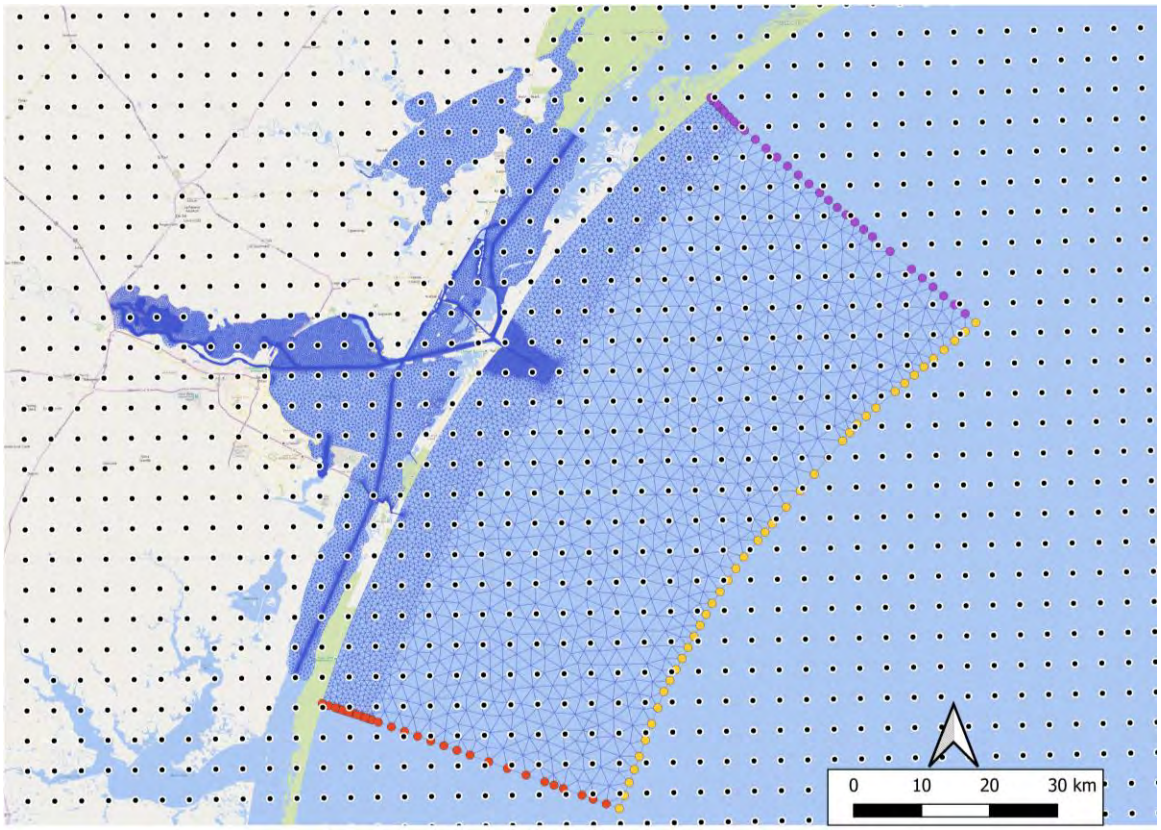

Figure 2.17: HYCOM model nodes and boundary of the computational mesh. Black dots are HYCOM model nodes, yellow dots show the offshore boundary of the mesh, purple lines show the northeast offshore boundary, orange dots show the southwest offshore boundary, and blue lines show the mesh elements.

2.2 Understandings of Physical Processes

2.2.1 Tide Propagation

This modeling study mainly focuses on Corpus Christi Bay, which connects to the other subtropical bays, such as Nueces Bay to northwest, Aransas Bay and Copano Bay on the northeast side, and Baffin Bay on the southwest side, through the Gulf Intracoastal Waterway (GIWW) (see Figure 2.18). The GIWW is a shallow water body running parallel to the shoreline of Gulf of Mexico (GOM) and has many man-made navigation channels. It is separated from the GOM by the longshore barrier islands, such as Mustang Island, Padre Island, and San Jose Island. These bays are connected to the GOM by a narrow entrance channel, Aransas Pass. There is a secondary inlet, Packery Channel. The tidal exchange between the GOM and the subtropical bays that have totally more than 1,000 km^2 in surface area is mainly through Aransas Pass, resulting in significantly strong current in the pass. The peak current speed in the pass reaches approximately 1.5 m/s (Williams et al., 1991; Brown et al., 2000, Whilden, 2015). On the other hand, this narrow channel also limits

the tidal exchange between the GOM and bays, resulting in significant attenuation of tides in Corpus Christi Bay.

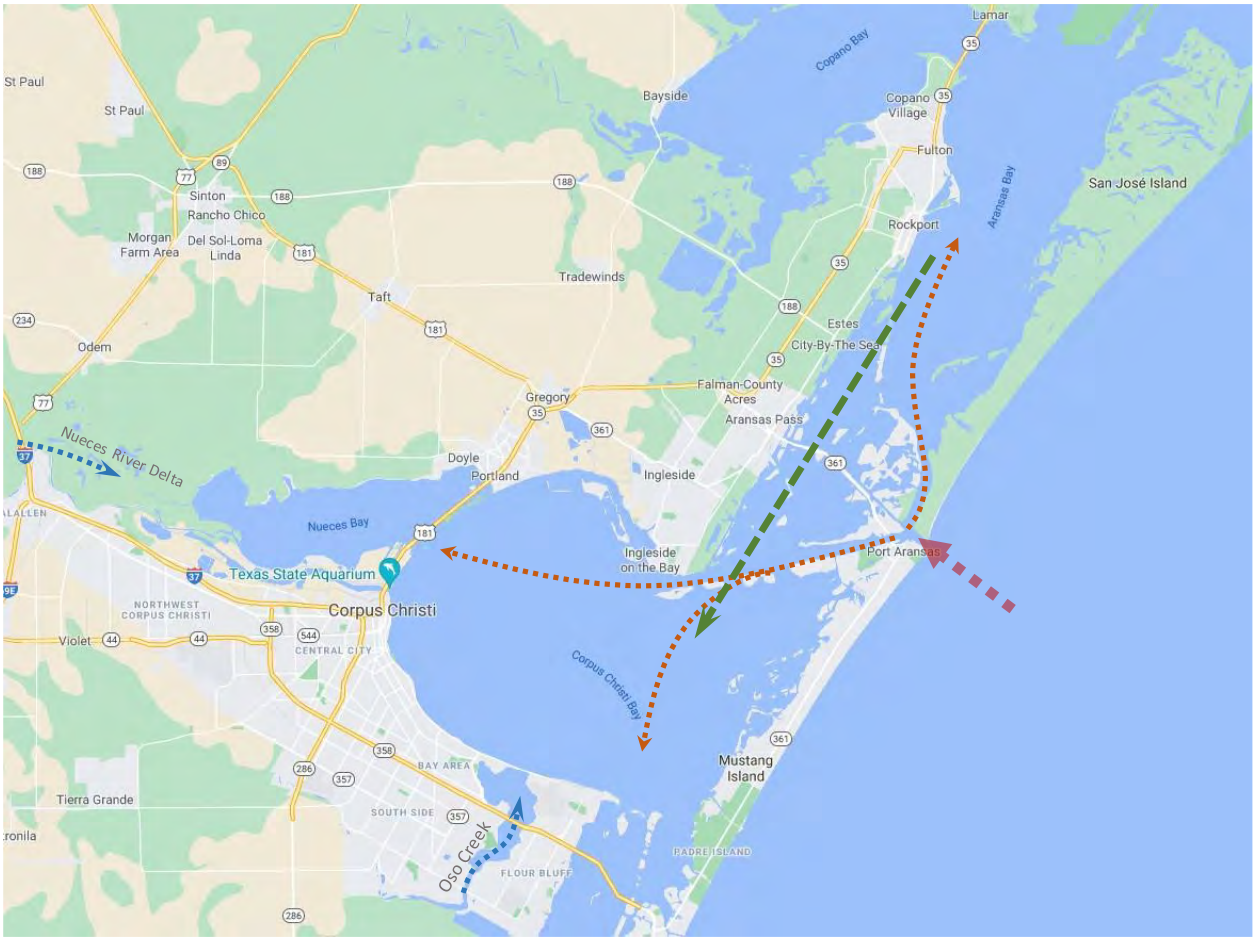

Figure 2.18: Understanding of local tide propagation. The orange arrows show the tide wave propagation directions. The green arrow shows the net flow along the intercoastal waterway. The blue arrows indicate the freshwater injections to the bays.

Data analysis of the measured water levels was carried out to understand the paths of tide propagation in the study area. Figure 2.19 to Figure 2.21 show the comparison of water levels measured at the stations (see locations in Figure 2.14) along three tide propagation paths as indicated in Figure 2.18. The Bob Hall Pier station is located in the offshore, therefore it represents the tide waves in the GOM. The tides in the GOM are primarily diurnal or mixed diurnal-semidiurnal with the tide range of about 0.7 m based on the measured water level at Bob Hall Pier.

These comparisons show three directions of tide wave propagation and the tide attenuation after the tide waves are transported from the GOM to the bays through Aransas Pass. The tide range at the Port Aransas is attenuated about 30%. The tides are further attenuated with the distance from Aransas Pass. Figure 2.19 shows the tide attenuation and phase lag along the northeast path of the intercoastal waterway, i.e., from the GOM, through Port Aransas, to Rockport and Aransas Wildlife Refuge. The lags in tide phase at these stations indicate the route of tide wave propagation in the northeast direction. The tide attenuation and the tide phase

lag from the GOM to USS Lexington are shown in Figure 2.20, indicating the other middle path of tide propagation along the Corpus Christi Navigation channel towards to Nueces Bay. Figure 2.21 shows the tide attenuation and the phase lag along the southwest direction of intercostal waterway from the GOM to Port Aransas, Packery Channel, South Bird Island, and Baffin Bay. The tide signal at Baffin Bay almost disappears. This also indicates that the secondary inlet at Packery Channel Inlet has an insignificant impact on the tide in the bays.

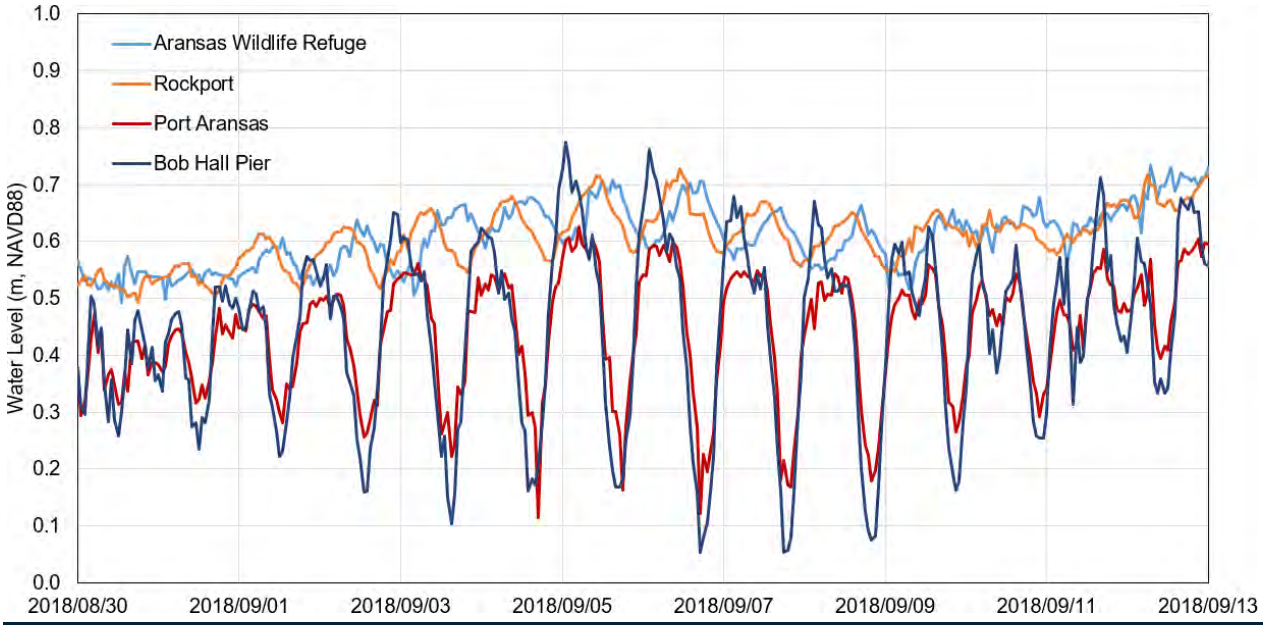

Figure 2.19: Tide propagation towards to northeast, indicated by the tide attenuation and phase lag from the GOM to Aransas Bay through Aransas Pass

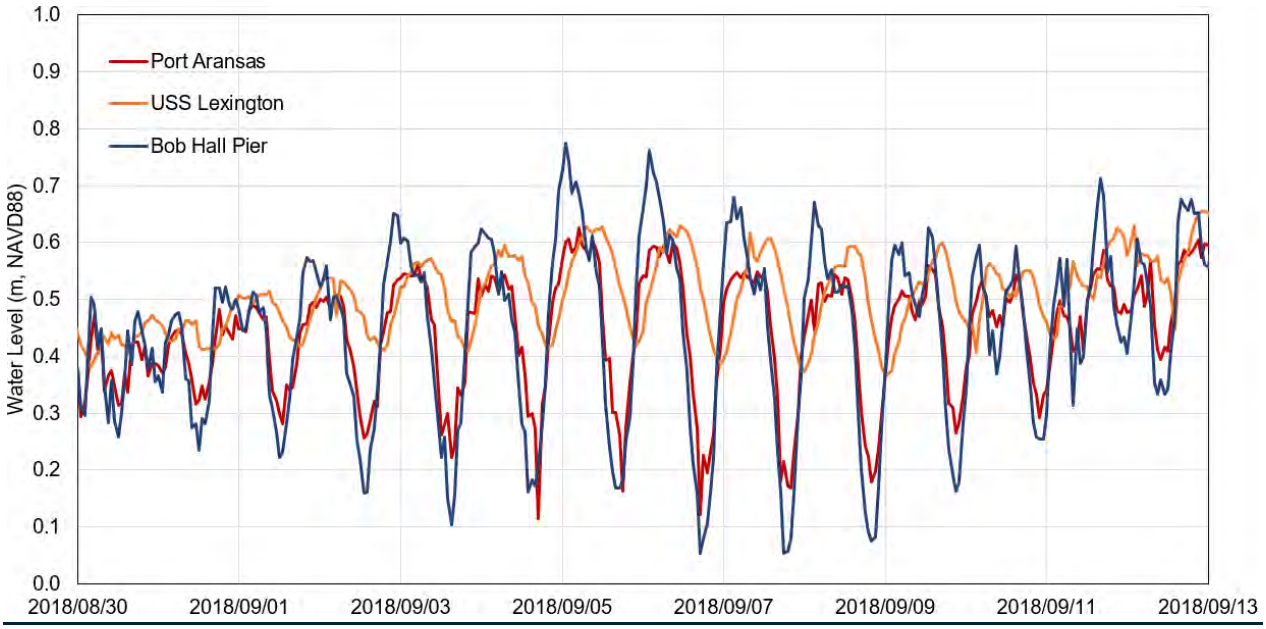

Figure 2.20: Tide propagation towards to northwest, indicated by the tide attenuation and tide phase lag from the GOM to USS Lexington through Aransas Pass

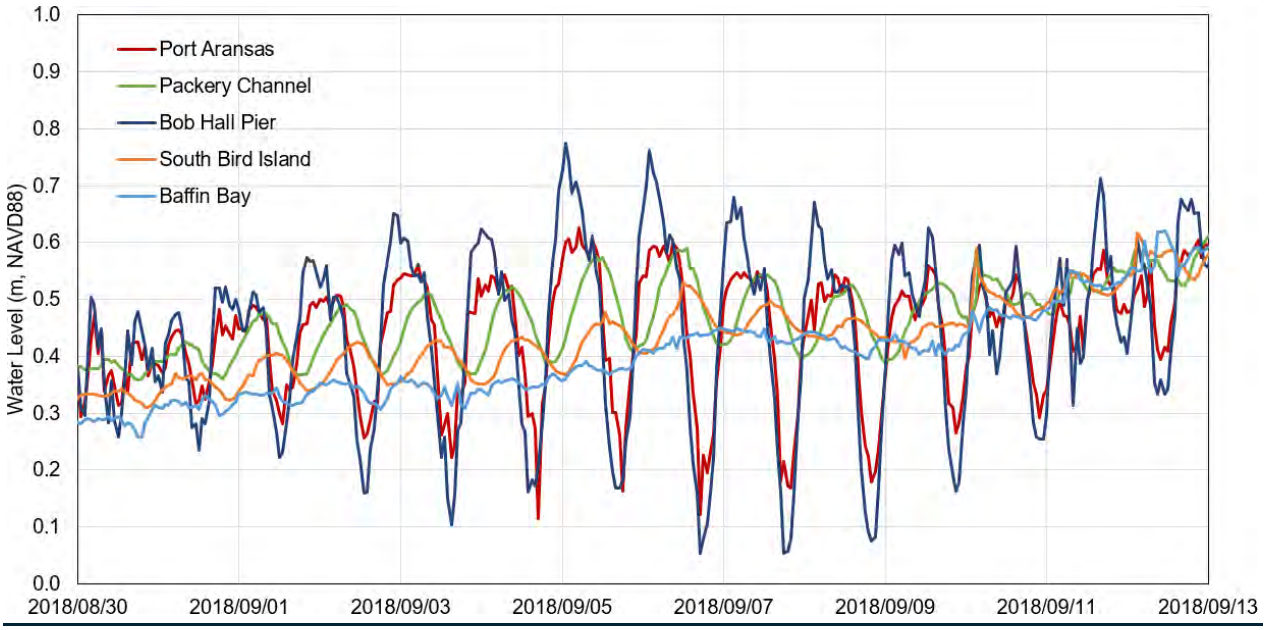

Figure 2.21: Tide propagation towards to southwest, indicated by the tide attenuation and tide phase lag from the GOM to Baffin Bay through Aransas Pass

The tide ranges at Rockport, Packery Channel, and the USS Lexington are only about 30% of the tide range in the GOM, i.e., the tides at these three stations are attenuated about 70%. It is also observed that the tide phases at these three stations are almost the same (see Figure 2.22). There is a constant water level difference between Rockport and Packery Channel, which indicates that there are likely net tide currents from Aransas Bay to Corpus Christi Bay through the GIWW as shown by the green arrow in Figure 2.18.

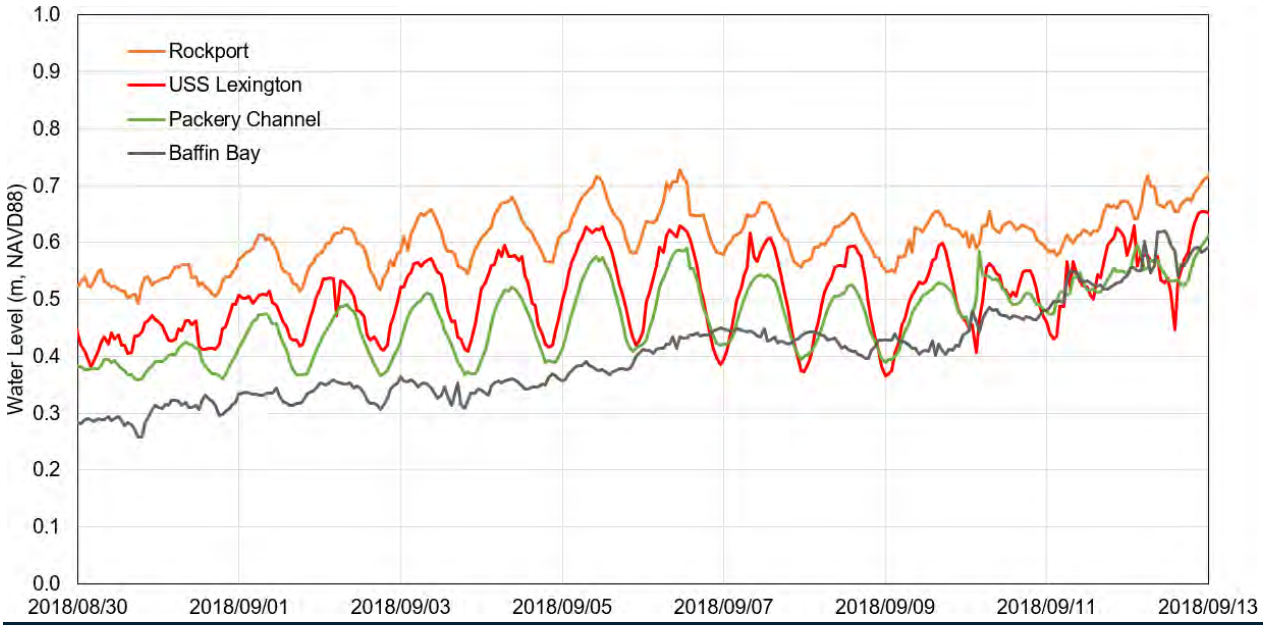

Figure 2.22: Water level difference along the Intercoastal Waterway. The water level at Rockport is always higher than that at Packery Channel.

2.2.2 Seasonal Variation of Wind

Hourly wind data measured at Bob Hall Pier was analyzed to understand the seasonal variation of local wind conditions. Figure 2.23 shows the rose plot from all wind data measured at Bob Hall Pier from 2005 to 2020. The figure indicates that the prevailing wind is from southeast. Since the study area is located on the northwest corner of the GOM, this prevailing wind likely results in the setup of water level at the study area. The monthly breakdown of the wind rose plots are shown in Figure 2.24. In the summer season from May to August, the prevailing wind is from southeast, which features the longest wind fetch in the GOM towards the project site. As a result, it likely produces the largest setup of water levels due to wind at the project site. In winter season from December to February, the prevailing wind is from north due to the frequent passages of cold fronts, which results in the set-down of water level in the GOM at the project site. In the remaining months, from March to April and from September to November, the prevailing wind is from both southeast and north which represents the transition of wind conditions between summer and winter seasons.

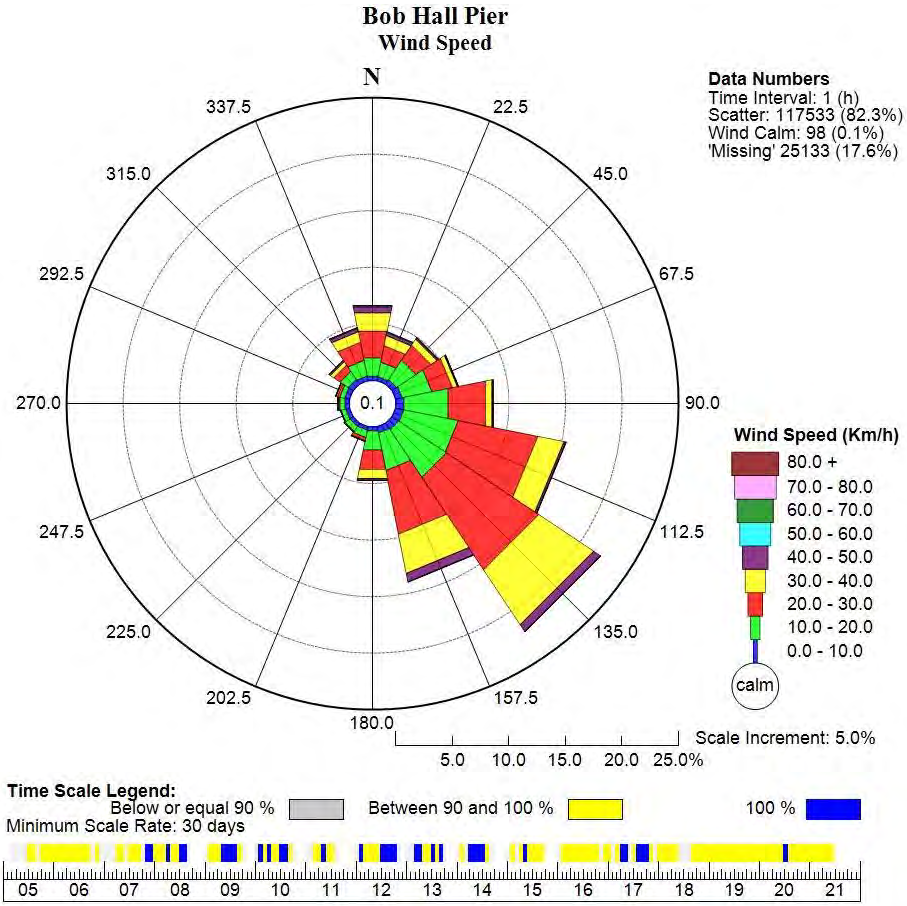

Figure 2.23: Rose plot of wind data measured at Bob Hall Pier (2005 to 2021)

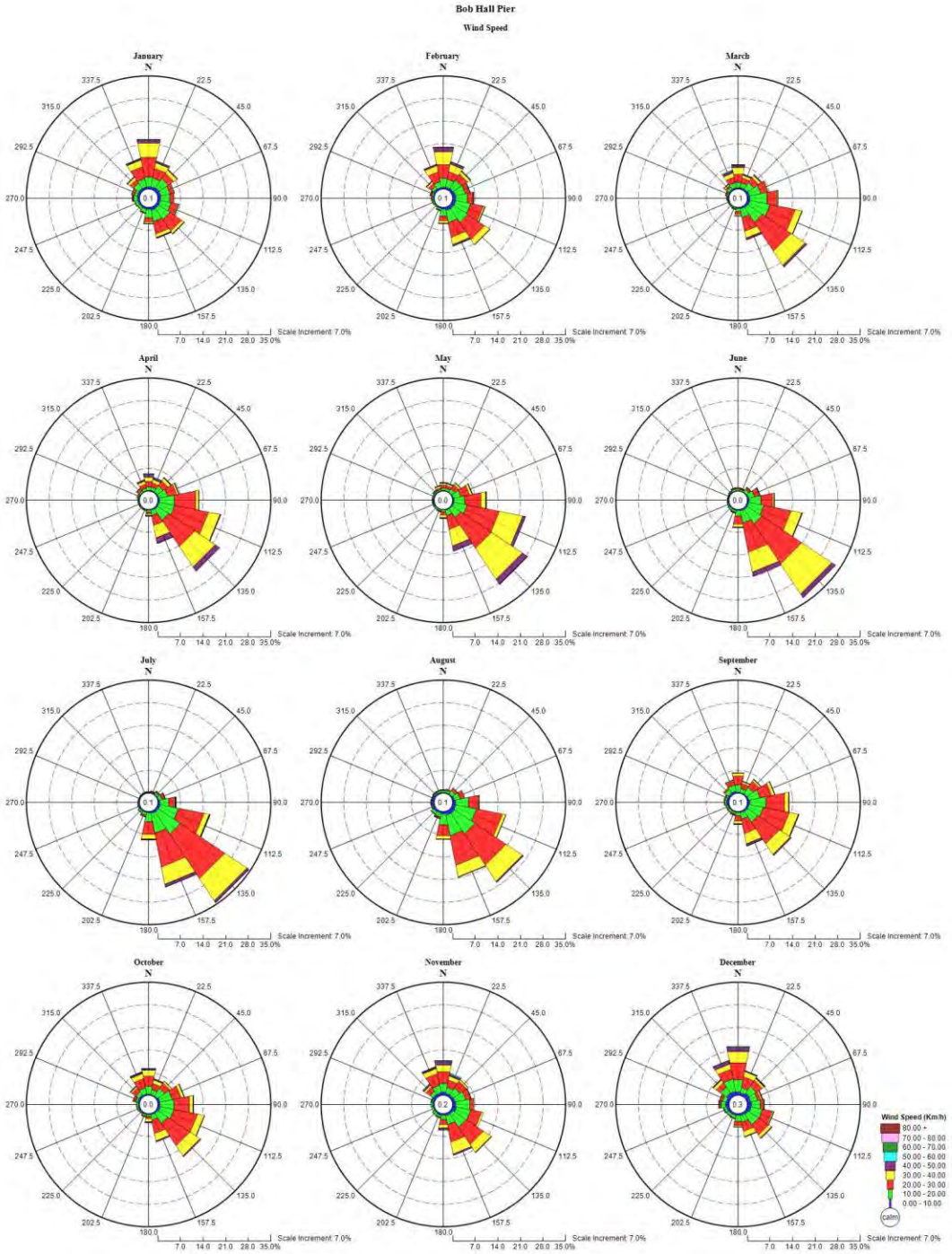

Figure 2.24: Monthly rose plot of wind data measured at Bob Hall Pier (2005 ~ 2021)

2.2.3 Seasonal Variation of Offshore Water Levels

Beside tides, the seasonal variation of water level in the GOM resulting from wind and the related oceanographic circulation has great contribution to the fluctuation of water level in these subtropical bays. As described in the previous section, the seasonal variation of water level at the offshore of the study area is driven by the seasonal sustained winds. The tropical storms (or hurricanes) cause large fluctuation of water level in the bays, but it is not sustainable. To understand the seasonal variations of offshore water level in the study area, tide signal was removed by subtracting water levels predicted using the selected major tide constituents from the measured water levels. The results are shown in Figure 2.25. The monthly averaged water level resulting from the sustained winds are shown in Figure 2.26. The seasonal variation of water level can be well explained by the seasonal changes of the prevailing wind direction in seasons in the GOM as described in Section 2.2.2 along with the related oceanographic circulation patterns. The water levels at the offshore of the project site are higher in late spring and fall. The highest offshore water level occurs in October, which is about 0.4 m ranging from 0.2 m to 0.7 m above mean sea level. The offshore water levels in winter season are low, which likely results from the predominant north winds associated with the passage of frequent cold fronts.

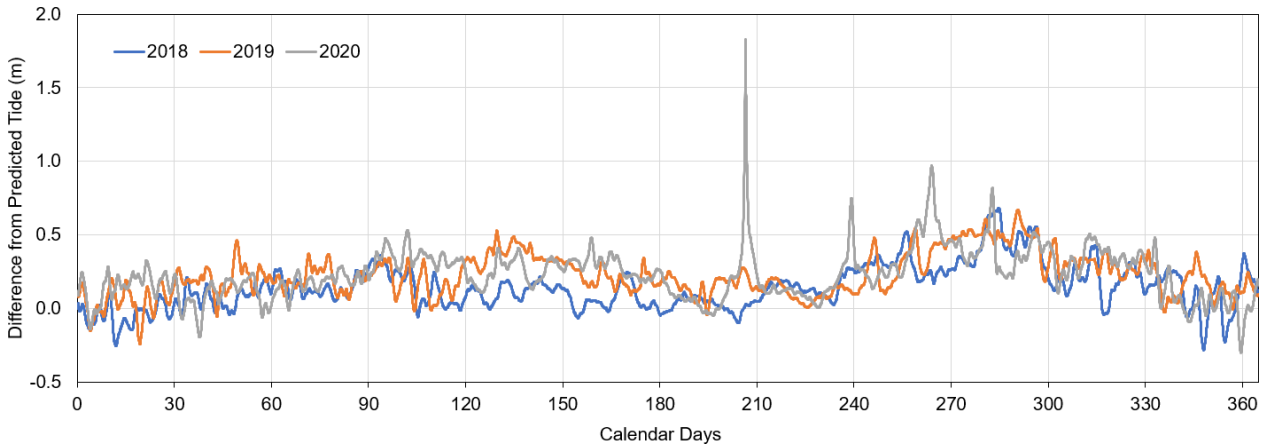

Figure 2.25: Seasonal variation of water level in the Gulf of Mexico calculated as the difference of water level measured at Bob Hall Pier and water level predicted by using tide constituents. The water level is referred to Mean Sea Level.

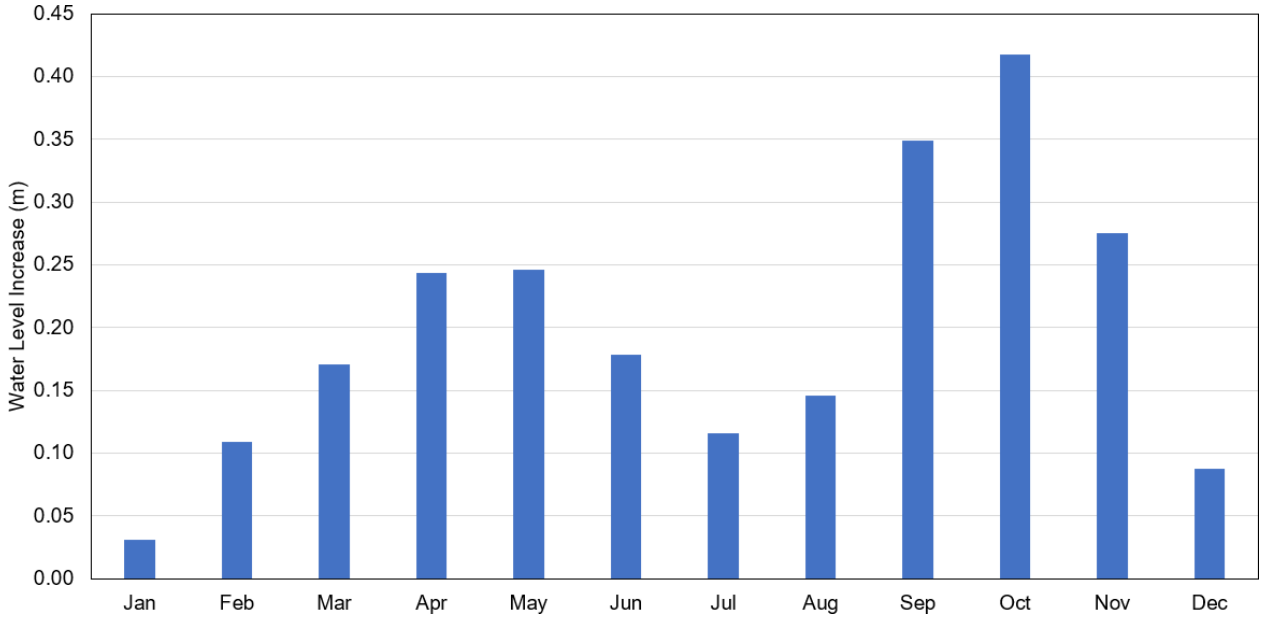

Figure 2.26: Monthly average variation of water levels at the offshore of project site resulting from seasonal wind variations

2.2.4 River Inflows

The Corpus Christi Bay receives freshwater from the Nueces River and Oso Creek through Nueces Bay and Oso Bay, respectively. Based on the measured discharge at Mathis in Nueces River, the average discharge in Nueces River is about 19 m^3/s, ranging from 1 m^3/s to 700 m^3/s. The monthly distribution of river discharge is shown in Figure 2.27 and indicates that the river has large high flow from May to November and low flow from December to April. Figure 2.28 provides annually averaged discharge in Nueces River, which shows significantly large variation of interannual river flow, ranging from 1 m^3/s in the dry years to 80 m^3/s in the wet years.

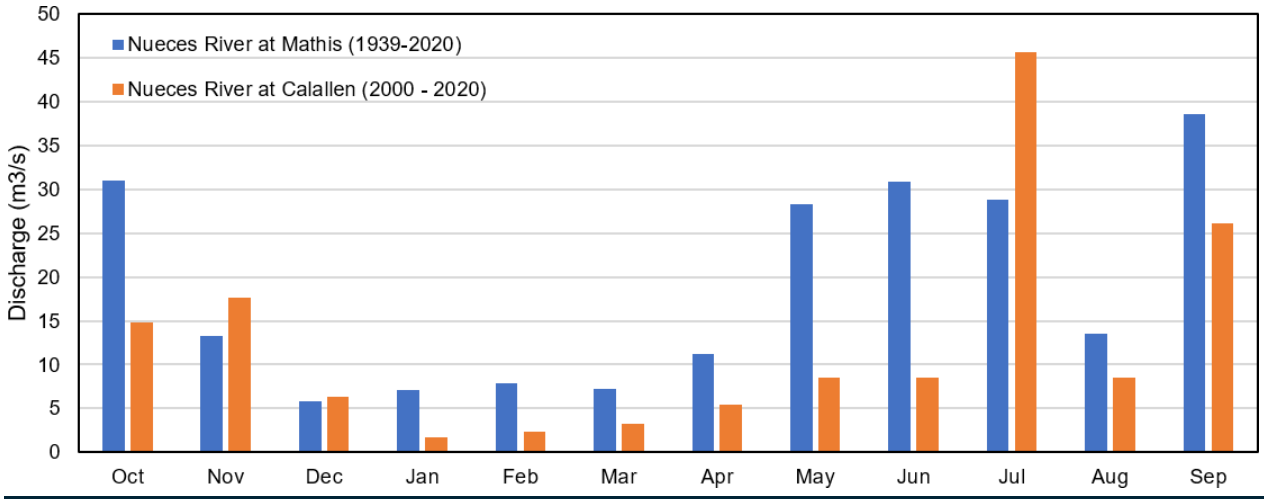

Figure 2.27: Seasonal Variation of River Discharge in Nueces River

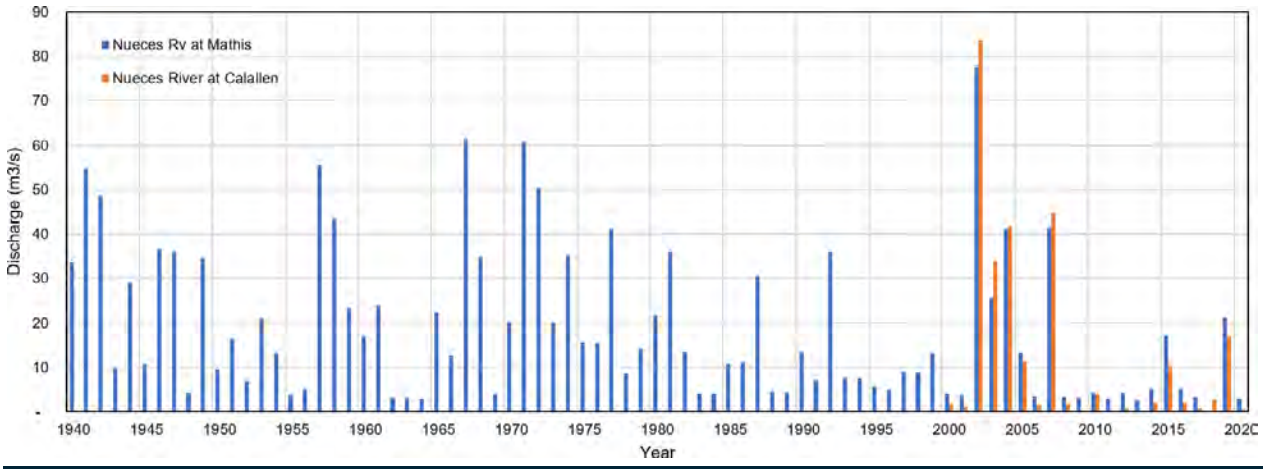

Figure 2.28: Annual average discharge in Nueces River

2.2.5 Salinity Sources

Understanding the salinity sources is essential for model calibration. There are many physical processes which drive salinity conditions in Corpus Christi Bay and Nueces Bay. The saltwater carried by tidal currents from the GOM is the origin of salinity in the bays. Figure 2.29 shows the measured salinity at the monitoring stations in the study area. The salinity in the intracoastal waterway (NPBSI and MANER4) and in Corpus Christi Bay (INPT) are the same level as the salinity in the GOM (TABS-D). Evaporation in dry season becomes important to drive salinity in shallow water areas to higher levels and sometimes even higher than in the GOM. The freshwater from the rivers and rainfalls results in significant decline of salinity in Nueces Bay (SALT01 and SALT03) due to dilution. When the river flow is large, the freshwater impact on salinity extends to Corpus Christi Bay through hydrodynamic advection. Stratification (i.e., higher salinity at the bottom than on the water surface) in the north part of Corpus Christi Bay was observed after a large river flow event in Nueces River (Islam et al, 2010). During extensive dry seasons, salinity in Nueces Bay and Baffin Bay becomes high and even exceeds the salinity level in Corpus Christi Bay and in the GOM (Ward & Armstrong, 1997). Carried by flood tide currents, this high saltwater can be transported to Nueces Delta resulting in the accumulation of salt in the delta marsh. The accumulation of salt in the marsh flat of Nueces River Delta was observed from satellite imagery (see Figure 2.30).

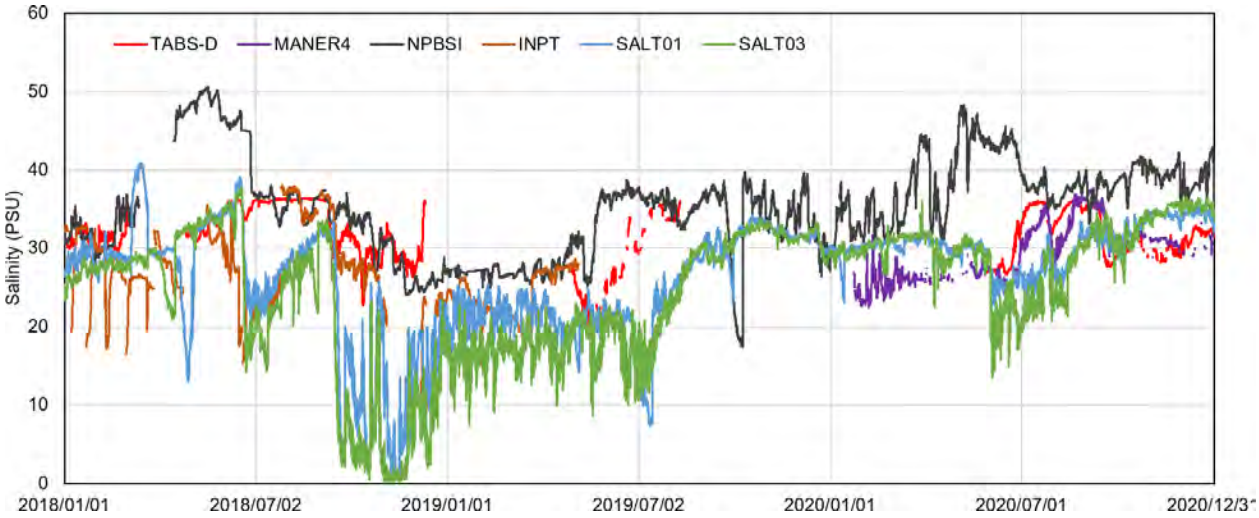

Figure 2.29: Measured salinity at the stations in the study area.

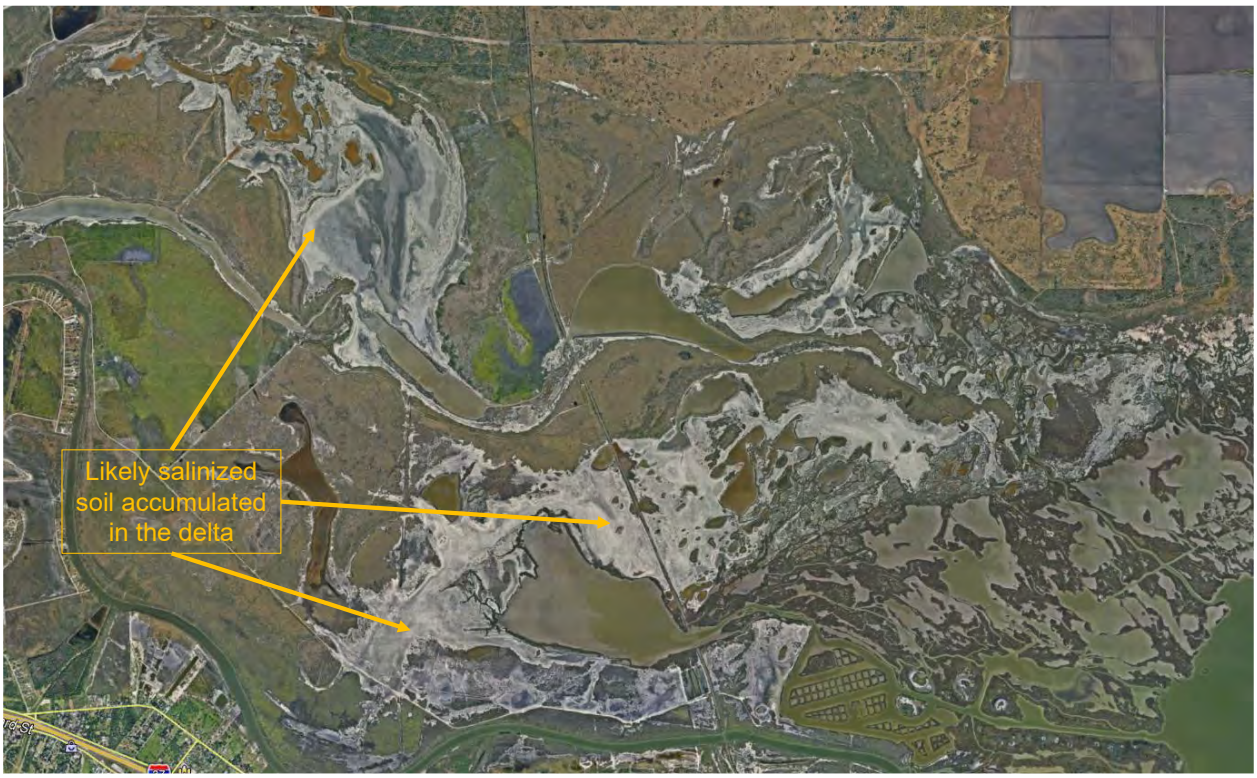

Figure 2.30: Salinized soil in Nueces Delta identified from satellite imagery

2.3 Data Gaps and Recommendations

Through the data collection and analysis, the following major data, which are required for model development, are missing:

- Bathymetry in Nueces Bay: There is no reliable bathymetry data in Nueces Bay. The Lidar Based bathymetry collected from the NOAA data source indicates a constant bed elevation of -0.1 m NAVD88, which is unlikely. The bathymetry in Nueces Bay is an important data set for the calculation of the tidal prism in Nueces Bay, and therefore, it could impact on the water exchange between Nueces Bay and Corpus Christi Bay significantly;
- Salinity data gap at Rockport: There is large temporal data gap of salinity at Rockport, which is used to develop the northeast open boundary condition for the open boundaries at the northeast of the intracoastal waterway;
- Storage of salt in Nueces River Delta: There is significant salt stored in the marsh flats of Nueces Bay. These salt deposits can be dissolved by rainfall and the flood flow of Nueces River and be carried to Nueces Bay by flood flows on the Nueces River.

3. Hydrodynamic and Salinity Model Development

3.1 Review of Previous Models

There are a few numerical models applied to Corpus Christi Bay areas to have been developed to simulate hydrodynamics and salinity in the Corpus Christi Bay area (Dawson & Phthina, 2001, Zhang, 2008 and 2010, Dawson *et al.*, 2011, Schoenbaechler *et al.*, 2011, Matsumoto *et al.*, 2001). Dawson and Pothina (2001) applied a three-dimensional (3D) model using finite element method, QUODDY4, to this study area to simulate hydrodynamics, temperature, and salinity. The report did not show the calibration result due to the model instability issues. In 2011, they applied another model, the University of Texas Bay and Estuary 3D (UTBEST3D), to the same areas to simulate hydrodynamics, temperature, and salinity. The model included tide, wind, and river inflow. Precipitation and evaporation were also considered. The model was able to reproduce water levels, though only by shifting the datum of measured data. Based on our data analysis, the model may not include (or may not reproduce) the net tidal currents from Aransas Bay to Corpus Christi Bay as described in Section 2.2.1. Our model tests indicate that including the net tidal currents significantly improves the water level calibration at USS Lexington.

Zhang (2008, 2010) applied OHSU's SELFE model to this area. The SELFE model is an open-source community-supported code using a semi-implicit finite-element/volume Eulerian-Lagrangian algorithm to solve the Navier-Stokes equations using a triangle mesh. The model simulated hydrodynamics, temperature and salinity and was calibrated against Year 2000 data.

Schoenbaechler *et al.* (2011) applied the TxBLEND model to Nueces Bay for support of freshwater resource management. The TxBLEND model is a two-dimensional (2D) depth-averaged model designed to simulate water circulation and salinity conditions in estuaries, which is an expanded version of the BLEND model specific to TWDB's needs (TWDB 1999). The model used a finite-element method with a triangular mesh. The model considered tide, wind, river inflow, precipitation, and evaporation and included the runoff from the ungagged catchments which directly drains to the Corpus Christi Bay. The model was extensively calibrated against measured data collected in 1994, 1995, 1999, through 2004. Similar to UTBEST3D model, the model underpredicted the mean water level at USS Lexington, which is likely associated with missing the net tidal currents from Aransas Bay to Corpus Christi Bay.

Matsumoto et al. (2001) applied the TxBLEND-3D model to assess the impacts of the Corpus Christi Ship Channel Improvement Project. The model was well calibrated against the measured current and salinity. The model may underestimate the stratification of salinity in Corpus Christi Bay. AECOM (2019) used the Delft3D model to assess the environmental impact of the FWP for the EIS study. Since the model was run in 2D mode, the model could not simulate the stratification in the bay.

All the above-mentioned models used the water level to control the offshore boundary conditions. These models may not appropriately simulate the long-shore currents in the GOM. The long-shore currents are necessary to estimate the cross-channel current speed in the outer channel, which is important information for navigation. The measured data at TABS-D shows that the long-shore current speed could be as high as 1 m/s.

3.2 Model Development

The model suite, MIKE21 and MIKE3, developed by Danish Hydraulic Institute (DHI), was selected to simulate hydrodynamics and salinity for this project. The main objective of this model study is to evaluate the impact of Corpus Christi Channel Deepening Project on the environment. The flexible mesh version of

DHI model was used to appropriately describe the complex shorelines and to refine the grid in the area of interest, e.g., along the navigation channel for this project. The model utilizes the finite volume method and can be used to simulate a range of hydraulic conditions, including tidal exchange, river flow and currents, wind driven current, density driven flow, and so on. The model is well known in the water resources and coastal community and has been extensively used by various government agencies, academia, and consultants to support surface water projects around the world. It is also a FEMA approved hydraulic and coastal model.

MIKE21 is a two-dimensional (2D) depth-averaged model, which has less computational demand. MIKE3 model is a three-dimensional (3D) model, which can be used to simulate the variation in water column, for example, stratification, but has much greater computational demand. To calibrate the model efficiently to meet with project schedule, MIKE21 was firstly used to perform the initial model calibration, and then MIKE3 was then used for the final model calibration and validation.

3.2.1 Model Domain

The model domain was selected to be centered on the project site (i.e., Aransas Pass) and includes the water bodies, which may be potentially impacted by the proposed project. It includes Corpus Christi Bay and its connected subtropical bays: Nueces Bay, Oso Bay, Redfish Bay, Aransas Bay, Copano Bay, and Baffin Bay. From Aransas Pass, the model domain extends to offshore about 50 km into the Gulf of Mexico to the -50 m NAVD88 contour, about 50 km north to Interstate Highway 37 including Nueces River Delta, and about 100 km along the GIWW. The two narrow connecting channels, Aransas Pass and Packery Channel, were included to make the connection between the bays and the GOM. Figure 3.1 shows the selected model domain.

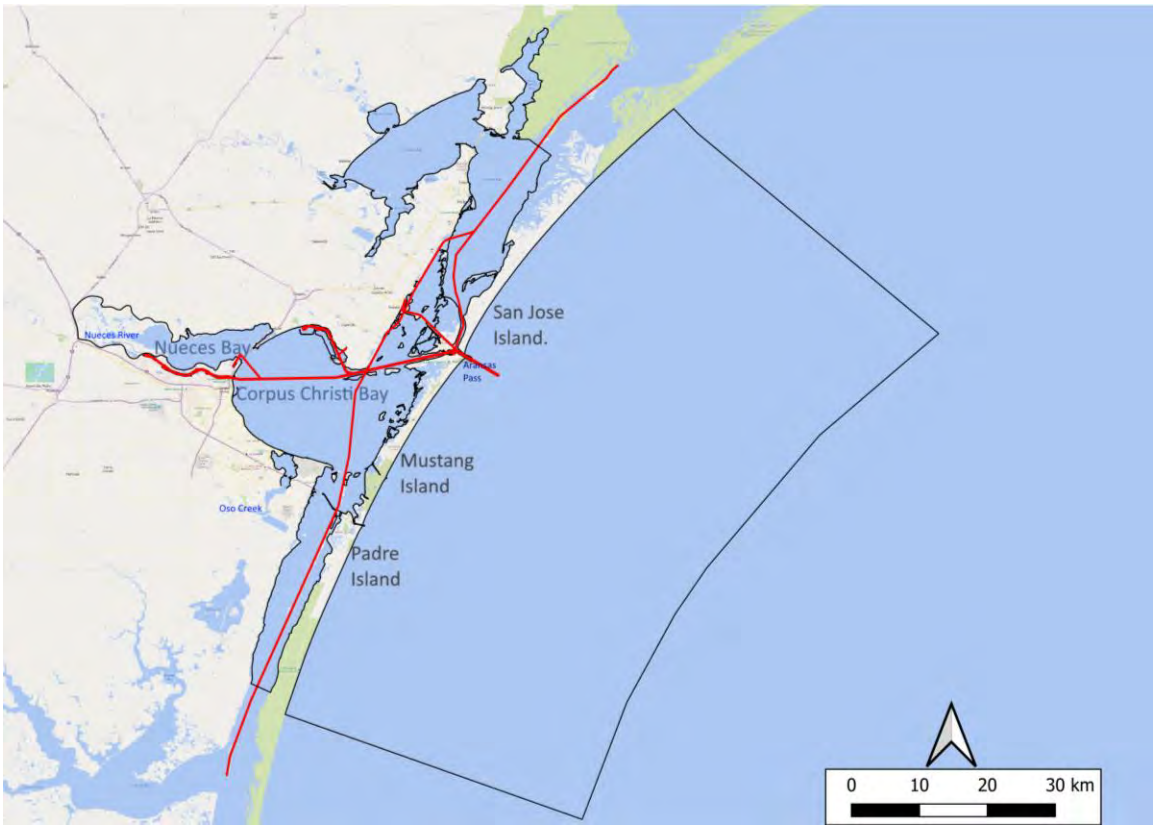

Figure 3.1: Model domain selected for this model assessment. The red lines show the existing navigation channels in the model domain.

3.2.2 Grid Generation

An unstructured mesh with the mixture of triangles and quadrilaterals was generated in the model domain. Mesh generation is one of the most important parts of the modeling strategy, since it defines the level of detail required while balancing computation time. The grid resolution varies depending on the hydrodynamic complexity and/or significance of an area. The mesh around the project site, along the navigation channels (both existing and proposed), the important narrow waterways, and the structures was significantly refined. Many test runs were performed to check whether there was sufficient grid resolution to simulate the complex flow patterns in the area of interest. The final model grid consists of 42,439 nodes and 80,015 elements (see Figure 3.2). The grid resolution in the navigation channel is about 30 m. The grid resolution in the bay and offshore was significantly reduced to reduce the computation time. The largest grid size is about 2,500 m. Figure 3.3 shows the variation in element resolution around Port Aransas.

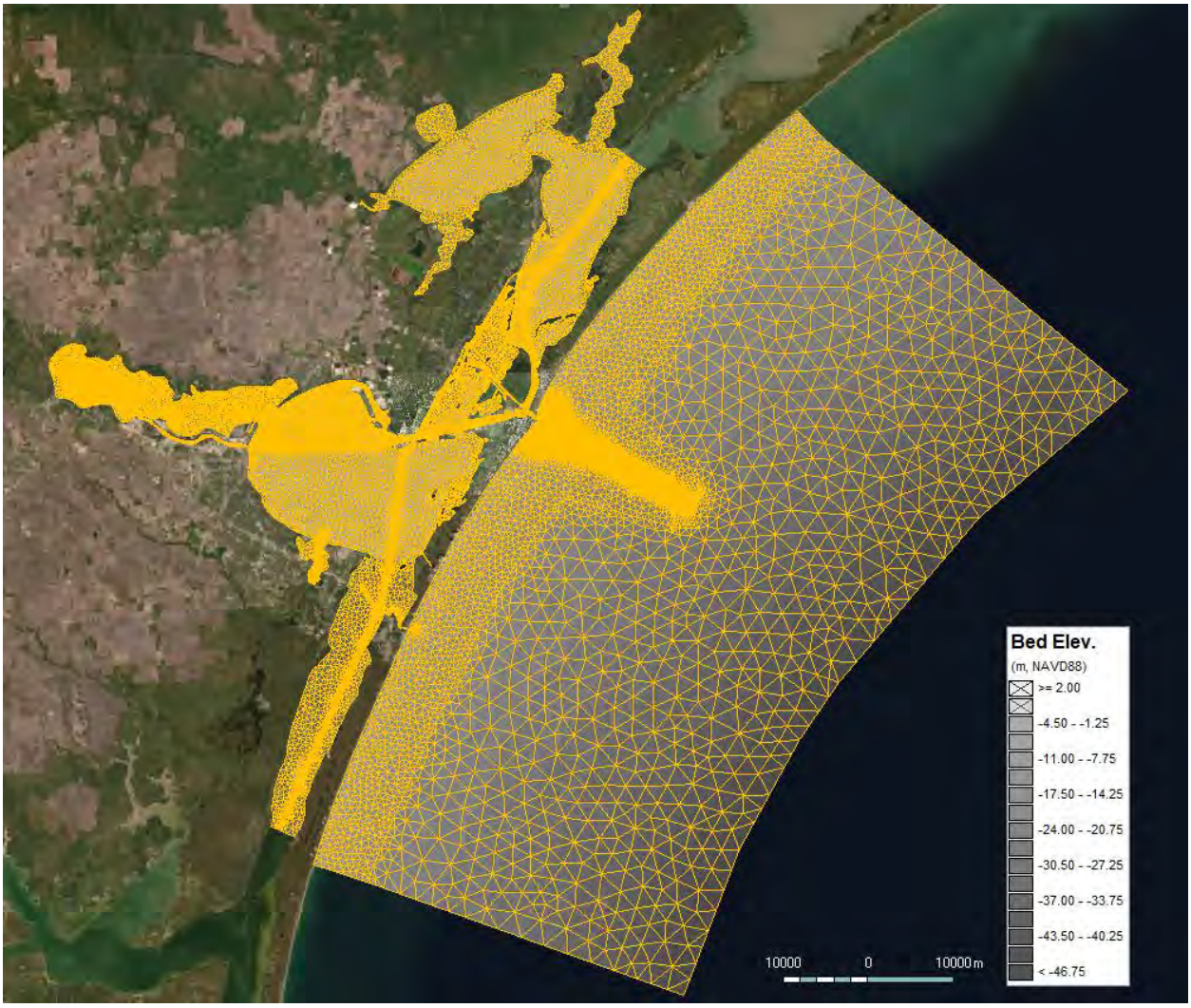

Figure 3.2: Final model mesh generated for this modeling study with mixture of triangles and quadrilaterals

Figure 3.3: Refinement of model mesh along the navigation channels

The bed elevations at the mesh nodes were interpolated from the assembled bathymetry data for the existing condition. Note that the bathymetry in Nueces Bay was modified during the calibration since there was no reliable bathymetry data available, which will be described in the next section. Figure 3.4 shows the interpolated bathymetry in the model domain, and Figure 3.5 shows the details of the bed elevation around Port Aransas.

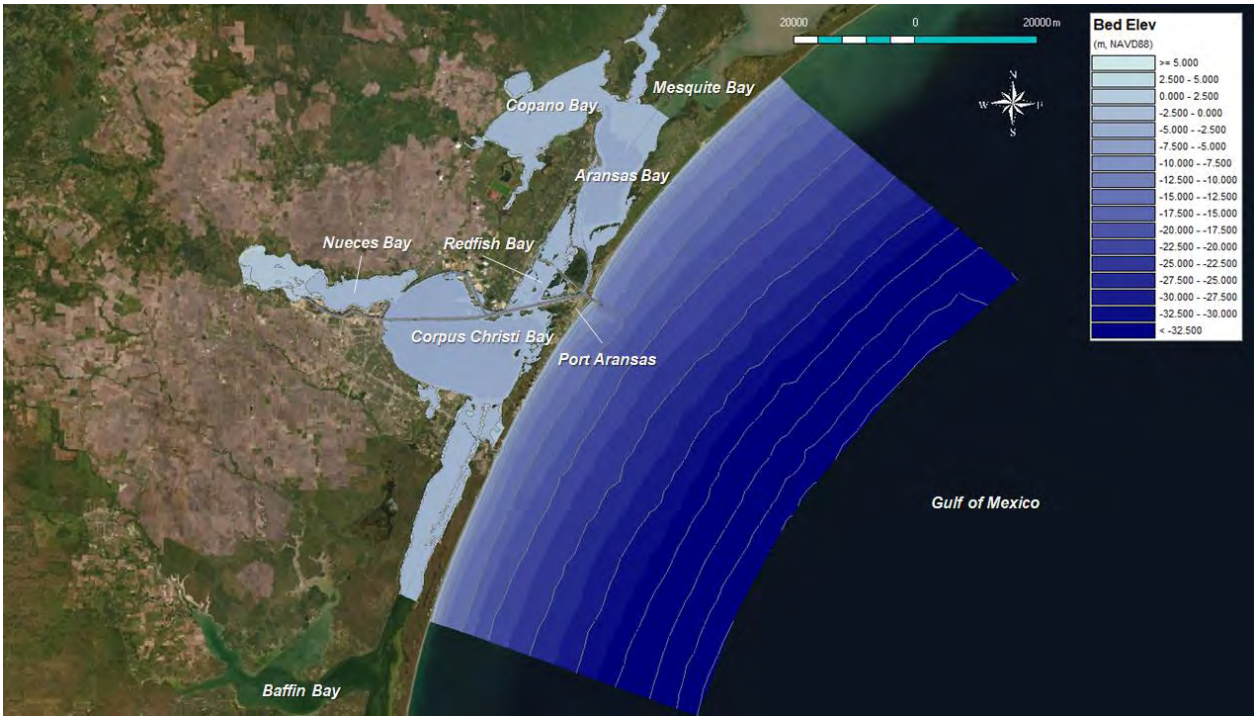

Figure 3.4: MIKE3 model domain and bathymetry in the existing condition

Figure 3.5: MIKE3 model bathymetry near Port Aransas in the existing conditions

3.2.3 Model Setup

The model requires the appropriate setup of initial conditions, open boundary conditions, driving forces, and physical parameters to correctly simulate the anticipated physical processes. Any errors from these inputs will result in inaccuracies in the simulation. Therefore, the measured data were used to develop the inputs to the model as much as possible.

3.2.3.1 Initial Conditions

The initial conditions for hydrodynamic simulation were set up as constant for water level and zero for flow velocity in the model domain. To avoid model instabilities, the start time of model simulation was carefully selected to coincide with slack tide time when the water level in at all open boundaries is at the same elevation to the extent as possible.

The initial conditions for salinity simulation were set up as a constant bay-wide for each individual bay, but varying bay-to-bay. Measured salinity at the simulation start time was used. No stratification in the water column was specified for the initial conditions.

3.2.3.2 Open Boundary Conditions

There are 10 open boundaries in the model domain which require specification of boundary conditions (BC) for model simulation. Table 3.1 lists the required details for the boundary conditions at these open boundaries, including:

- Open Boundary: Open boundary name;
- BC Type: the type of physical variable used to control the open boundary conditions;
- Variation: indicates whether the boundary conditions are varied (or constant) in time, horizontal space, and vertical column;
- Method: indicates the method to develop the boundary condition from the source data;
- Data Sources: indicates the data used to build the boundary condition.

Additional information on developing boundary conditions for certain open boundaries are described below.

Table 3.1: Open boundary conditions for hydrodynamic simulation

Open Boundary	BC Type	Variation	Method	Data Sources
Offshore	Water level	Time series and spatially varied	Extracted from HYCOM model and adjusted with measured water level	HYCOM model output
Offshore NE	Unit width flow flux	Time series and varied on boundary and water column	Extracted from HYCOM model	HYCOM model output
Offshore SW	Unit width flow flux	Time series and varied on boundary and water column	Extracted from HYCOM model	HYCOM model output

Open Boundary	BC Type	Variation	Method	Data Sources
Rockport	Water level	Time series and constant on boundary	Interpolated from measured water levels	Water levels measured at Rockport and Aransas Wildlife Refuge
Baffin Bay	Water level	Time series and constant on boundary	Measured water levels	Water levels measured at Baffin Bay
Oso Creek	Discharge	Time series	Measured discharge and adjusted for ungaged watershed	Discharge measured USGS gage and TrRR output
Nueces River	Discharge	Time series	Measured discharge and adjusted for ungaged watershed	Discharge measured USGS gage and TrRR output
Aransas River	Discharge	Time series	Measured discharge	Discharge measured USGS gage
Mission River	Discharge	Time series	Measured discharge	Discharge measured USGS gage
Copano Creek	Discharge	Time series	Measured discharge	Discharge measured USGS gage

The boundary condition for the offshore open boundary was controlled by water level and was extracted from HYCOM model output. However, the water levels from the HYCOM model are significantly different from the water level measured at Bob Hall Pier. By analyzing the water level difference, it was found that the HYCOM model likely did not include seasonal variation of water levels in the GOM fully as described in Section 2.2.3. Therefore, the following steps were performed to adjust the offshore water levels for boundary conditions:

- Calculate the difference of hourly water levels measured at Bob Hall Pier and predicted by HYCOM model;
- Perform the 25-hour moving average on the water level difference by removing tidal signals;
- Add the smoothed water level difference to the offshore water level predicted by HYCOM.

Discharges from Nueces River and Oso Creek were developed based on the daily discharge measured at the USGS gages. The runoff from the ungagged watershed for these inflows were added by using the predicted runoff from TxRR model. For Nueces River, the return flows from the water usage facilities were also added.

Salinity was defined at all 10 open boundaries for salinity simulation. Table 3.2 shows the setup of the salinity boundary conditions.

Table 3.2: Open boundary conditions for salinity simulation

Open Boundary	BC Type	Variation	Method	Data Sources
Offshore	Salinity	Time series and spatially constant	Gap filled salinity	Measured at TABS-D
Offshore NE	Salinity	Time series and spatially constant	Gap filled salinity	Measured at TABS-D
Offshore SW	Salinity	Time series and spatially constant	Gap filled salinity	Measured at TABS-D
Rockport	Salinity	Time series and spatially constant	Gap filled salinity	Measured at MANER4
Baffin Bay	Salinity	Time series and spatially constant	Gap filled salinity	Measured at NPBSI
Oso Creek	Salinity	Constant	Fresh water	0 PSU
Nueces River	Salinity	Time series and spatially constant	Measured salinity with adjustment	Measured at SALT05, SALT01, SALT03
Aransas River	Salinity	Constant	Fresh water	0 PSU
Mission River	Salinity	Constant	Fresh water	0 PSU
Copano Creek	Salinity	Constant	Fresh water	0 PSU

There were outliers and large data gaps in the measured salinity data. All measured salinity data was first processed by filtering the outliers. The data gaps were filled by using neighboring gage data if available. The filled data gaps in salinity were revised during the model calibration.

The salinity for Nueces River inflow was developed based on the measured salinity at SALT05. However, the model tests indicated that the conveyance capacity of Nueces River downstream the USGS gage at Calallen is small. There are several small branches connected to the Nueces River, which diverts the freshwater to the ponds and shallow marshes in the delta, mixes with high salt water in the ponds and shallow marshes, and empties to Nueces Bay. Additionally, flooding over the Nueces Delta occurs during large river flow events. The flooding river freshwater associated with river floods could dissolve the salt soil accumulated in the delta marsh and eventually drain to Nueces Bay with high salinity. Many model tests were carried out during the model calibration. It was concluded that good model calibration could not be achieved if the measured salinity at SALT05 was used to control the salinity from Nueces River since MIKE3 model has no capability to account for above-mentioned physical processes. Therefore, the adjustment of salinity boundary conditions for Nueces River was made by using the information provided from the measured salinity at SALT01 and SALT03.

3.2.3.3 Driving Forces

Wind

Wind is one of the important forces driving the currents in the bays which is considered in this study. By analyzing the wind data measured at the meteorological stations in the model domain, wind direction is mostly constant in space under the normal weather conditions, except for the spatial variability during tropical storms. Since this model study mainly focuses on normal meteorological conditions, time-varying and spatially constant wind was implemented in the model. The hourly wind data measured at Bob Hall Pier was the most

representative of average wind conditions in the open water of the study area and therefore was used for this modeling study.

Precipitation

Precipitation (or rainfall) was considered in the model setup, because it can be a freshwater source for the salinity simulation, although it may not have significant impact on hydrodynamics. Based on the comparison of daily precipitation data (which are available at many stations), the precipitation can be very localized and significantly varied in space. The precipitation increases from inland moving offshore, e.g., from Nueces River catchment to Port Aransas and Rockport, due to the lake affect. However, there was insufficient precipitation data available to develop a spatially varied precipitation dataset. Therefore, time-varying but spatially constant precipitation was used in the model, developed from the hourly precipitation data measured at Port Aransas. A scale factor was introduced to account for spatial variation, which was considered to be a calibration parameter.

Evaporation

Evaporation can cause increases in salinity, particularly in shallow waters. The impact may be greater during dry seasons. Therefore, the evaporation was considered in the model. Initially, a monthly average evaporation rate estimated by NOAA was used. With this data, the model did not produce the good calibration against the measured data. Therefore, the daily evaporation measured at the NOAA Station at Mathis (USC00415661) was used for the model. Since the gage is located inland, the evaporation over open waters could be greater than in the inland. Therefore, a scale factor was introduced as a calibration parameter.

Runoff

There are five catchments which directly drain to Corpus Christi Bay and Nueces Bay as shown in Figure 2.8. The daily runoffs from these catchments were provided from TxRR model output or estimated from the daily precipitation. For each catchment, the runoff was evenly divided into a few point sources that were implemented in the model. The locations of point sources were selected visually at the locations of small ditches using satellite imagery. The runoff is considered as freshwater (no salinity).

3.2.3.4 Physical and Numerical Parameters

There are several physical and numerical parameters which were determined through the model calibration. Table 3.3 lists the primary physical and numerical parameters and their final values determined through iterations of model runs during the model calibration.

Table 3.3: Primary physical and numerical parameters determined through the mode calibration

Physical Parameters	Variation	Value or Range	Notes
Roughness	Varied spatially	0.015 ~ 0.023	Determined from hydrodynamic model calibration
Wind Drag Coefficient	Constant in space and varied with wind speed	0.0013 (U_{10} <= 7 m/s) 0.0024 (U_{10} >= 25 m/s)	Determined from hydrodynamic model calibration
Horizontal eddy viscosity	Varied spatially	0.28 for Smagorinsky coefficient	Calculated by using Smagorinsky formulae
Vertical eddy viscosity	Varied spatially	Calculated from model	Using two-equation closure $\kappa - \varepsilon$ model
Horizontal diffusivity	Constant in space	10	Determined from salinity model calibration
Vertical diffusivity	Varied spatially	1 (scale factor)	Scale to vertical eddy viscosity

Bed roughness is one of the most important physical parameters for model calibration. Many sensitivity tests with roughness were performed to check response of surface elevation and current velocity to roughness variations. The final map of Manning's M values, ranging from 43 to 67, which corresponds to the Manning's n roughness from 0.023 to 0.015, as shown in Figure 3.6.

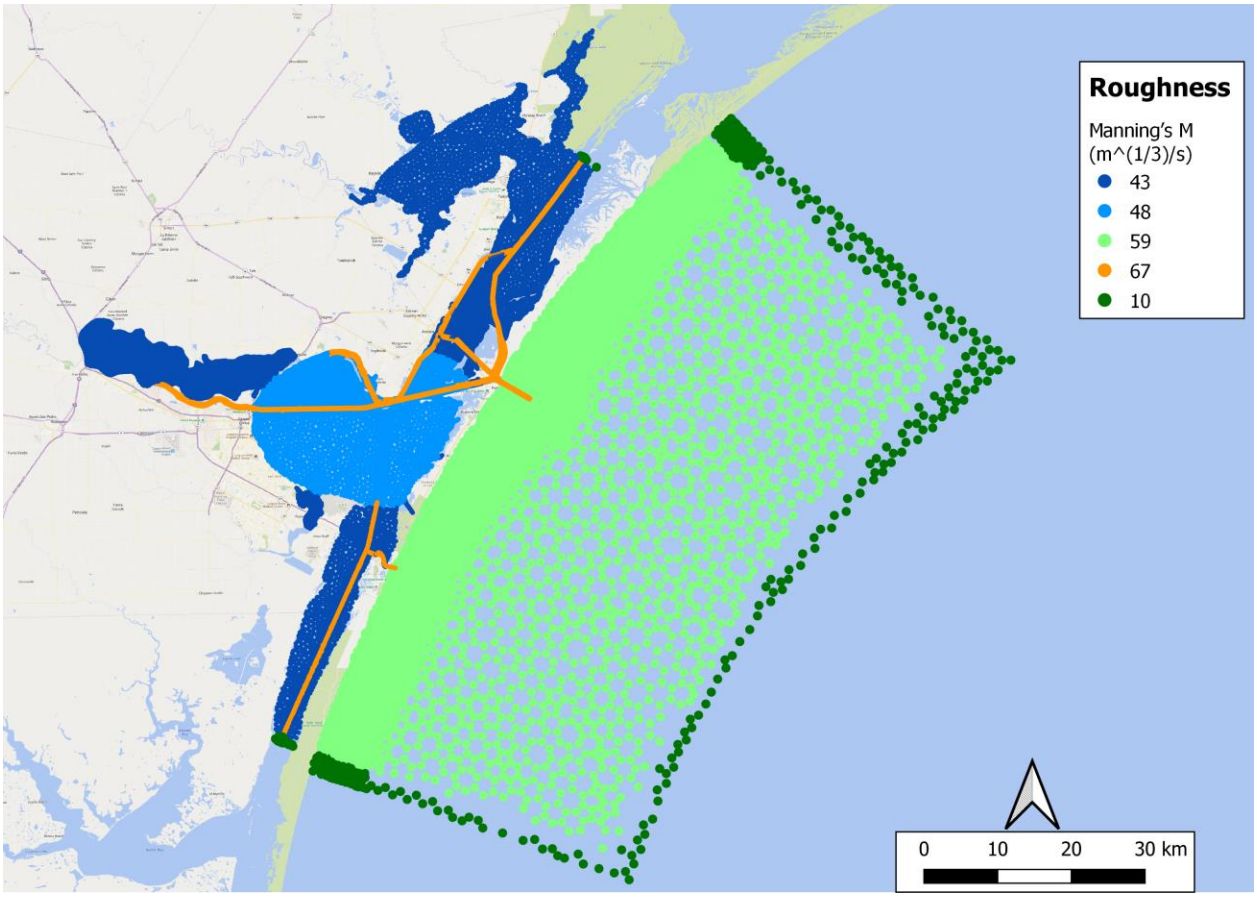

Figure 3.6: Bed roughness

3.3 Model Calibration and Validation

3.3.1 Simulation Periods

Three simulation periods with three-month duration each were selected for model calibration and validation based on the conditions of river inflows, wind, and salinity mixing in the Corpus Christi Bay. The three-month duration is sufficiently long to cover the full variation of tides. To understand the representative dynamics in the selected simulation periods, statistical analysis of the measured discharge and wind data was carried out. Figure 3.7 shows the monthly average discharge measured in Nueces River and their corresponding cumulative frequency, based on daily discharge measured at Nueces River, Calallen (USGS gage 08211500) in the period from October 1, 1997, to September 30, 2020. Figure 3.8 shows the monthly average wind speed and monthly maximum wind speed, based on the hourly wind data measured at Bob Hall Pier in the period from 2018 to 2020. Table 3.4 shows the three selected periods and the representative river flow, wind conditions, and physical processes.

Table 3.4: Selected simulation periods for model calibration and validation

Simulation Period	Start Date	Duration	Conditions
Period 1	June 1, 2018	90 days	• Normal river flow • Average wind • Salinity recovery from a rainfall event • Some salinity stratifications
Period 2	September 1, 2018	90 days	• Above-normal river flow (the 95th Percentile) • Average and below average wind • Salinity dilution with large river flow • Strong salinity stratification
Period 3	July 1, 2020	90 days	• Normal river flow • Above-normal wind with hurricanes • Well mixed salinity mixing in the bays

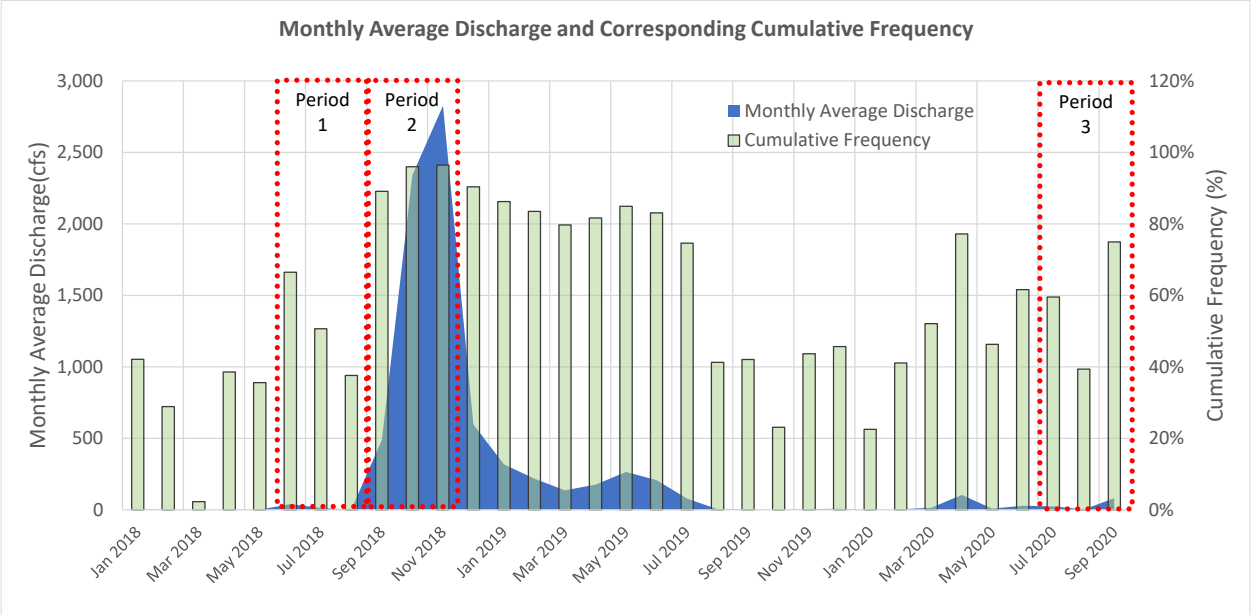

Figure 3.7: Monthly average discharge from Nueces River and the corresponding cumulative frequency of the discharge

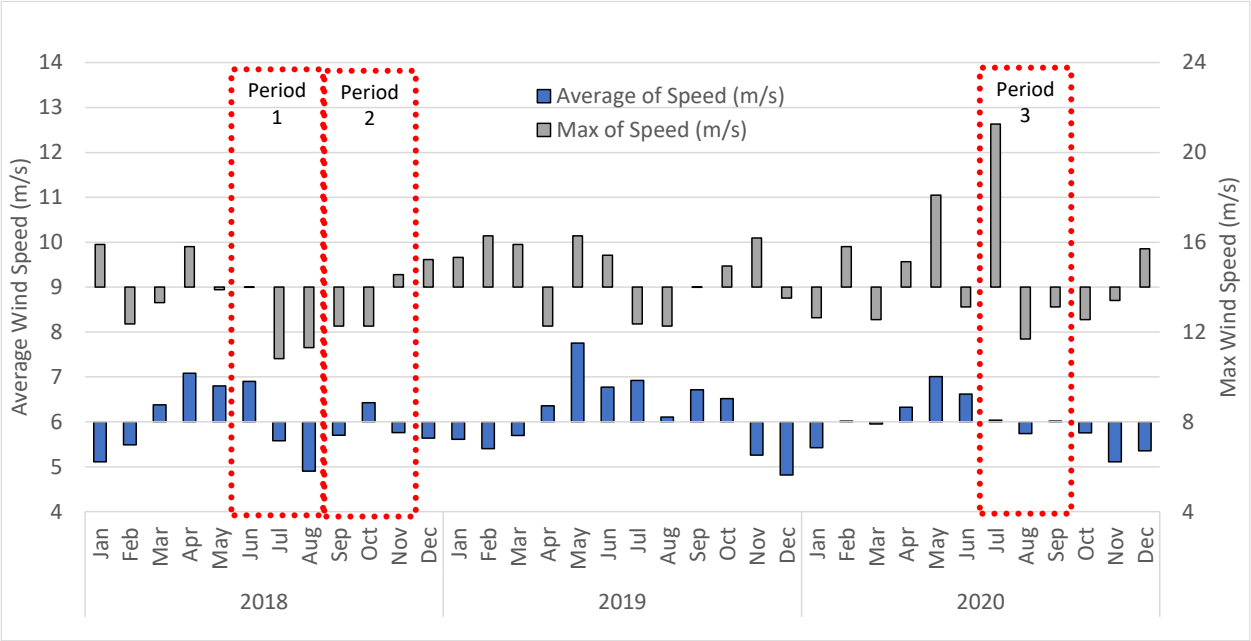

Figure 3.8: Monthly average wind speed and monthly max wind speed in Bob Hall Pier

3.3.2 Model Calibration

Period 2 was selected for model calibration since it covers the most complicated physical processes for hydrodynamics and salinity, including:

- The season features high water level in the bay, impacted by the seasonal variation of water level in the GOM as described in Section 2.2.3 (see Figure 2.25);
- Large freshwater inflow from Nueces River, resulting in significant dilution of salinity in Nueces Bay;
- Normal sustained wind from southeast;
- Strong stratification in Corpus Christi Bay, resulting from large river inflow and week mixing in the normal wind condition.

In the model calibration, the predicted water levels, current speed and direction, and salinity were compared with the measured data to evaluate the proficiency of model prediction. Periods 1 and 3 were used for model validation.

3.3.2.1 Water Levels

Figure 3.9 to Figure 3.11 show the comparisons of model predicted water level with the measured water level at Bob Hall Pier, Port Aransas, and USS Lexington, respectively. The plots showing the comparison of water level at other two other stations are attached in Appendix A. To evaluate the model prediction accuracy, three key performance indicators: bias, mean absolute error (MAE), and root mean square error (RMSE) were calculated as listed in Table 3.5. All three indicators shows that the model predicts water level well. The overall prediction error is less than 7 cm, based on the RMSE.

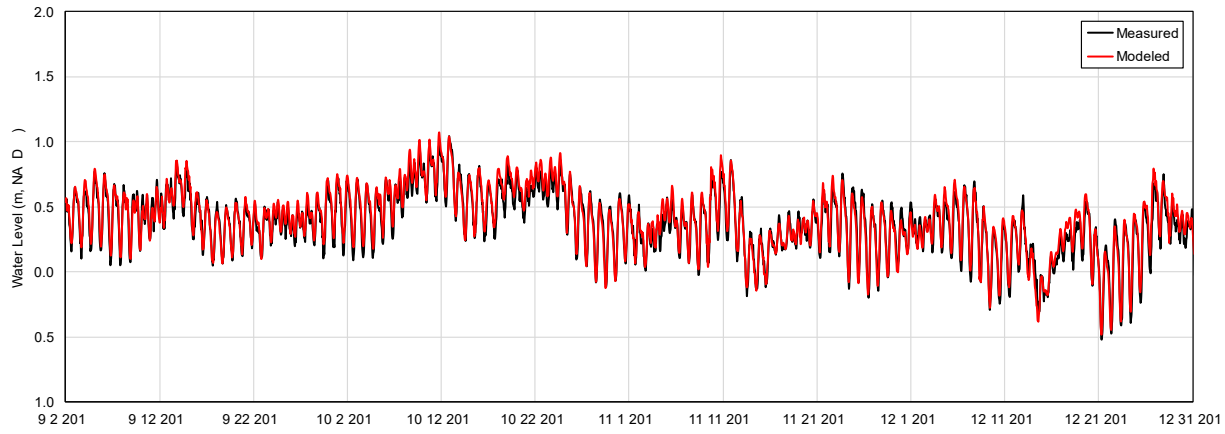

Figure 3.9: Comparison of the model predicted water level (red) to the measured water level (black) at Bob Hall Pier

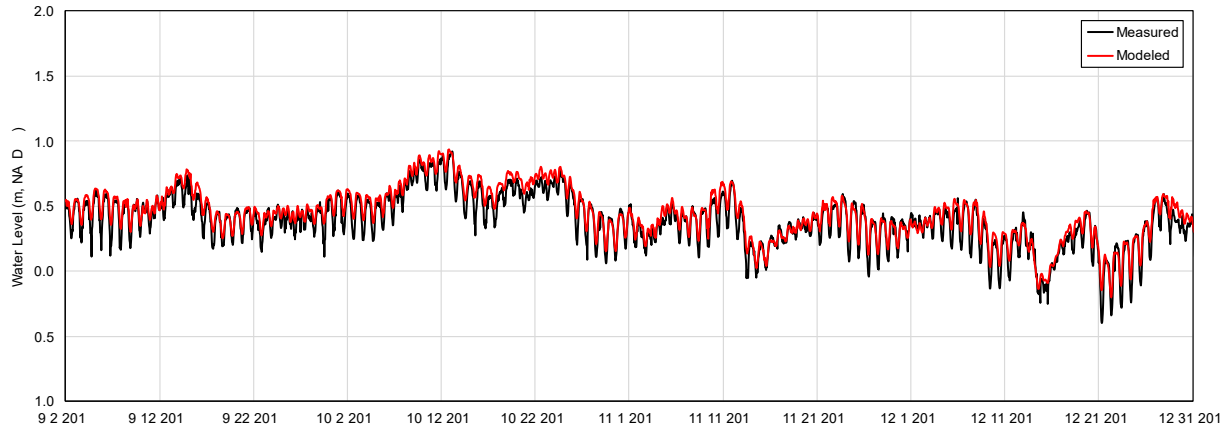

Figure 3.10: Comparison of the model predicted water level (red) to the measured water level (black) at Port Aransas

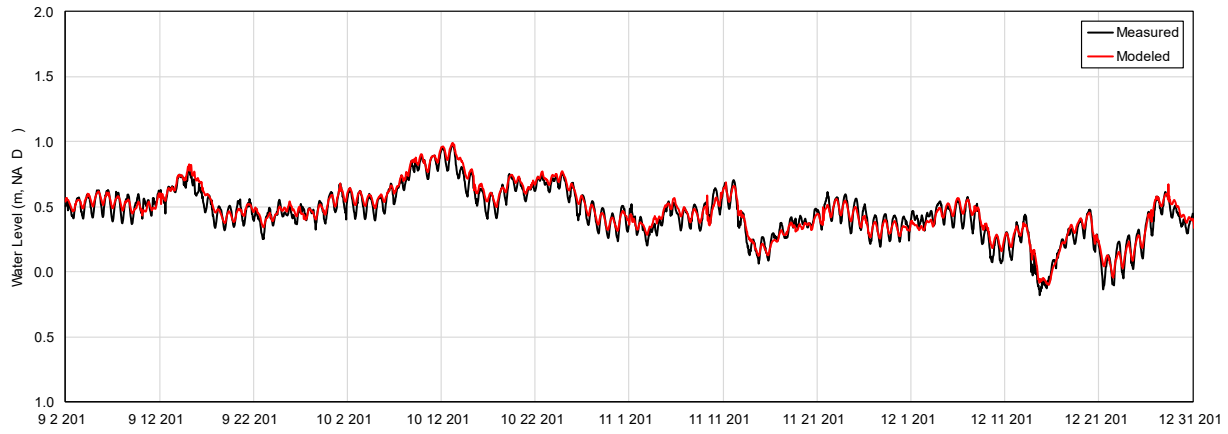

Figure 3.11: Comparison of the model predicted water level (red) to the measured water level (black) at USS Lexington

Table 3.5: Key performance indicators (KPI) of model prediction on water level in Period 2

KPI	Rockport	Port Aransas	USS Lexington	Packery Channel	Bob Hall Pier
BIAS (m)	-0.05	0.05	0.02	0.03	0.02
MAE (m)	0.05	0.06	0.04	0.04	0.05
RMSE (m)	0.05	0.07	0.05	0.06	0.06
R^2	0.98	0.92	0.94	0.92	0.96

Figure 3.12 shows the attenuation of tidal amplitude of tidal constituent O1 in percentage compared with its tidal amplitude at the head of the jetties in the outer channel. O1 is one of the major tidal constituents in the study area. The figure also shows the tidal phase lag in hours relative to its tidal phase at the jetty head, which is consistent with the understandings of tidal propagations as described in Section 2.2.1.

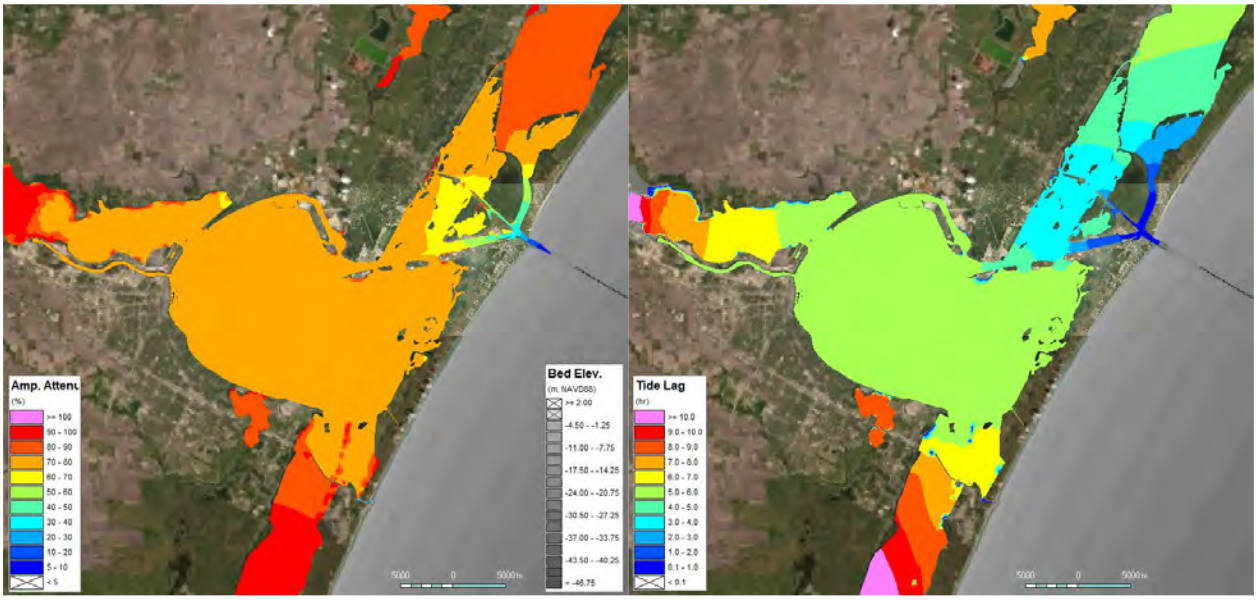

Figure 3.12: Tidal amplitude attenuation in percentage (left) and phase lag in hours (right) of O1 tidal constituent

3.3.2.2 Currents

Figure 3.13 and Figure 3.14 shows the comparison of model predicted flow velocity vectors with the measured data at Port View in Aransas Pass (CC0301) and at the navigation channel of MADS (CC0401). The flow vectors are broken down into U component with positive value pointing to east and V component with positive value pointing to north. Additional plots for velocity comparison are attached in Appendix A. The KPIs for the model prediction on flow velocity are listed in Table 3.6. The KPIs indicate that the model predicts flow vectors reasonably well. The model may underestimate the flow speed in Aransas Pass slightly, which may result from the underestimation of flow from the Redfish Bay due to the large grid resolution and/or due to the HYCOM model underprediction of long-shore currents in the GOM.

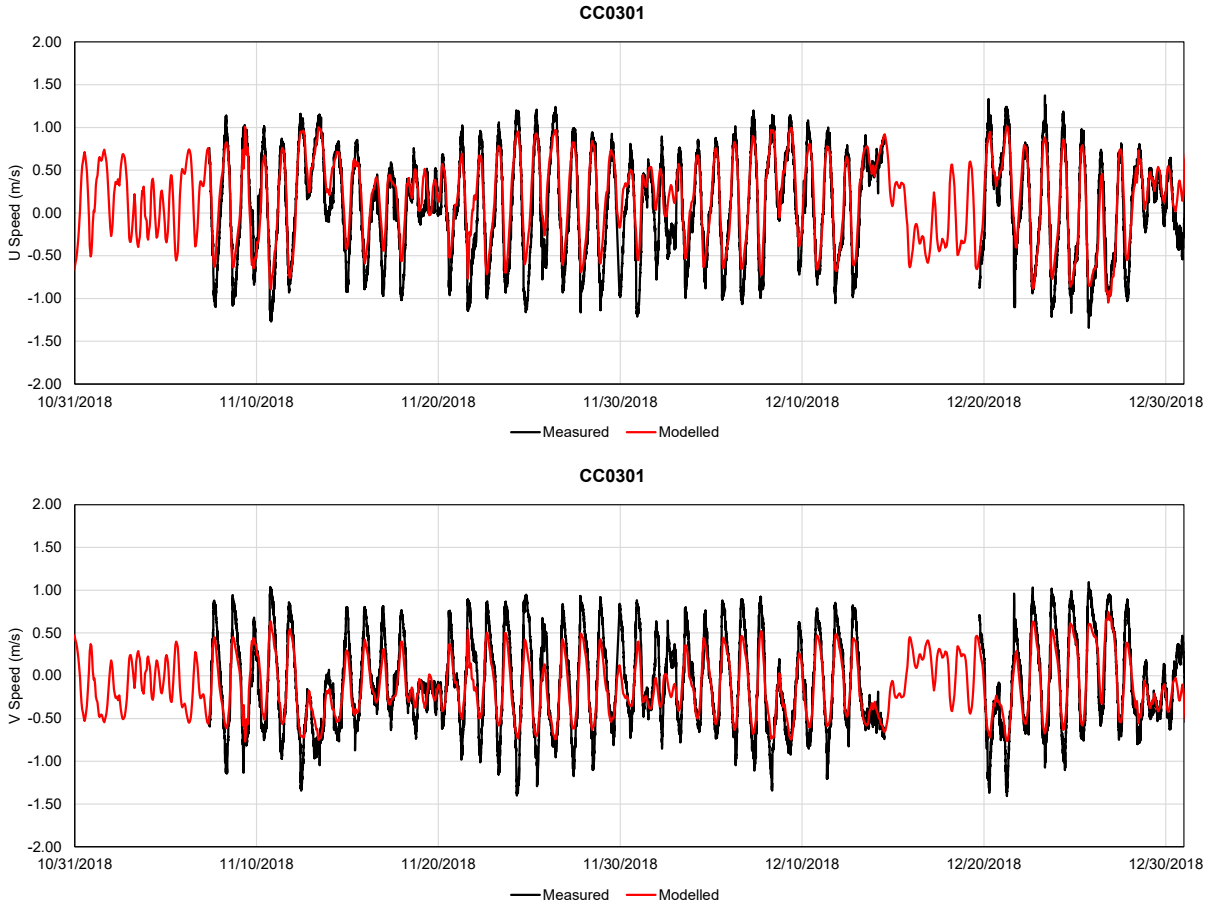

Figure 3.13: Comparison of model predicted flow velocity components, U (east) and V (north), with the measured data at Port View (CC0301)

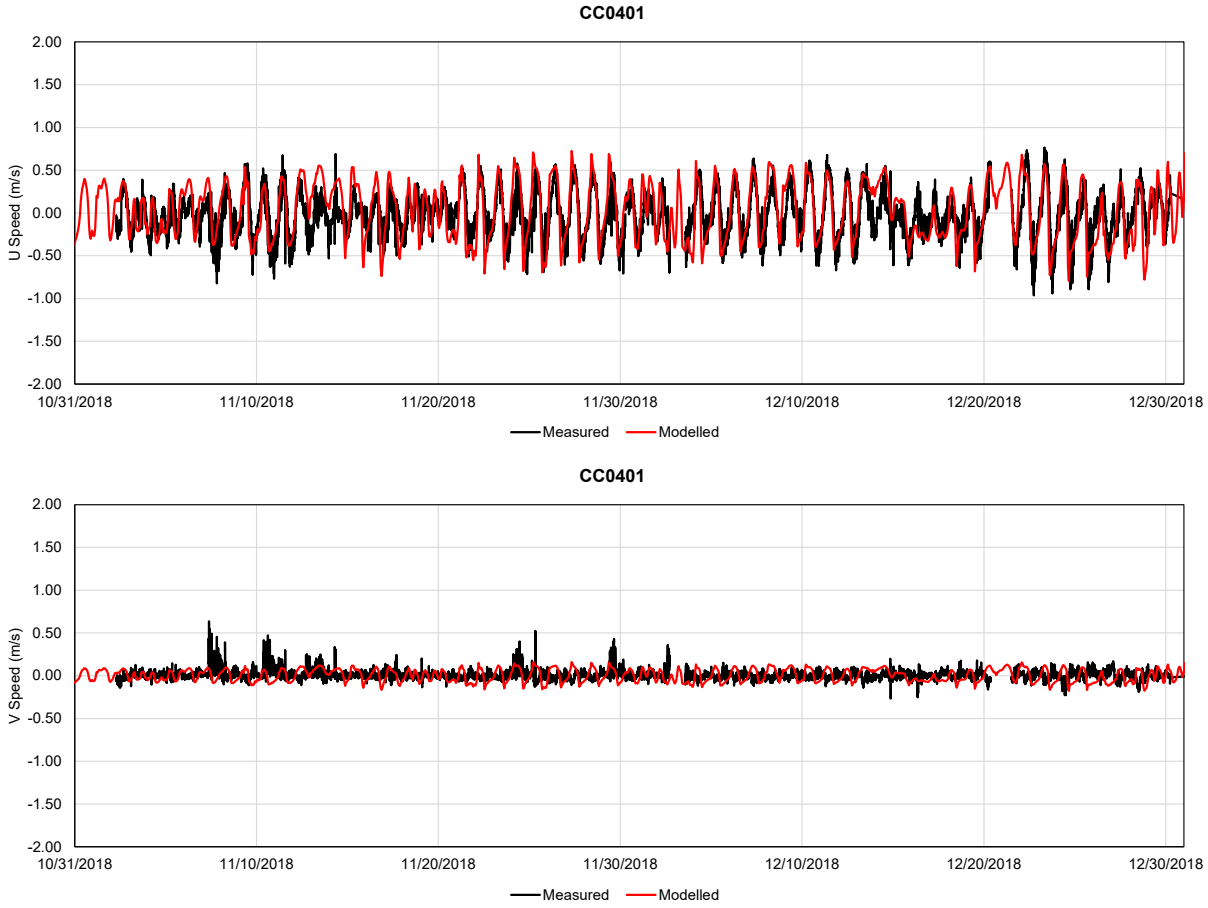

Figure 3.14: Comparison of model predicted flow velocity components, U (east) and V (north), with the measured data at MADS (CC0401)

Table 3.6: Key performance indicators of model prediction on current speed in Period 2

KPI	TABS-D	CC0101	CC0303	CC0401 (MADS)
BIAS (m/s)	0.04	0.08	0.02	0.01
MAE (m/s)	0.17	0.18	0.20	0.14
RMSE (m/s)	0.22	0.23	0.25	0.18
R^2	0.19	0.30	0.87	0.46

Figure 3.15 and Figure 3.16 show the flow vectors on water surface (black) around the inner basin with 3D flow vectors (red) in the selected locations during a flood tide and an ebb tide, respectively. During the flood tide, more water flows to Corpus Christi Bay, which likely results from the constant difference of water level between Rockport and Packery Channel (see Section 2.2.1). During ebb tide, the 3D flow structure is found beyond the jetties in the outer channel. The flow direction near the seabed is different from the flow direction on the water

surface, which likely results from the interaction of the strong flow from the Pass and the long-shore currents in the GOM.

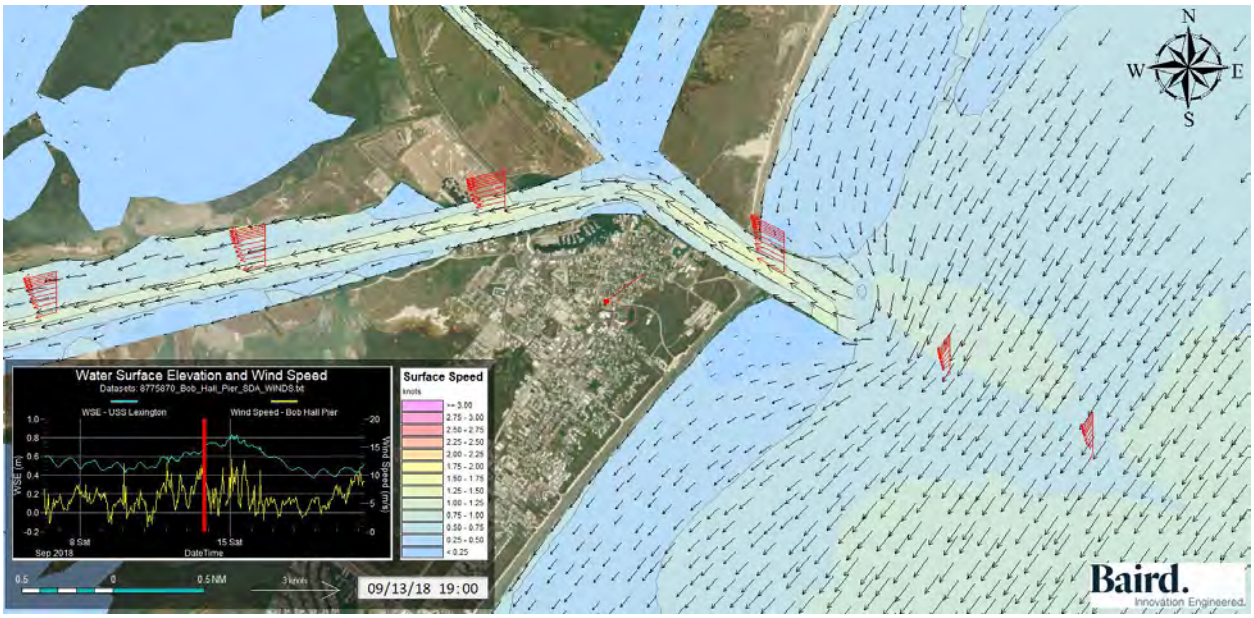

Figure 3.15: Flow patterns on water surface around the inner basin during a flood tide. The red stacked vectors are the flow vectors in water column predicted by the model. The red barb shows the wind speed and direction (from) measured at Bob Hall Pier

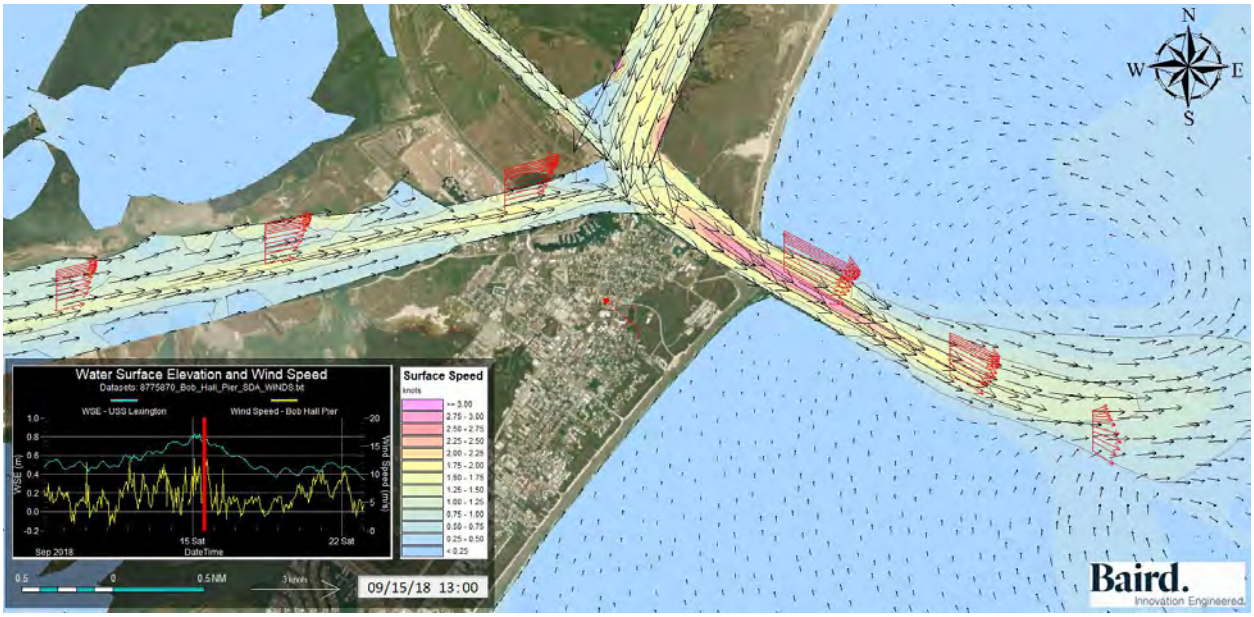

Figure 3.16: Flow patterns on water surface around the inner basin during an ebb tide. The red stacked vectors are the flow vectors in water column predicted by the model. The red barb shows the wind speed and direction (from) measured at Bob Hall Pier

To better understand the net tidal currents, which is an indicator of net salinity and sediment transport direction, the residual of tidal currents was calculated by averaging velocity components, U (easting) and V (northing), over the period from September 8, 2018 14:00 to November 30, 2018 22:00 (from neap tide to neap tide). The flow vectors of net tidal currents over the entire model domain are shown in Figure 3.17. The net current vectors zoomed to Corpus Christi Bay are shown in Figure 3.18. A log scale of flow speed was used for the vector plot to make small net current visible. The large net currents from Aransas Bay heading to Corpus Christi Bay (see Figure 3.19) likely results from the constant difference of water levels between Rockport and Packery Channel, which may be explained by the large inflows from the three rivers to Copano Bay. The net currents in Nueces Bay are always heading to Corpus Christ Bay due to the input of Nueces River. In Corpus Christi Bay, the net current speed is very small (< 4 cm/s). The net currents are heading to the GOM in the navigational channel from MODA to Port Aransas but heading to the Corpus Christi Port in the west section of navigation channel in Corpus Christi Bay.

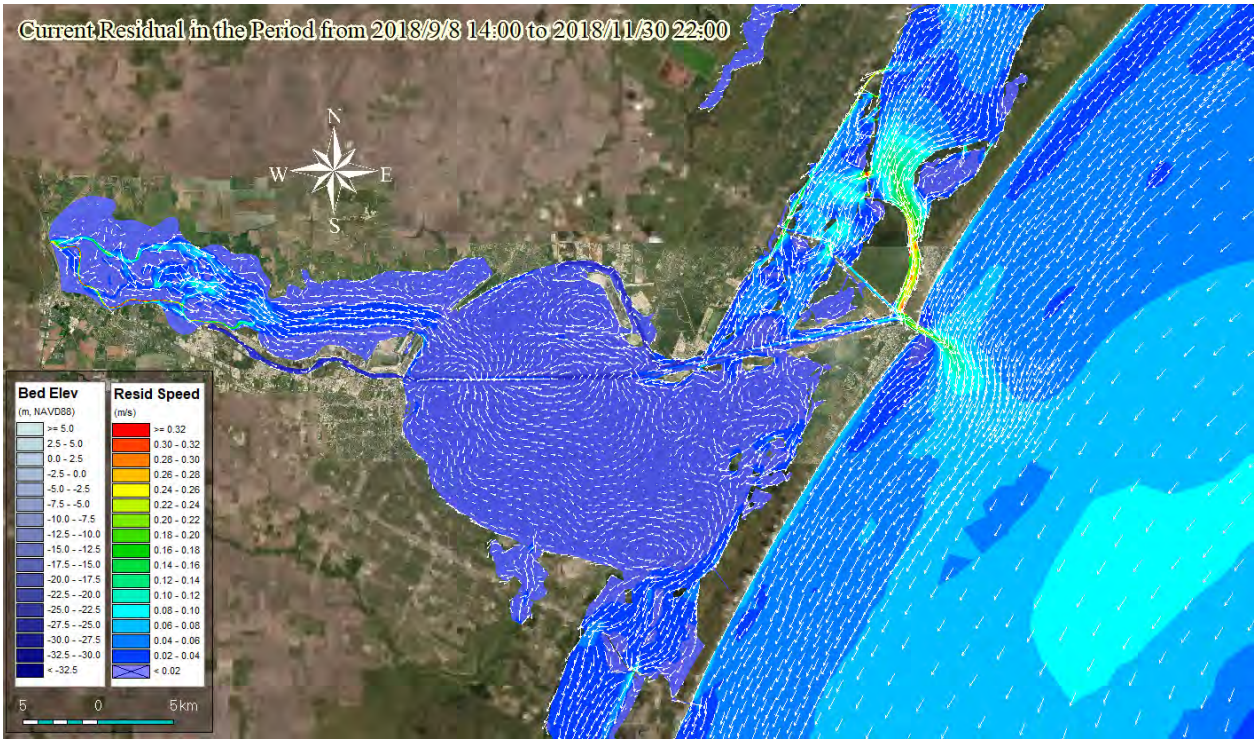

Figure 3.17: Residual currents in the model domain calculated from the depth-averaged velocity in the period from 2018/9/8 14:00 to 2018/11/30 22:00. Vector length is in the log scale of flow speed.

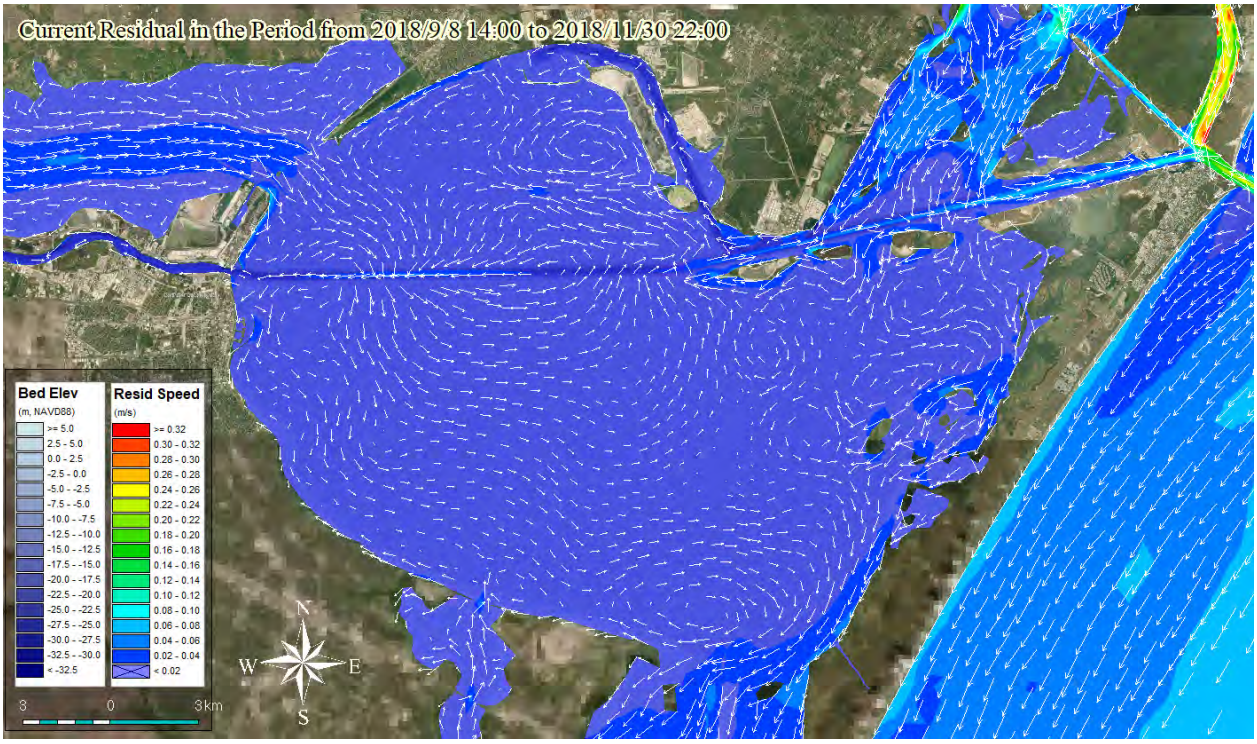

Figure 3.18: Residual currents in Corpus Christi Bay calculated from the depth-averaged velocity in the period from 2018/9/8 14:00 to 2018/11/30 22:00.

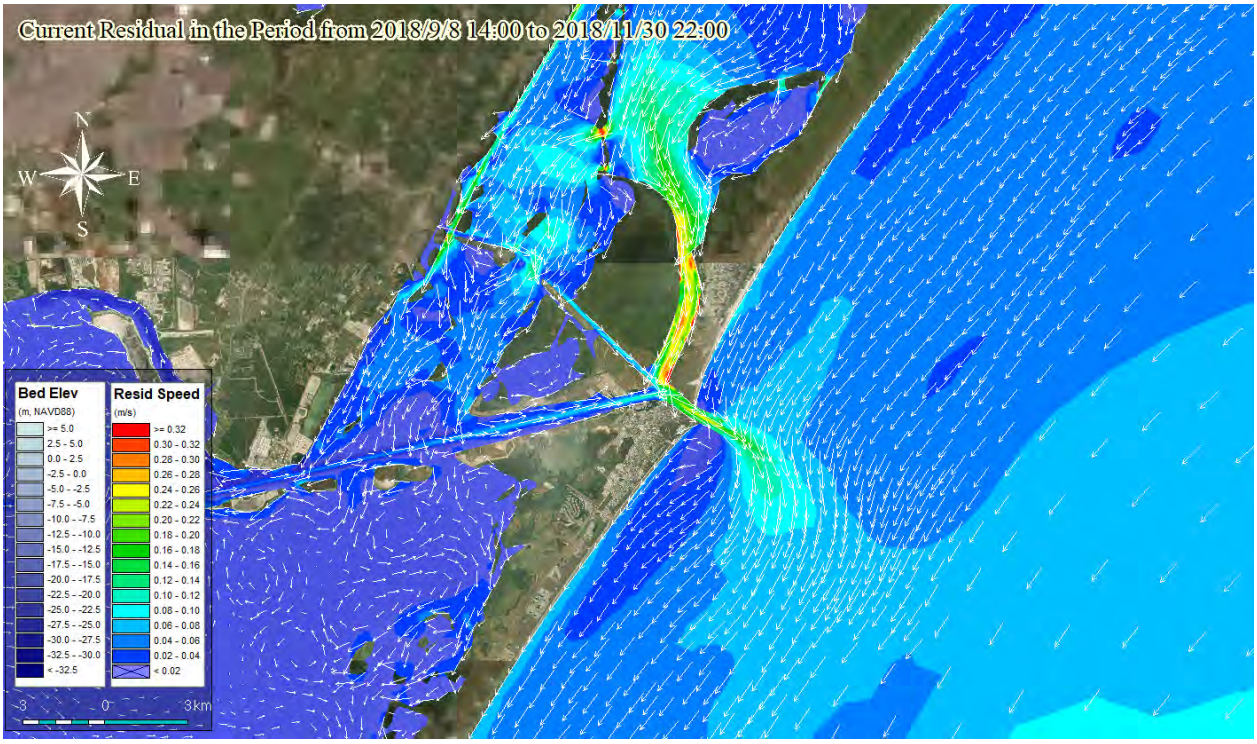

Figure 3.19: Residual currents in the GOM, Redfish Bay, Aransas Bay, and the inner basin calculated from the depth-averaged velocity in the period from 2018/9/8 14:00 to 2018/11/30 22:00.

3.3.2.3 Salinity

Figure 3.20 shows the comparison of model predicted salinity with the measured salinity at five stations (see locations in Figure 2.16). The KPIs for model prediction of salinity are listed in Table 3.7. The overall model prediction error on salinity is about 5 PSU (it is noted that there are several periods with gaps and noticeable calibration drift in measured salinities). The model predicts the salinity in Nueces Bay reasonably well and was able to reproduce the significant reduction of salinity due to the freshwater dilution during a large river flow event as well as salinity recovery during lower inflow periods.

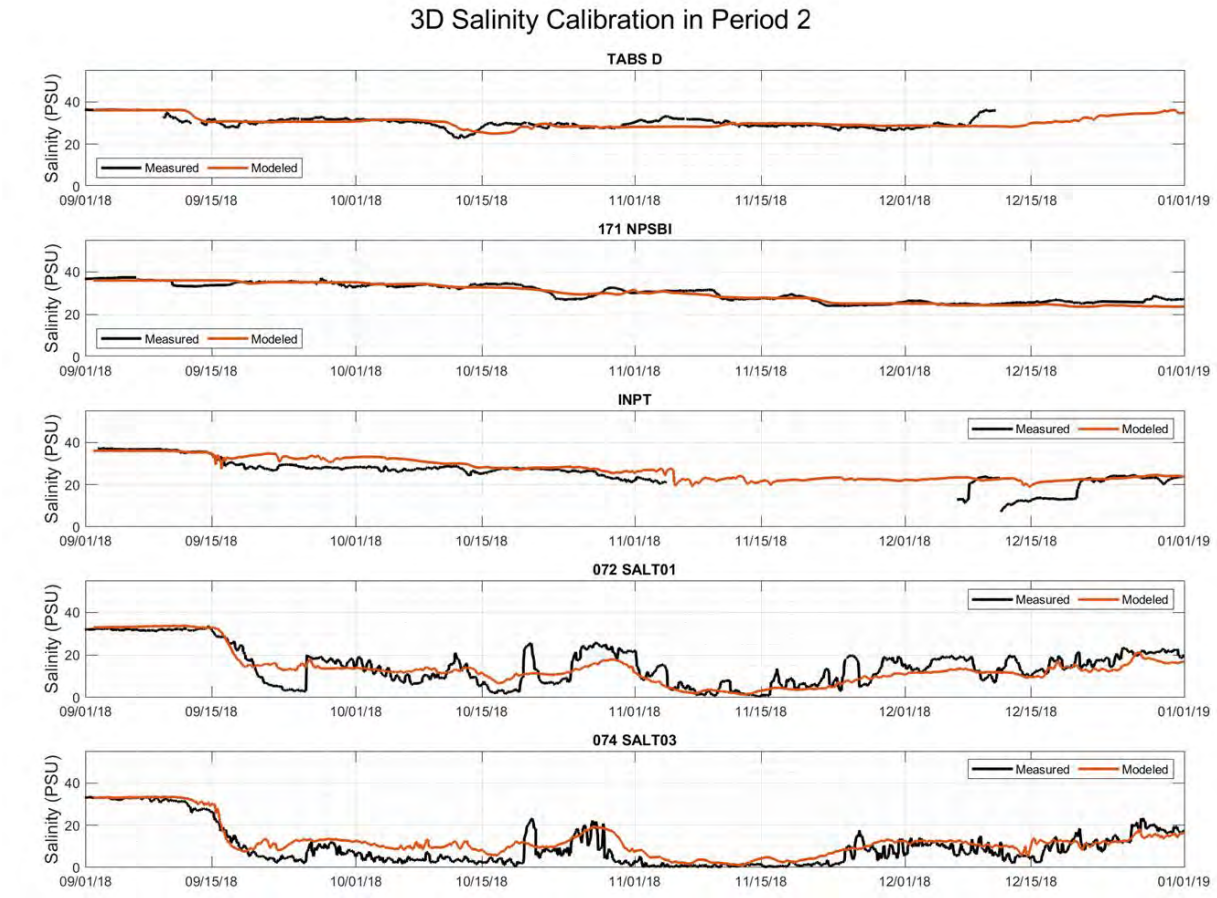

Figure 3.20: Comparison of model predicted salinity with measured data in Period 2

Table 3.7: Key performance indicators of model prediction on salinity in Period 2

KPI	074 SALT03	072 SALT01	INPT	171 NPSBI	TABS D
BIAS (psu)	-2.8	1.1	-2.8	0.3	0.3
MAE (psu)	3.8	3.8	3.2	1.2	1.7
RMSE (psu)	4.7	4.7	4.3	1.5	2.3
R2	0.84	0.73	0.75	0.90	0.33
Measured Mean (psu)	9.7	14.9	25.9	30.1	30.0
Predicted Mean (psu)	12.5	13.9	27.1	29.8	30.3

Figure 3.21 and Figure 3.22 show the snapshots of model predicted salinity at the time following a large river flow event on water surface and near the lakebed seabed (approximately at -4 m NAVD88), respectively. The comparison of the two figures indicates that there is strong salinity stratification (more than 10 PSU difference) in the northern part of Corpus Christi Bay. Figure 3.23 shows the salinity profile extracted at the navigation

channel which is indicated by the red star in Figure 3.22. In the navigation channel below -6 m NAVD88, the salinity is high and does not mix with the top layers well. The stratification predicted by the model is consistent with the measured data which was described in Islam *et al.* (2010).

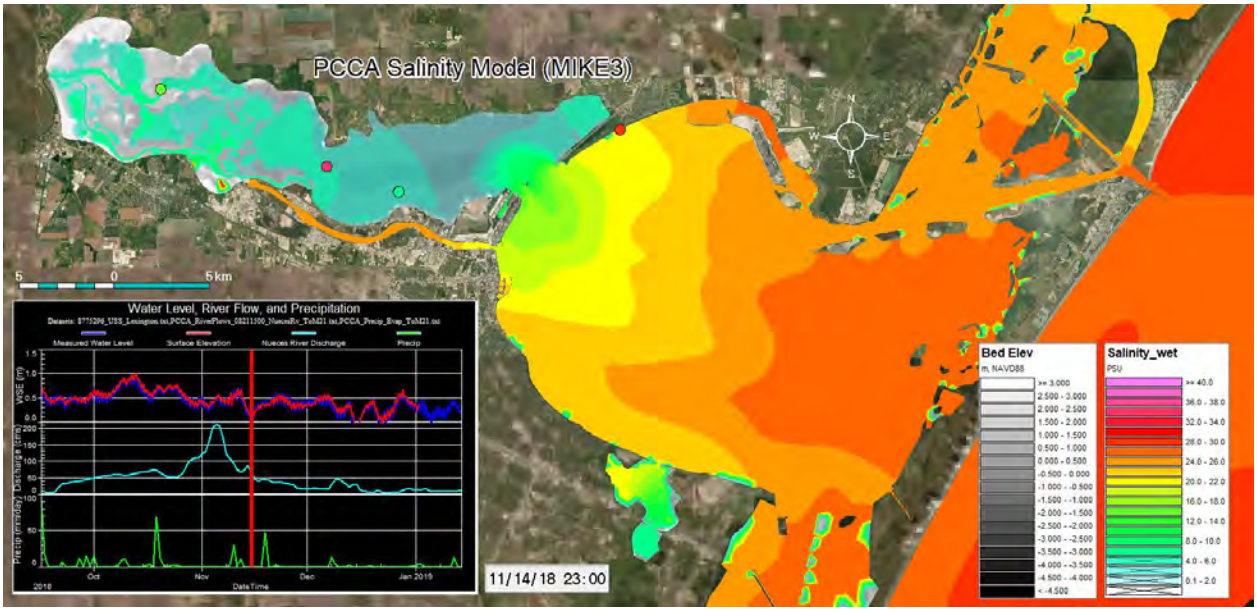

Figure 3.21: Snapshot of modeled salinity on water surface after a large river flow event

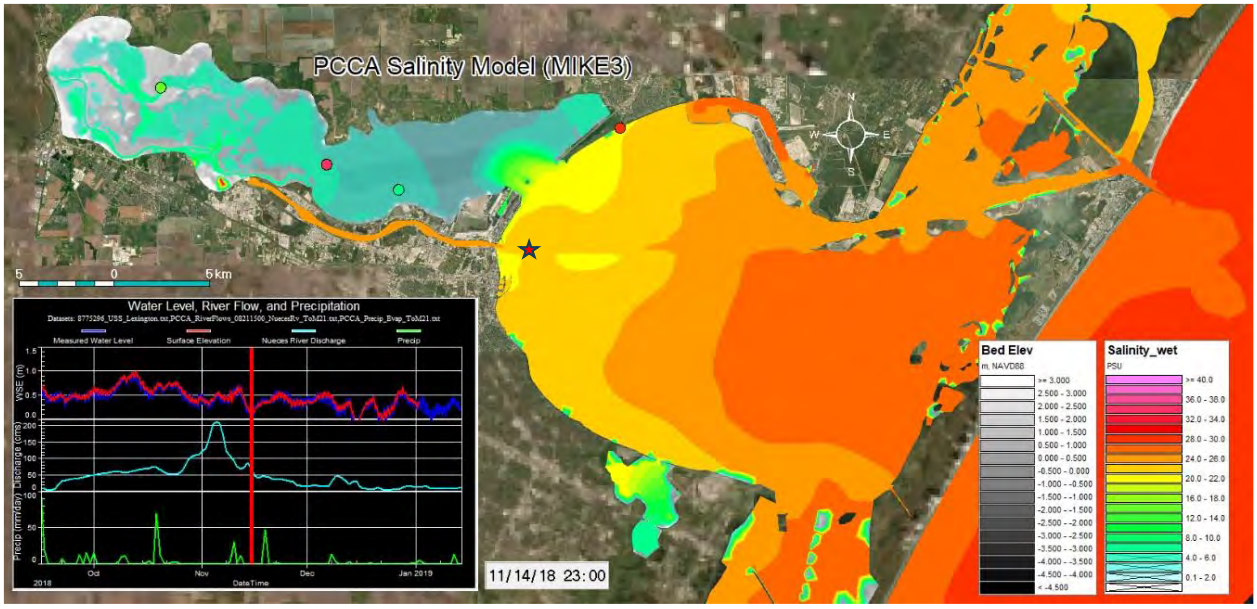

Figure 3.22: Snapshot of modeled salinity near the seabed (approximately -4 m, NAVD88) after a large river flow event

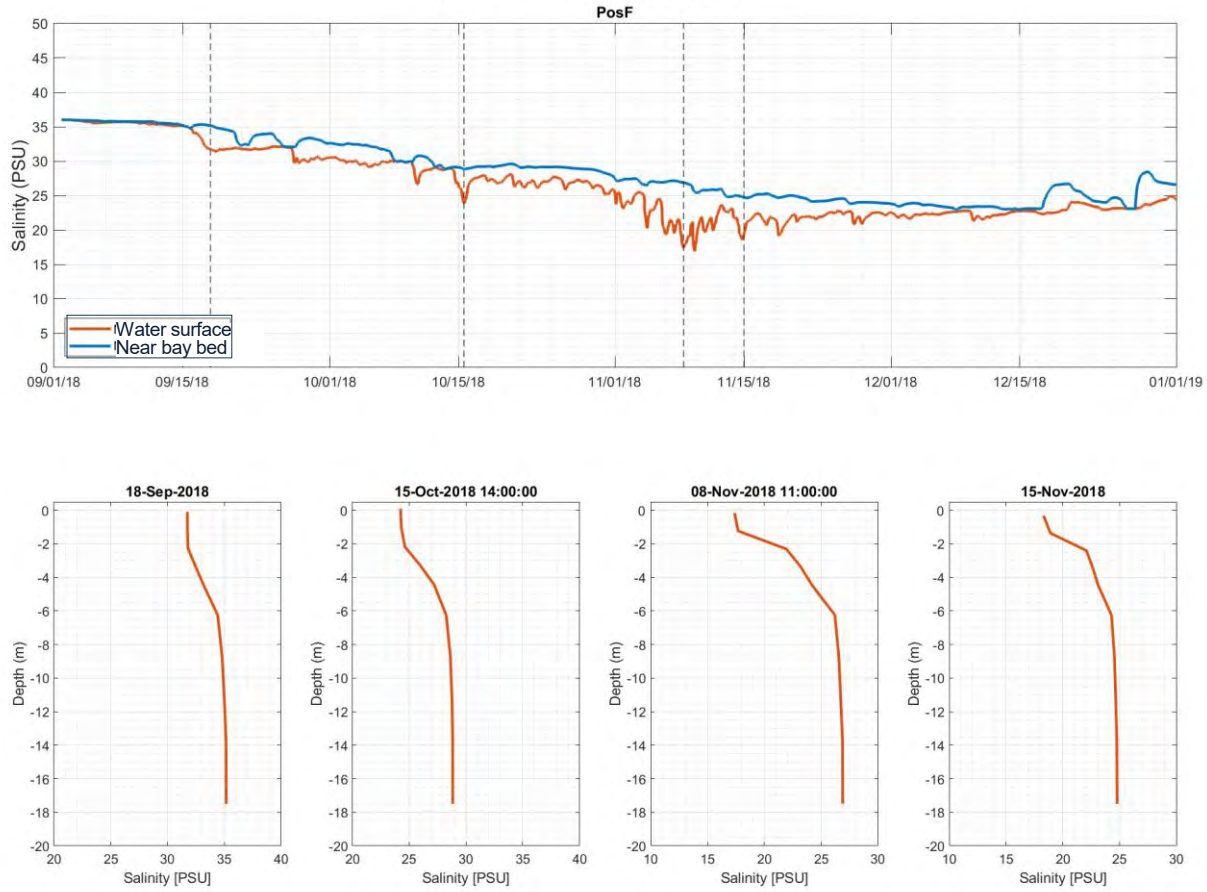

Figure 3.23: Salinity stratification predicted by the model. Top: model predicted salinity on water surface (orange) and near the bay bed (blue) extracted at the position of the red star shown in Figure 3.22. Bottom: snapshots of salinity profiles which times are indicated by vertical dash lines shown on the top plot.

3.3.3 Model Validation

The calibrated model was validated in Period 1 and Period 3. During the model validation, all parameters determined in the model calibration such as roughness, wind drag coefficient, eddy viscosity, diffusivity, scale factors for precipitation and evaporation were applied in the model validation. All open boundaries in the model validation periods were developed from the measured data using the same approaches as used for the model calibration. For some salinity boundaries, the approach to fill data gaps in the measured data was revised to achieve the better results during the model validation period.

3.3.3.1 Water Levels

Figure 3.24 and Figure 3.25 show the comparison of model predicted water level against the measured data at USS Lexington in Period 1 and Period 3, respectively. The plots of water level comparison at the other stations are provided in Appendix A. Table 3.8 and Table 3.9 list the key performance indicators of model prediction of water levels in Period 1 and Period 3, respectively. The model predicted the water levels well and the

prediction errors are less 5 cm. The model may slightly underestimate the tide range at USS Lexington, which likely results from the uncertainty of bathymetry in Nueces Bay (see Section 2.3). Note the occurrence of Hurricane Hanna (Category 1 hurricane), which storm eye passed through Corpus Christi and made landfall on July 25, 2020, and the other two tropical storms on August and September, 2020 in Period 3. The model predicted the storm surges caused by the storms reasonably well.

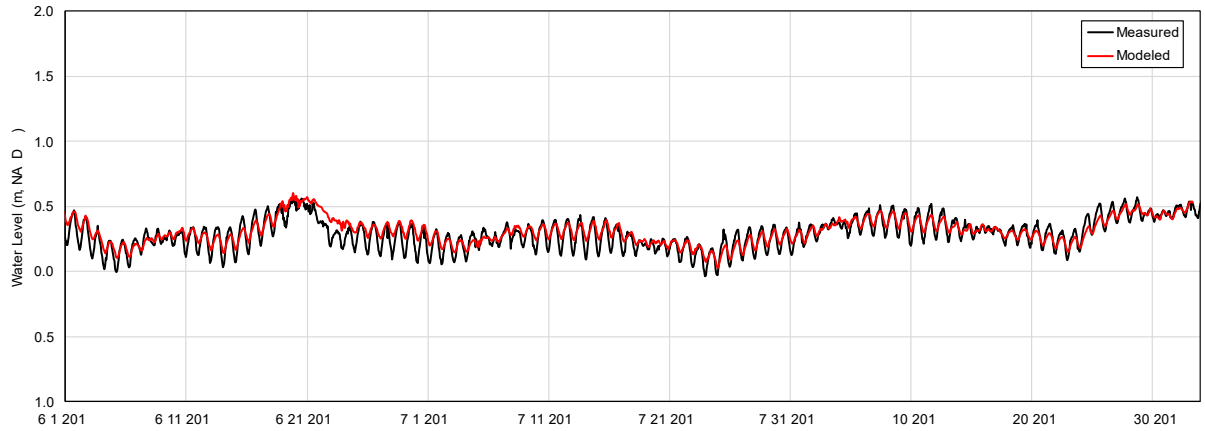

Figure 3.24: Comparison of model predicted water level with the measured data at USS Lexington in the model validation (Period 1)

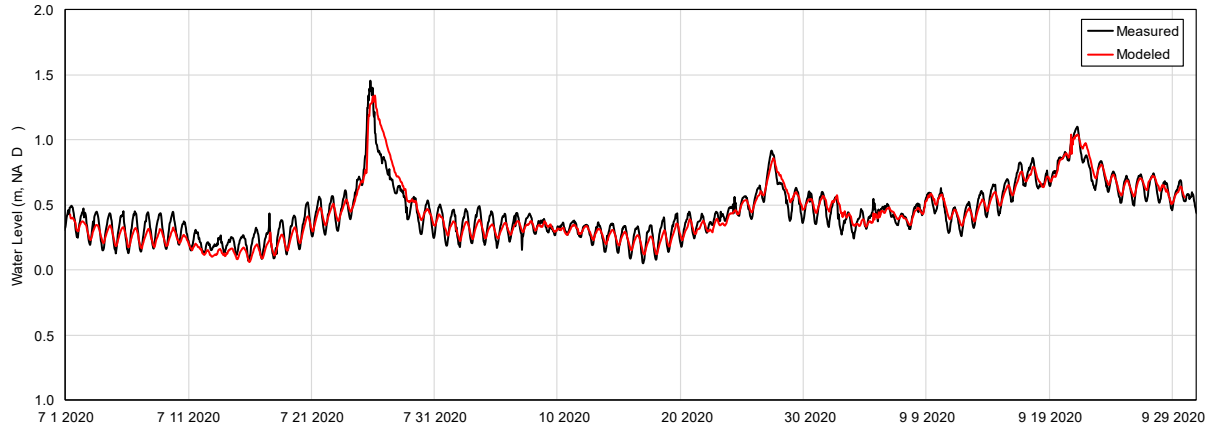

Figure 3.25: Comparison of model predicted water level with the measured data at USS Lexington in the model validation (Period 3)

Table 3.8: Key performance indicators of model validation of water levels in Period 1

KPI	Rockport	Port Aransas	USS Lexington	Packery Channel	Bob Hall Pier
BIAS (m)	-0.05	0.03	0.01	-0.03	0.05
MAE (m)	0.05	0.03	0.01	0.03	0.05
RMSE (m)	0.05	0.04	0.02	0.03	0.06
R^2	0.96	0.88	0.78	0.89	0.9

Table 3.9: Key performance indicators of model validation of water levels in Period 3

KPI	Rockport	Port Aransas	USS Lexington	Packery Channel	Bob Hall Pier
BIAS (m)	-0.05	0.04	-0.01	0.03	0.01
MAE (m)	0.05	0.05	0.05	0.04	0.06
RMSE (m)	0.05	0.07	0.06	0.06	0.08
R^2	0.99	0.94	0.93	0.94	0.93

3.3.3.2 Currents

Figure 3.26 and Figure 3.27 show the comparison of model predicted flow vectors, which break down into U (easting) component and V (northing) component, with the available measured data at current stations in Period 1 and Period 3, respectively. The two stations are located at the outer navigation channel (see Figure 2.15). The currents at Station CC0101 (AP Buoy) are mainly driven by the long-shore currents, while the currents at Station CC0201 (Aransas Pass LB6) results from the interaction of the strong channel currents from Aransas Pass and the long-shore currents with impact of the two parallel jetties.

Table 3.10 and Table 3.11 list the key performance indicators of model prediction of currents in Period 1 and Period 3, respectively. Station TABS-D (Offshore Buoy 42048), Station CC0301 (Port Aransas, Channel View), and CC0401 (MODA Currents) have been included where measured data is available. Plots for the additional stations are presented in Appendix A.

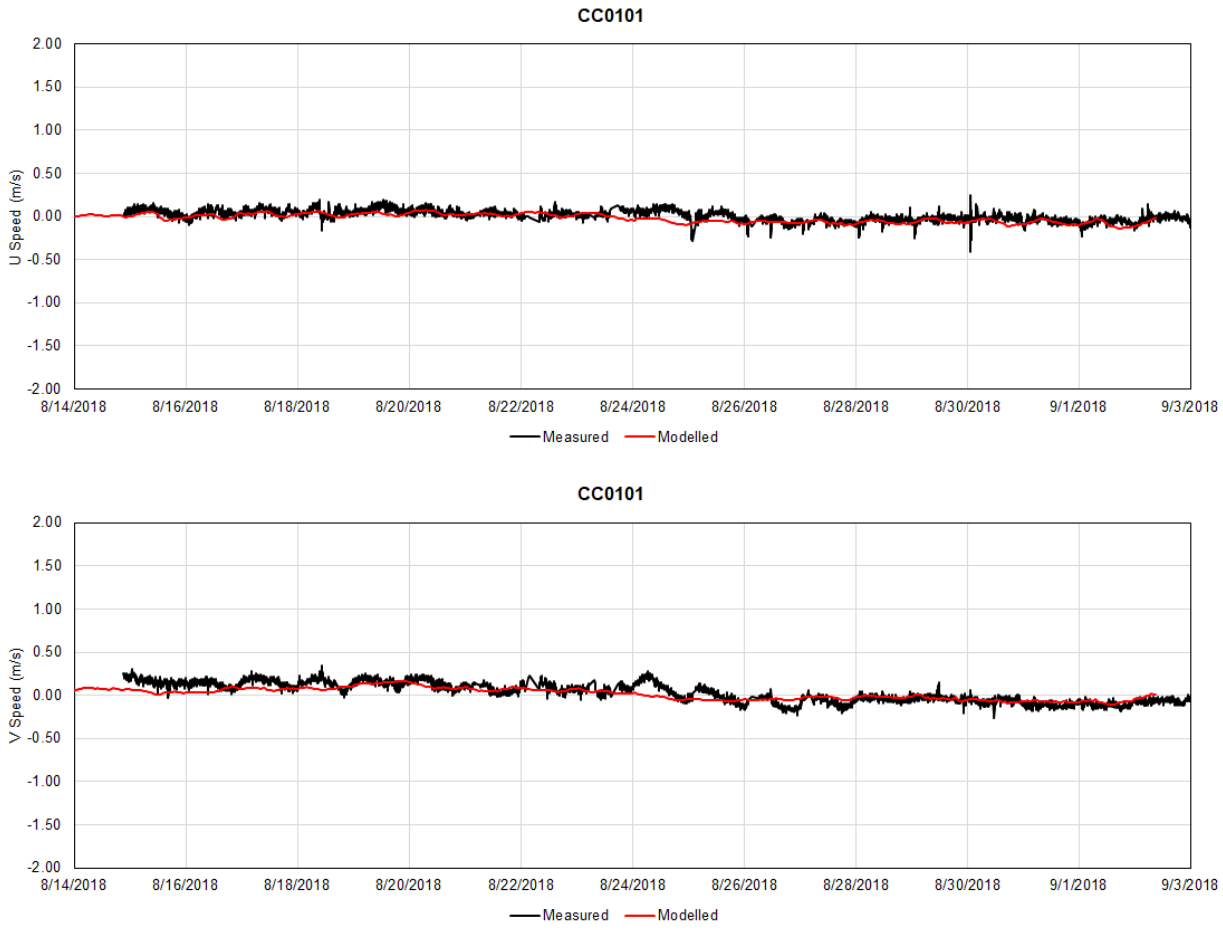

Figure 3.26: Comparison of model predicted flow velocity components with the measured data in the model validation (Period 1)

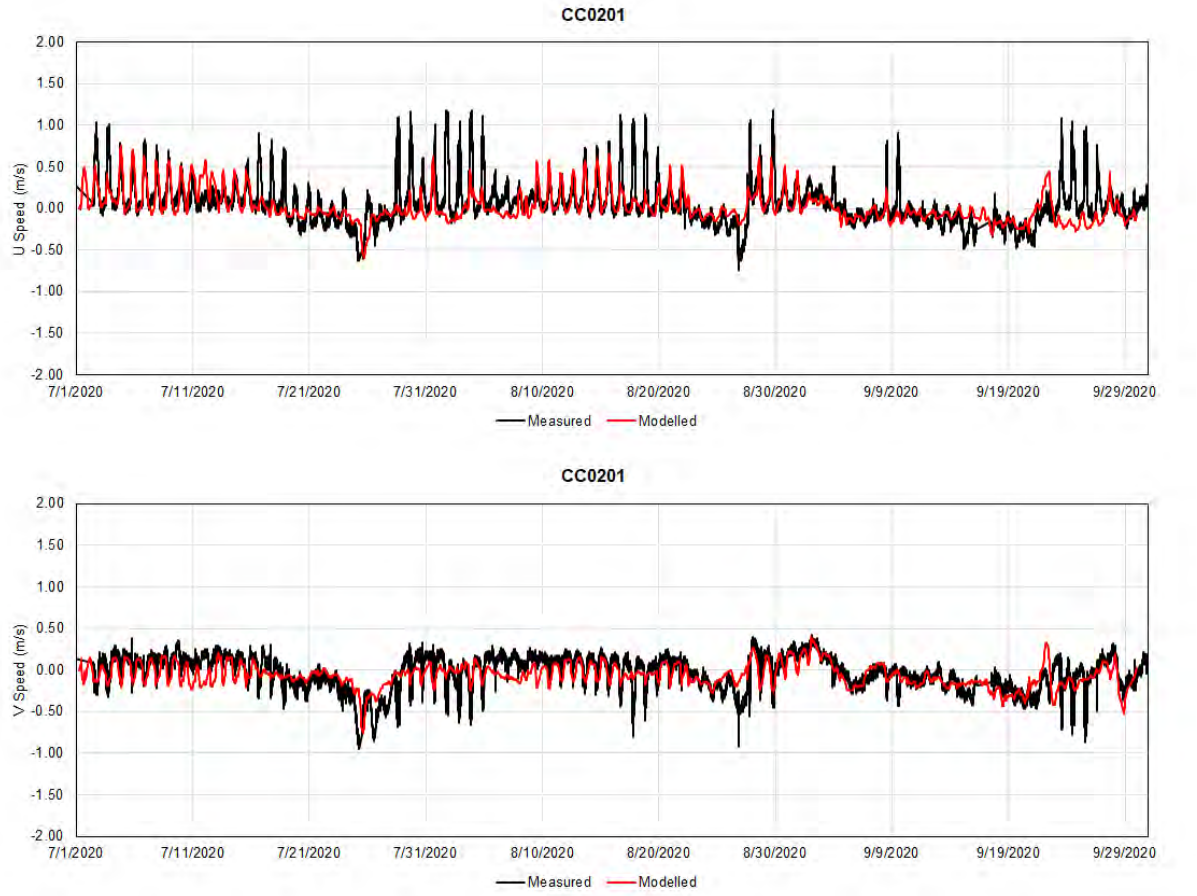

Figure 3.27: Comparison of model predicted flow velocity components with the measured data in the model validation (Period 3)

Table 3.10: Key performance indicators of model prediction of flow vectors in Period 1

KPI	TABS-D	CC0101	CC0401
BIAS (m/s)	-0.08	-0.03	-0.03
MAE (m/s)	0.10	0.06	0.14
RMSE (m/s)	0.13	0.07	0.18
R^2	0.32	0.5	0.44

Table 3.11: Key performance indicators of model prediction on flow vectors in Period 3

KPI	TABS-D	CC0201	CC0301	CC0401
BIAS (m/s)	0.04	-0.04	0.03	0.01
MAE (m/s)	0.16	0.13	0.18	0.10
RMSE (m/s)	0.22	0.19	0.23	0.13
R^2	0.08	0.35	0.86	0.65

3.3.3.3 Salinity

Figure 3.28 and Figure 3.29 show the comparison of model predicted salinity against the measured data at five stations in Period 1 and Period 3, respectively. The key performance indicators of model prediction are listed in Table 3.12 and Table 3.13, respectively. Note that R^2 may not be a good indicator for salinity, which does not significantly change with time, although the time series plots show the good agreement of predicted salinity with the measured salinity. Instead, the two additional indicators, mean measured salinity and mean predicted salinity, were added in the tables to indicate the degree of the model prediction errors. Overall, the model predicted the salinity reasonably well. The RMSE is less than 7 PSU and 4 PSU for Period 1 and Period 3, respectively. Note that there are large data gaps and data noise in the measured salinity data, including some indications of calibration drift, which may affect the evaluation of model prediction errors.

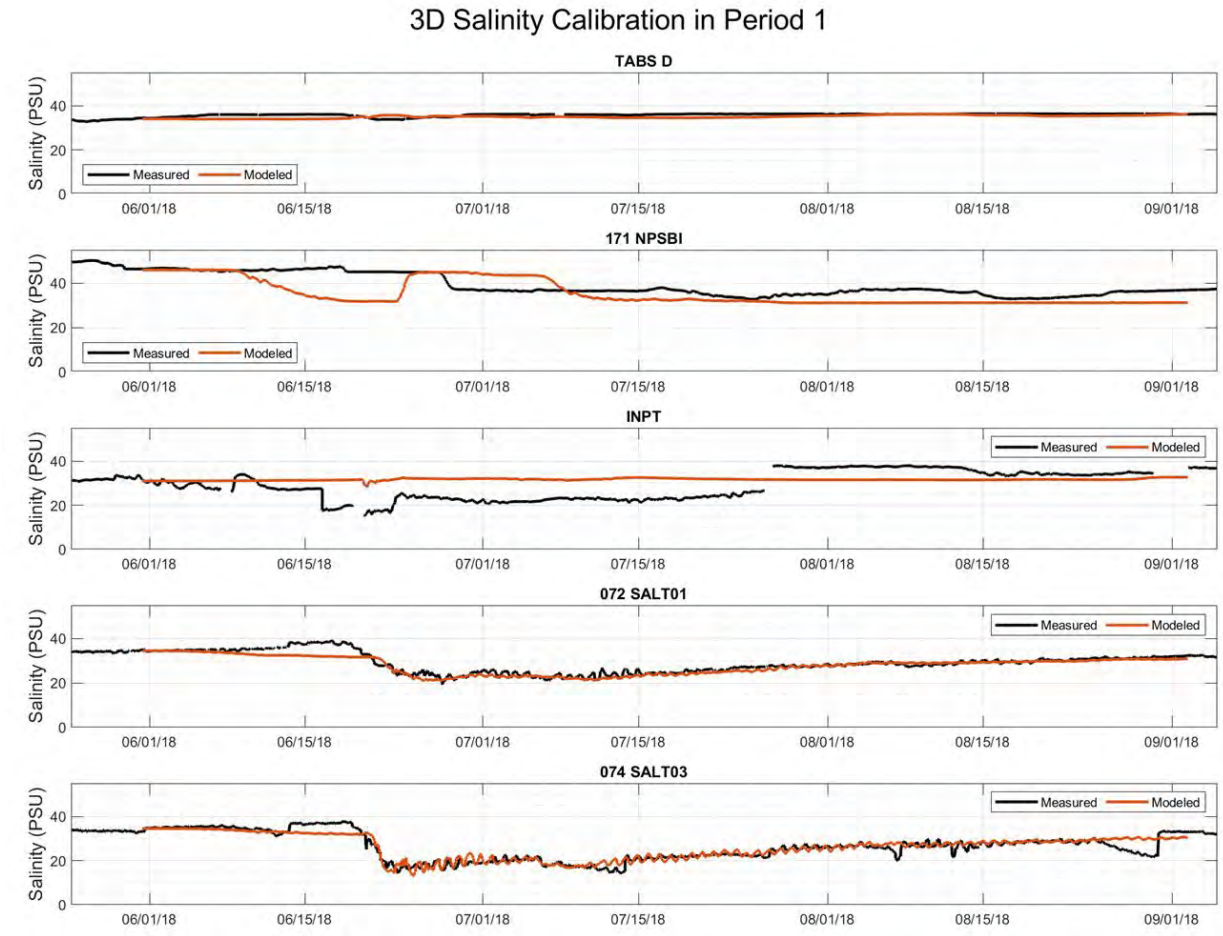

Figure 3.28: Comparison of model predicted salinity with the measured data in the model validation (Period 1)

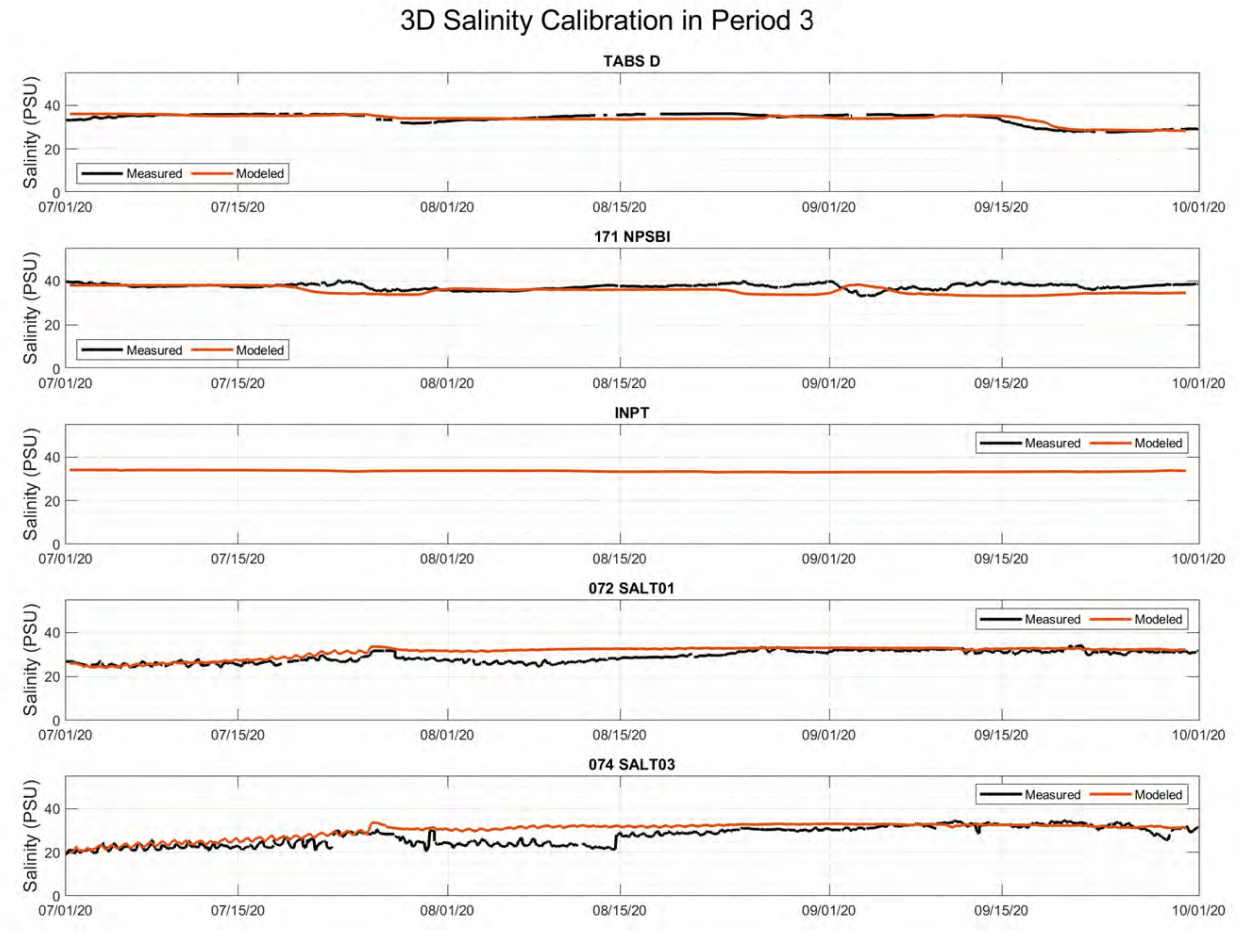

Figure 3.29: Comparison of model predicted salinity with the measured data in the model validation (Period 3)

Table 3.12: Key performance indicators of model prediction of salinity in Period 1

KPI	074 SALT03	072 SALT01	INPT	171 NPSBI	TABS D
BIAS (psu)	-0.1	1.0	-2.7	0.3	0.9
MAE (psu)	1.7	1.3	5.9	4.9	1.0
RMSE (psu)	2.4	2.0	6.9	5.5	1.2
R^{2*}	0.85	0.86	0.16	0.06	0.04
Measured Mean (psu)	26.0	29.0	28.8	35.8	35.9
Predicted Mean (psu)	26.1	28.0	31.6	35.4	35.0

*R^2 should not be used as a performance indicator when the variation of salinity with time is small.

Table 3.13: Key performance indicators of model prediction of salinity in Period 3

KPI	074 SALT03	072 SALT01	INPT	171 NPSBI	TABS D
BIAS (psu)	-2.7	-2.1	ND*	1.9	0.1
MAE (psu)	3.0	2.3	ND	2.3	1.1
RMSE (psu)	4.0	2.9	ND	2.9	1.4
R^2	0.52	0.51	ND	0.03	0.69
Measured Mean (psu)	27.5	29.0	ND	37.4	33.9
Predicted Mean (psu)	30.2	31.1	33.4	35.5	33.8

*ND – no measured data

3.4 Sensitivity Tests

Many sensitivity tests were carried out during the model development and calibration to understand the performance of the variation of model results with input parameters. Only the tests that significantly impacted the model performance results are described in this section.

3.4.1 Grid Resolution

Grid resolution was first tested during grid generation. The grid resolution depends on the complexity of bathymetry, shorelines, and structures. The model stability and computational time were also considered during grid generation. A high-resolution grid was used in the areas of complex shorelines and along the navigation channels where the study was focused. The sensitivity tests indicate that the grid resolution has some impact on the model results if there are insufficient grids distributed along the narrow openings.

3.4.2 Offshore Open Boundary Conditions

Many sensitivity tests were carried out by applying different approaches to construct the offshore boundary conditions; observations are described below:

- Using the predicted tide from the major tide constituents with the DHI MIKE utility cannot reproduce the seasonal water level variation in both the GOM and in the subtropical bays. The model significantly underpredicts long-shore currents (driven by oceanographic currents, not wave momentum) in the GOM;
- Using the measured water level at Bob Hall Pier can reproduce the offshore water level at the offshore reasonably well but significantly underpredicts the mean water level in Corpus Christi Bay, e.g., at USS Lexington. The long-shore current in the GOM is also underpredicted;
- Using the HYCOM model results without water level adjustment can produce reasonably large, long-shore currents but cannot reproduce the water levels in the bays well.

Finally, the offshore boundary conditions were developed by using the HYCOM modeled currents to control the northeast and southwest open boundaries and using adjusted water level from the HYCOM predicted water level and measured data at Bob Hall Pier (see details in Section 3.2.3.2). A good calibration result was achieved with this approach.

3.4.3 3D Impacts

Sensitivity tests on the 3D model impact were carried out by performing the model runs using the same grid and the same model setting using both MIKE21 model (2D) and MIKE3 model (3D). The predicted water levels and depth-averaged flow velocity were compared. The results show that there is no significant difference in water level and depth-averaged flow velocity predicted by using these two models.

However, a 3D model is required to correctly simulate both hydrodynamics and salinity for this study. Wind generally produces reversed current in the deep water, e.g., the navigation channel of Corpus Christi Bay, to the current on water surface as shown in Figure 3.18. Strong alongshore currents in the gulf result in significant difference of current direction in water columns of the outer channel (see Figure 3.16). The cross-channel currents in the outer channel are important information for navigation simulation. When there is a large river inflow from Nueces River, there is the significant stratification of salinity in the Corpus Christi Bay (see Figure 3.22 and Figure 3.23). All above-mentioned 3D profiles of currents and salinity cannot be produced by the 2D model and therefore a 3D model is required.

3.4.4 Diffusivity Coefficient

Sensitivity tests on diffusivity coefficient for salinity simulation were performed. There are two approaches to set up the diffusivity coefficient for salinity: a) scale to the eddy viscosity which was calculated by the hydrodynamic model; and b) user specified values. The sensitivity tests show that the salinity is sensitive to diffusivity and therefore this parameter is regarded as a calibration parameter.

3.4.5 Evaporation and Precipitation

Many sensitivity tests on evaporation and precipitation were performed during the model development. The results show that the hydrodynamics are not sensitive to evaporation and precipitation but the salinity in shallow water is sensitive to evaporation and precipitation. Therefore, these two parameters are regarded as the calibration parameters for salinity model.

3.5 Model Uncertainties

3.5.1 Bathymetry in Nueces Bay

The bathymetry in Nueces Bay is identified as a significant data gap during the model development. The bathymetry downloaded from NOAA data source indicates a constant bed elevation of -0.1 m NAVD88, which is incorrect as historical satellite images (see Figure 3.30) show that there are many small channels in and between Nueces Bay and connected to Corpus Christi Bay. The bathymetry in Nueces Bay is important to calculate tide prism in of Nueces Bay, and therefore, it significantly impacts on the tidal exchange between Nueces Bay and Corpus Christi Bay.

Figure 3.30: The connecting channels between Nueces Bay and Corpus Christi Bay in the historical satellite images

In the current present model, a representative bathymetry dataset of Nueces Bay was constructed based on information available in previous model reports (Li & Hodges, 2015), discussions with hydrographic surveyors familiar with the area, and satellite imagery and was adjusted to achieve an acceptable model calibration and validation. The final model bathymetry for Nueces Bay is shown in Figure 3.31.

Figure 3.31: The finally constructed bathymetry in Nueces Bay

3.5.2 Salt in Nueces Delta

There is large volume of salt stored in Nueces Delta, which has been observed in satellite imagery (see Figure 2.30). This salt storage has impacts on the salinity in Nueces Bay. During a large rainfall event, these salts are dissolved by rain and runoff and carried to the bay. Additionally, during a large river flow event, flooding may occur in the delta and dissolve the stored salt, resulting in high salinity in Nueces Bay. During the model calibration, it was recognized that the salt storage in the delta cannot be ignored, otherwise, a reasonable salinity calibration cannot be achieved in Nueces Bay. Unfortunately, there is very limited information on salt storage in the delta. In this model, the boundary conditions for salinity at the open boundary of Nueces River and the salinity with the runoff to the delta was developed to account for the dissolution of salt in the delta and adjusted during the calibration (see Section 3.3.2.3 for more details).

3.5.3 Salinity Data Gap in Aransas Bay

There are large temporal data gaps in the measured salinity, which is required to construct the boundary conditions for salinity along the open boundary of Aransas Bay. The salinity in Aransas Bay has been identified to be an important source to Corpus Christi Bay since there is a net flow along the intercoastal waterway from Aransas Bay to Corpus Christi Bay. Unlike water level, it is more difficult to fill data gaps for salinity using the other stations. In this model, the boundary condition for salinity in Aransas Bay was developed by using the measured data from stations further to the northeast along the GIWW (e.g., CHKN in San Antonio Bay).

3.5.4 HYCOM Model Prediction

To better understand the accuracy of HYCOM model, the flow velocity was extracted from the HYCOM model at the NOAA monitoring station, TABS-D, at a depth of -2 m NAVD88. Figure 3.32 shows the comparison of the HYCOM modeled velocity with the measured data at TABS-D in time series. Figure 3.33 shows the correlation of velocity components (U (easting) and V (northing)) between the HYCOM model prediction and

the measured data. These plots show that the HYCOM model underpredicted the currents at TABS-D significantly (about 65% less). This means that the HYCOM model underpredicted the alongshore currents in the GOM. Since the HYCOM model results were used to develop the offshore boundary condition, it may bring uncertainty to the developed model.

Figure 3.34 shows the comparison of water level predicted by the HYCOM model with the water level measured at Bob Hall Pier. The HYCOM model predicted tide signals well. However, the model underpredicts surges produced by wind, which have a seasonal variation as described in Section 2.2.3. Nevertheless, in this model calibration, the offshore boundary condition of water level was constructed by using HYCOM predicted water levels and adjusted with the seasonal variation of water level based on the measured water level at Bob Hall Pier as shown in Figure 3.34. With this adjustment, a good water level calibration was achieved.

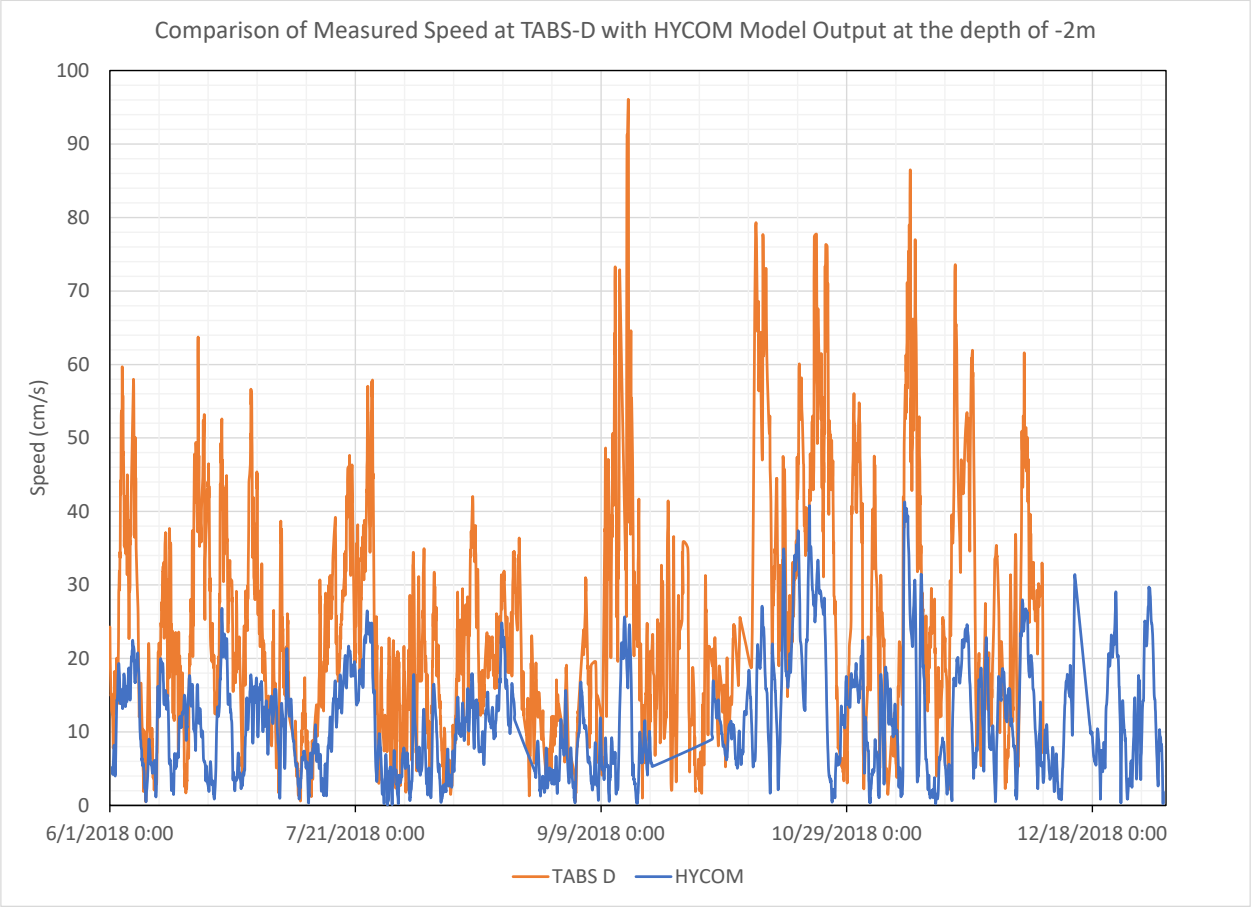

Figure 3.32: Comparison of HYCOM predicted current speed with the measured data at TABS-D

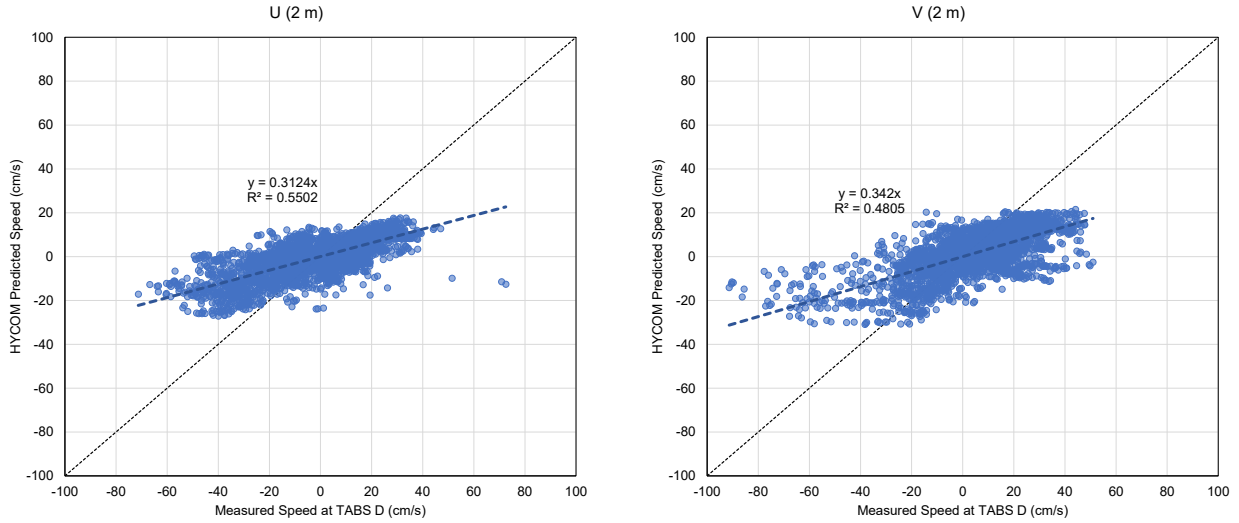

Figure 3.33: Correlation of HYCOM Predicted Velocity Components with the measured data at TABS-D.

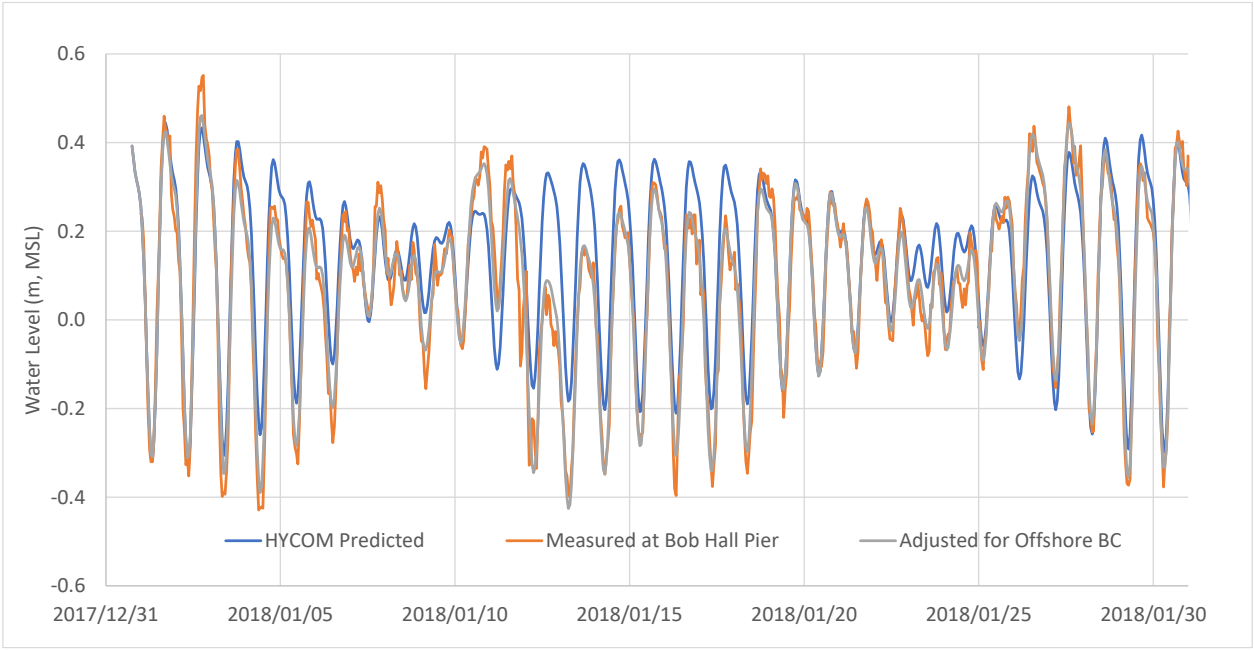

Figure 3.34: Comparison of HYCOM predicted water level with the measured water level at Bob Hall Pier

4. Impact Assessment for Future With Project

4.1 Production Model Runs

The main objective of this modeling study is to evaluate the impact of Future With Project (FWP) compared to Future Without Project (FWOP). The Future Without Project is the 54 ft channel deepening project that has been approved and is now in construction. The navigation channel in the FWOP is being dredged from the Port of Corpus Christi to the GOM to -54 ft MLLW (-16.6 m NAVD88), including Humble Basin and the Turning Basin (see Figure 4.1). The FWP is the proposed project to dredge the Corpus Christi navigation channel to -75 ft MLLW (-23.65 m NAVD88) from approximately Light #1 near Port Aransas to the GOM (see Figure 4.2). Both two project scenarios were simulated by using the developed 3D model, which was calibrated and validated against the field data (see Section 3.3).

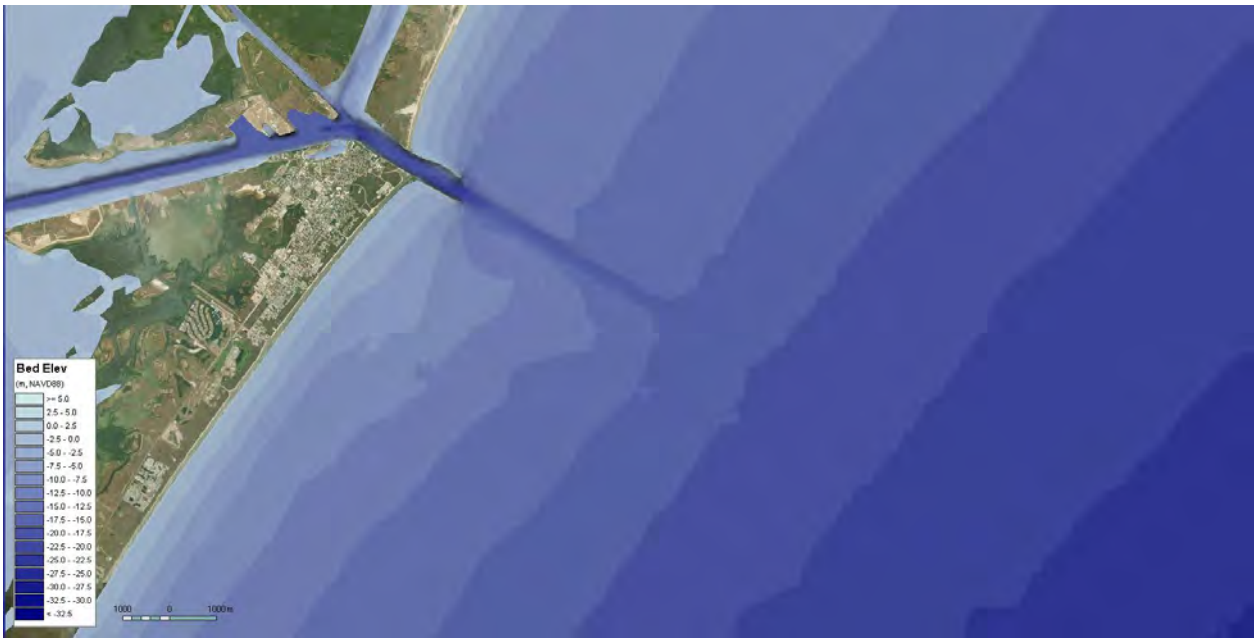

Figure 4.1: Bathymetry used for FWOP production model runs

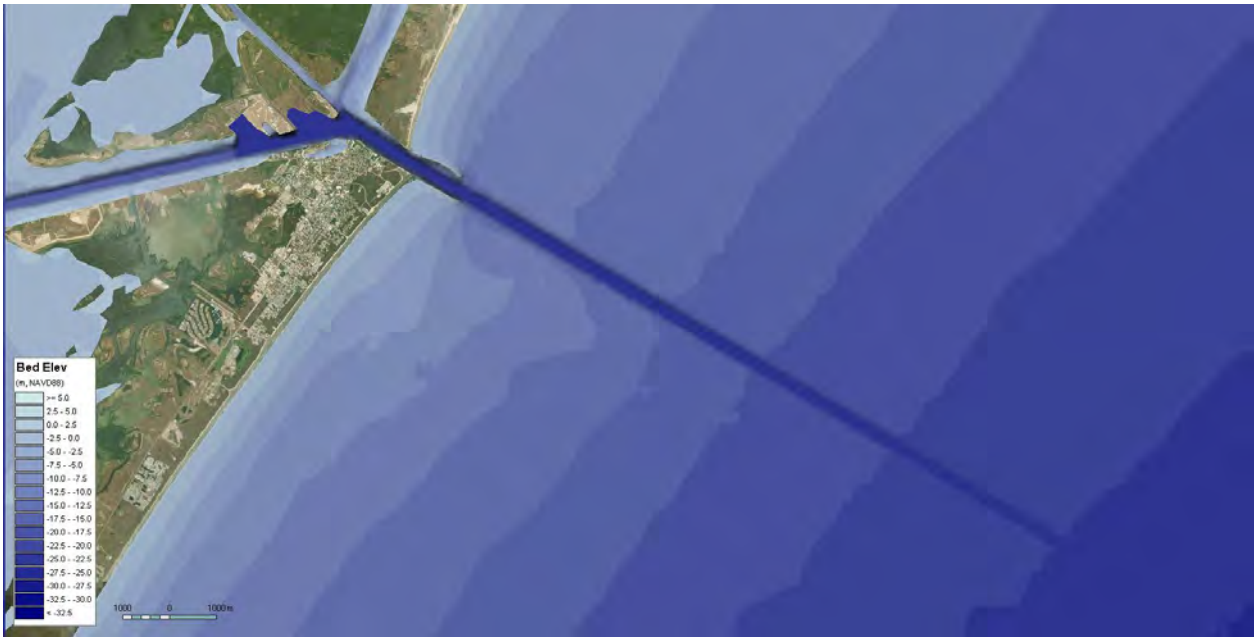

Figure 4.2: Bathymetry used for the FWP production model runs

The model production runs for both two project scenarios were carried out for the three periods that were selected for model calibrations and validations. The duration for each model run is three months. The representation of driving forces for these three periods are described in Section 3.3.1. To evaluate the impact of the FWP with strong wind conditions, the river inflow from Nueces River is forced to zero in Period 3. A total of six runs were carried out with the model.

To minimize the impacts from the other numerical factors (e.g., grid), all model runs were carried out using the same grid. The grid along the section of navigation channel that was deepened to 54 ft for the FWOP conditions and will be deepened to 75 ft for the FWP conditions was refined to appropriately represent the post-project bathymetry as shown in Figure 4.3. The same boundary conditions and physical and numerical parameters, except the bathymetry in the dredge areas, are used for all production model runs.

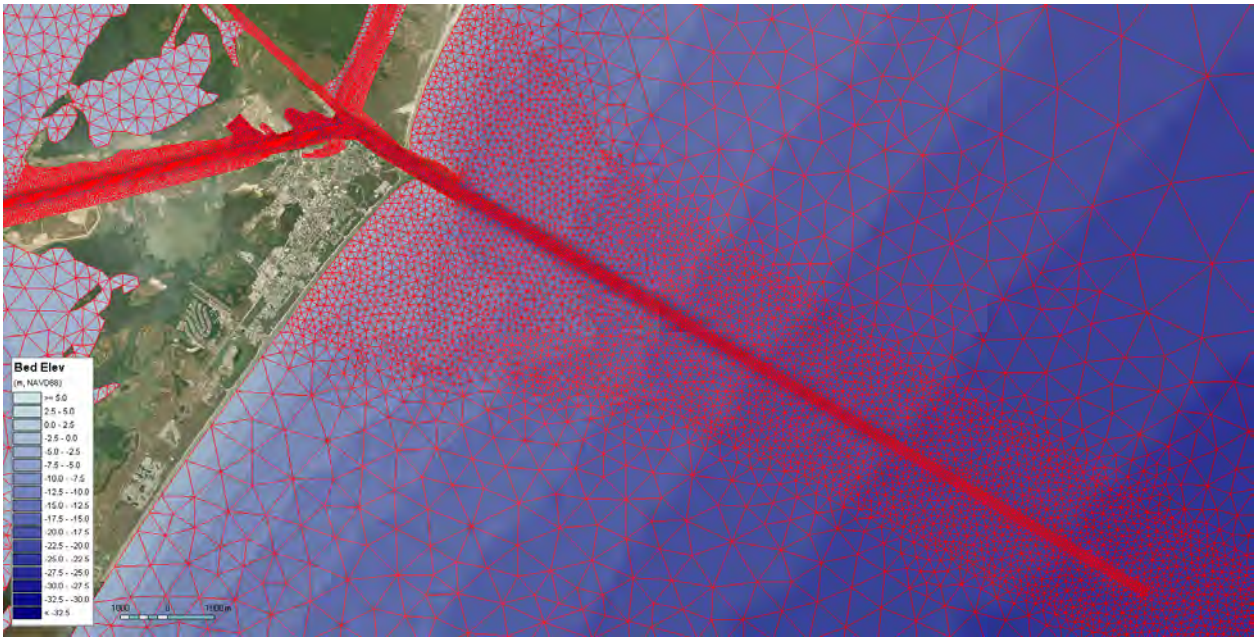

Figure 4.3: Refinement of model grid in the vicinity of the FWP construction areas

All production model runs output the results in one-hour intervals, including water level, velocity vectors (speed and direction), and salinity. The impacts of the FWP were assessed by comparing water level, current speed, and salinity between the FWP and FWOP scenarios in time and in 3D space. To better understand the impact, statistical analysis was carried out through entire simulation period (excluding the warmup period) and the outputs include mean, range, and standard deviation of the changes between FWP and FWOP. The post-processing of model results was mainly carried out by using Baird in-house software, Spatial Data Analyzer (SDA), which is a powerful tool to visualize and analyze the dynamic data in time and 3D space that are typically generated by models with GIS capability. The results were also extracted at the selected locations (see Figure 4.4) to represent the bays of interest in this analysis.

Figure 4.4: Selected stations to represent the bays of interest in the impact assessment

4.2 Impact to Water Levels

4.2.1 Mean Water Level

The changes in water level caused by the FWP were first analyzed by subtracting the hourly water levels predicted in the FWOP scenario from these predicted in the FWP scenario. A statistical analysis of the difference of hourly water levels was then carried out. Figure 4.5 shows the change of mean water level caused by the FWP in Period 2, which shows a decrease of mean water level less than 1 cm. The plots for the change of mean water levels in Period 1 and Period 3 are attached in Appendix B.1.1, which show similar results. This indicates that the FWP is unlikely to change mean water levels in the bays.

Figure 4.5: Impact of FWP to mean water levels as compared to FWOP during Period 2

4.2.2 High Tide and Low Tide

To understand the details of water level change caused by the FWP in the tide environment, the predicted water levels in the inner channel (see Figure 4.4 for location), where there is the largest water level change observed from the model result, are compared between FWP and FWOP, as shown in Figure 4.6. In the FWP, the water levels at high tide increase, and the water levels at low tide decrease.

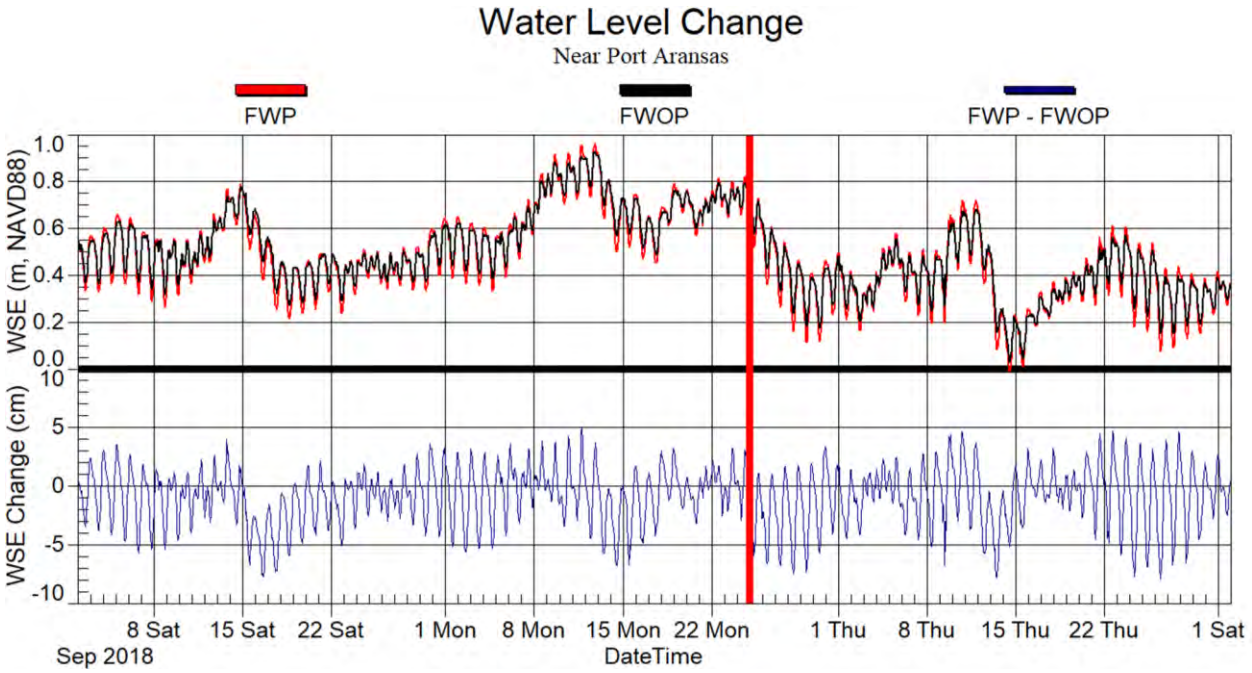

Figure 4.6: Comparison of predicted water levels for FWP and FWOP

To quantitively estimate the change, the high tides (i.e., the highest water level in a tide cycle) were analyzed from the model hourly output with the following steps:

- Calculate high tide predicted for both FWP and FWOP in all tidal cycles;
- Calculate the difference of high tide between FWP and FWOP for all tidal cycles;
- Perform the statistical analysis of high tide difference which outputs the mean, minimum, maximum, and standard deviation.

Figure 4.7 shows the average increase of high tide caused by the FWP in Period 2 and the similar plots for Period 1 and Period 3 are attached in Appendix B.1.2. Table 4.1 shows the increase of high tides caused by the FWP at the selected stations, which was combined from the results of all three modeling periods. The model predicted that the increase of high tide is less than 2 cm in Corpus Christi Bay and Redfish Bay. The maximum increase of high tide occurs at Humble Basin which is about 4 cm. It is unlikely that the FWP would cause any flooding issues in the vicinity of the proposed dredge area.

Figure 4.7: The average increase of high tide caused by FWP in comparing with FWOP in Period 2

Table 4.1: Increase of high tide caused by the FWP

Station	High Tide Change (cm)			Percentage
	Mean	Minimum	Maximum	
Outer Channel	0.0	-0.2	0.1	0%
Aransas Pass	0.4	-0.2	1.8	1%
Inner Channel	1.0	-1.5	3.8	2%
Redfish Bay	0.3	-1.1	1.6	1%
Corpus Christi Bay	0.2	-1.1	1.5	1%
USS Lexington	0.2	-1.2	1.5	1%
Nueces Bay	0.1	-1.4	1.2	0%
Packery Channel	0.1	-0.8	1.3	0%
Rockport	0.1	-0.3	0.6	0%

Using a similar approach, the lowering of low tides was calculated, and the results are shown in Figure 4.8. Similar plots for Period 1 and Period 3 are attached in Appendix B.1.2. Table 4.2 shows the lowering of low tide caused by the FWP, which was integrated from model results for all three modeling periods. The model predicted that the FWP would cause less than 4 cm drop of low tide in Corpus Christi Bay and Redfish Bay. The maximum drop of low tide occurs in the inner channel near Humble Basin which is about 10 cm. This small drop of low tide unlikely causes a navigation risk.

Figure 4.8: The average drop in low tide caused by the FWP in comparing with the FWOP in Period 2

Table 4.2: Drop in low tide caused by the FWP

Station	Low Tide Change (cm)			Percentage
	Mean	Minimum	Maximum	
Outer Channel	0.0	-0.1	0.0	0%
Aransas Pass	0.3	-0.1	0.0	0%
Inner Channel	-2.8	-9.4	-4.8	-7%
Redfish Bay	-1.0	-3.7	-1.7	-3%
Corpus Christi Bay	-0.9	-2.9	-1.3	-2%
USS Lexington	-0.9	-2.7	-1.4	-2%
Nueces Bay	-0.6	-2.0	-1.2	-2%
Packery Channel	-0.3	-1.0	-0.5	-1%
Rockport	-0.2	-0.5	-0.4	0%

4.2.3 Tidal Range

The pattern of water level change mentioned above (i.e., the increase in high tide and lowering of low tide) implies that the FWP will increase the tidal range in the vicinity of the project site. To quantitively evaluate the increase of tidal range caused by the FWP, two approaches were applied to calculate the tide range change:

- Using tidal harmonic analysis from the hourly water levels to estimate the relative change of tidal amplitude in percentage;

- Performing the statistical analysis on the tidal ranges which are directly calculated from the hourly water levels for all tidal cycles to estimate the absolute tidal range change.

A tide harmonic analysis with 26 major tidal constituents was carried out by using the three-month hourly water levels predicted by the model in Period 2. Figure 4.9 and Figure 4.10 show the comparison of the tidal amplitudes of these major tide constituents between FWP and FWOP at the selected locations (see locations in Figure 4.4) for Period 2. Similar plots are attached in Appendix B.1.3 for Periods 1 and 3. The slopes of the linear fitting lines (without intercept) as shown in the plots indicates the degree of relative increase in tidal amplitude. The percentage of tidal amplitude increase can be calculated by subtracting one from the slope of the fitting lines, which are listed in Table 4.3. The model predicted tidal amplitude increases about 11% in Redfish Bay, 8% in Corpus Christi Bay, 7% in Nueces Bay, and 3% at Rockport. The tidal amplitude at the inner channel near Port Aransas has the largest increase which is about 17%. There is no significant change in tidal amplitudes in Aransas Pass and the outer channel. Note that the tidal ranges in these locations are small and therefore the actual increase in tidal ranges may not be significant despite the fact the percentage of increase is significant.

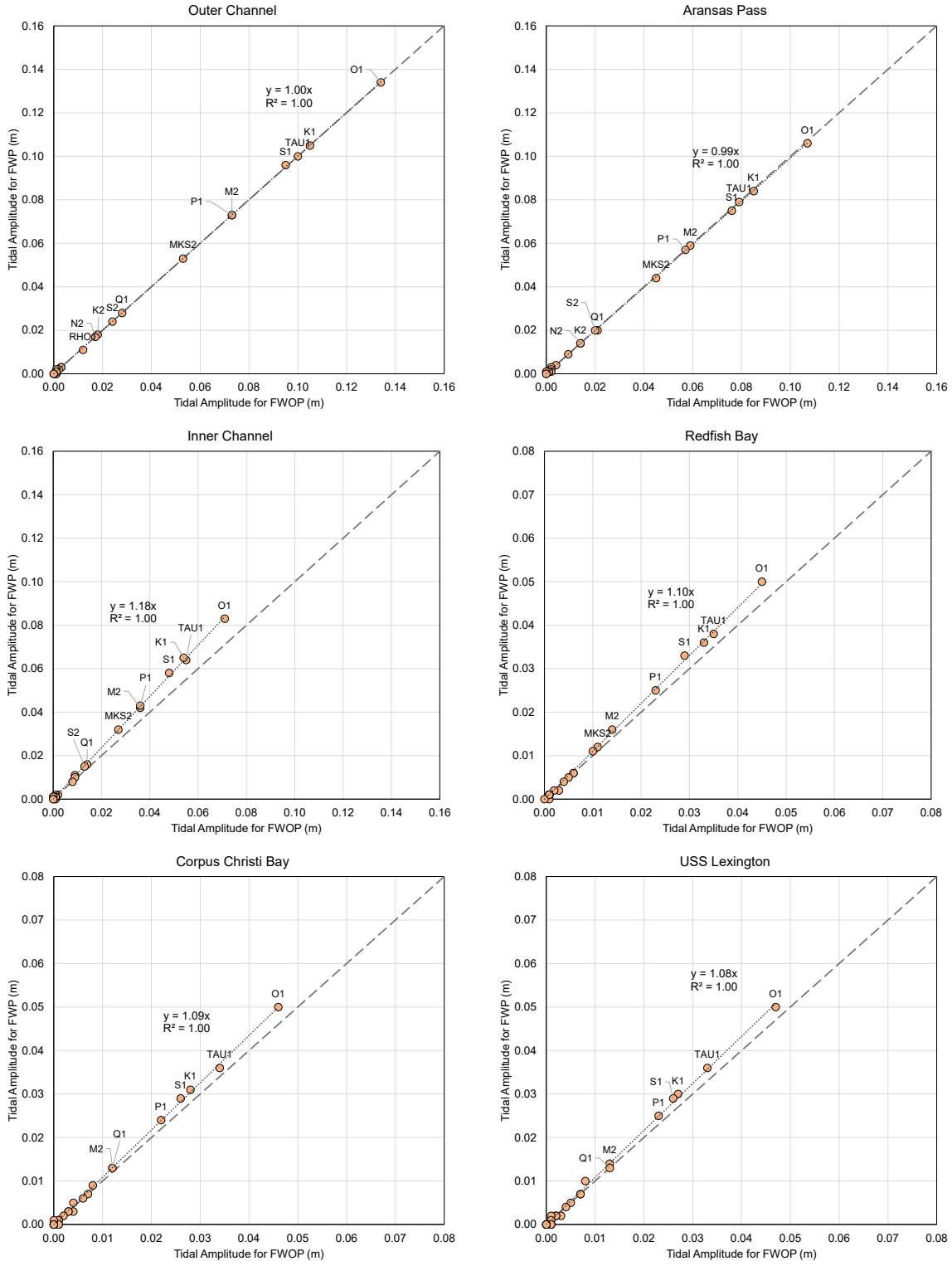

Figure 4.9: Comparison of tide amplitudes between FWP and FWOP in for Period 2

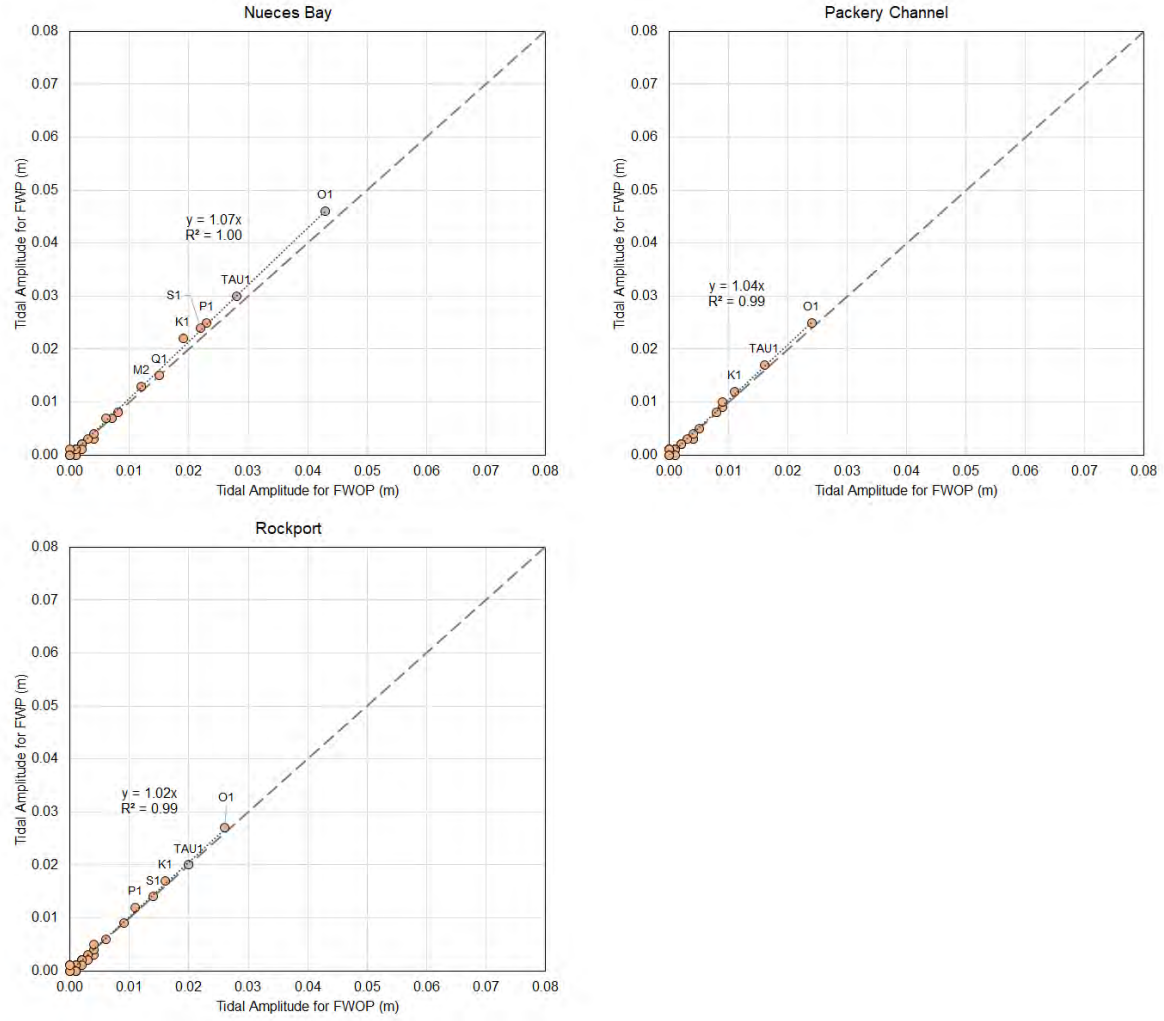

Figure 4.10: Comparison of tide amplitudes between FWP and FWOP in Period 2 (continued)

Table 4.3: Relative increase of tide amplitudes caused by the FWP

Locations	Tide Amplitude Increase (%)			
	Period 1	Period 2	Period 3	Average
Outer Channel	0%	0%	0%	0%
Aransas Pass	0%	-1%	0%	0%
Inner Channel	16%	18%	16%	17%
Redfish Bay	11%	10%	11%	11%
Corpus Christi Bay	7%	9%	9%	8%
USS Lexington	8%	8%	9%	8%
Nueces Bay	6%	7%	7%	7%

Locations	Tide Amplitude Increase (%)			
	Period 1	Period 2	Period 3	Average
Packery Channel	5%	4%	7%	5%
Rockport	4%	2%	4%	3%

To quantitively estimate the absolute increase of tidal range, the spatially varied tidal ranges over three-month periods were calculated (totally about 80 tide cycles). Figure 4.11 shows the average tidal range change in centimeters for Period 2. Similar plots for Period 1 and Period 3 are attached in Appendix B.1.3. Table 4.4 lists the average tidal range increase with the minimum and maximum values found in the three simulation periods. The model predicted that the average tidal range increase is about 4 cm at the inner channel near Port Aransas, ranging from 0.3 cm to 9 cm. The average tidal range increase at Corpus Christi Bay and Redfish Bay is less than 2 cm, ranging from -0.1 cm to 4 cm.

The percentage of tidal range increase in the model domain for Period 2 is shown in Figure 4.12. The percentage of tidal range increase listed in Table 4.4 is consistent to the percentage of tide amplitude increase listed in Table 4.3. Although the percentage is significant, the absolute tidal range changes are actually small (e.g., in the order of 1 cm or less), which may not result in significant impacts on the environment in Corpus Christi Bay and Redfish Bay, in Baird's opinion. A noticeable impact on the tidal range is limited to the Navigation Channel from Point Mustang to the inner basin.

Table 4.4: Change of tide range caused by the FWP

Station	Tide Range Change (cm)			Percentage of Average Change
	Mean	Minimum	Maximum	
Outer Channel	-0.1	-0.3	0.2	0%
Aransas Pass	0.1	-0.8	2.0	0%
Inner Channel	3.8	0.3	9.0	16%
Redfish Bay	1.2	-0.1	3.0	8%
Corpus Christi Bay	1.1	0.0	4.0	7%
USS Lexington	1.1	0.0	4.0	7%
Nueces Bay	0.8	-0.6	3.0	4%
Packery Channel	0.4	-0.3	1.0	4%
Rockport	0.3	-0.1	2.0	3%

Figure 4.11: Average tide range increase caused by the FWP for Period 2

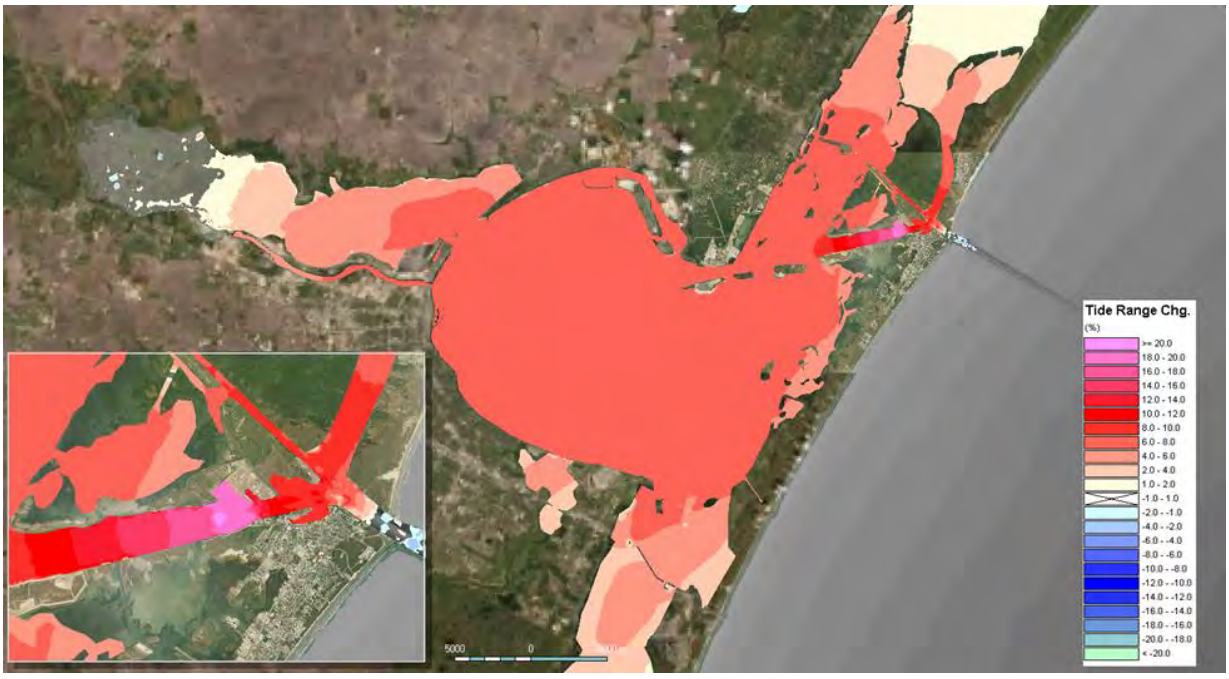

Figure 4.12: Percentage of tide range increase caused by FWP for Period 2

The predicted increase in tidal range due to the FWP is consistent with the hydrodynamic analysis from the 2007 Moffatt & Nichol report "*Matagorda Ship Channel Improvement Project, Point Comfort, Texas*". Located approximately 100 km northeast of Corpus Christi, the project features deepening the Matagorda Ship Channel from 38 ft Mean Low Tide (MLT) to 44-46 ft MLT and double widening the channel width. MIKE3 modeling predicted that the tidal range in Matagorda Bay would be increased by about 20% as a result of the channel deepening and widening.

4.3 Impact to Current Speed

Figure 4.13 presents the impact of the FWP on depth-averaged current speed as compared to the FWOP in Period 2. Similar plots of the depth-averaged speed change in Period 1 and Period 3 are provided in Appendix B.2. The change of current speeds on the water surface and at the depths of -5 m and -10 m NAVD88 are also plotted, which shows the similar patterns in the current speed change as observed in the depth-averaged current speed change. These plots are also attached in Appendix B.2. Table 4.5 lists the summary of depth-averaged speed change caused by the FWP at the selected stations in all three periods.

Overall, the impact of FWP on the current speed is limited to the proposed dredge areas and the navigation channel extending about 15 km to Port Ingleside from the proposed dredge area near Port Aransas. There is no significant impact on currents in Corpus Christi Bay, Redfish Bay, and Nueces Bay. The model predicted that the FWP would reduce current speeds through the proposed dredge area, which results from deepening the navigation channel. The mean current speed at Aransas Pass is reduced by about 7 cm/s on average and up to 19 cm/s as a maximum. The current speed increases in the Corpus Christi Channel from Port Aransas to Port Ingleside where the water depth remains unchanged. The current speed at the inner channel near Port Aransas increases about 3 to 4 cm/s, up to 11 cm/s. Increases in current speed may raise navigation concerns and the current speed change may result in local morphological change.

Figure 4.13: The change of depth-averaged speed caused by the FWP in for Period 2

Table 4.5: Change of depth averaged speed caused by the FWP at the selected locations

Station	Flow Speed Change (cm/s)			Percentage
	Mean	Minimum	Maximum	
Outer Channel	-1.6	-18.5	12.6	-17%
Aransas Pass	-6.5	-18.7	8.8	-14%
Inner Channel	2.9	-5.8	10.5	8%
Redfish Bay	0.0	-0.6	0.6	1%
Corpus Christi Bay	0.1	-0.3	0.4	3%
USS Lexington	0.0	-0.4	0.5	0%
Nueces Bay	0.1	-0.9	0.9	2%
Packery Channel	0.1	0.0	0.2	0%
Rockport	0.0	-0.2	0.2	0%

To better illustrate the impact of FWP on tidal range and current speed, four cross-sections in the navigation channels around the inner basin are selected as shown in Figure 4.14. Using the hourly model outputs, the wet cross-section area, total discharge, and cross-section averaged speed are calculated. Figure 4.15 demonstrates how the percentage of discharge change from the hourly discharge results is determined. The plot shows the comparison of calculated discharge passing through Aransas Pass (cross-section A) between FWOP (referred to x-axis) and FWP (referred to y-axis) in Period 2. The percentage change of discharge caused by the FWP is then determined by the slope of the fitting line minus one. The plot shows the increase of discharge through Aransas Pass during both flood tides (negative discharge) and ebb tides (positive discharge) constantly.

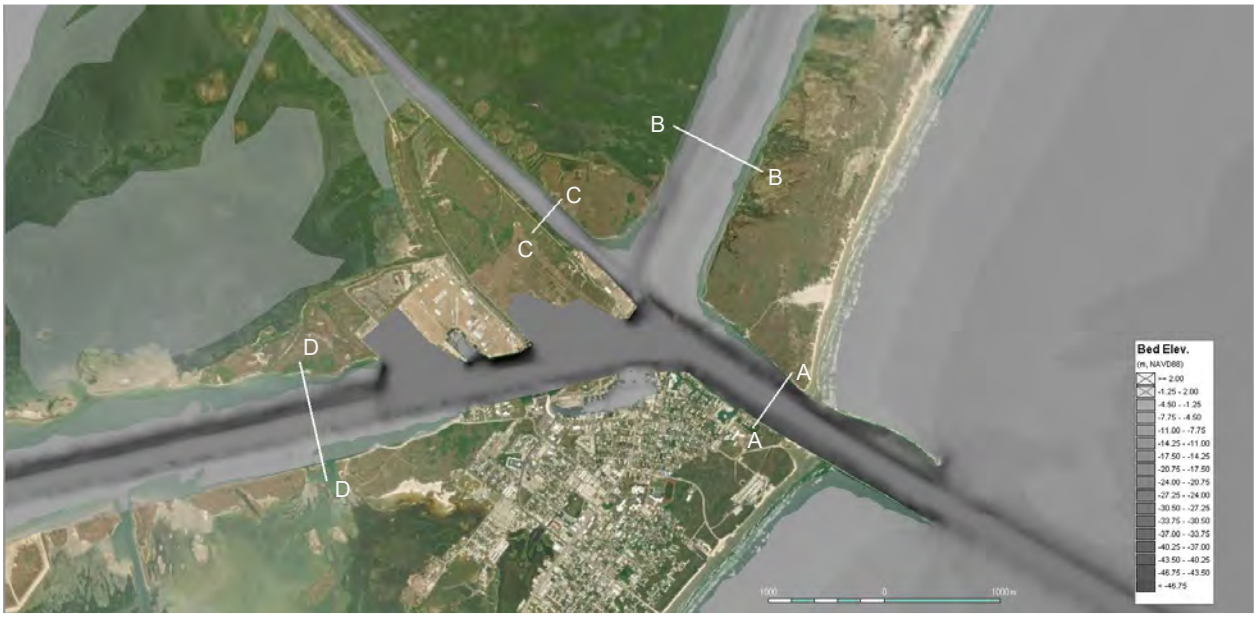

Figure 4.14: Locations of cross-sections to calculate discharge

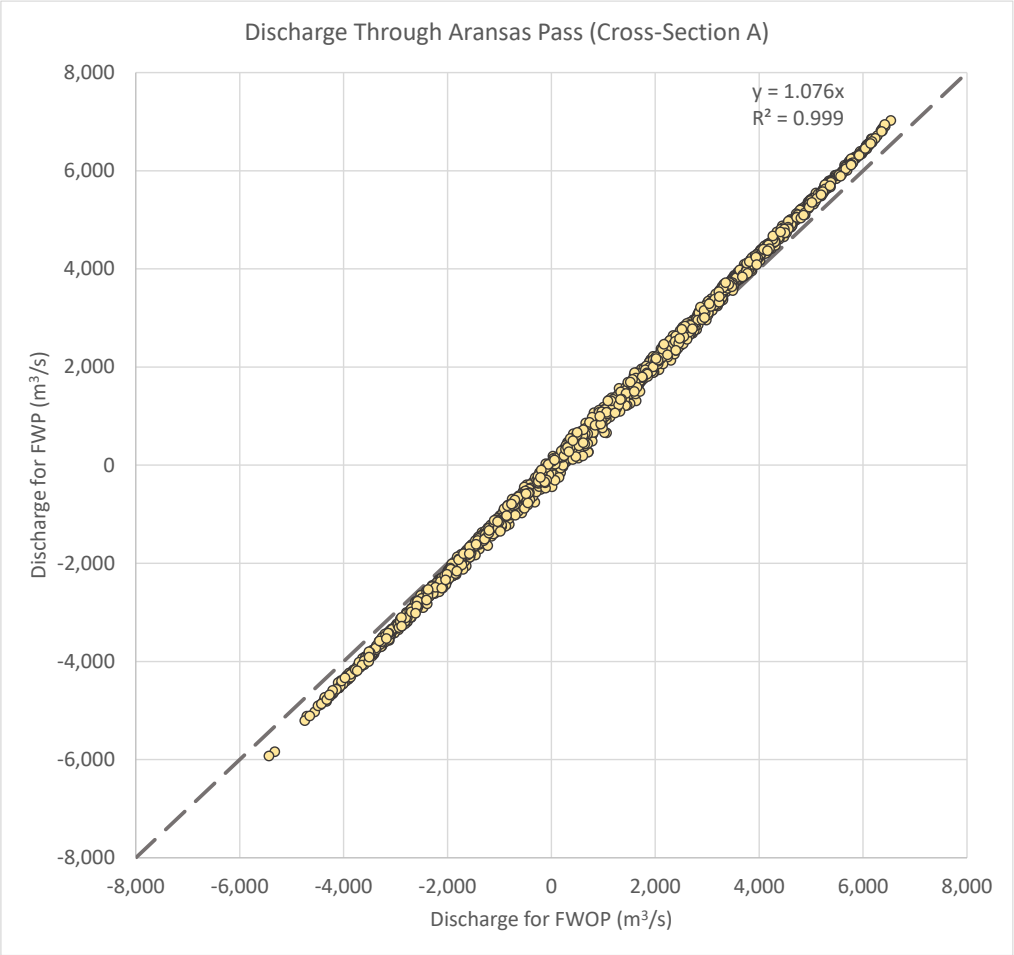

Figure 4.15: Comparison of discharge between FWOP and FWP along Cross-Section A-A in for Period 2

Table 4.6 lists the percentage of changes in cross-section area, cross-section averaged current speed, discharge, and net flow caused by the FWP, which are averaged from all three model runs for all three periods. Aransas Pass is the primary outlet of the bays to the GOM. Figure 4.16 shows the discharge variations through these four cross-sections in both FWOP and FWP scenarios and provides the flow distribution in these three branches connected to Aransas Pass. The peak flow discharge in the pass is about 6,000 m^3/s in normal conditions and could reach more than 9,000 m^3/s during storms.

Deepening the navigation channel in Aransas Pass significantly increases the cross-sectional wet area, which is about 20%. This results in the increase of conveyance capacity in the pass. As a result, tidal exchange between the bays and the GOM significantly increases. The model predicts that the discharge through the pass increases by about 8% although the cross-section averaged speed reduces about 10% due to water depth increase.

In response to the discharge increase in Aransas Pass, the discharges increase about 3% to Aransas Bay and Redfish Bay and about 8% to Corpus Christi Bay after the construction of the FWP. As the result, the tidal range and current speeds in the navigation channels to these bays increases accordingly because the cross-

sections to Aransas Bay (B-B), Redfish Bay (C-C), and Corpus Christ Bay (D-D) remain unchanged after the FWP.

The net flow, which is the net water volume through the cross-sections in the simulation periods, decreases at the cross-section to Redfish Bay but increase at the cross-section to Corpus Christi Bay. This indicates that there is an increase in net flow from Redfish Bay to Corpus Christi Bay after the FWP construction.

Table 4.6: Percentage changes of area, discharge, and net flow caused by FWP in four cross-sections around the inner basin

Cross-Section	A-A	B-B	C-C	D-D
Connected Bay	Aransas Pass	To Aransas Bay	To Redfish Bay	To Corpus Christi Bay
Area	20%	0%	0%	0%
Speed	-10%	3%	3%	9%
Discharge	8%	3%	3%	8%
Net Flow	2%	0%	-3%	5%

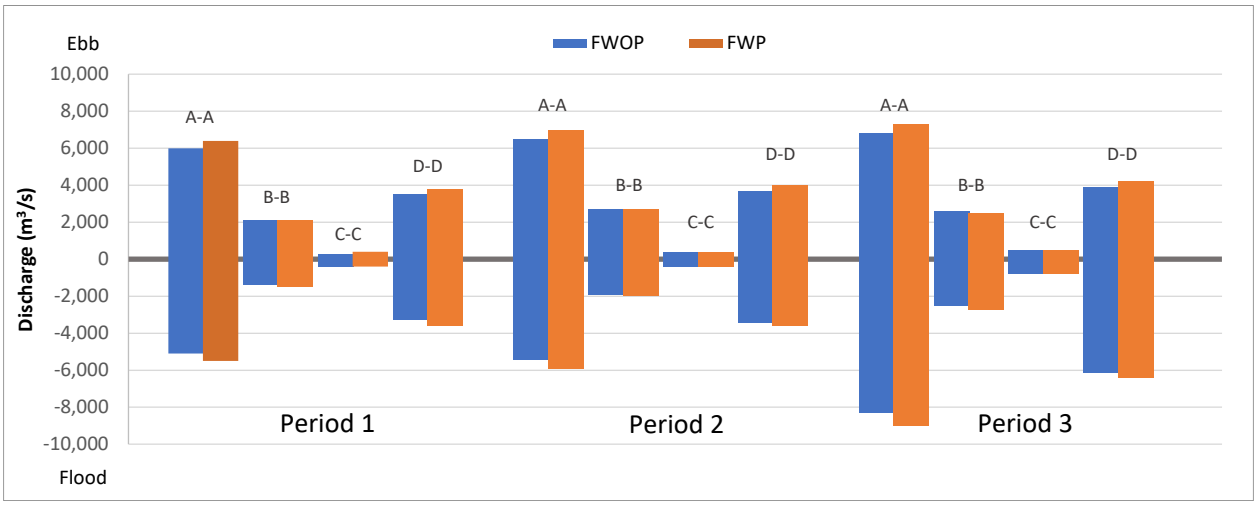

Figure 4.16: Comparison of discharge variation through four cross-sections between FWOP and FWP in three modeling periods

4.4 Impact to Salinity

The impact of FWP on salinity was assessed by comparing the salinity predicted in the FWP scenario with the salinity predicted in the FWOP scenario in time and 3D space. The salinity change caused by the FWP was calculated as the difference of salinity predicted by the FWP and FWOP. The model results show that the salinity change are similar in the vertical column. To better understand the impact, a statistical analysis on the salinity change was performed for all time steps and all layers in the 3D model mesh. Figure 4.17 shows the salinity change averaged over time and water column during Period 2. The average change in salinity caused by FWP is very small. Figure 4.18 shows the range of salinity change, which was calculated as the maximum

salinity change minus the minimum salinity change. It indicates that the FWP may cause some disturbing change in salinity of less than ±3 PSU in the proposed dredge area and the connected navigation channels. Note that the large range of salinity change in the very shallow water (generally at a few inches water depth) likely results from the wetting and drying process in the model (i.e., the cell may be dry in one model run but the cell is wet in the other model run). Table 4.7 lists the average salinity change, minimum and maximum, and percentage at the selected stations. It is concluded that the FWP is unlikely to cause significant impact on salinity in these bays.

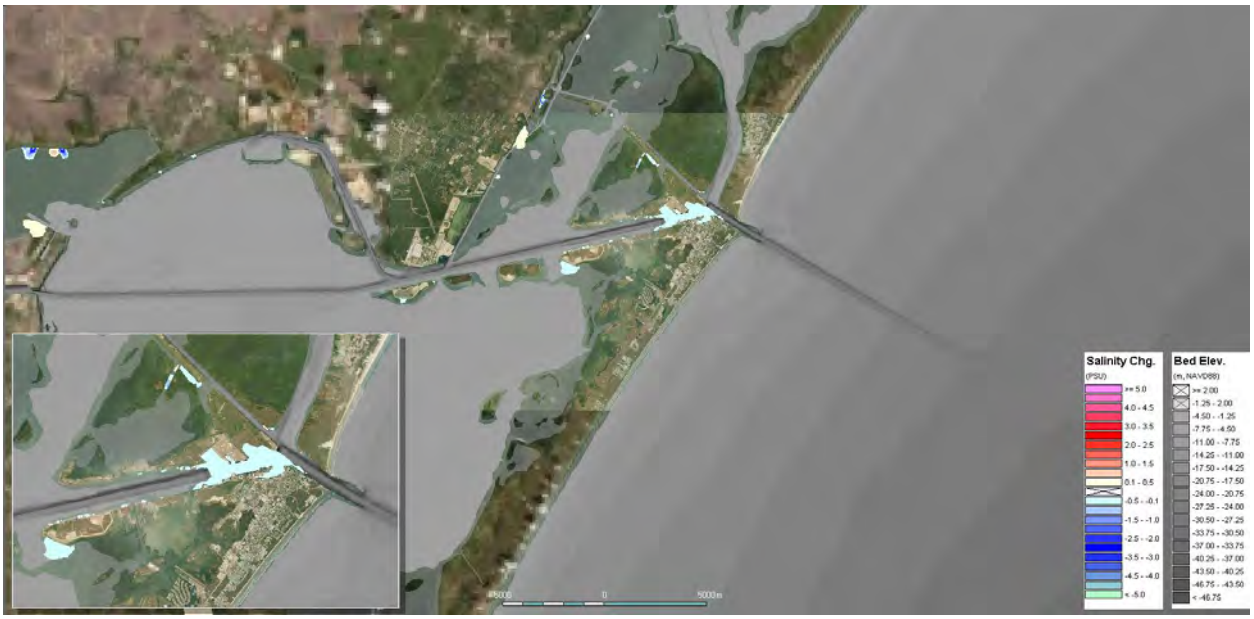

Figure 4.17: Average salinity change caused by FWP in Period 2

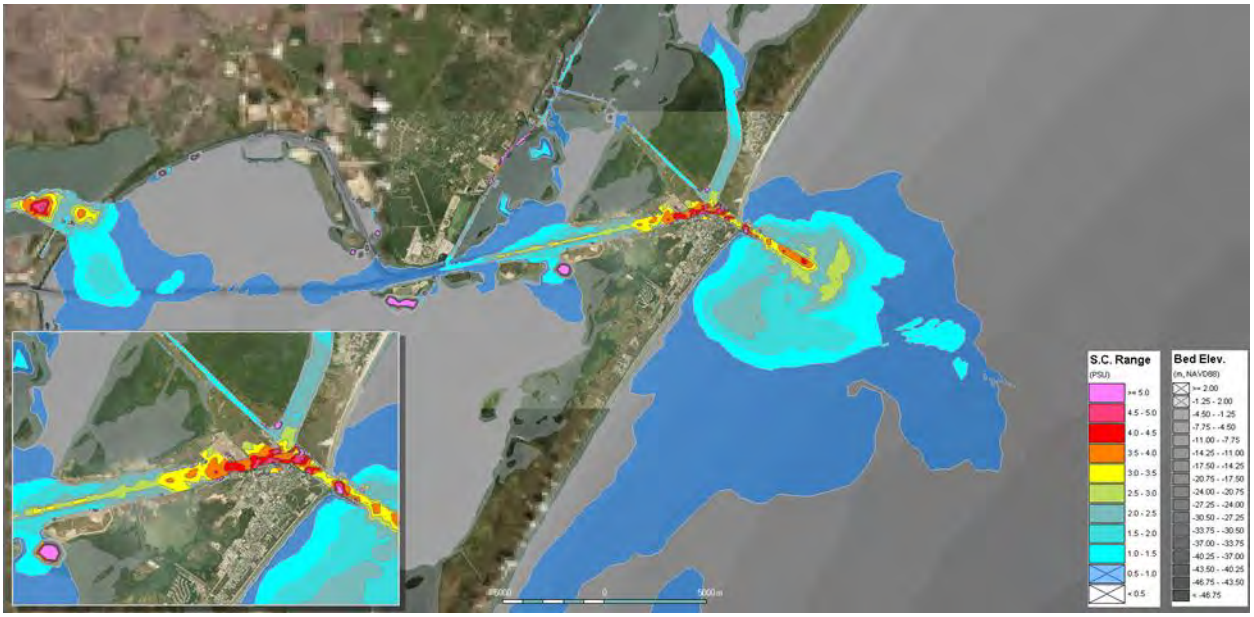

Figure 4.18: Range of salinity change (max change minus min change) caused by FWP in Period 2.

Table 4.7: Change of salinity caused by FWP at the selected stations in comparing with FWOP

Station	Salinity Change (PSU)			Percentage
	Mean	Minimum	Maximum	
Outer Channel	0.0	-1.1	1.9	0.0%
Aransas Pass	-0.1	-3.0	2.2	-0.2%
Inner Channel	-0.1	-2.7	1.2	-0.2%
Redfish Bay	0.0	-0.2	0.2	0.0%
Corpus Christi Bay	0.0	-0.1	0.1	0.0%
USS Lexington	0.0	-0.3	0.1	0.0%
Nueces Bay	0.0	-0.4	0.3	0.0%
Packery Channel	0.0	-0.2	0.1	-0.1%
Rockport	0.0	-0.1	0.1	0.0%

4.5 Long-term Impact Assessment

The above-mentioned impact assessment was based on the model runs in the selected three-month periods. Three-month simulation may be insufficient to cover the full ranges of tide fluctuation and the seasonal variations of meteorological-oceanographic conditions in the Gulf of Mexico. Three long-term model runs with the simulation period of one year were carried out to verify and extend the impact assessment for the scenarios of the existing condition (EC), FWOP, and FWP. The sensitivity tests indicate that the 2D model produces the results similar to the 3D model in term of depth average currents/salinity and water levels (see Section 3.4.3). Instead using the 3D version of MIKE3 (hereafter refer to the short-term 3D model), a 2D depth-average model of MIKE21 (hereafter refer to the long-term 2D model) was used to reduce the computational time. The simulation period is selected from June 1, 2018 to June 1, 2019, which includes Period 1 and Period 2 selected for the 3D model calibrations (see Section 3.3) and the production runs (see Section 4.1). All model settings, including grid, open boundary conditions, and model parameters, are the same as these used in the short-term 3D model, except the bathymetry. The 2D model outputs water level, flow velocity, and salinity in one-hour interval. This section documents the impacts of FWP compared with FWOP from the long-term 2D model results.

4.5.1 Impacts to Water Levels

By using the same methodology as the 3D model, tide harmonic analysis on the hourly outputs of water levels from the long-term 2D model was carried out. Figure 4.19 shows the QQ plots of tide amplitudes for 26 major tide constituents predicted for the FWOP (shown in x-axis) and the FWP (shown in y-axis) at Inner Channel (approximately Channel Stationing +100+00) and Corpus Christi Bay (see locations in Figure 4.4). The QQ plots for other stations are attached in Appendix B. The percentage of tide amplitude increase is calculated as the subtraction of one from the slope of the fitting lines, which are listed in Table 4.8. The results show that the impacts of the FWP on tide amplitudes predicted by the long-term 2D model are consistent to that predicted by the short-term 3D model. The largest increase of tidal amplitudes occurs at the inner channel near Port Aransas (approximate Channel Stationing +100+00), which is an increase of approximately 15%. The increases in tidal amplitudes are approximately 10% in Redfish Bay, 9% in Corpus Christi Bay, 7% in Nueces

Bay, and 3% at Rockport. There is no significant change in tidal amplitudes in Aransas Pass and the outer channel.

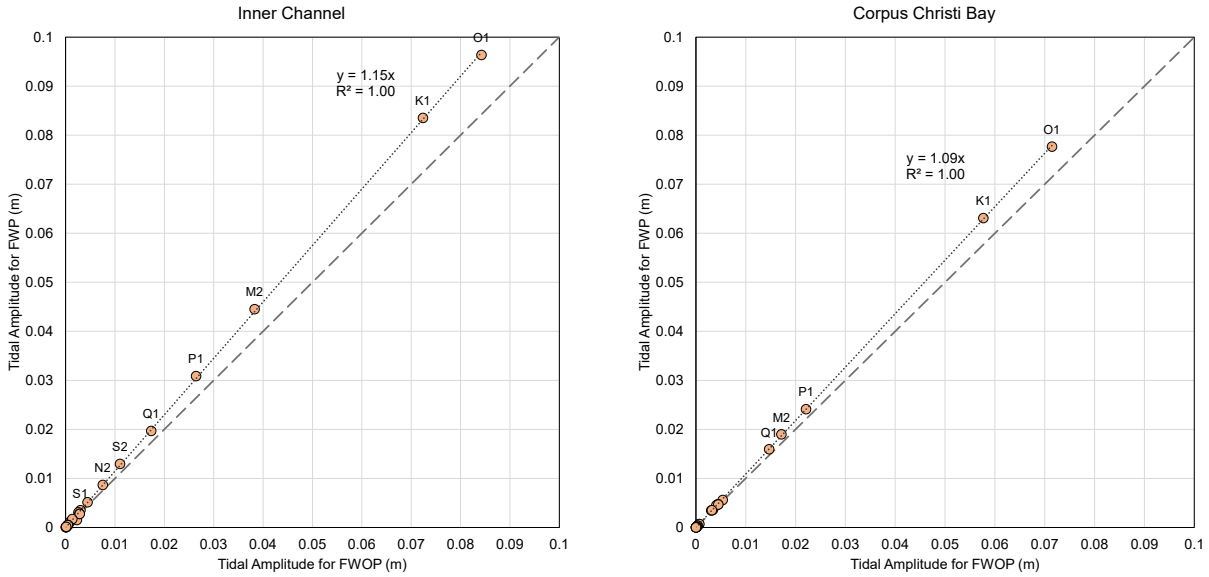

Figure 4.19: Increase of tidal amplitudes for FWP compared to FWOP in Inner Channel (left) and Corpus Christi Bay (right)

Tide ranges are also calculated from the hourly 2D model outputs. Figure 4.20 shows the average tidal range change in centimeters based on the long-term 2D model results. Table 4.8 lists the average tidal range increase with the minimum and maximum values predicted by the long-term 2D model. The model predicted that the average increase of tidal range is approximately 3.5 cm at the inner channel near Port Aransas, ranging from -0.1 cm to 8 cm. The average tidal range increase at Corpus Christi Bay and Redfish Bay is less than 2 cm, ranging from -0.2 cm to 4 cm. The result is consistent to that found from the short-term 3D model.

To better understand the impact of tide range on water levels, the change of tide ranges was extracted and plotted in Figure 4.22. The location of the profile and channel stationing number are shown in Figure 4.21. The envelop and heat map represents the envelope and distribution of tide range change at these points along the navigation channel. The largest tide range increase is found in the channels from Stationing 0+00 to 300+00.

Table 4.8: Change in Tide Range and Tide Amplitudes for 26 Major Tide Constituents for FWP compared to FWOP

Stations	Tide Range Change				Increase of Tide Amplitude (%)
	Mean (cm)	Minimum (cm)	Maximum (cm)	Percentage (%)	
Outer Channel	0.0	-1.8	1.3	0%	0%
Aransas Pass	0.0	-1.4	1.7	0%	0%
Inner Channel	3.4	-0.1	7.9	13%	15%
Redfish Bay	1.8	-0.2	3.8	8%	10%
Corpus Christi Bay	1.8	-0.2	3.5	8%	9%

USS Lexington	1.8	-0.4	3.6	8%	9%
Nueces Bay	1.2	-0.6	2.7	6%	7%
Packery Channel	0.5	-0.7	1.6	6%	8%
Rockport	0.2	-0.3	0.6	1%	3%

Figure 4.20: Mean tide range change caused by the FWP relating to the FWOP

Figure 4.21: Longitudinal profile along the navigation channel to Corpus Christi Bay. The red dot is the location to which the channel stationing refers (positive channel stationing is the channel towards Corpus Christi Bay)

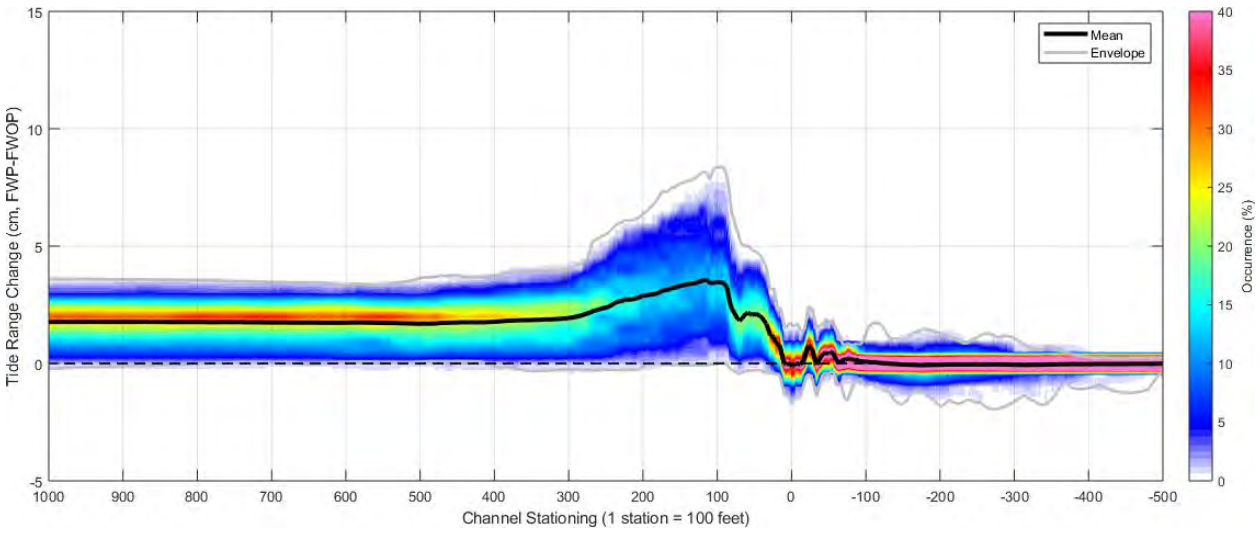

Figure 4.22: Tide range change caused by the FWP in comparing with the FWOP along the navigation channel. The thick black line represents the average change. The envelope enclosed by two grey lines represents the minimum and maximum changes found in the one-year model run. The heat map represents the distribution of the changes. Dash horizontal line represents no change

4.5.2 Impacts to Current Speed

The change in depth-average current speed comparing the FWP to the FWOP was calculated as from the long-term 2D model results. Statistical analysis for hourly current speed changes was also carried out. Figure 4.23 shows the mean change in depth-average current speed comparing the FWP to FWOP. The impact to the current speed predicted by the long-term 2D model is consistent with the short-term 3D model. The impact is focused along the proposed dredged areas and the navigation channel extending about 15 km to Port Ingleside from the proposed dredge area. There is no significant impact on currents in Corpus Christi Bay, Redfish Bay, and Nueces Bay. In average, the FWP will reduce current speeds through the proposed dredge area and increase the current speed in the Corpus Christi Channel from Port Aransas to Port Ingleside where the water depth remains unchanged.

Increases in current speed may affect navigation and modeled currents have been integrated into the vessel maneuvering simulations conducted for the project by others. Figure 4.24 shows the mean change in the depth-average current speed comparing the FWP to the FWOP. The envelope and heat map shown in the plot represents the minimum and maximum change to the current speed comparing the FWP to FWOP and their distribution. The large envelope in the outer channel (at approximate channel stationing -200+00) likely results from the eddy location change in that area where the currents from Aransas Pass meet with the Gulf longshore currents.

Figure 4.23: The change of depth-averaged speed caused by the FWP compared with the FWOP

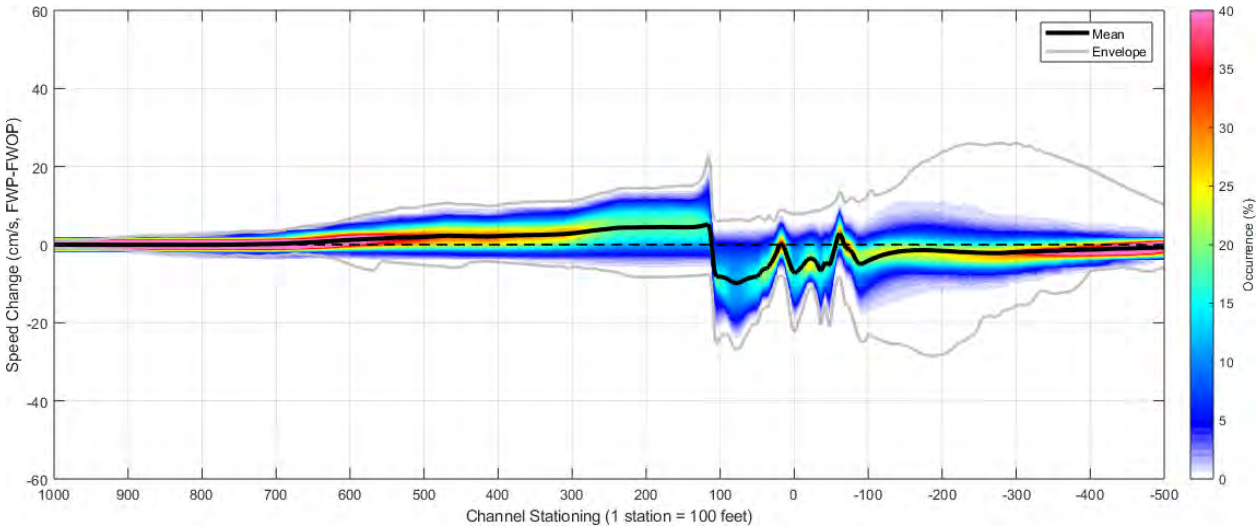

Figure 4.24: Depth-averaged current speed change caused by the FWP in comparing with the FWOP along the navigation channel. The thick black line represents the average change. The envelope enclosed by two grey lines represents the minimum and maximum changes found in the one-year model run. The heat map represents the distribution of the changes. Dash horizontal line represents no change

4.5.3 Impacts to Salinity

Like the findings from the short-term 3D model, the FWP would not cause significant salinity change on average (see Figure 4.25) but it may cause short term changes in the range of +/- 3 PSU in the proposed dredge area and the connected navigation channels (see Figure 4.26). Figure 4.27 shows the mean salinity change and the distribution of salinity changes along the navigation channel.

Figure 4.25: Average salinity change comparing FWP compared with the FWOP

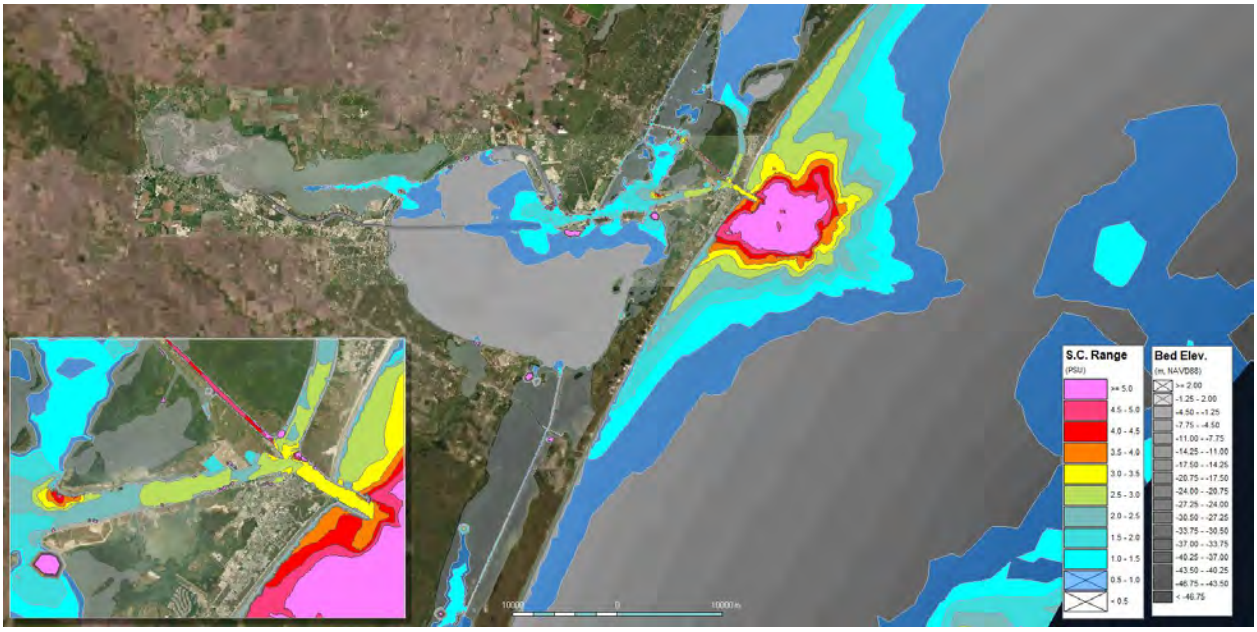

Figure 4.26: Range of salinity change (max change minus min change) comparing the FWP with the FWOP

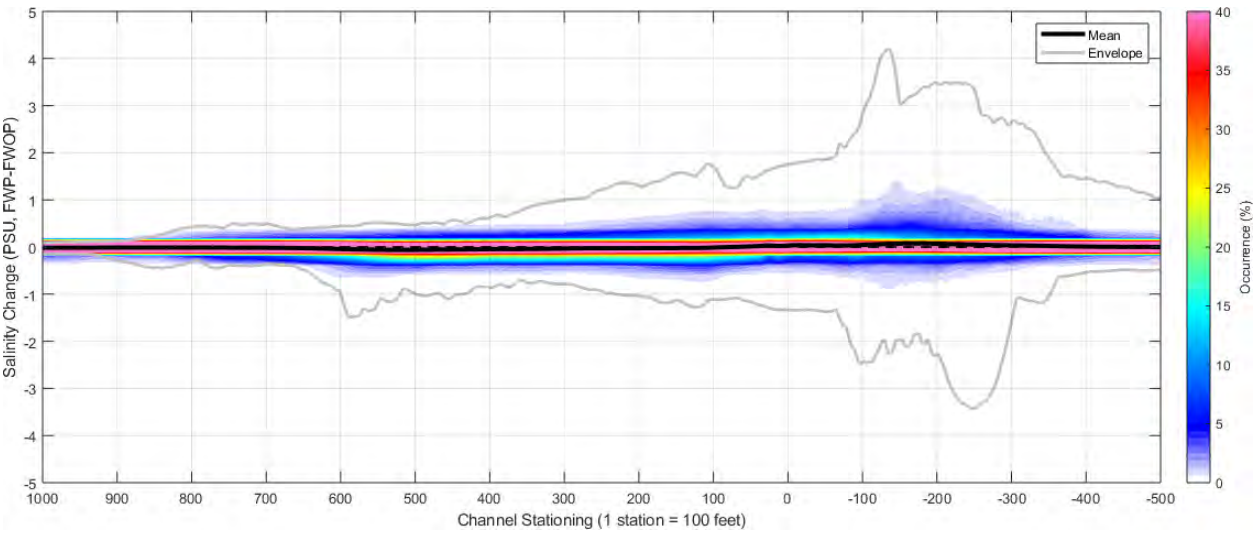

Figure 4.27: Depth-averaged salinity change caused by the FWP in comparing with the FWOP along the navigation channel. The thick black line represents the average change. The envelope enclosed by two grey lines represents the minimum and maximum changes found in the one-year model run. The heat map represents the distribution of the changes. Dash horizontal line represents no change

5. Impact Assessment for Future Without Project

The Future Without Project (FWOP) is currently in construction. The impacts caused by the FWOP were also evaluated to compare the results from the long-term 2D model with these for the existing conditions. The approaches used for impact assessment for FWP (see Section 4) were also used for this assessment.

5.1 Impacts to Water Levels

By comparing with the existing condition, the FWOP may cause a slight drop (less than 1 cm) in mean water level in the Corpus Christi Bay and its surround waters (see Figure 5.1), a small increase (less than 1 cm) on high tide (see Figure 5.2), and a slight drop on low tide (less than 2 cm) (see Figure 5.3).

Figure 5.1: Impact of FWOP on mean water levels compared with existing conditions

Figure 5.2: The average increase of high tide caused by FWOP compared with existing conditions

Figure 5.3: The average drop in low tide caused by FWOP compared with existing conditions

Through tide harmonic analysis, the impacts of the FWOP on tidal amplitudes at the two selected stations of Inner Channel (approximately Channel Stationing +100+00) and Corpus Christi Bay are shown in Figure 5.4. Similar plots for other selected stations are attached in Appendix C. Note that the slopes of the linear fitting lines (without intercept) shown in the plots indicates the degree of relative increase in tidal amplitude if the slopes are larger than one. The relative increases of tidal amplitudes calculated from the fitting lines are listed

in Table 5.1. This indicates that the FWOP could cause the tidal amplitude increases about 15% in Redfish Bay, about 16% in Corpus Christi Bay, and about 13% in Nueces Bay. There is no significant increase of tide amplitude at Rockport. The tidal amplitude at Inner Channel (Channel Stationing 100+00) has the greatest increase which is about 18%.

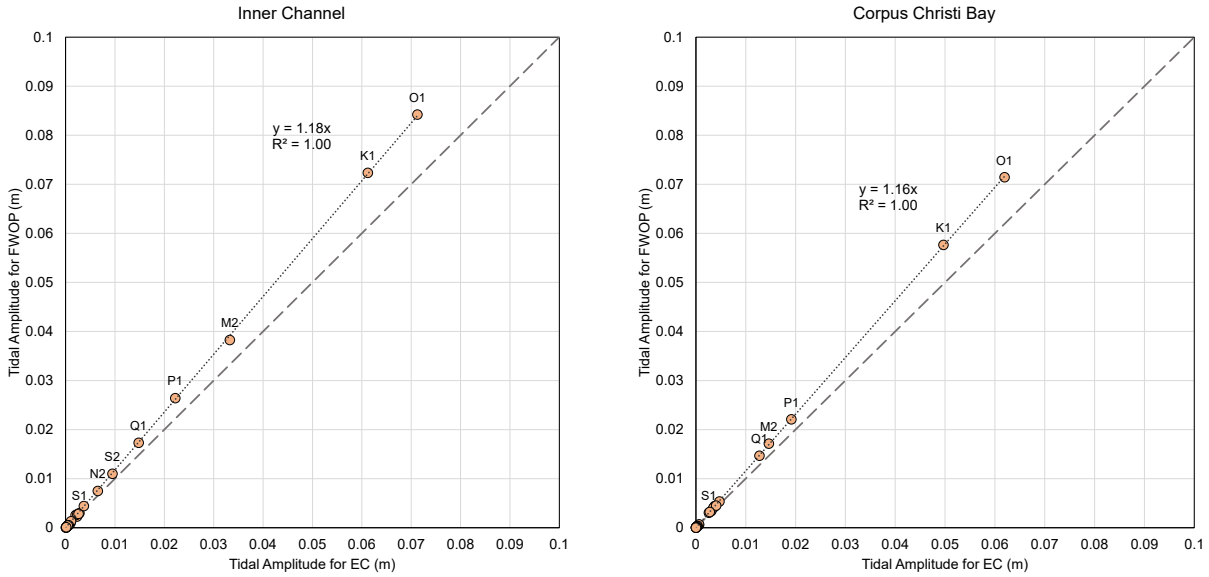

Figure 5.4: Increase of tidal amplitude caused by FWOP at Inner Channel and Corpus Christi Bay

To quantitively evaluate the impact of FWOP on tide range, the tide ranges were calculated from the hourly output of water levels produced by the one-year model runs and the statistical analysis on tide range changes were carried out. The results are shown in Figure 5.5 and listed Table 5.1. The FWOP results in approximately 3 cm increase in tide range in Corpus Christi Bay and its sounding areas but results in less impact on Rockport.

Table 5.1: Change of tide range and tidal amplitudes caused by the FWOP relating to the EC

Stations	Tide Range Change				Tidal Amplitude Increase (%)
	Mean (cm)	Minimum (cm)	Maximum (cm)	Percentage (%)	
Outer Channel	-0.1	-0.8	0.7	0%	0%
Aransas Pass	-0.4	-1.4	0.8	-1%	-1%
Inner Channel	3.4	-0.1	6.5	15%	18%
Redfish Bay	2.3	-0.4	4.4	12%	15%
Corpus Christi Bay	2.6	-0.7	4.7	14%	16%
USS Lexington	2.5	-0.7	4.7	13%	16%
Nueces Bay	1.8	-1.3	3.9	9%	13%
Packery Channel	0.8	-0.9	2.5	9%	14%
Rockport	0.0	-0.4	0.3	0%	1%

Figure 5.5: Average change of tide range caused by the FWOP in comparison of the existing condition

Figure 5.6 shows the average, the envelope, and distribution of tide range change comparing the FWOP to existing conditions along the navigation channel. It shows that most tide range increase is in the areas adjacent to the navigation channel from 100+00 to 300+00. There is slight decrease in Aransas Pass and no change in the outer channels beyond the jetties.

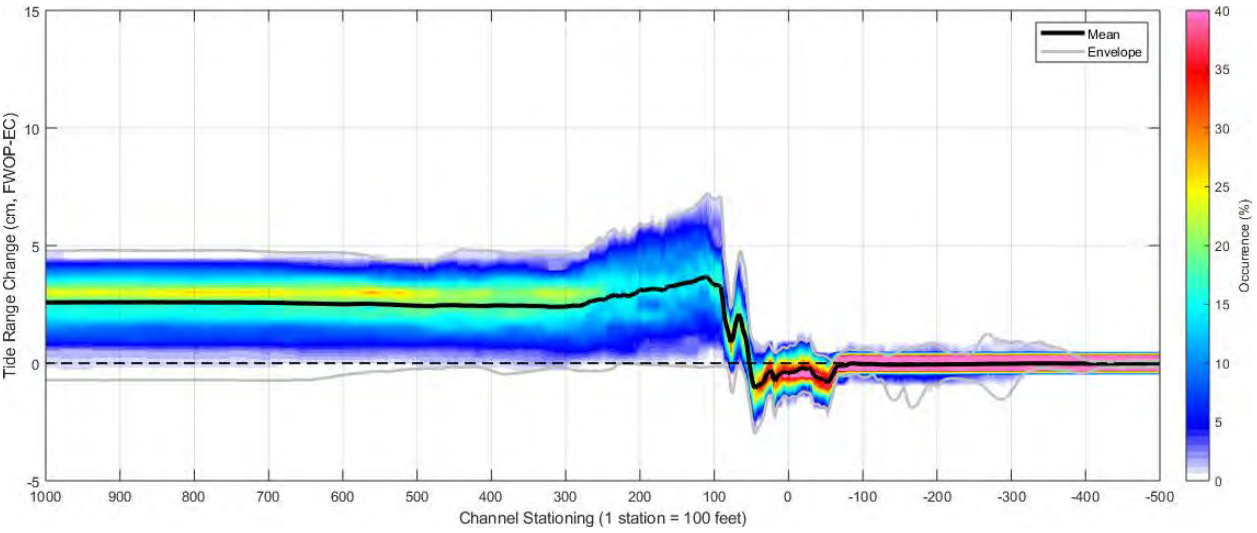

Figure 5.6: Tide range change caused by the FWOP in comparing with the existing conditions along the navigation channel. The thick black line represents the average change. The envelope enclosed by two grey lines represents the minimum and maximum changes found in the one-year model run. The heat map represents the distribution of the changes. Dash horizontal line represents no change

5.2 Impacts to Current Speed

Figure 5.7 shows the average change in depth-average current speed comparing the FWOP to the existing conditions. The current speed changes along the navigation channel are plotted in Figure 5.8. In the average, the FWOP could cause the flow velocity increases from Station +100+00 to the Corpus Christi Bay, but the speed decreases in the inner channel where there are two basins proposed. The flow velocity in Aransas Pass could slightly increase but no change is expected in the outer channel.

Figure 5.7: The change in depth-averaged speed comparing the FWOP with existing conditions

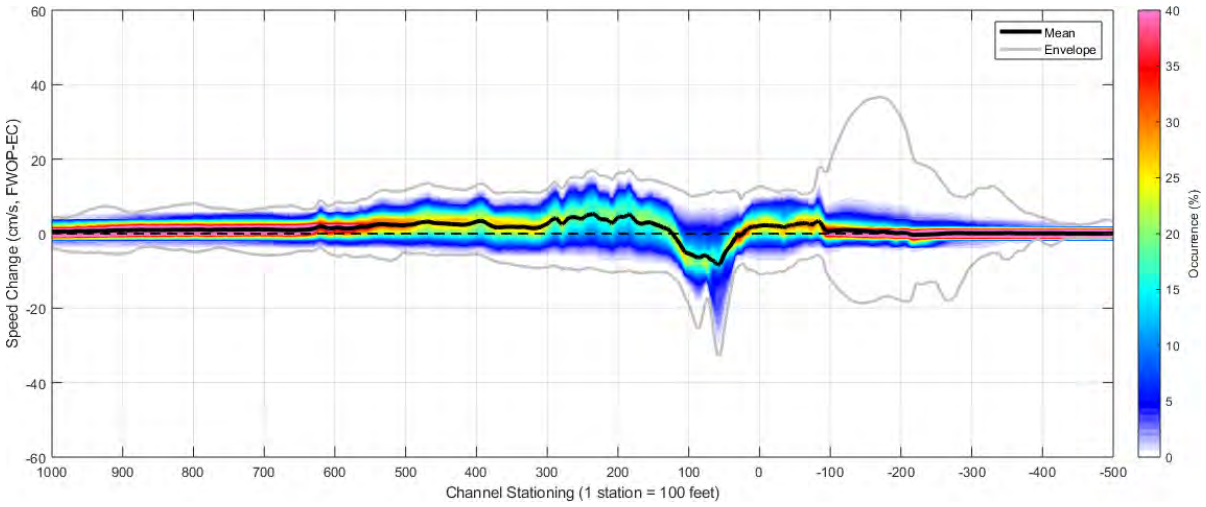

Figure 5.8: Depth-averaged current speed change caused by the FWOP in comparing with the existing conditions along the navigation channel. The thick black line represents the average change. The envelope enclosed by two grey lines represents the minimum and maximum changes found in the one-year model run. The heat map represents the distribution of the changes. Dash horizontal line represents no change

5.3 Impacts to Salinity

Figure 5.9 shows the mean of salinity change comparing the FWOP with existing conditions. It indicates that there is no significant salinity change. However, like the FWP, the FWOP could cause some short term change in salinity which is less than 3 PSU in the navigation channels and in the nearshore areas around the outer channel (see Figure 5.10). The profile of salinity change along the navigation channel are shown in Figure 5.11.

Figure 5.9: Average salinity change comparing FWOP with existing conditions

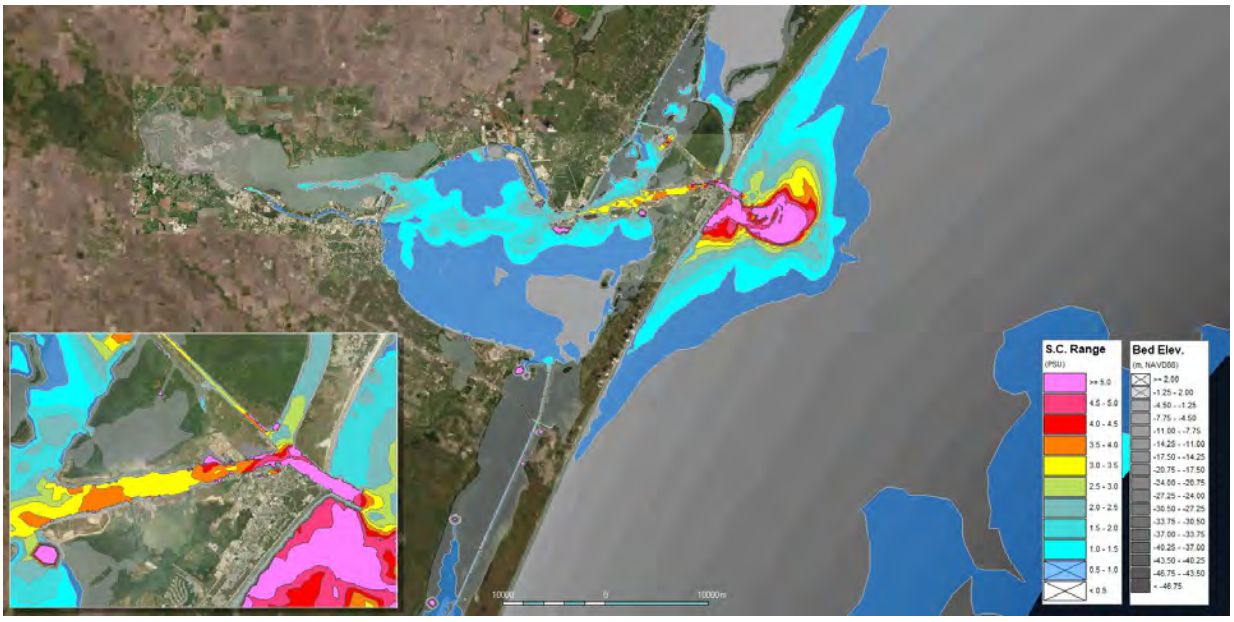

Figure 5.10: Range of salinity change (max change minus min change) comparing the FWOP with existing conditions

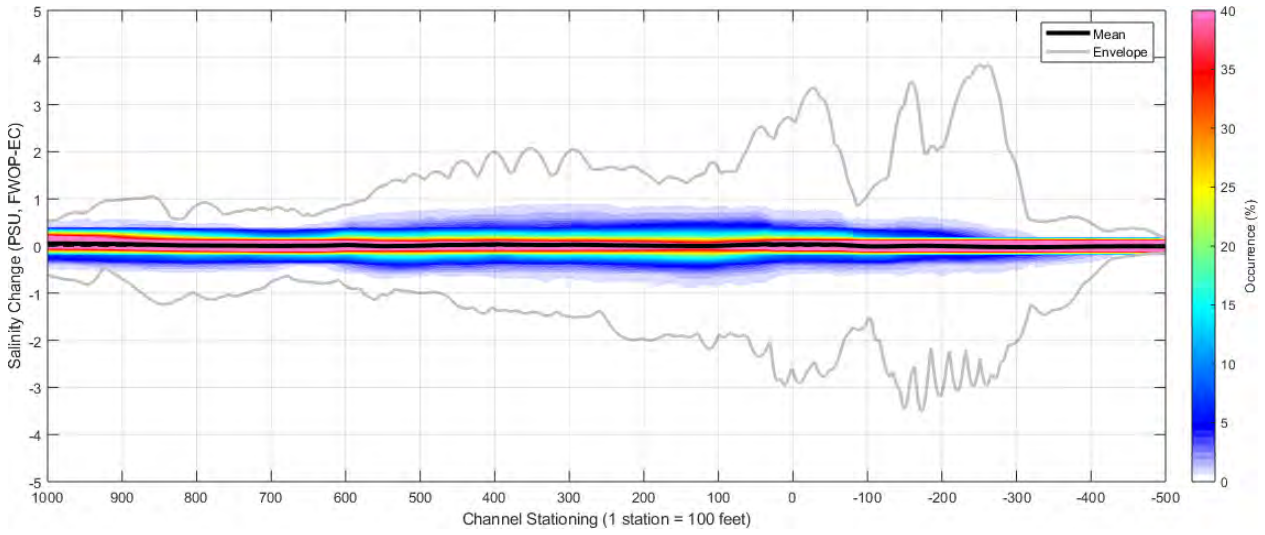

Figure 5.11: Depth-averaged salinity change caused by the FWOP in comparing with the existing conditions along the navigation channel. The thick black line represents the average change. The envelope enclosed by two grey lines represents the minimum and maximum changes found in the one-year model run. The heat map represents the distribution of the changes. Dash horizontal line represents no change

6. Cumulative Impacts for Future With Project

The impacts of FWP on tide range and current speed in the navigation channels could be accumulated from the two stages of channel deepening projects since these two projects (i.e., FWOP and FWP) have similar impacts on tide range and current speed, as described in Section 4 and Section 5. The impact can be assessed by comparing the model results for FWP with these for the existing conditions. The cumulative impacts may become significant.

Figure 6.1 shows the comparison of tide amplitudes for 26 major tide constituents predicted for the FWP and for the existing conditions at the inner channel and Corpus Christi Bay. The comparison plot of tide amplitudes for the other stations are attached in Appendix D. The tide amplitude increases about 36% at the inner channel and about 26% in Corpus Christi Bay. Table 6.1 shows the cumulative impacts of the FWP on tide range and tide amplitudes in comparing with the existing conditions at the selected stations. The cumulative impacts of the FWP to tide ranges along the navigation channels are shown Figure 6.2. The model results indicate that the cumulative impacts caused by the FWP is almost equal to the summary of the FWP impacts (*vs* FWOP) and the FWOP impacts (*vs* the existing condition). The greatest impact on tide ranges appears at the inner channel (Channel Stationing 100+00), where the tide range increases about 7 cm on average and about 14 cm in maximum. In Corpus Christi Bay and Redfish Bay, the tide range increases about 4 cm in average and 8 cm in maximum.

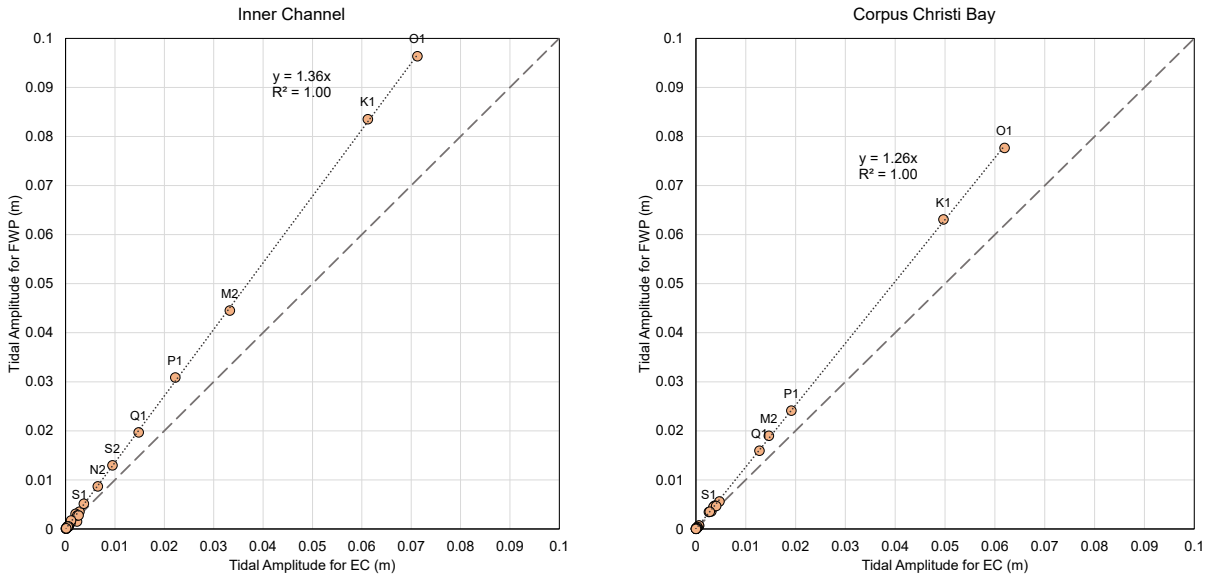

Figure 6.1: Cumulative increase of tidal amplitude caused by FWP in comparing with the existing conditions at Inner Channel and Corpus Christi Bay

Table 6.1: Cumulative impacts of FWP on tide range and tide amplitudes compared with the existing conditions

Stations	Tide Range Change				Tide Amplitude Increase (%)
	Mean (cm)	Minimum (cm)	Maximum (cm)	Percentage (%)	
Outer Channel	-0.1	-2.4	1.3	0%	0%
Aransas Pass	-0.4	-2.1	1.1	-1%	-1%
Inner Channel	6.8	0.6	14.1	29%	36%
Redfish Bay	4.1	-0.4	8.1	21%	27%
Corpus Christi Bay	4.3	-0.9	8.1	23%	26%
USS Lexington	4.3	-1.1	8.2	22%	26%
Nueces Bay	3.0	-1.8	6.6	15%	21%
Packery Channel	1.4	-1.5	4.1	15%	22%
Rockport	0.2	-0.4	0.8	2%	3%

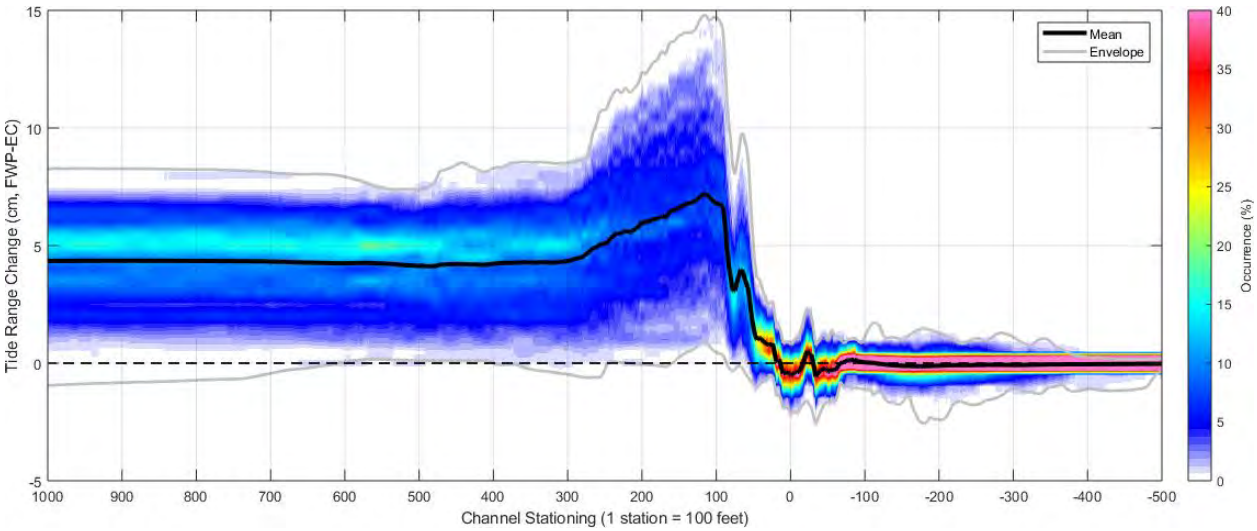

Figure 6.2: Tide range change caused by the FWP in comparing with the existing conditions along the navigation channel. The thick black line represents the average change. The envelope enclosed by two grey lines represents the minimum and maximum changes found in the one-year model run. The heat map represents the distribution of the changes. Dash horizontal line represents no change

Figure 6.3 shows the cumulative impact of the FWP on the depth-average current speed compared to existing conditions along the navigation channel. The greatest impact to the current speed appears around Channel Stationing 200+00. The depth-average current speed increases about 10 cm/s in average and about 30 cm/s in maximum. The current speed decreases about 18 cm/s in average and 50 cm/s in maximum in the proposed dredge basins in the channel segment from Channel Stationing 100+00 to 50+00. The flow speed in Aransas Pass to the gulf reduces slightly in average.

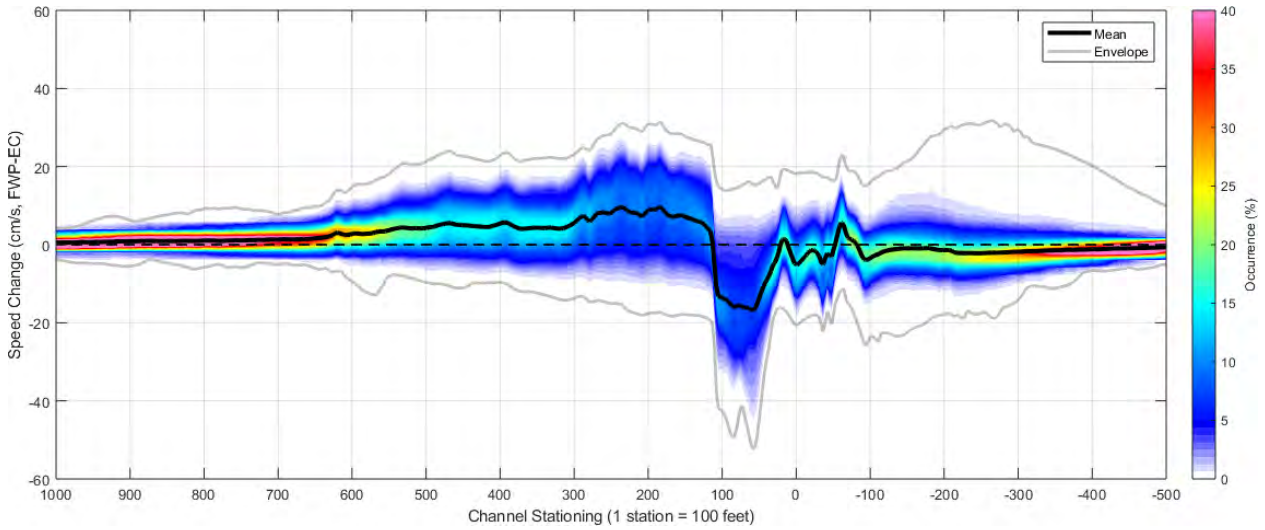

Figure 6.3: Depth-averaged current speed change caused by the FWP in comparing with the existing conditions along the navigation channel. The thick black line represents the average change. The envelope enclosed by two grey lines represents the minimum and maximum changes found in the one-year model run. The heat map represents the distribution of the changes. Dash horizontal line represents no change

Figure 6.4 shows the cumulative change of salinity caused by the FWP along the navigation channel. The average salinity change is insignificant (< 1 PSU). However, the range of salinity change, i.e., the instantaneous change of salinity over one year, is about +/- 4 PSU.

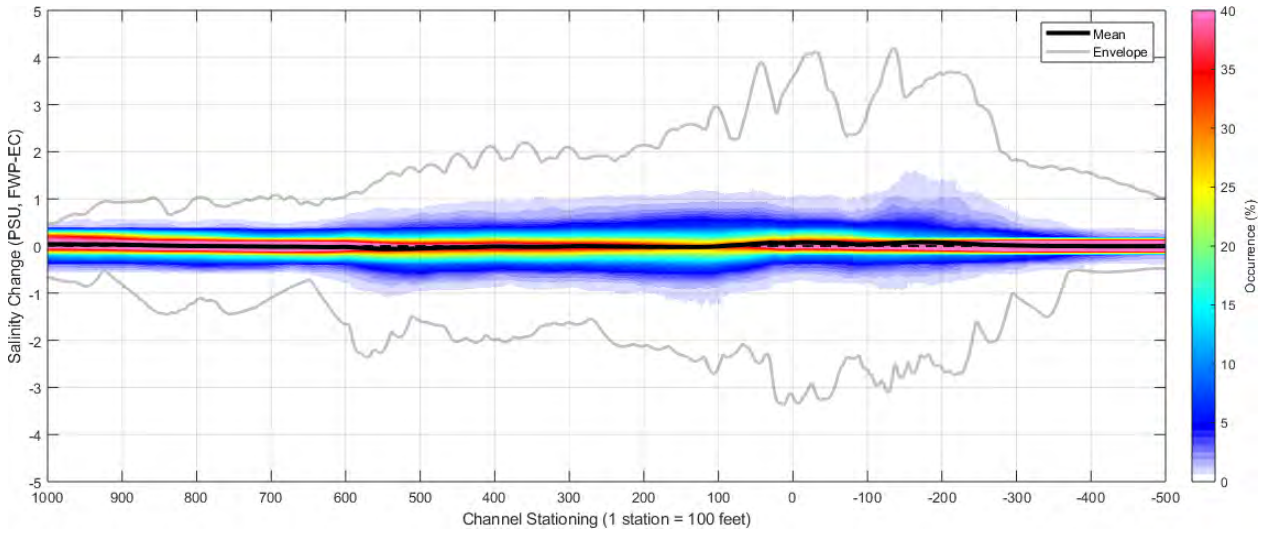

Figure 6.4: Depth-averaged salinity change caused by the FWP in comparing with the existing conditions along the navigation channel. The thick black line represents the average change. The envelope enclosed by two grey lines represents the minimum and maximum changes found in the one-year model run. The heat map represents the distribution of the changes. Dash horizontal line represents no change

7. Conclusions and Uncertainties

7.1 Conclusions

The following conclusions are made from this modeling assessment.

7.1.1 Impact on Water Levels

The impact of the Future With Project (FWP) scenario on water levels was assessed by comparing the model predicted water levels with the Future Without Project (FWOP) scenario. The findings are summarized below:

- The FWP is unlikely to cause changes to the mean water level in the subtropical secondary bays, which are connected to Aransas Pass, including Corpus Christi Bay, Nueces Bay, Redfish Bay, Packery Channel, and Aransas Bay. There is a slight reduction of less than one centimeter (cm), in mean water level in these bays;
- The FWP may increase tidal range in the subtropical secondary bays, depending on the distance from Aransas Pass. The model predicts increases in tidal range up to 2 cm in Corpus Christi Bay and Redfish Bay. The increase of tidal range decreases with the distance from Aransas Pass. The greatest impact on tidal range is limited in the Corpus Christi Navigation channel from Point Mustang to Humble Basin. The model predicts that the tidal range in this area increases about by 4 cm ranging from 0.3 cm to 9 cm;
- In the FWP, the tidal amplitudes of the selected tide constituents increase in the subtropical bays. The relative increases of tidal amplitudes are about 11% in Redfish Bay, 8% in Corpus Christi Bay, 7% in Nueces Bay, and less than 5% in Packery Channel and Aransas Bay. The greatest increase of tidal amplitudes (about 17%) is in the Corpus Christi Channel near Humble Basin;
- The FWP may cause a slight rise in high tide, which is less than 1 cm on average and at most 2 cm in the bays of interest. The rate of increase in high tide decreases with distance from Aransas Pass;
- The FWP may also cause a slight drop of low tide, which is less than 1 cm on average and 4 cm at maximum in the bays of interest connected to Aransas Pass. The amount of lowering of tides decreases with the distance from Aransas Pass;
- Overall, the impact of FWP on water level is insignificant. It is unlikely to increase the flood risk associated with changes in high tide or navigation risk associated with the changes in low tide and mean sea level in the Corpus Christi Bay. The impact on water level should be limited to the segment of the navigation channel from Point Mustang to Humble Basin.

7.1.2 Impact on Current Speeds

The impact of FWP on current speed was assessed by comparing current speeds in both FWP and FWOP scenarios in 3D space and the discharges at the selected cross-sections around the inner basin. The findings are summarized below:

- The impact of FWP on current speed in Corpus Christi Bay, Nueces Bay, Redfish Bay, Aransas Bay is insignificant. The change in current speed caused by the FWP is less than 1 cm/s;
- The FWP causes a reduction of the current speeds in the proposed dredge areas from Humble Basin to the outer channel in the GOM. The current speed in Aransas Pass reduces about 14% overall, ranging from -19 cm/s (reduction) to 9 cm/s (increase) with an average of -7 cm/s. This is a result of the deepened navigation channel, which increases the cross-sectional area in Aransas Pass by about 20%. The reduction of current speed may result in significant morphological change in the pass which is assessed in the other tasks;

- The FWP causes an increase in current speed in the navigation channels that connect to the Aransas Pass but will not be dredged in the FWP. The current speed in the Corpus Christi Navigation Channel near Humble Basin increases by 8%, which is about 3 cm/s on average and ranging from -6 cm/s to 11 cm/s. This likely results from the increase in discharge (about 8% increase) through the channel while the cross-section area remains unchanged. The increase in current speed reduces gradually from Humble Basin to Point Mustang.

7.1.3 Impact on Salinity

The impact of the FWP on salinity was assessed by comparing model predicted salinity in both FWP and FWOP scenarios in 3D space. The findings are summarized below:

- The FWP would not cause the significant change of salinity in the subtropical secondary bays. The average change of salinity caused by the FWP is less than 1 PSU;
- The FWP may result in a small disturbance change in salinity (about ±3 PSU) in the vicinity of the proposed dredged area;
- When the river flow in the Nueces River is large, the FWP may cause some small disturbance change in salinity (about ±3 PSU) at the outlet of Nueces Bay.

7.2 Uncertainties

The following uncertainties were found through this modeling analysis which are summarized below:

- A significant data gap for the model development is the bathymetry in Nueces Bay. There is limited bathymetric data for Nueces Bay. The bathymetry in Nueces Bay is important to calculate tide exchange between Nueces Bay and Corpus Christi Bay. This data gap was addressed by developing a model through constructing representative bathymetry of Nueces Bay based on available information to achieve good model calibration and validation;
- There is limited information on the amount of salt stored in Nueces Delta. The stored salt is a salt source for salinity in Nueces Bay. During a large rainfall event, these salts are dissolved by the rain and carried by the runoff to the bay. During a large river flow events that causes significant flooding in the delta, the flooding also dissolves the salt and results in a high salinity level in Nueces Bay. The model was developed to overcome this uncertainty by constructing the boundary conditions for salinity from Nueces River and Delta runoff based on the measured salinity data at SALT05 and NUDE3 stations (both are on the delta) to achieve a better salinity calibration in Nueces Bay;
- There is a large temporal data gap in the measured salinity data in Aransas Bay. The salinity at the open boundary of Aransas Bay has been identified to be a salinity source to Corpus Christi Bay. The model was developed to address this uncertainty by filling the data gaps using measured data on further northeast stations along the ICW (e.g., CHKN in San Antonio Bay);
- By comparing with measured data at TABS-D in the GOM, the HYCOM model significantly underpredicted the longshore current speed in the GOM. Since HYCOM model result was used for offshore boundary conditions in this model, the uncertainty may impact the model prediction of current speed at the outer channel.

8. References

AECOM (2019). Corpus Christi Ship Channel Deepening Project: Impacts to Tidal Flows in Corpus Christi Bay

Brown, C.A., G.A. Jackson and D.A. Brooks (2000). Particle Transport Through a Narrow Tidal Inlet Due to Tidal Forcing and Implications for Larval Transport. J. Geophys. Res. 105, 24141–24156.

Dawson, C. and Pothina, D. (2001). Hydrodynamic simulation of the Corpus Christi Bay Area Using QUODDY4, Part I. Universion of Texas at Austin

Dawson, C., Proft, J., and Aizinger, V. (2011). UTBEST3D Hydrodynamic Model Verification of Corpus Christi Bay. Technical Report for Texas Water Development Board

Freese and Nichols, Inc. (2020). *Data Gap Analysis, Corpus Christi Ship Channel Improvement Project Environmental Impact Statement,* Port of Corpus Christi Authority (Job No. PCA20166)

Islam, M.S., Bonner, J.S., Page, C., and Ojo, T.O. (2010). Integrated Real-Time Monitoring System to Investigate the Hypoxia in a Shallow Wind-Driven Bay. *Environ Monit Assess.* DOI 10.1007/s10661-010-1316-8

Li, Z. and Hodges, B.R. (2015). Modeling Salinity Fluxes in the Nueces Delta, Technical Report to TWDB

Linacre, E. (1977). A simple formula for estimating evaporation rates in various climates, using temperature data alone, *Environmental Science, Agricultural Meteorology*. DOI:10.1016/0002-1571(77)90007-3

Matsumoto, J., Austin, B., Paternostro, C., and Powell, G. (2001). Three-dimensional Modeling Study of the Corpus Christi Ship Channel Improvement Project: Preferred Plan. Technical Report, Texas Water Development Board (TWDB)

Moffatt & Nichol (2007). Matagorda Ship Channel Improvement Project, Point Comfort, Texas. Hydrodynamic and Salinity Model. Prepared for Calhoun County Navigation District. Revision 0.

Perales, Jerome, Gu, R., and Maidment, D.R. (2000). Developing a GIS-TxRR Model, Center for Research in Water Resources, University of Texas at Austin.

Schoenbaechler, C, Matsumoto J., Lu, Q.G, and Negusse, S (2011). TxBLEND Model Calibration and Validation for the Nueces Estuary. Technical Report

Schoenbaechler, Caimee, Guthrie, C.G., Lu, Q.G (2011). Coastal Hydrology for the Nueces Estuary: Hydrology for Version #TWDB201101 with Updates to Diversion and Return Data for 2000-2009. Texas Water Development Board.

TWDB. (1999). User's Manual for the Texas Water Development Board's Hydrodynamic and Salinity Model: TxBLEND. Texas Water Development Board, Austin, Texas

Ward, G.H. and Armstrong N.E. (1997). Ambient Water, Sediment and Tissue Quality of Corpus Christi Bay Study Area: Present Status and Historical Trends. Center for Research in Water Resources, The University of Texas at Austin.

Whilden, K.A. (2015). Investigation of Tidal Exchange and the Formation of Tidal Vortices at Aransas Pass, Texas, USA. *A Dissertation for Ph.D,* Texas A&M University

Williams, R.G., T.D. Bethem, G.W. French and H.R. Frey (1991). Corpus Christi Bay Current Prediction Quality Assurance Miniproject. NOAA Tech. Memo. NOS OMA 60. US Department of Commerce

Zhang, Y.J. (2008). Corpus Christi Bay Testbed, Technical Report, Oregon Health & Science University (OHSU).

Zhang, Y.J. (2010). Inter-model comparison for Corpus Christi Bay Testbed, Technical Report, Oregon Health & Science University (OHSU).

Appendix A

Calibration Figures

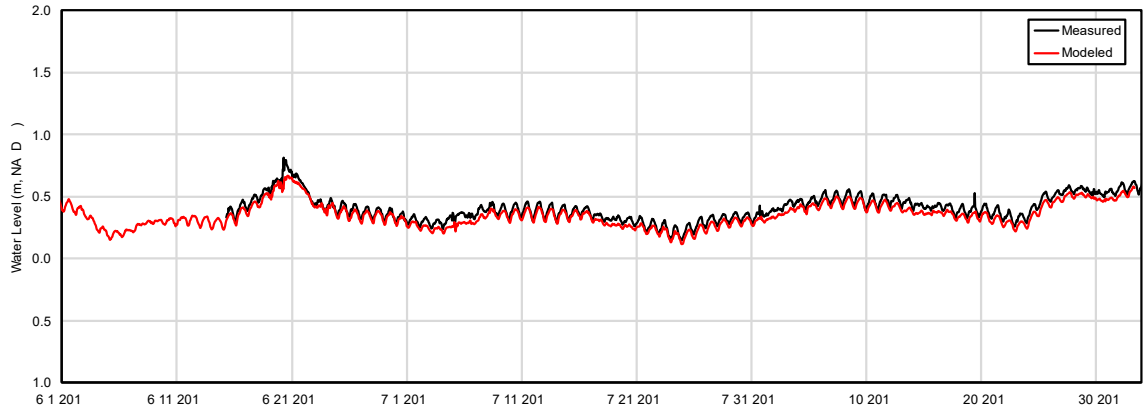

Figure A.1: Comparison of the model predicted water level (red) to the measured water level (black) at Rockport during Period 1

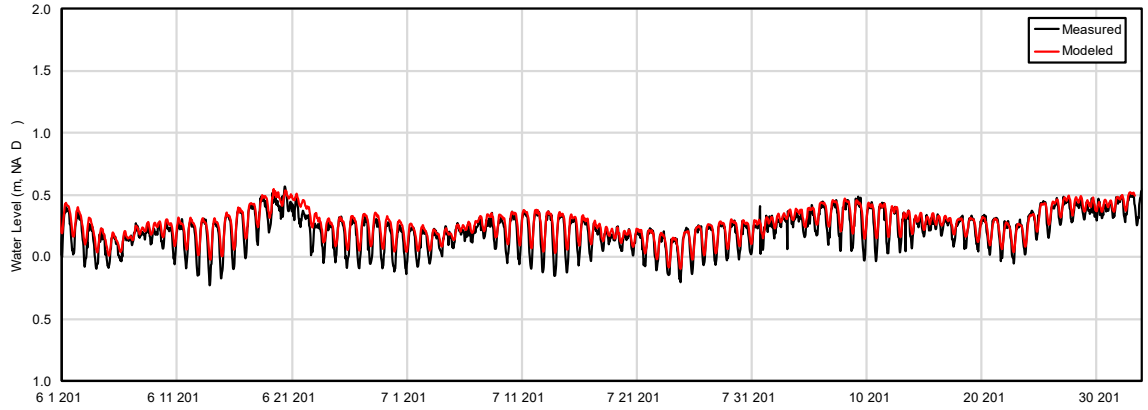

Figure A.2: Comparison of the model predicted water level (red) to the measured water level (black) at Port Aransas during Period 1

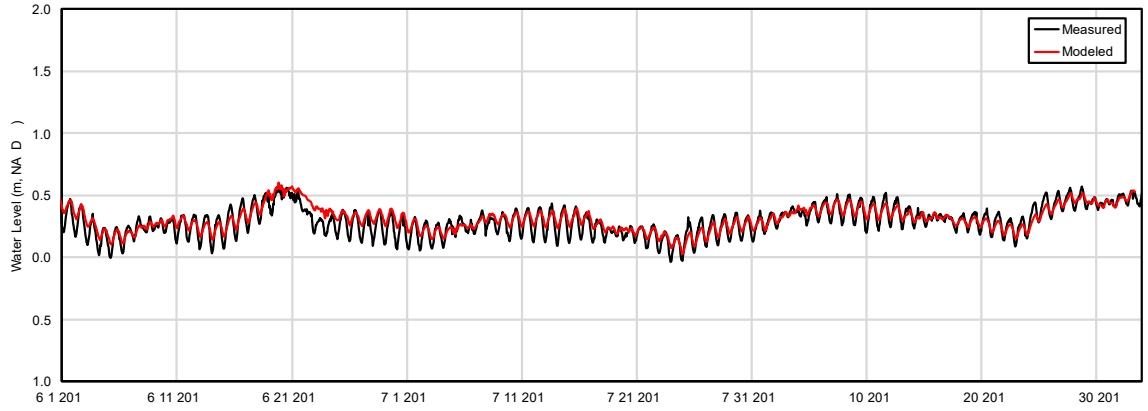

Figure A.3: Comparison of the model predicted water level (red) to the measured water level (black) at USS Lexington during Period 1

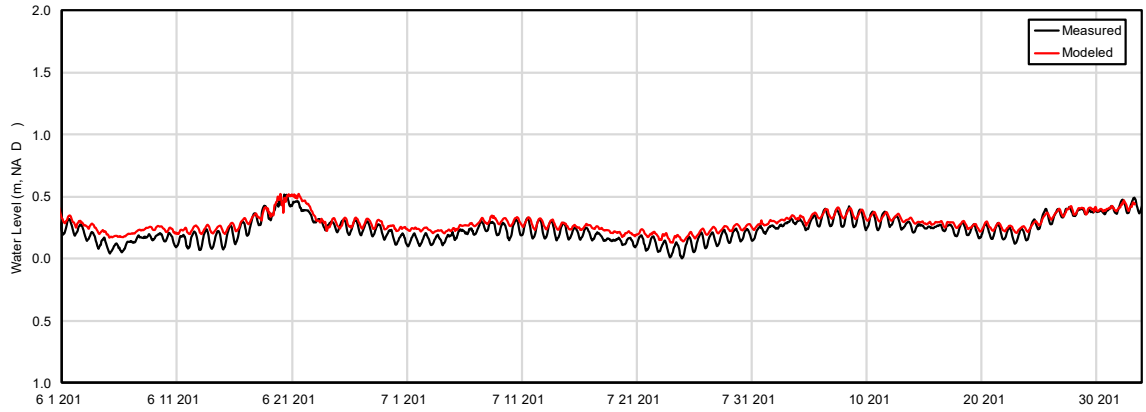

Figure A.4: Comparison of the model predicted water level (red) to the measured water level (black) at Packery Channel during Period 1

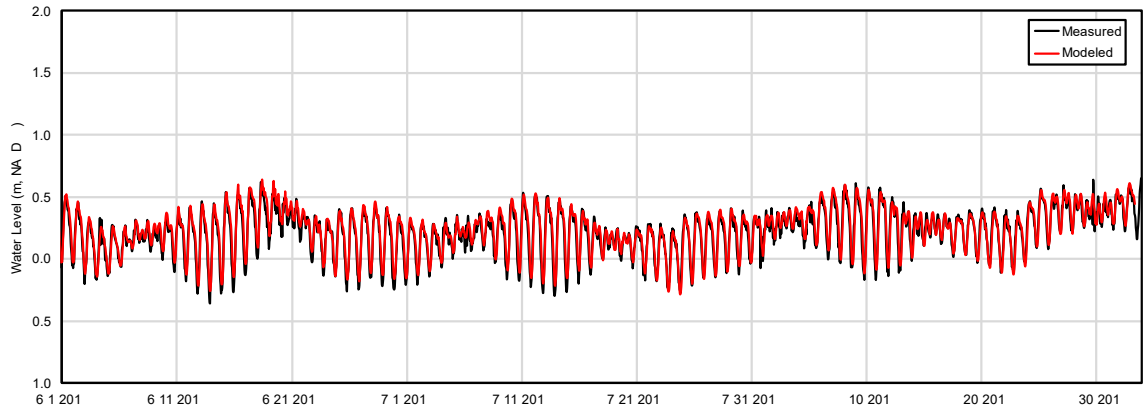

Figure A.5: Comparison of the model predicted water level (red) to the measured water level (black) at Bob Hall Pier during Period 1

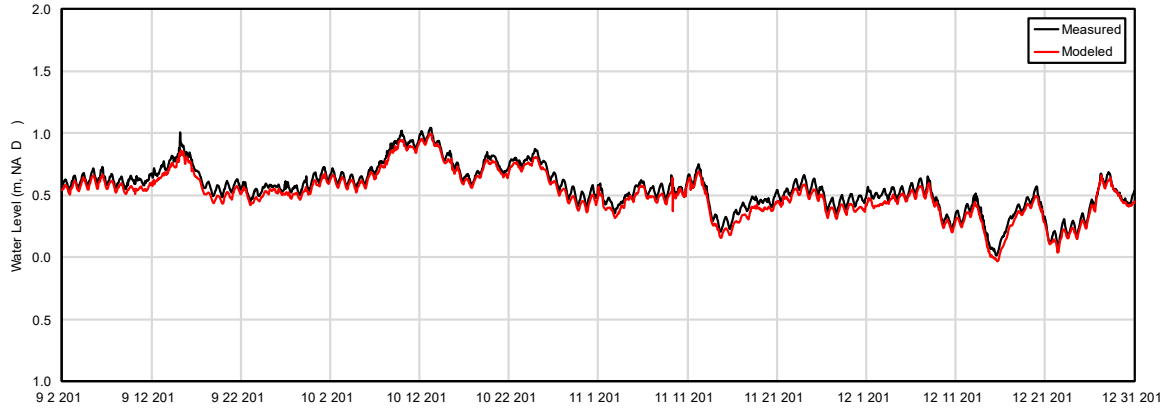

Figure A.6: Comparison of the model predicted water level (red) to the measured water level (black) at Rockport during Period 2

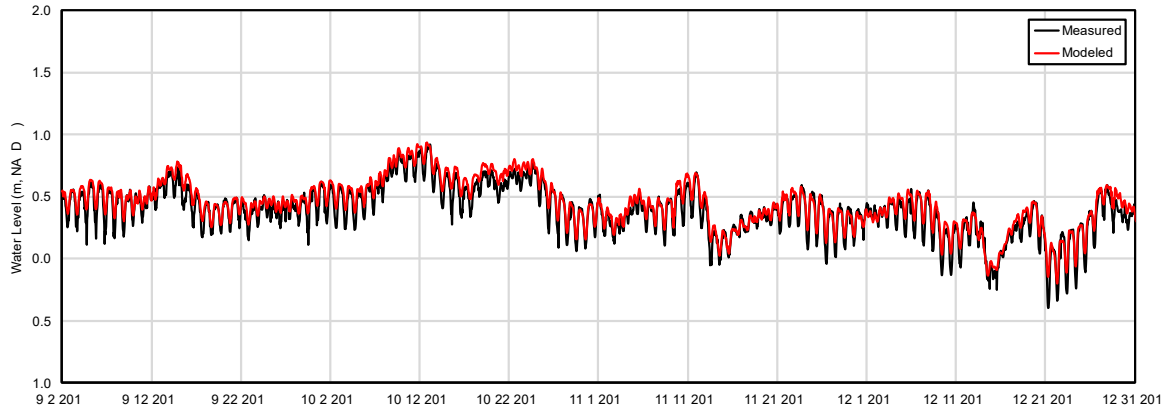

Figure A.7: Comparison of the model predicted water level (red) to the measured water level (black) at Port Aransas during Period 2

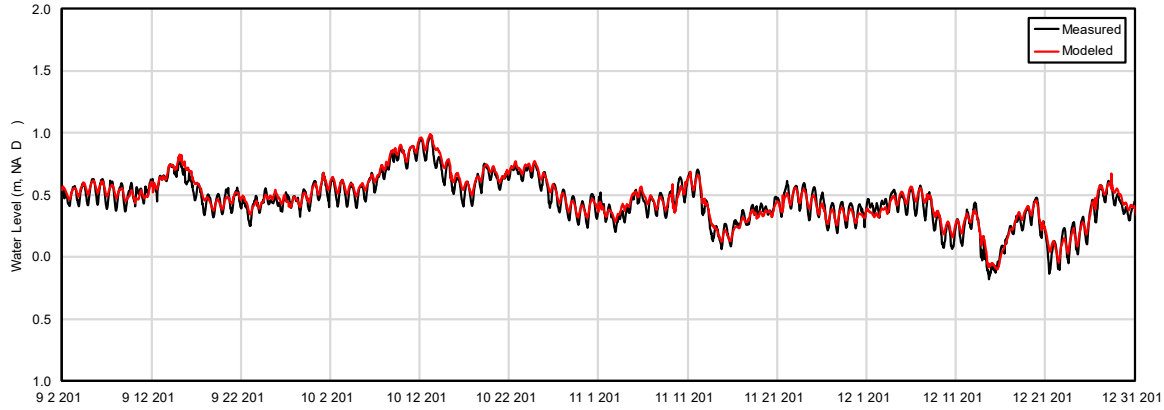

Figure A.8: Comparison of the model predicted water level (red) to the measured water level (black) at USS Lexington during Period 2

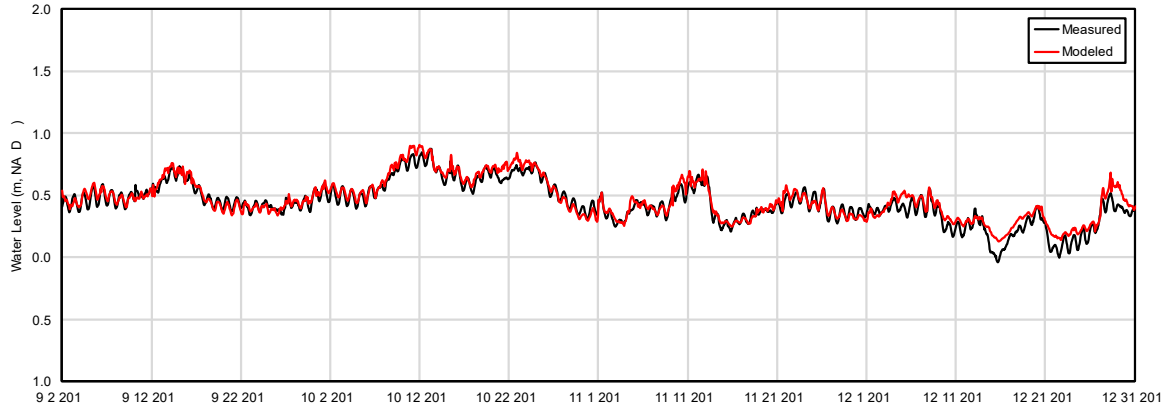

Figure A.9: Comparison of the model predicted water level (red) to the measured water level (black) at Packery Channel during Period 2

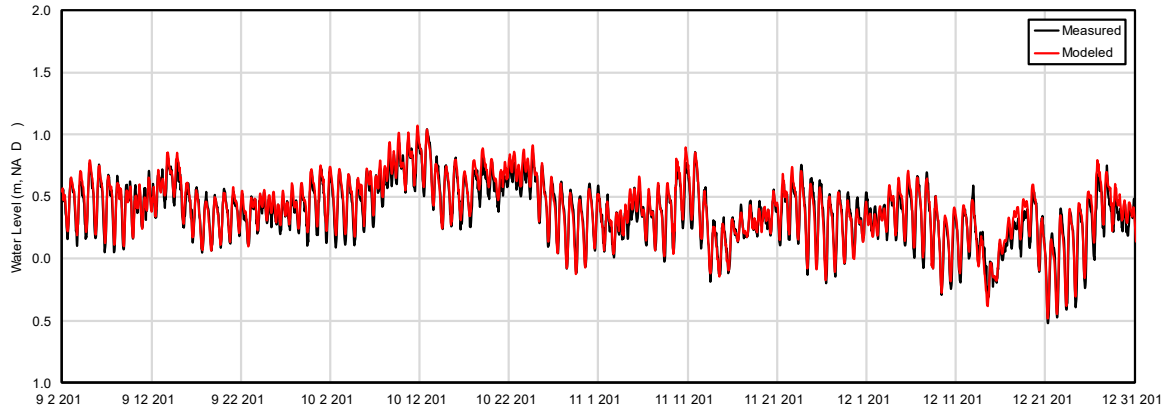

Figure A.10: Comparison of the model predicted water level (red) to the measured water level (black) at Bob Hall Pier during Period 2

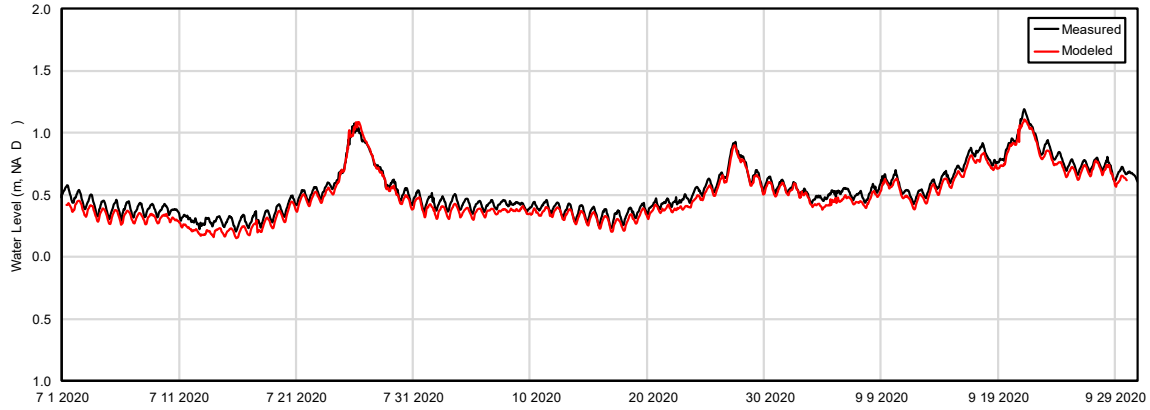

Figure A.11: Comparison of the model predicted water level (red) to the measured water level (black) at Rockport during Period 3

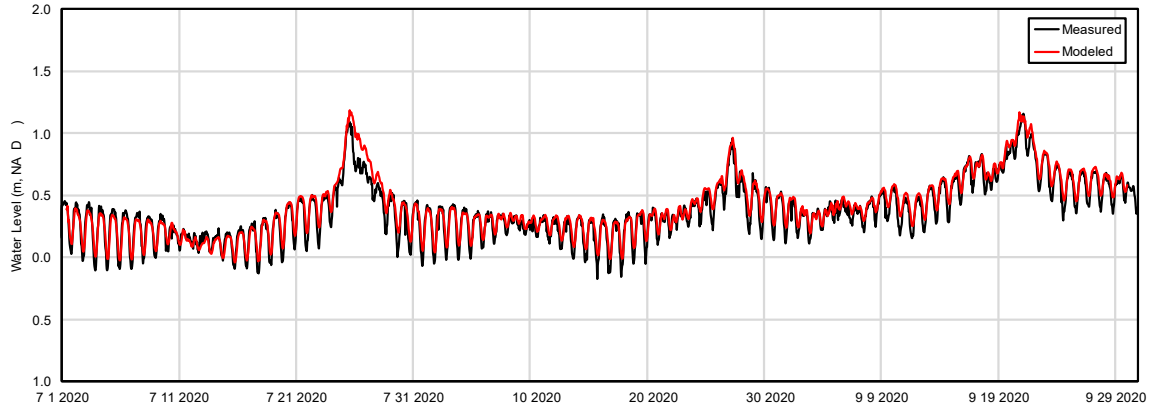

Figure A.12: Comparison of the model predicted water level (red) to the measured water level (black) at Port Aransas during Period 3

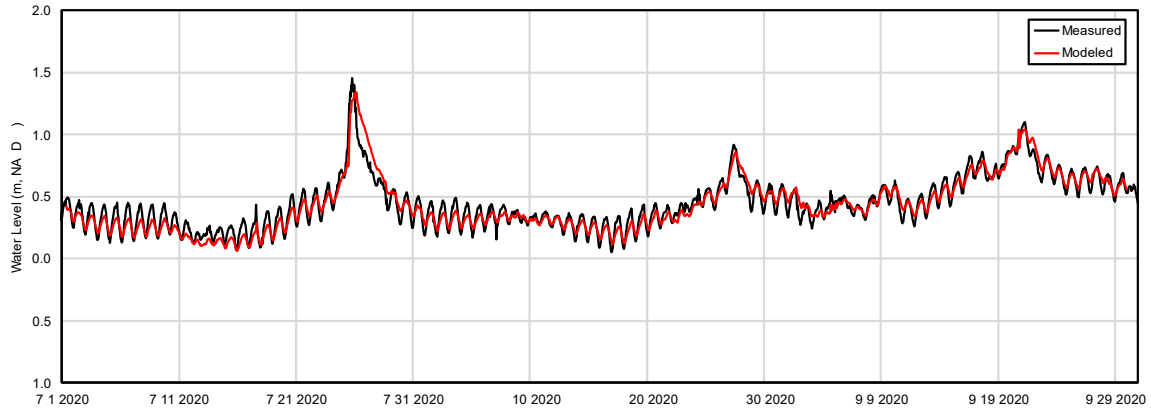

Figure A.13: Comparison of the model predicted water level (red) to the measured water level (black) at USS Lexington during Period 3

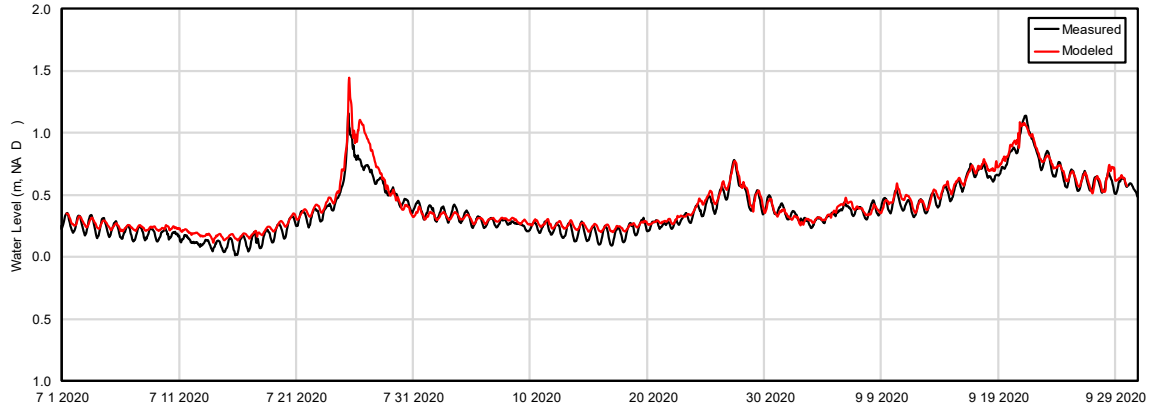

Figure A.14: Comparison of the model predicted water level (red) to the measured water level (black) at Packery Channel during Period 3

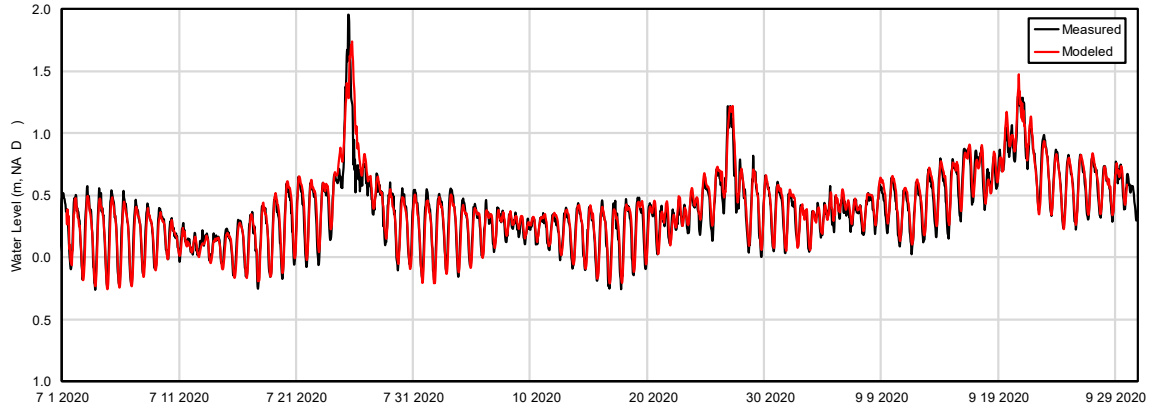

Figure A.15: Comparison of the model predicted water level (red) to the measured water level (black) at Bob Hall Pier during Period 3

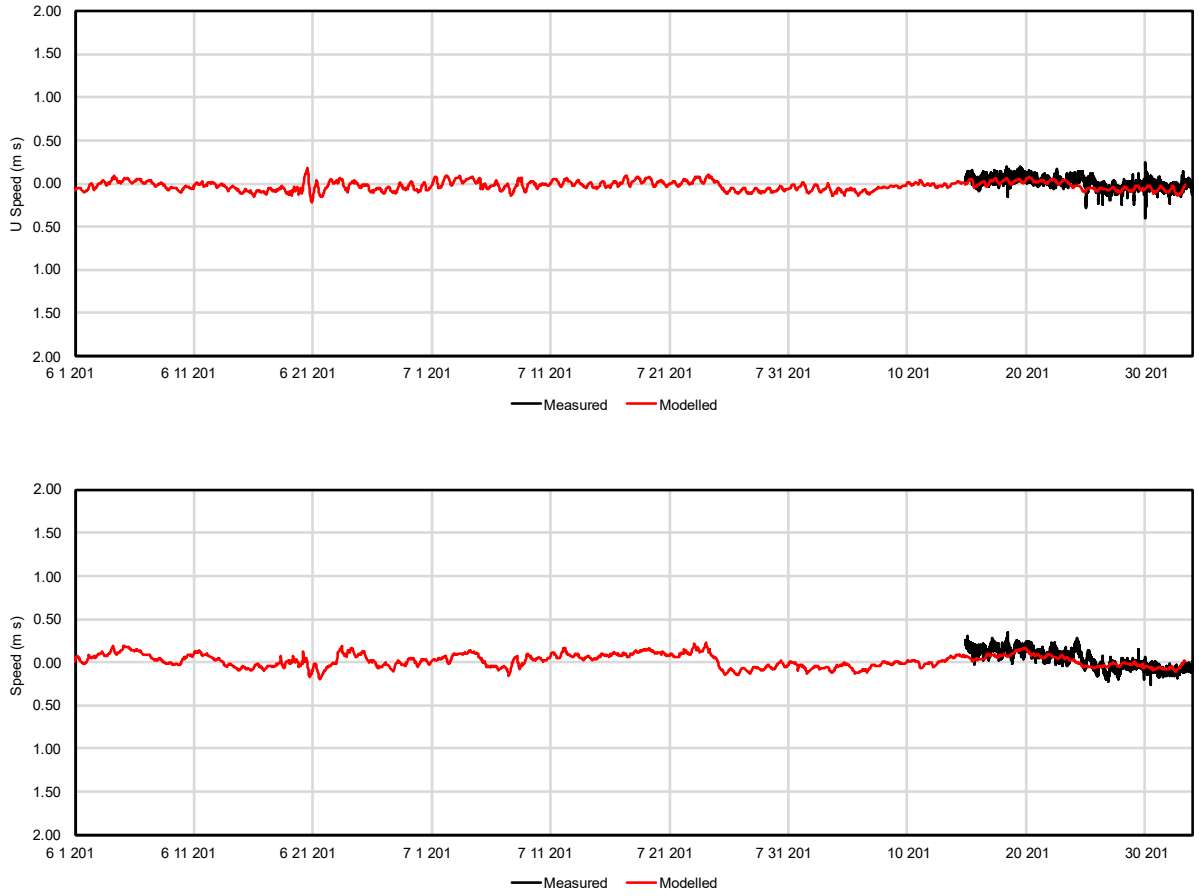

Figure A.16: Comparison of model predicted flow velocity components, U (east) and V (north), with the measured data at CC0101 during Period 1

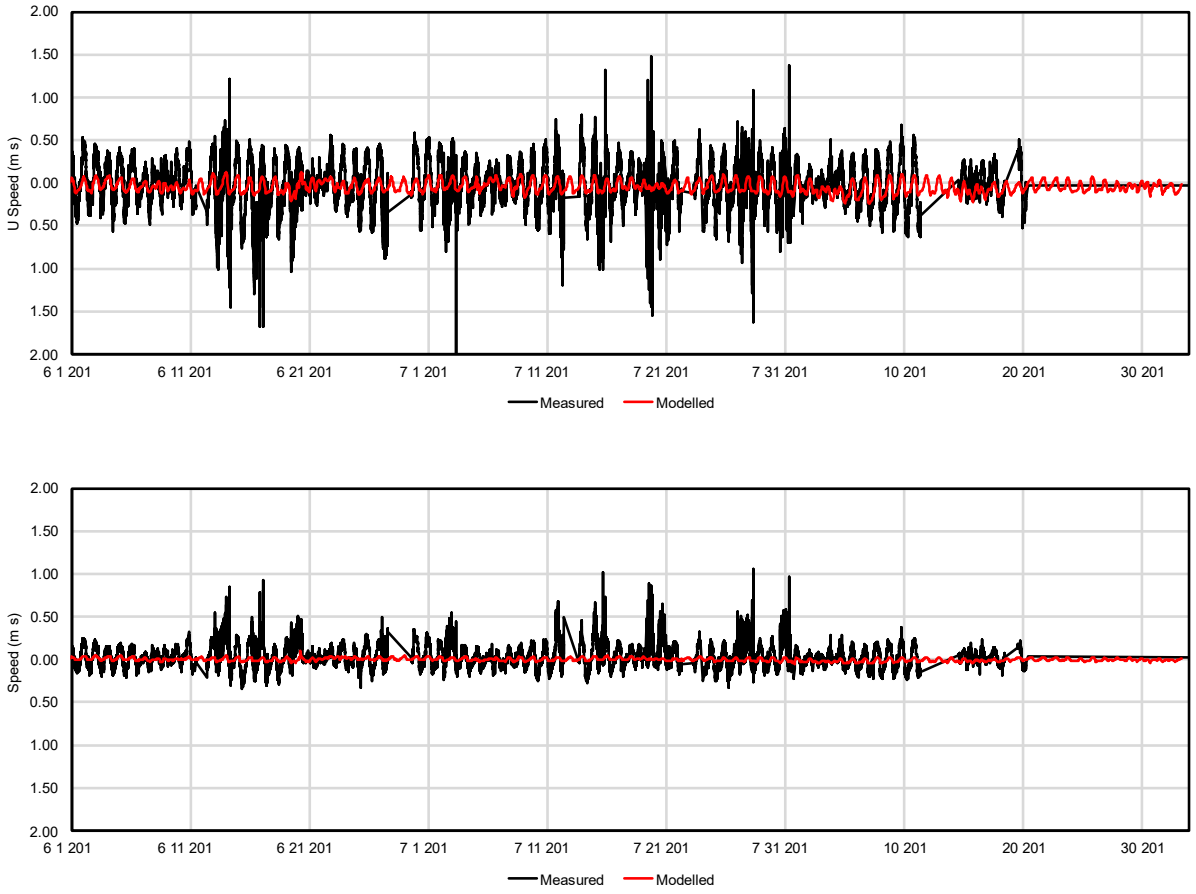

Figure A.17: Comparison of model predicted flow velocity components, U (east) and V (north), with the measured data at CC0401 during Period 1

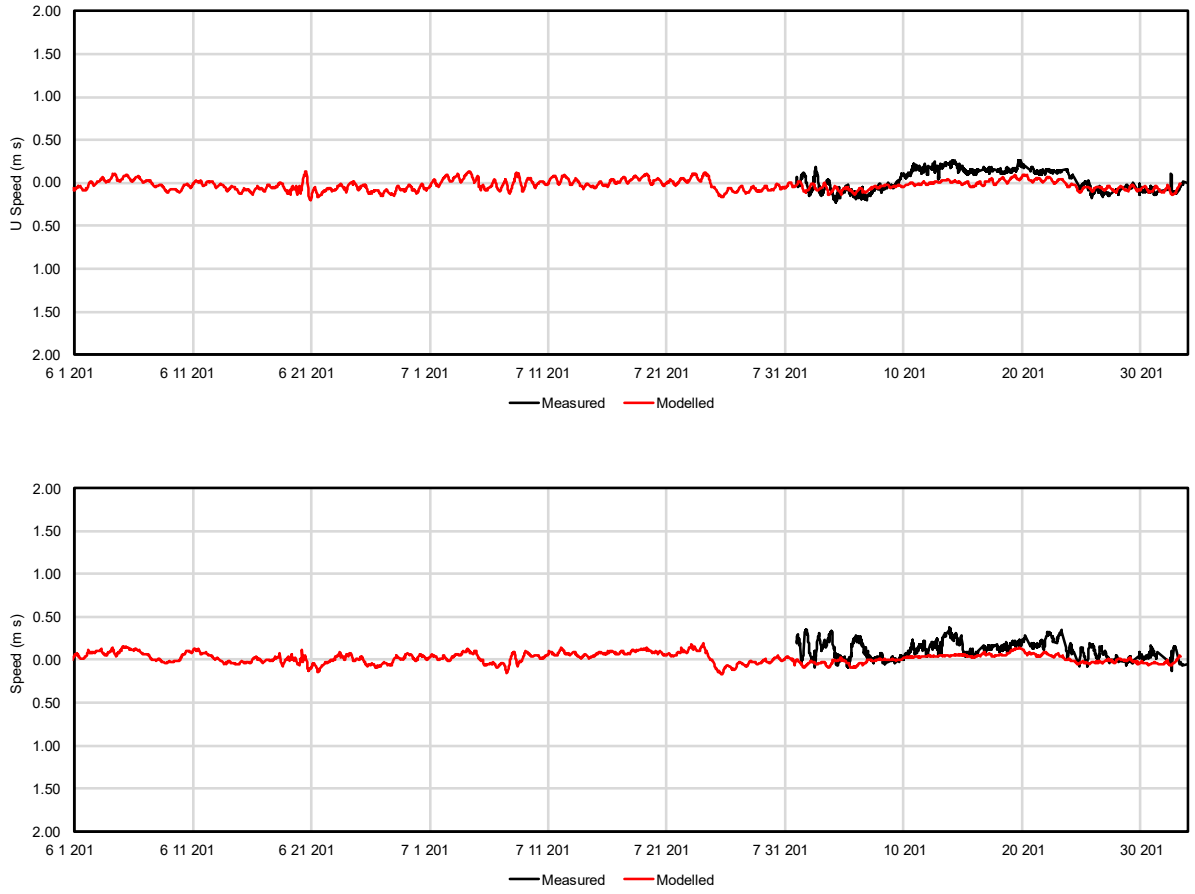

Figure A.18: Comparison of model predicted flow velocity components, U (east) and V (north), with the measured data at TABS-D during Period 1

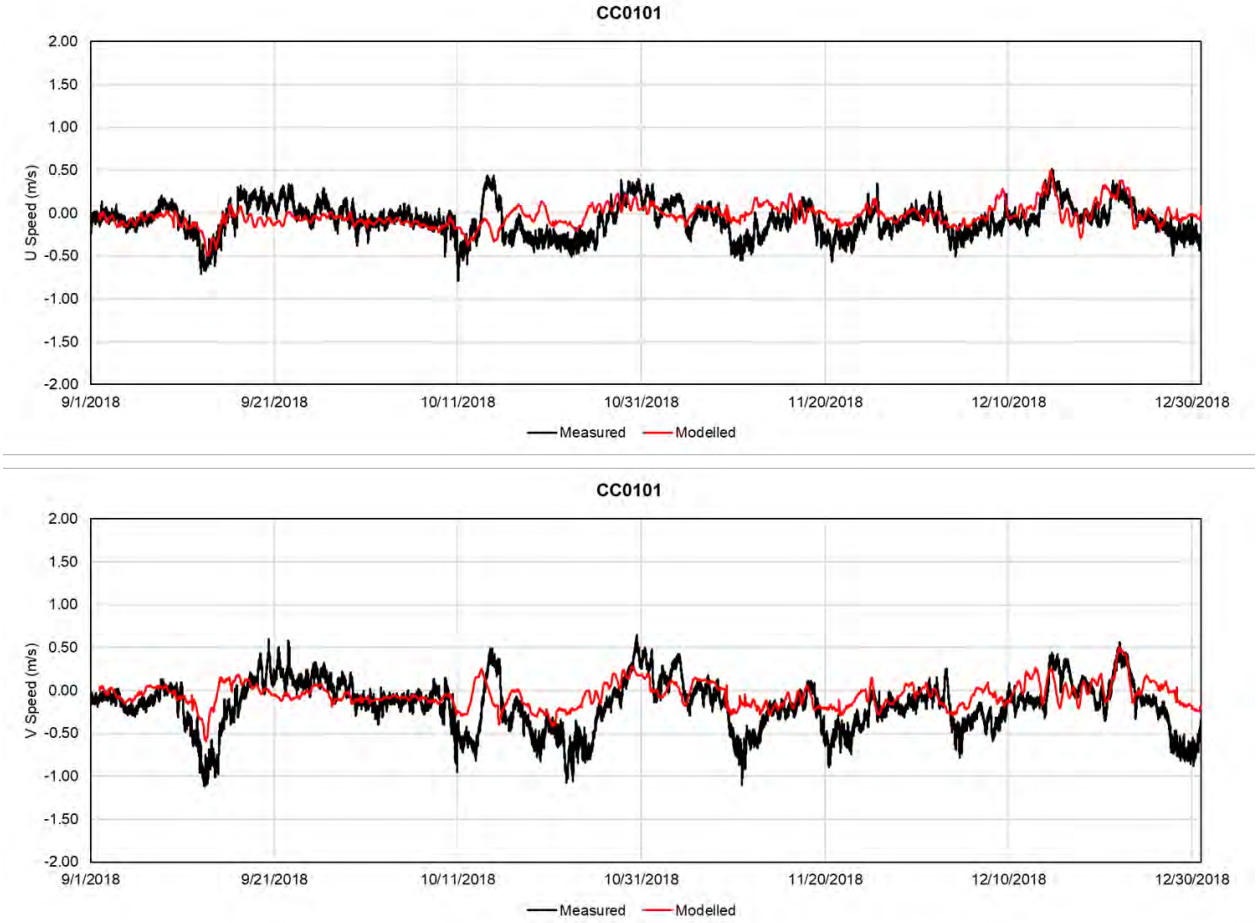

Figure A.19: Comparison of model predicted flow velocity components, U (east) and V (north), with the measured data at CC0101 during Period 2

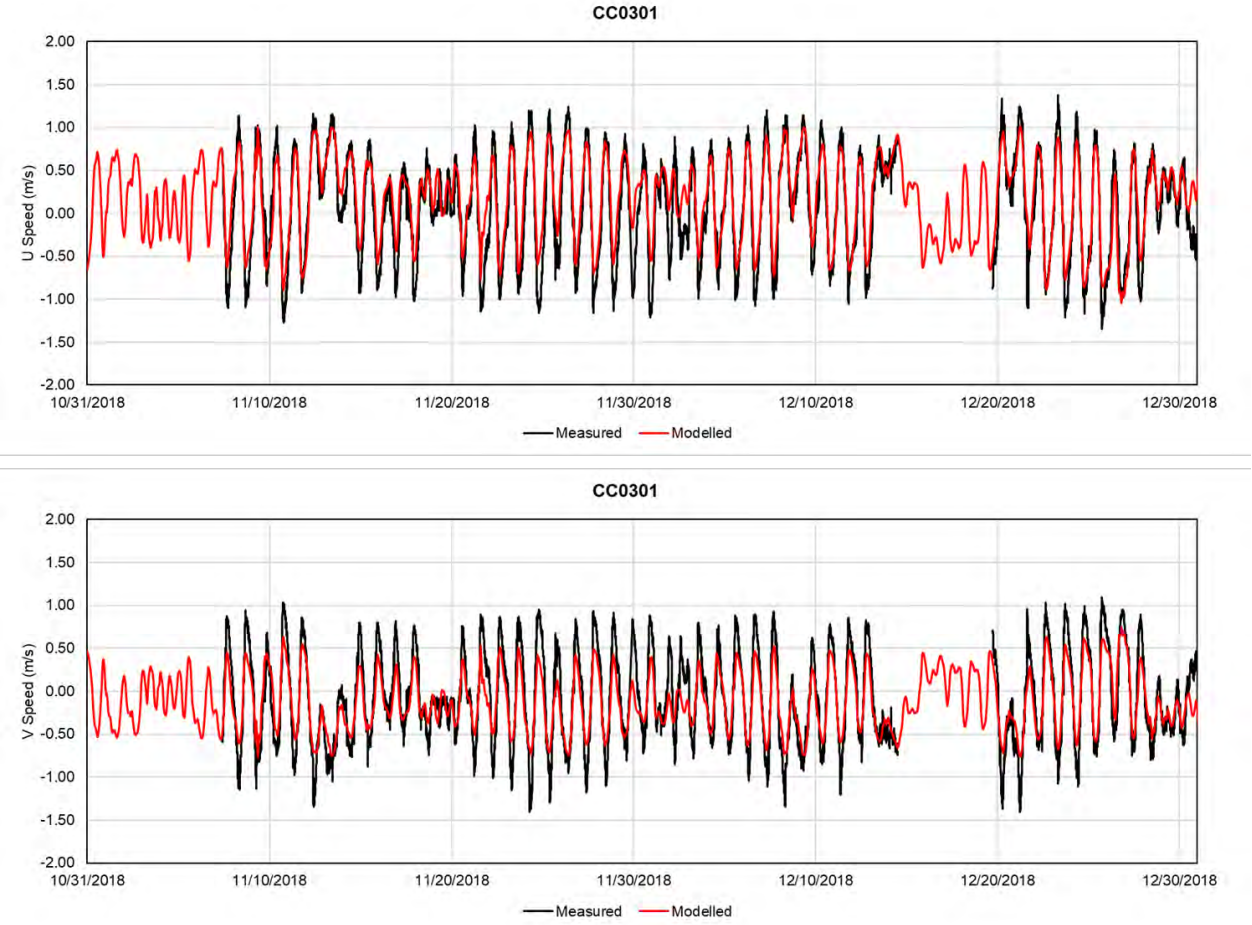

Figure A.20: Comparison of model predicted flow velocity components, U (east) and V (north), with the measured data at CC0301 during Period 2

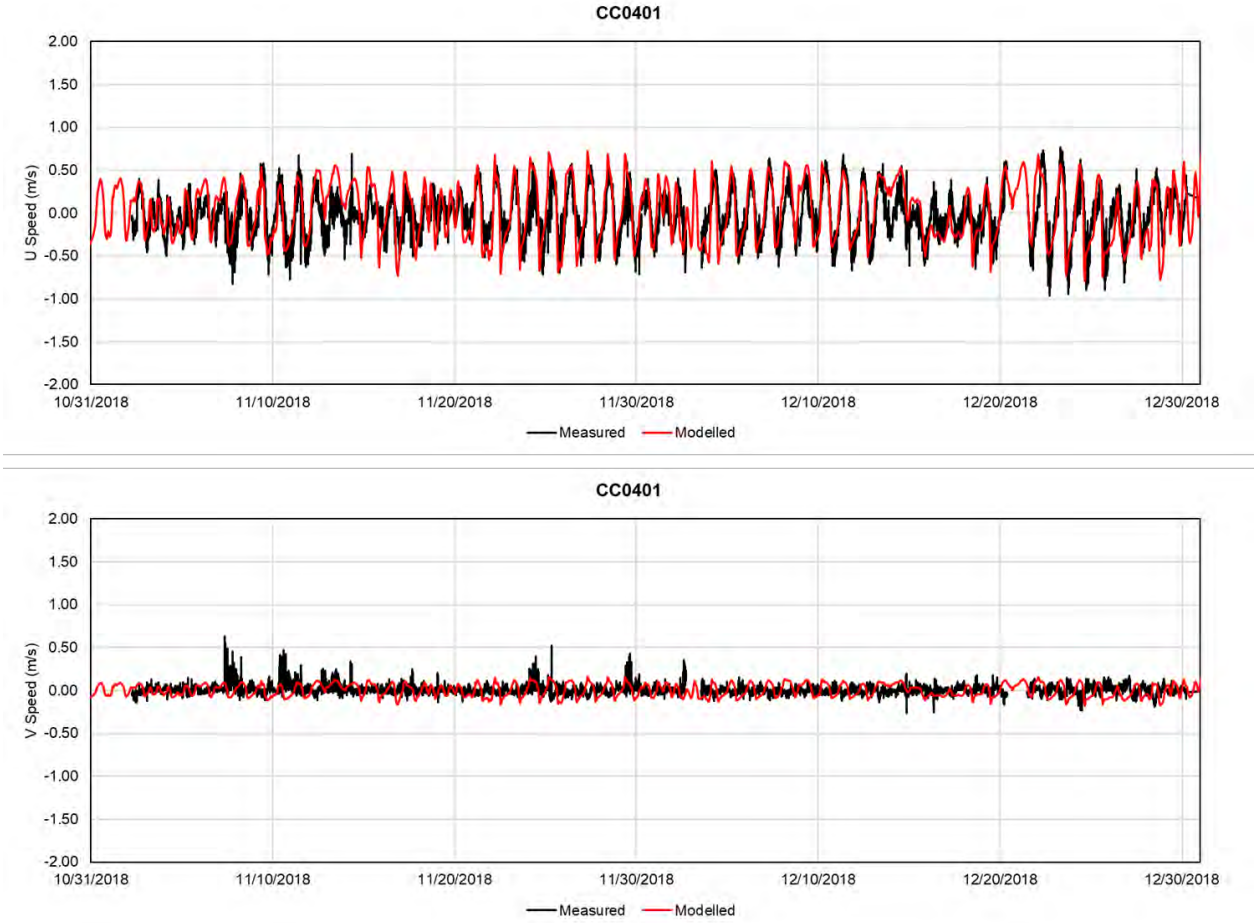

Figure A.21: Comparison of model predicted flow velocity components, U (east) and V (north), with the measured data at CC0401 during Period 2

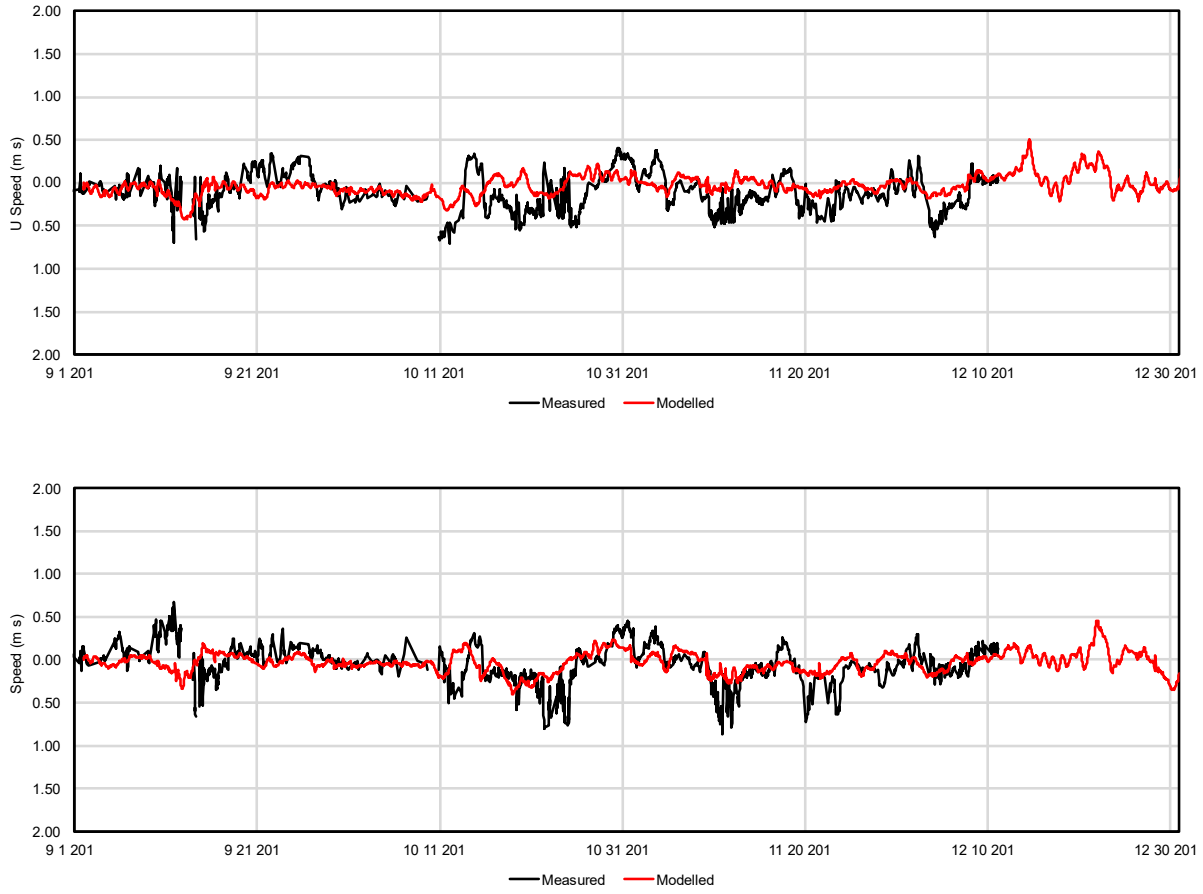

Figure A.22: Comparison of model predicted flow velocity components, U (east) and V (north), with the measured data at TABS-D during Period 2

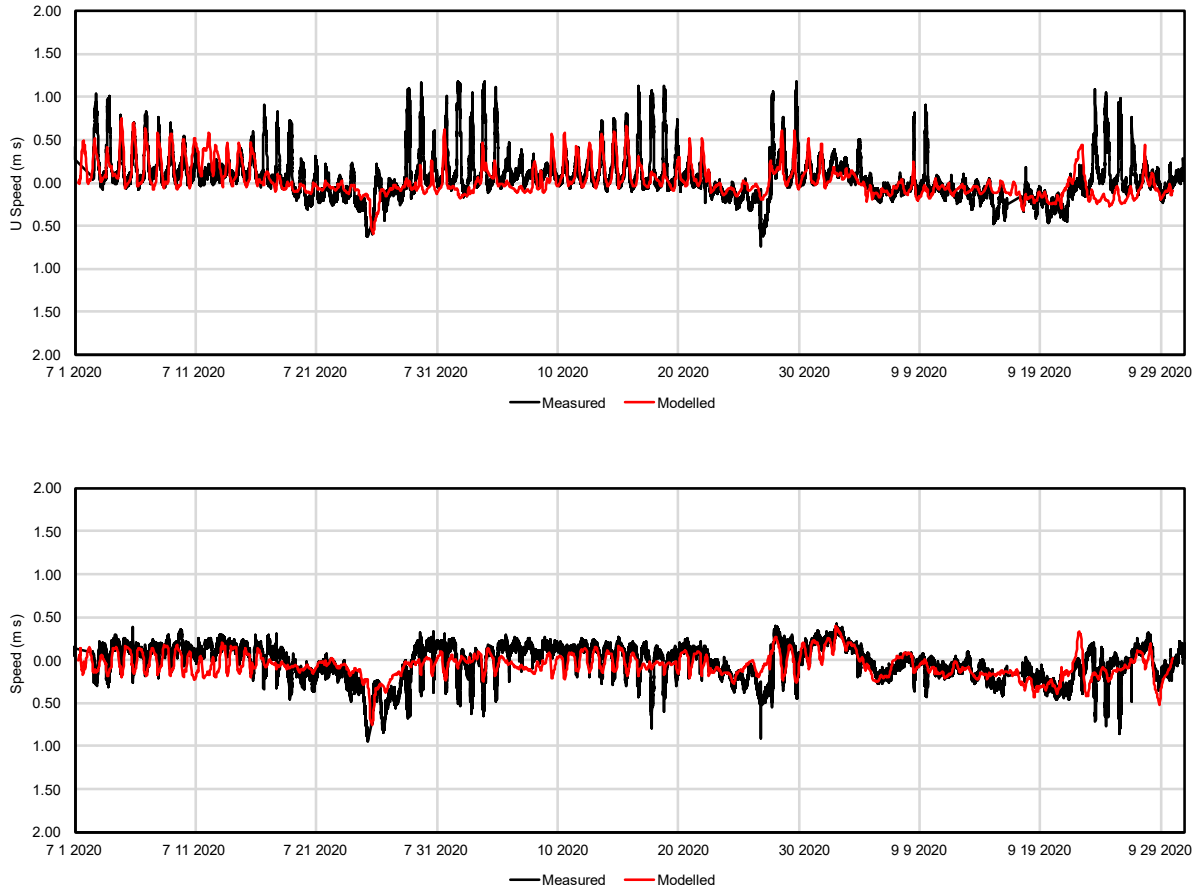

Figure A.23: Comparison of model predicted flow velocity components, U (east) and V (north), with the measured data at CC0201 during Period 3

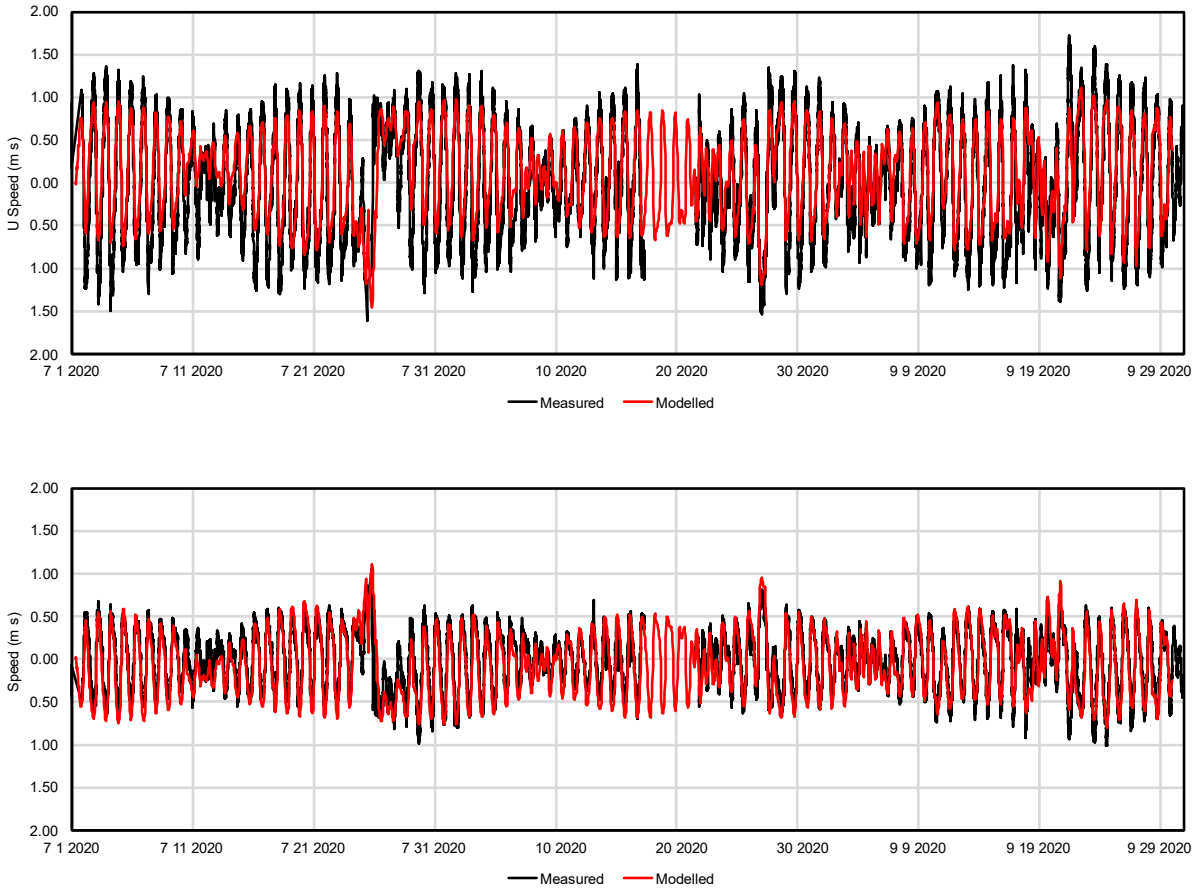

Figure A.24: Comparison of model predicted flow velocity components, U (east) and V (north), with the measured data at CC0301 during Period 3

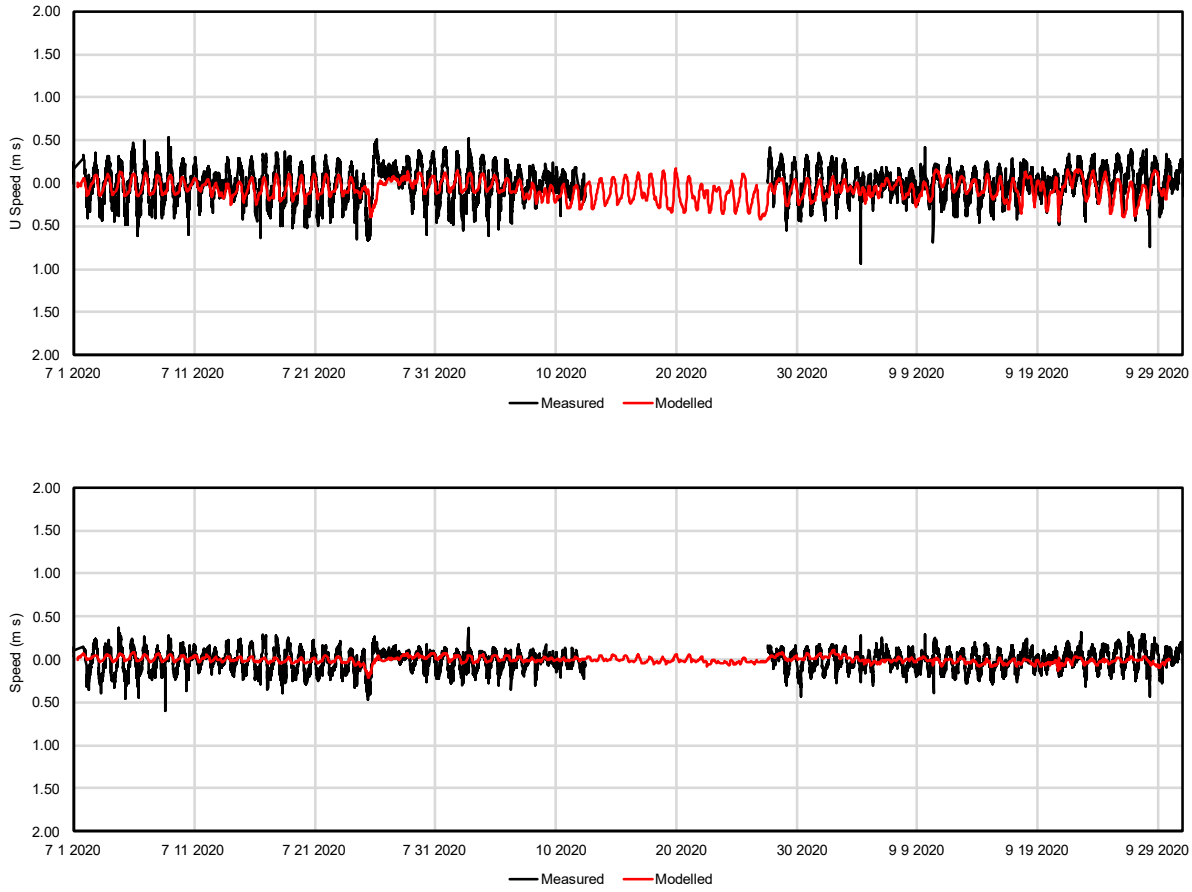

Figure A.25: Comparison of model predicted flow velocity components, U (east) and V (north), with the measured data at CC0401 during Period 3

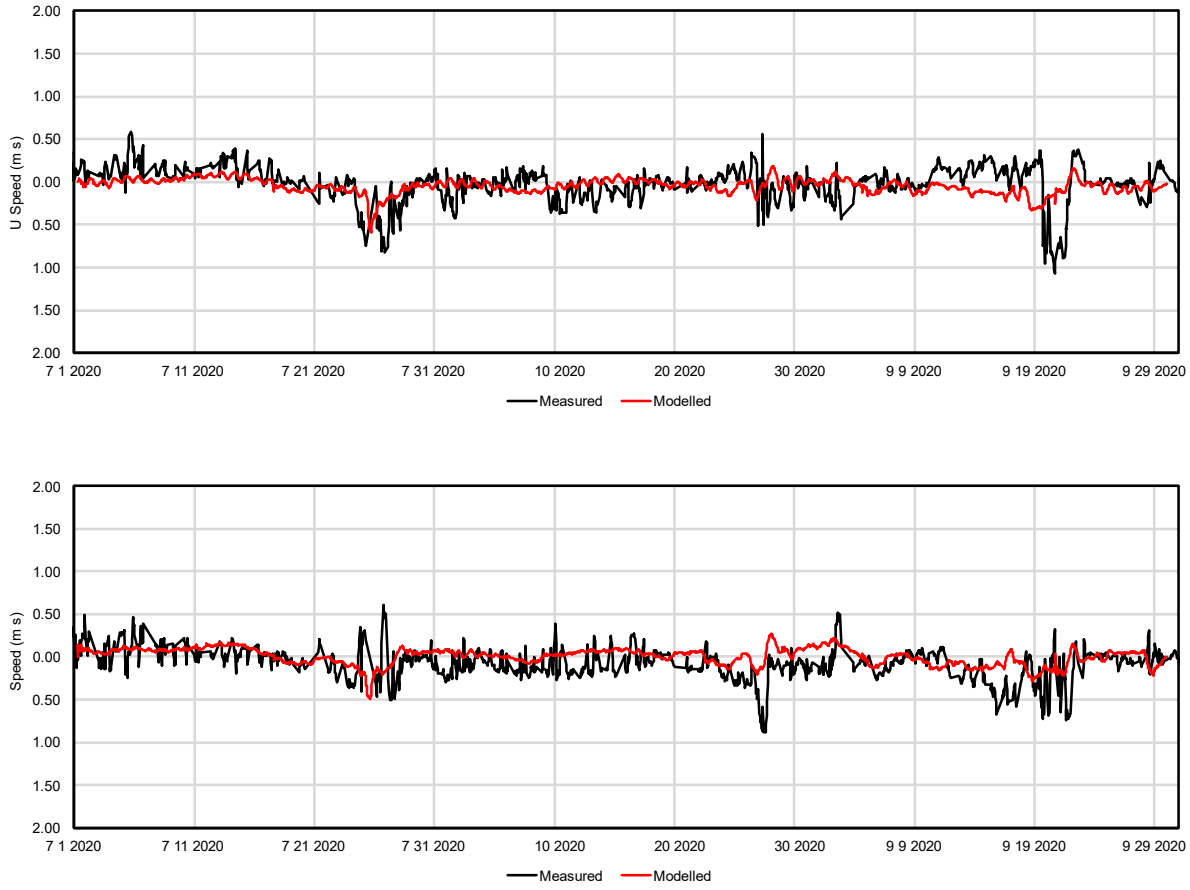

Figure A.26: Comparison of model predicted flow velocity components, U (east) and V (north), with the measured data at TABS-D during Period 3

Appendix B

Impact of Future With Project

B.1 Impacts on Water Level

B.1.1 Mean Water Level

Figure B.1: Change of mean water level caused by the FWP in Period 1

Figure B.2: Change of mean water level caused by the FWP in Period 2

Figure B.3: Change of mean water level caused by the FWP in Period 3

B.1.2 High Tide and Low Tide

Figure B.4: Average change of high tide caused by the FWP in Period 1

Figure B.5: Average change of high tide caused by the FWP in Period 2

Figure B.6: Average change of high tide caused by the FWP in Period 3

Figure B.7: Average change of low tide caused by the FWP in Period 1

Figure B.8: Average change of low tide caused by the FWP in Period 2

Figure B.9: Average change of low tide caused by the FWP in Period 3

B.1.3 Tide Range

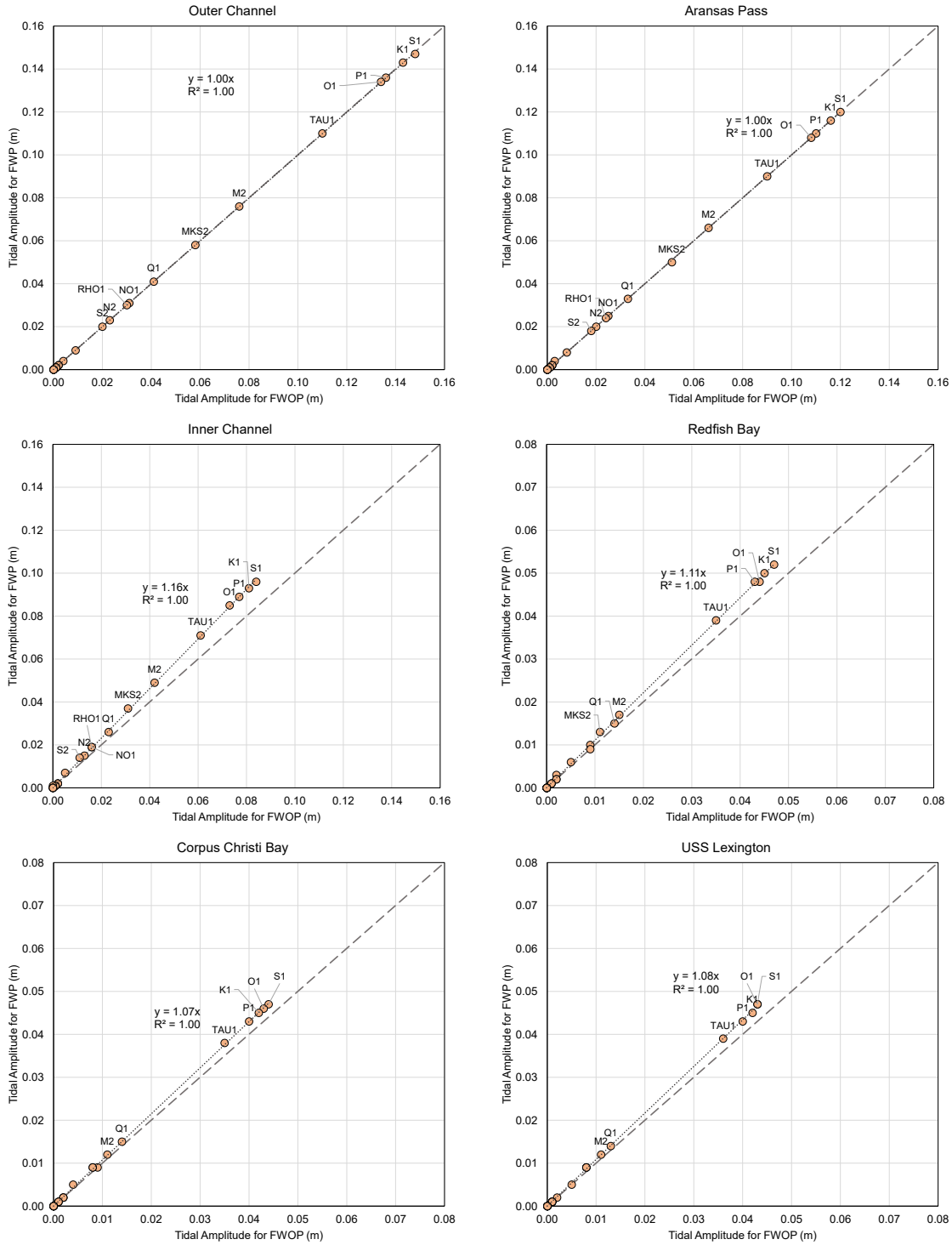

Figure B.10: Comparison of tide amplitudes between FWP and FWOP in Period 1

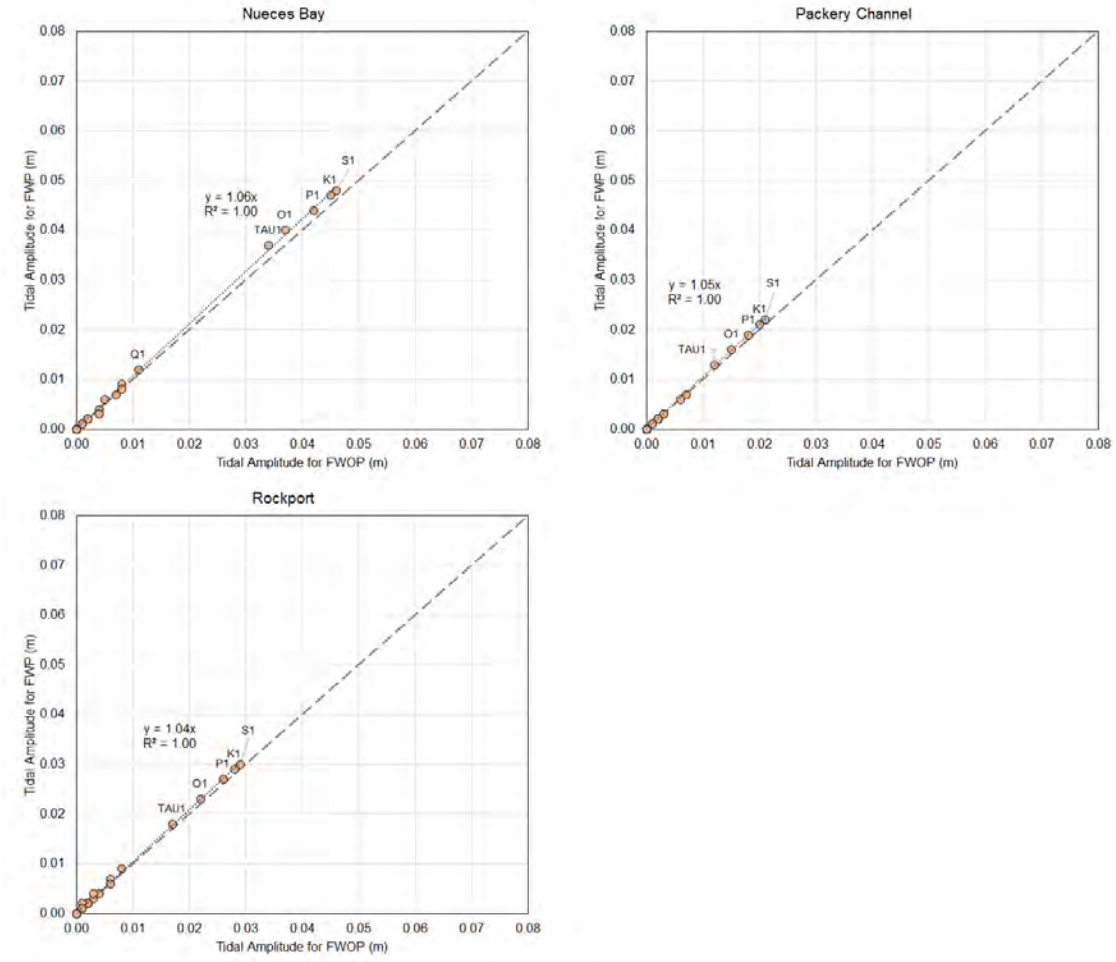

Figure B.11: Comparison of tide amplitudes between FWP and FWOP in Period 1 (continued)

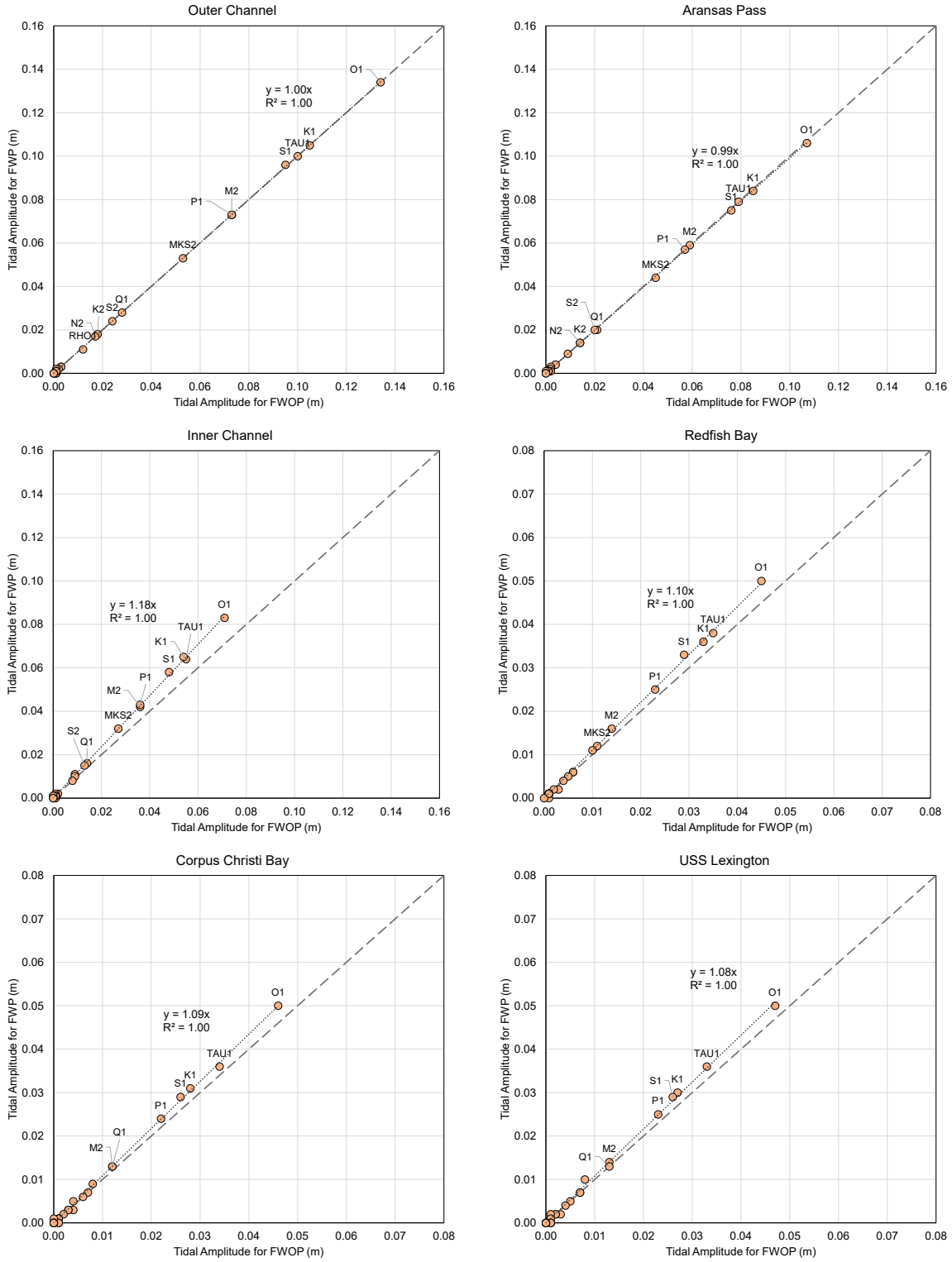

Figure B.12: Comparison of tide amplitudes between FWP and FWOP in Period 2

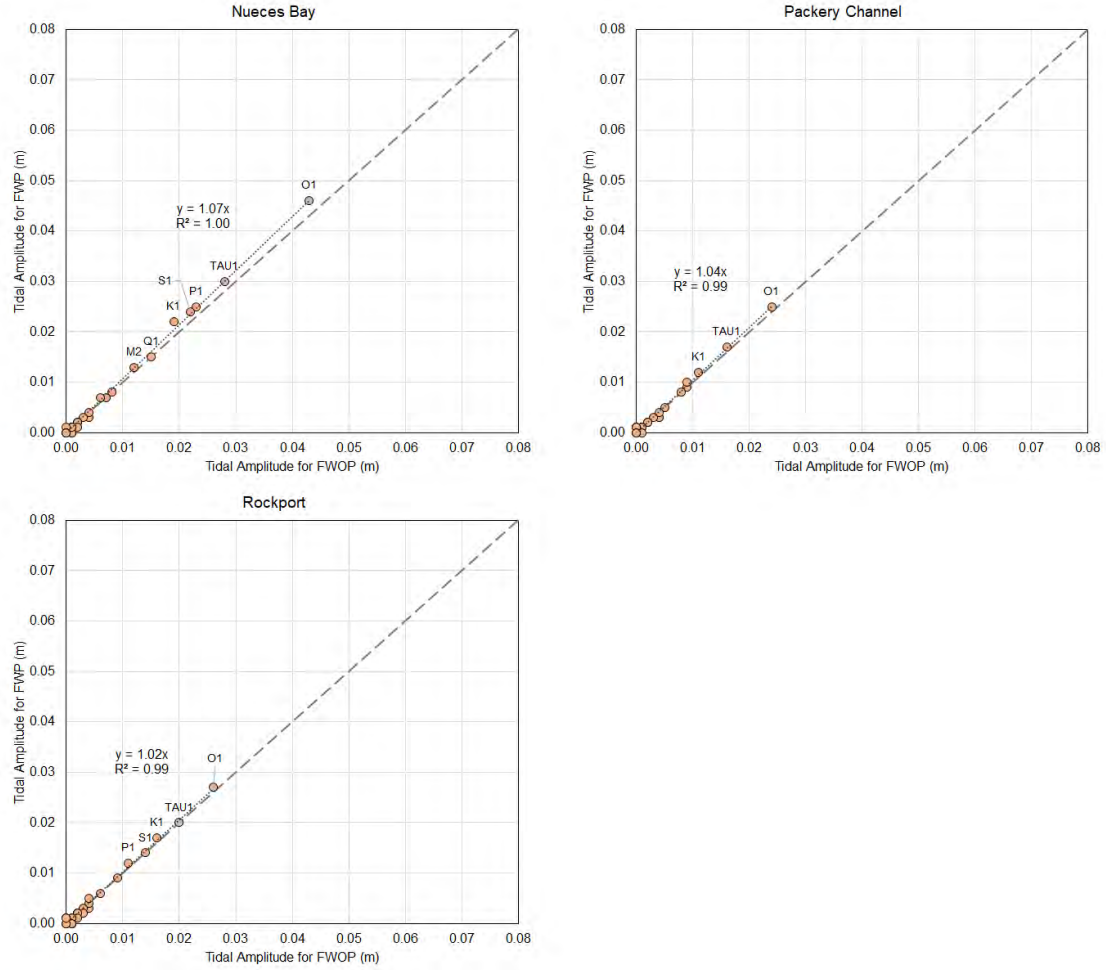

Figure B.13: Comparison of tide amplitudes between FWP and FWOP in Period 2 (continued)

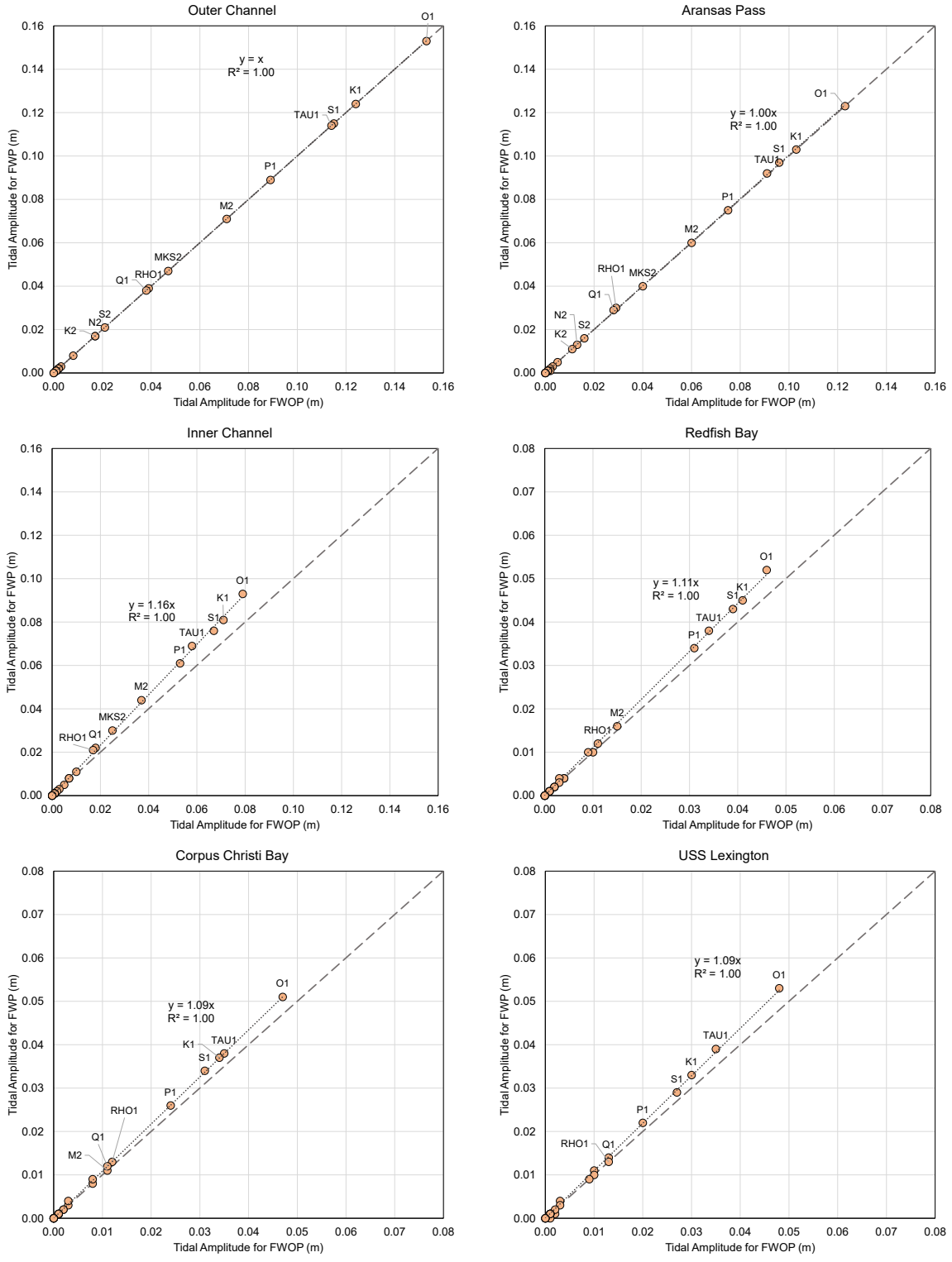

Figure B.14: Comparison of tide amplitudes between FWP and FWOP in Period 3

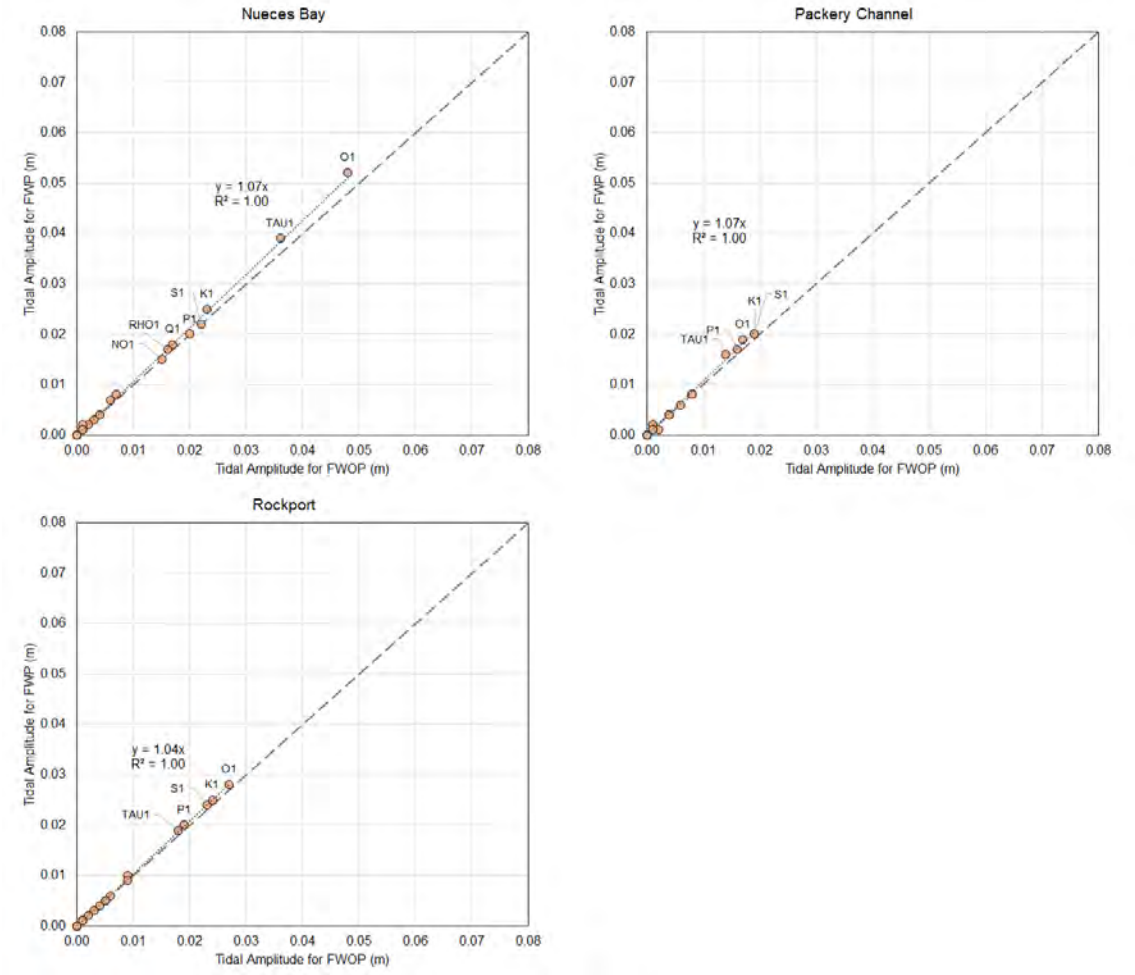

Figure B.15: Comparison of tide amplitudes between FWP and FWOP in Period 3 (continued)

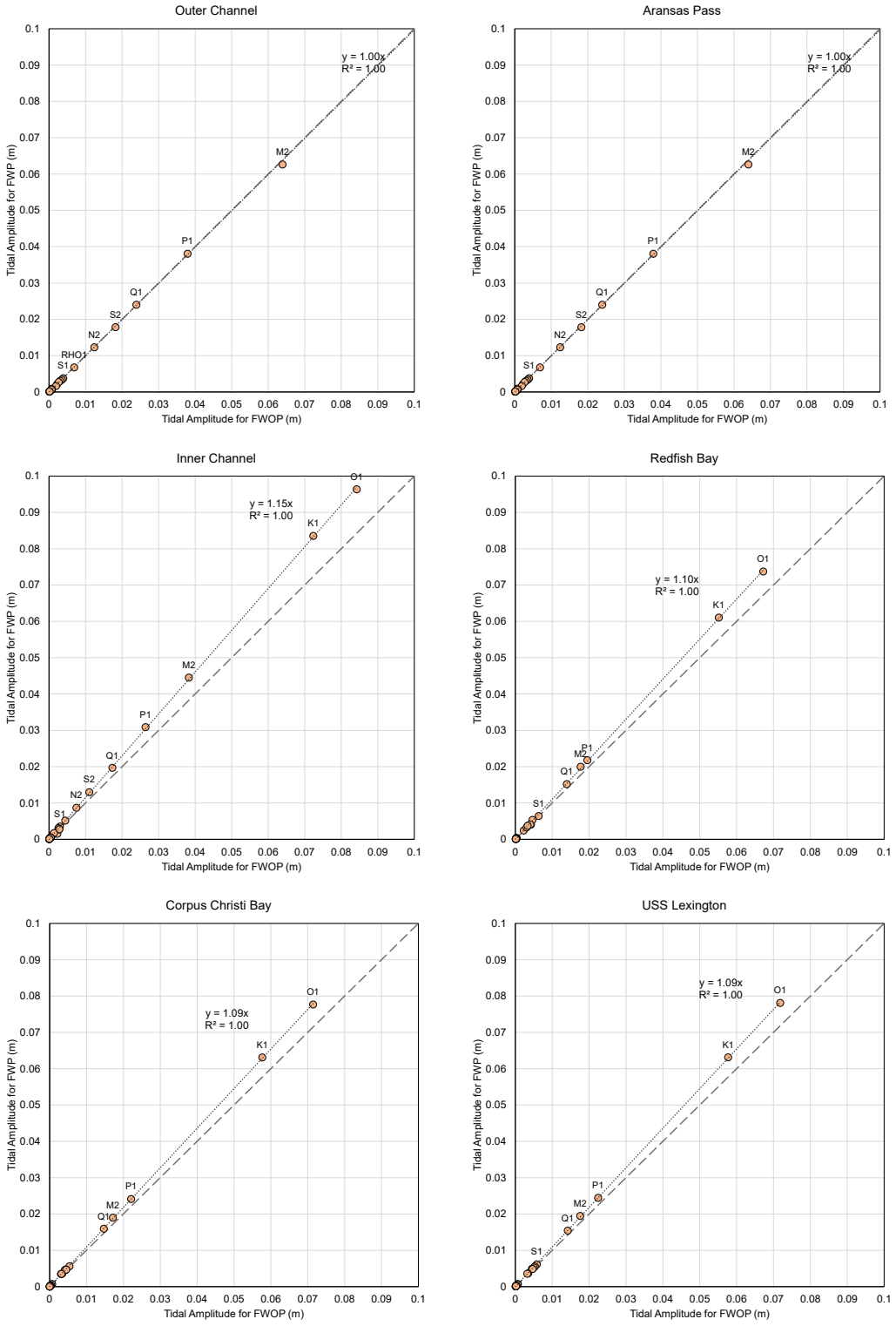

Figure B.16: Comparison of tide amplitudes between FWP and FWOP from one-year run

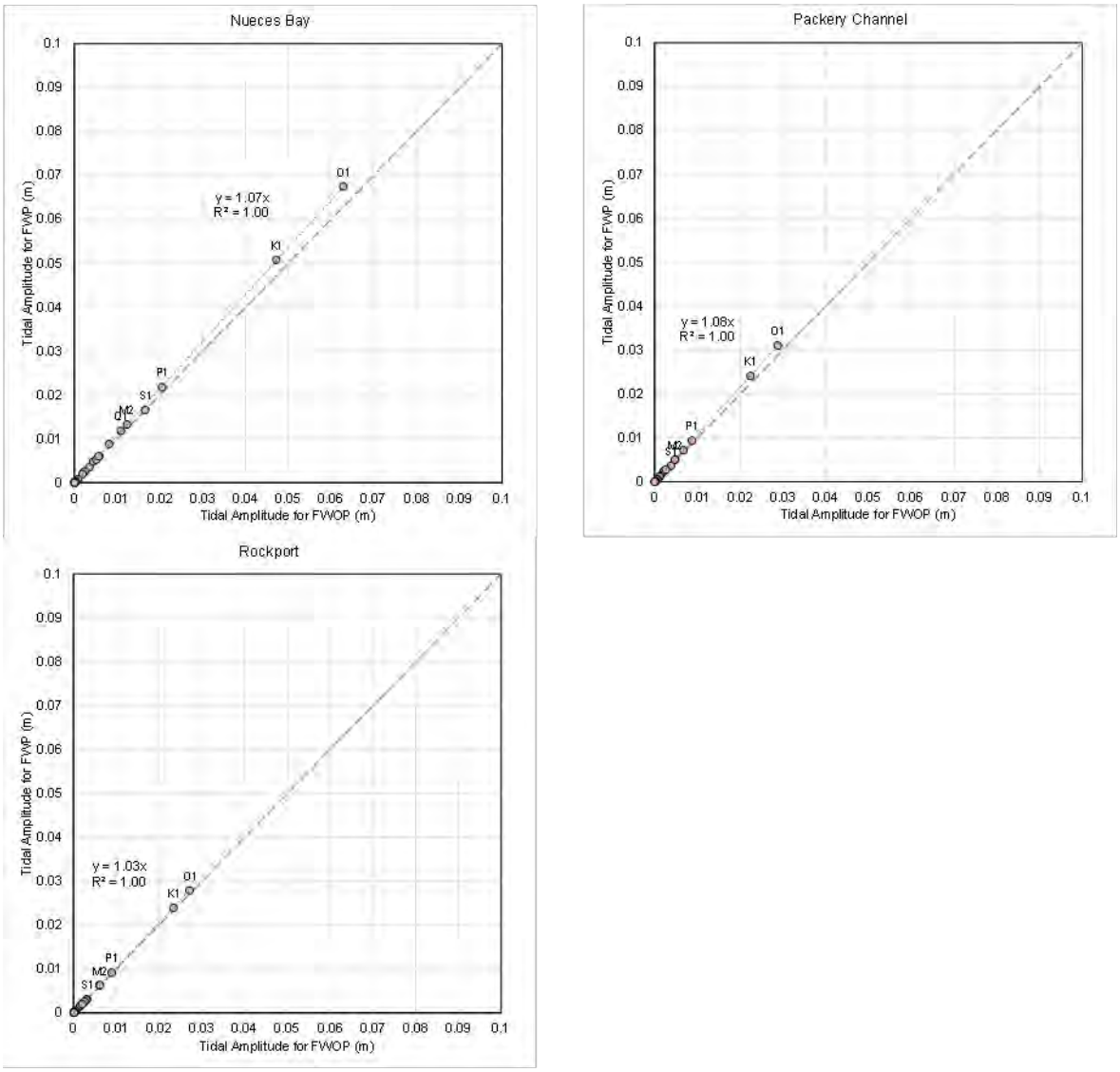

Figure B.17: Comparison of tide amplitudes between FWP and FWOP from one-year run (continued)

Figure B.18: Average Change of Tide Range Caused by FWP in Period 1

Figure B.19: Average Change of Tide Range Caused by FWP in Period 2

Figure B.20: Average Change of Tide Range Caused by FWP in Period 3

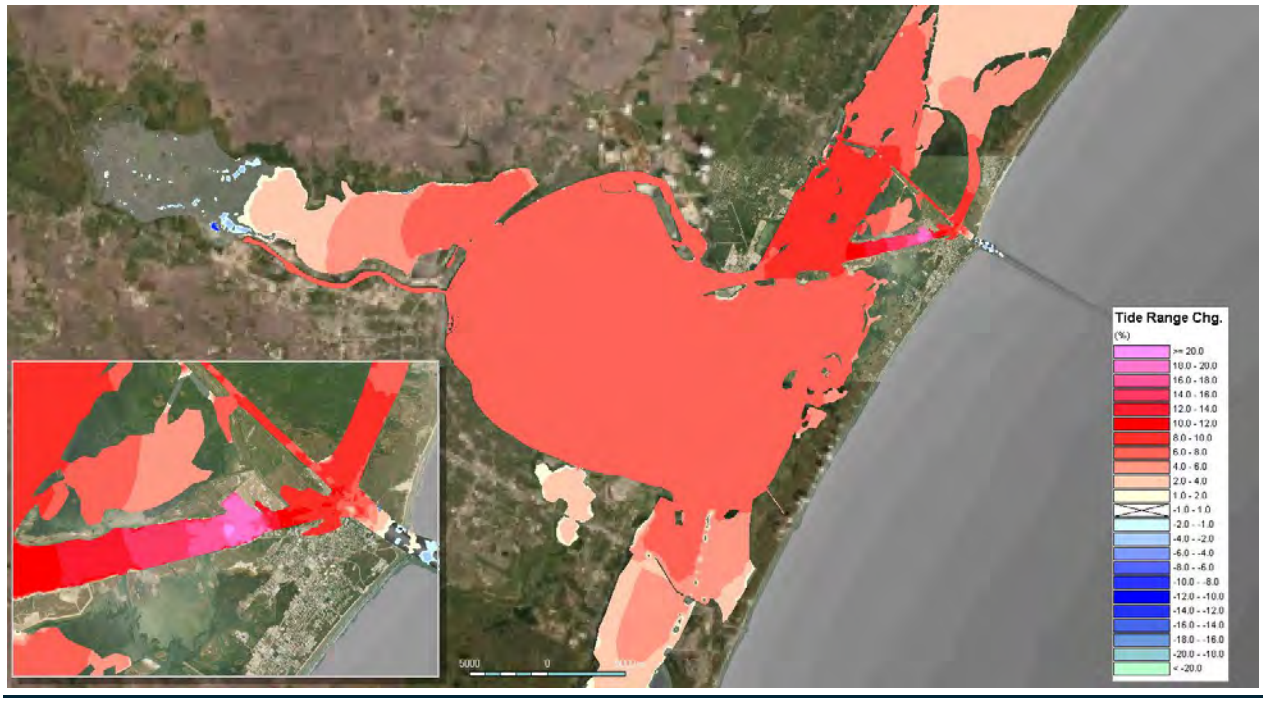

Figure B.21: Percentage of tide range change caused by the FWP in Period 1

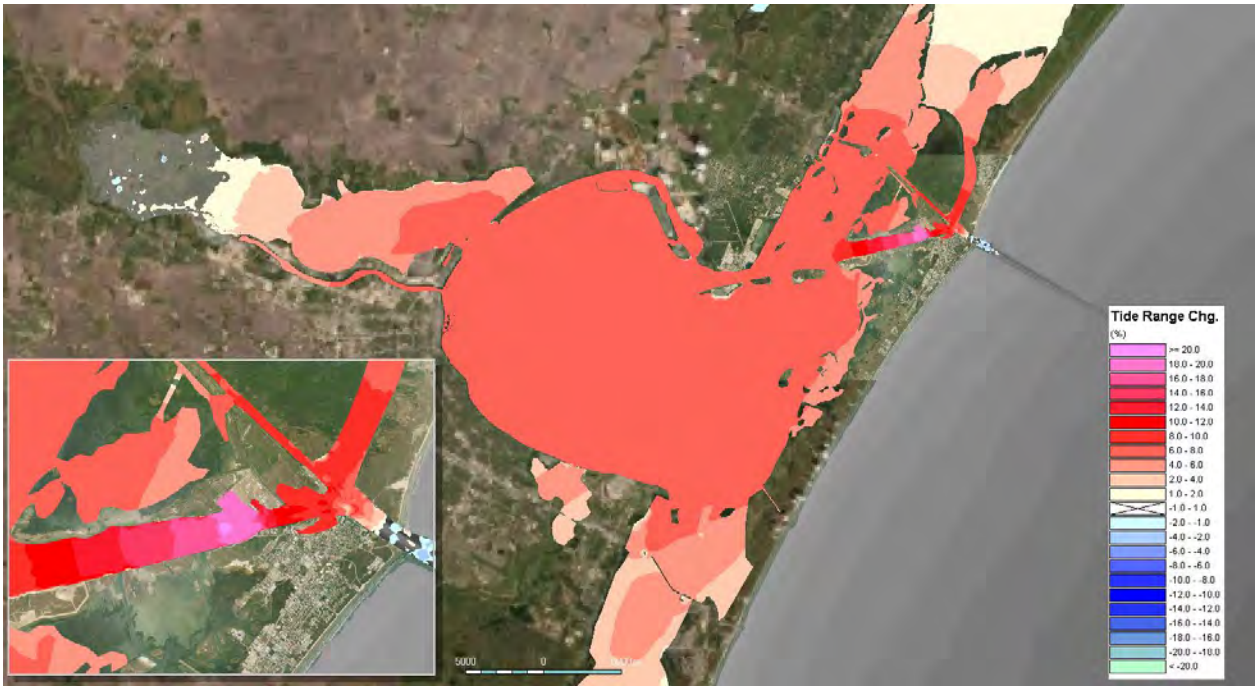

Figure B.22: Percentage of tide range change caused by the FWP in Period 2

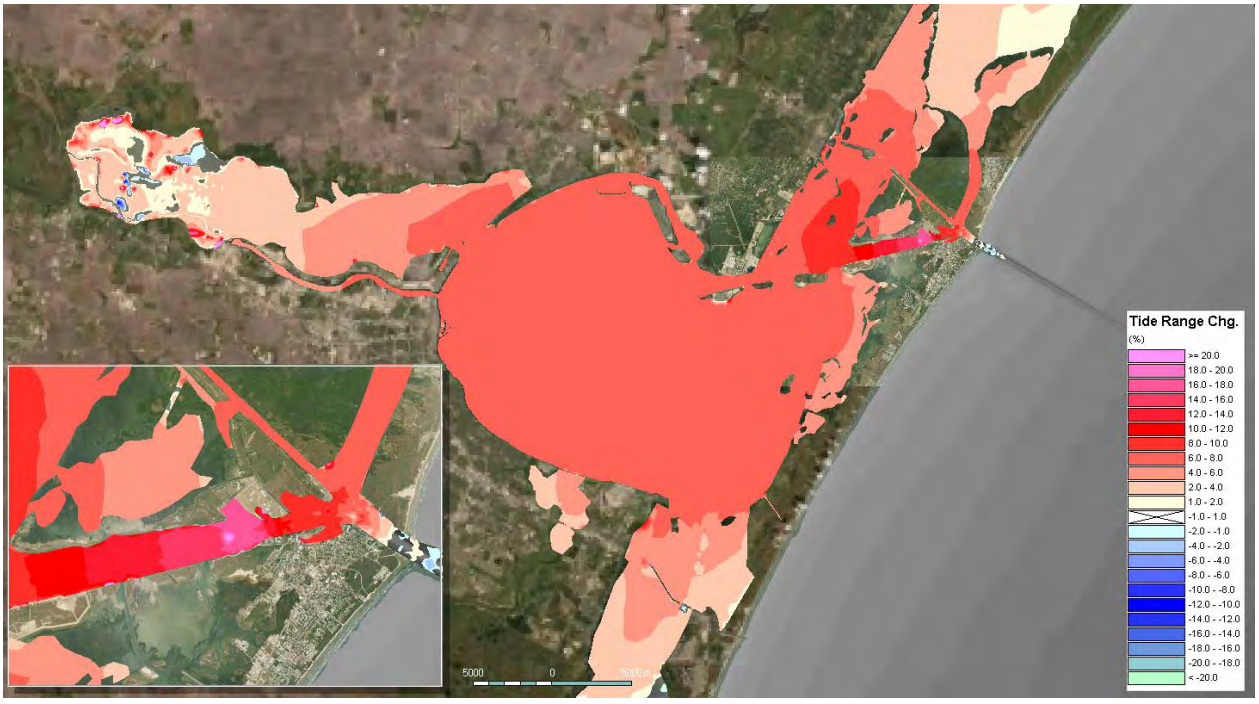

Figure B.23: Percentage of tide range change caused by the FWP in Period 3

B.2 Impact on Currents

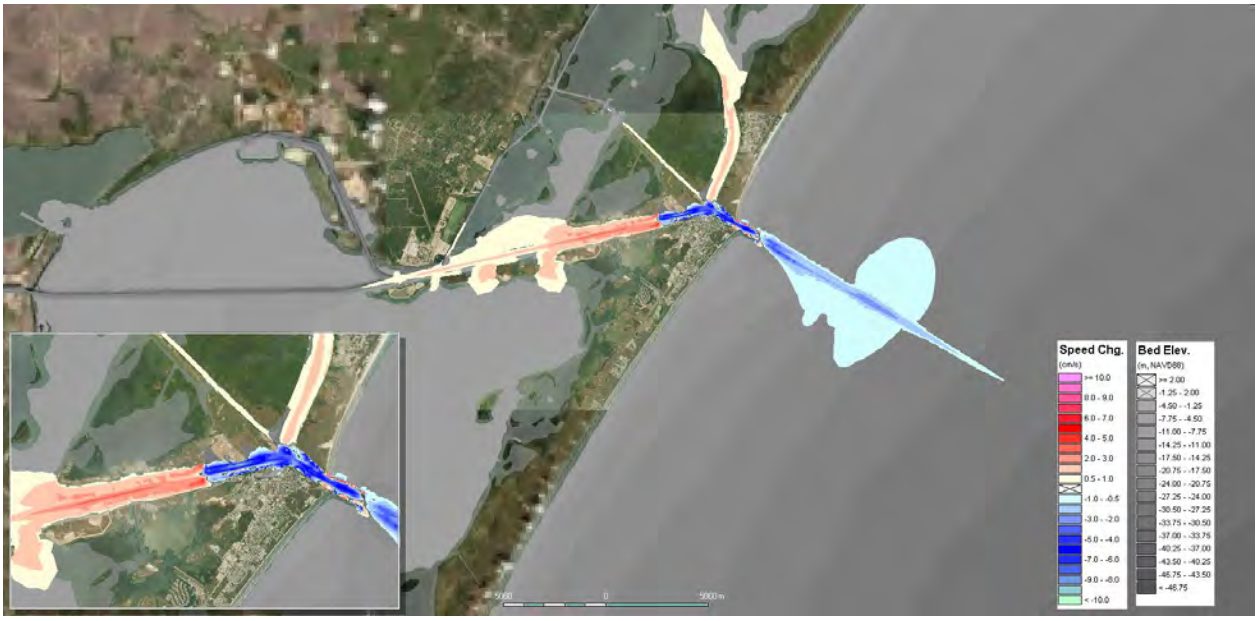

Figure B.24: Depth averaged speed change caused by the FWP in Period 1

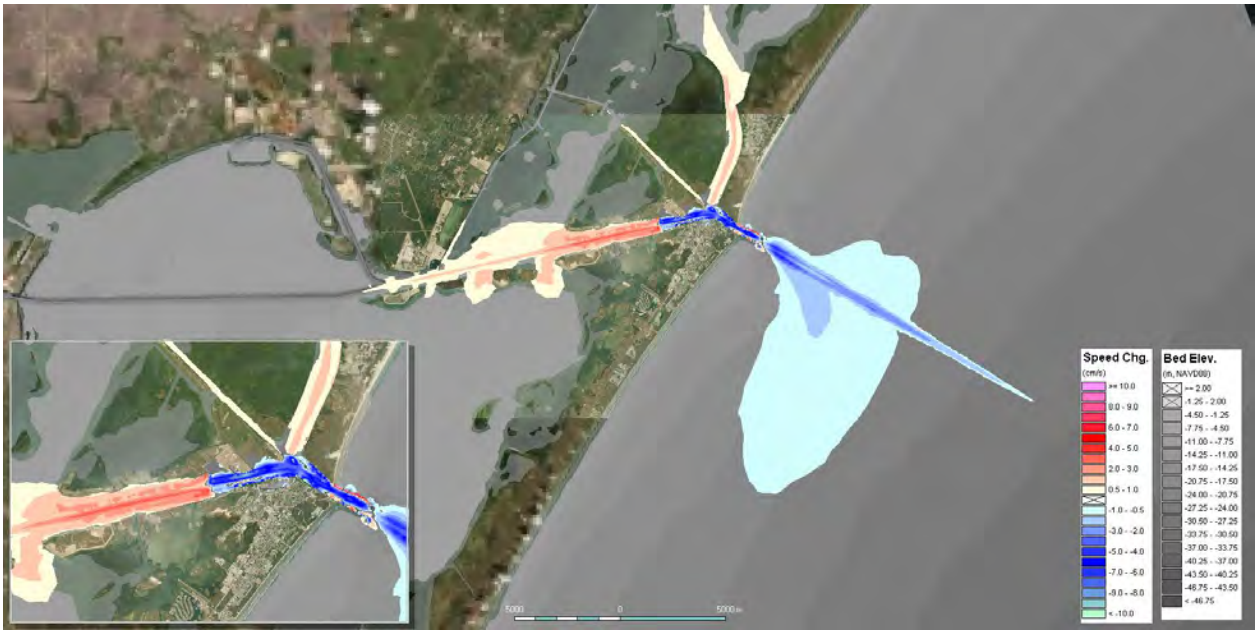

Figure B.25: Depth averaged speed change caused by the FWP in Period 2

Figure B.26: Depth averaged speed change caused by the FWP in Period 3

Figure B.27: Average flow speed change on water surface in Period 1

Figure B.28: Average flow speed change at the elevation of -5 m (NAVD88) in Period 1

Figure B.29: Average flow speed change at the elevation of -10 m (NAVD88) in Period 1

Figure B.30: Average flow speed change on water surface in Period 2

Figure B.31: Average flow speed change at the elevation of -5 m (NAVD88) in Period 2

Figure B.32: Average flow speed change at the elevation of -10 m (NAVD88) in Period 2

Figure B.33: Average flow speed change on water surface in Period 3

Figure B.34: Average flow speed change at the elevation of -5 m (NAVD88) in Period 3

Figure B.35: Average flow speed change at the elevation of -10 m (NAVD88) in Period 3

B.3 Impact on Salinity

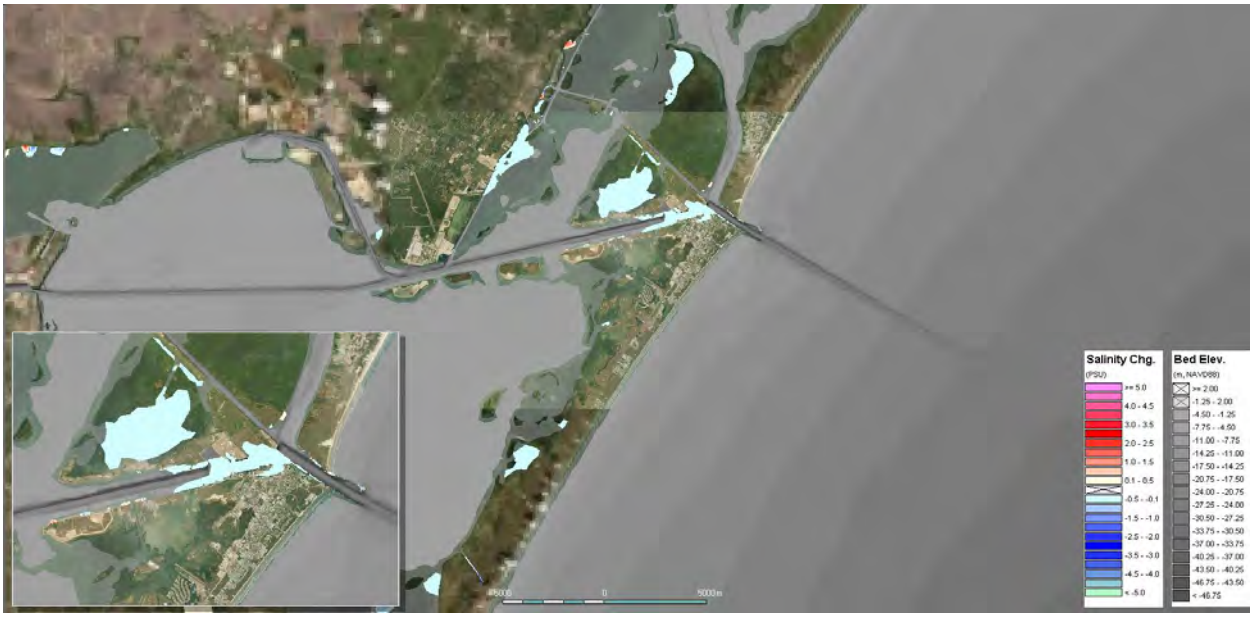

Figure B.36: Average salinity change caused by FWP in Period 1

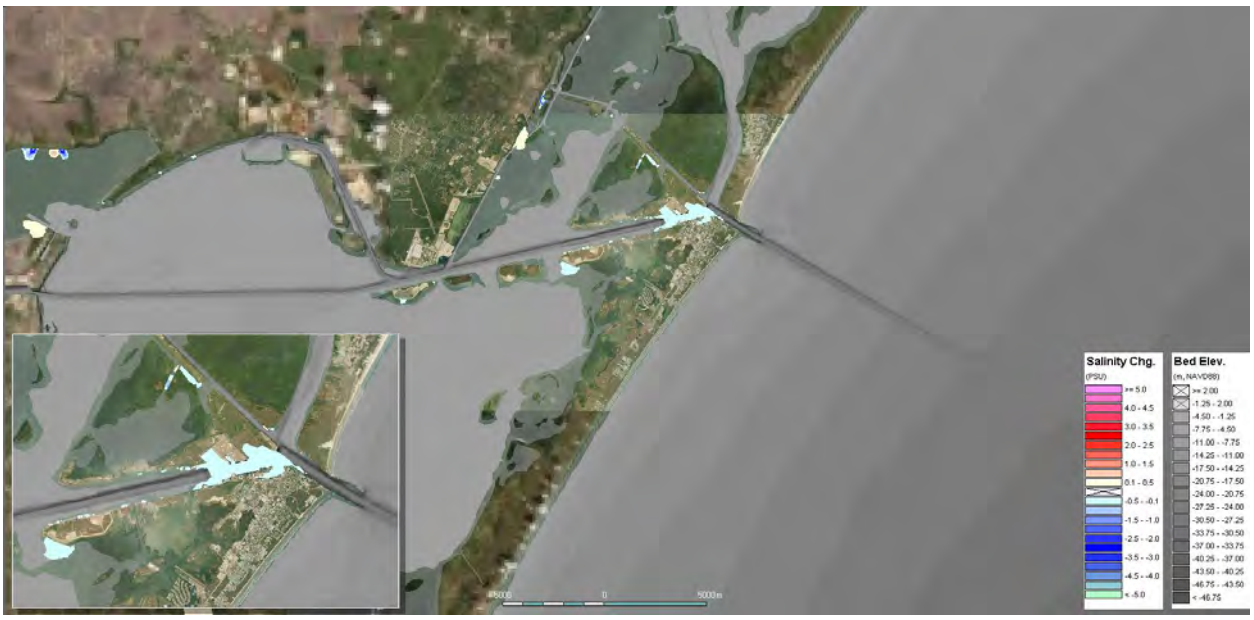

Figure B.37: Average salinity change caused by FWP in Period 2

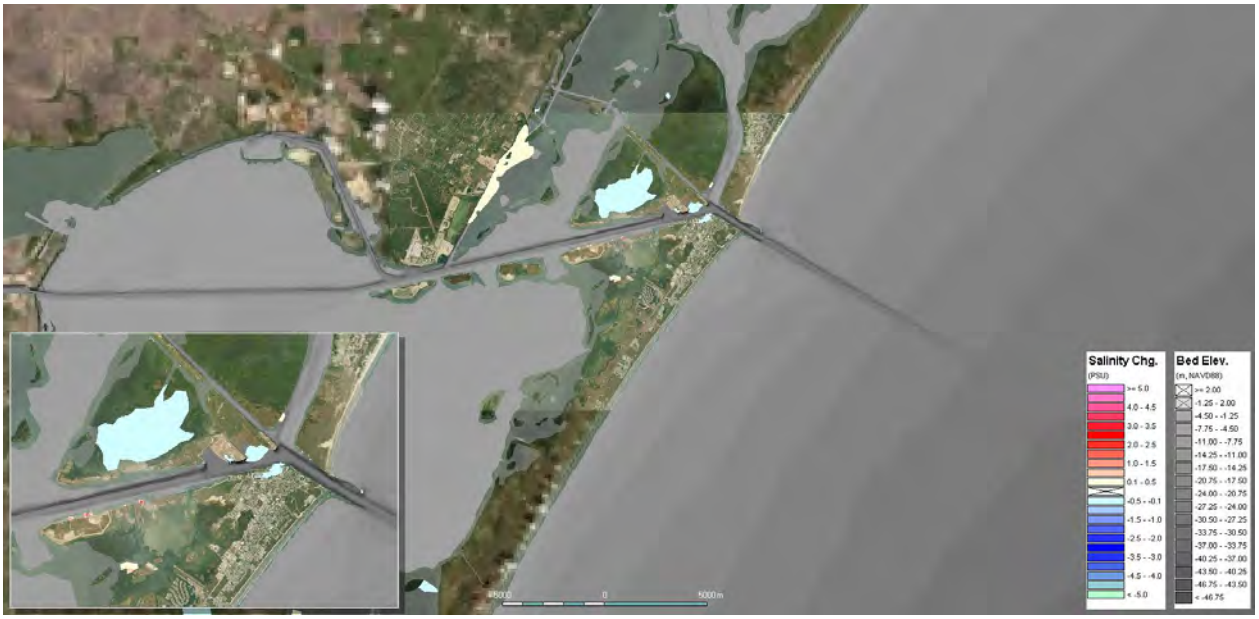

Figure B.38: Average salinity change caused by FWP in Period 3

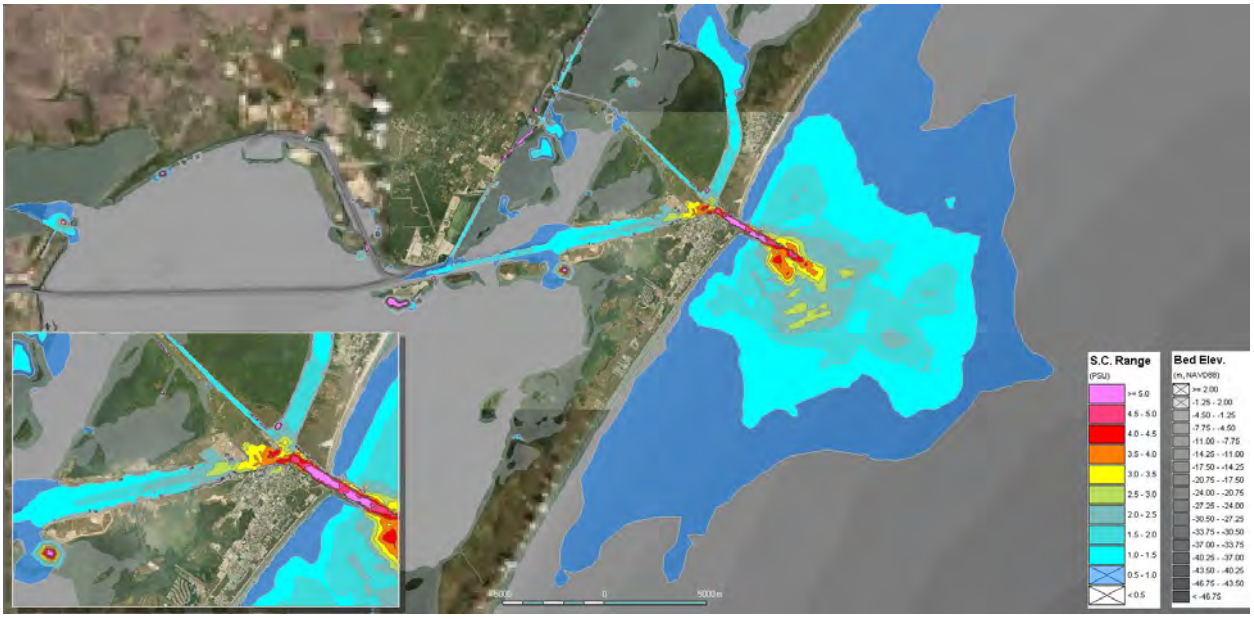

Figure B.39: Range of salinity change caused by FWP in Period 1

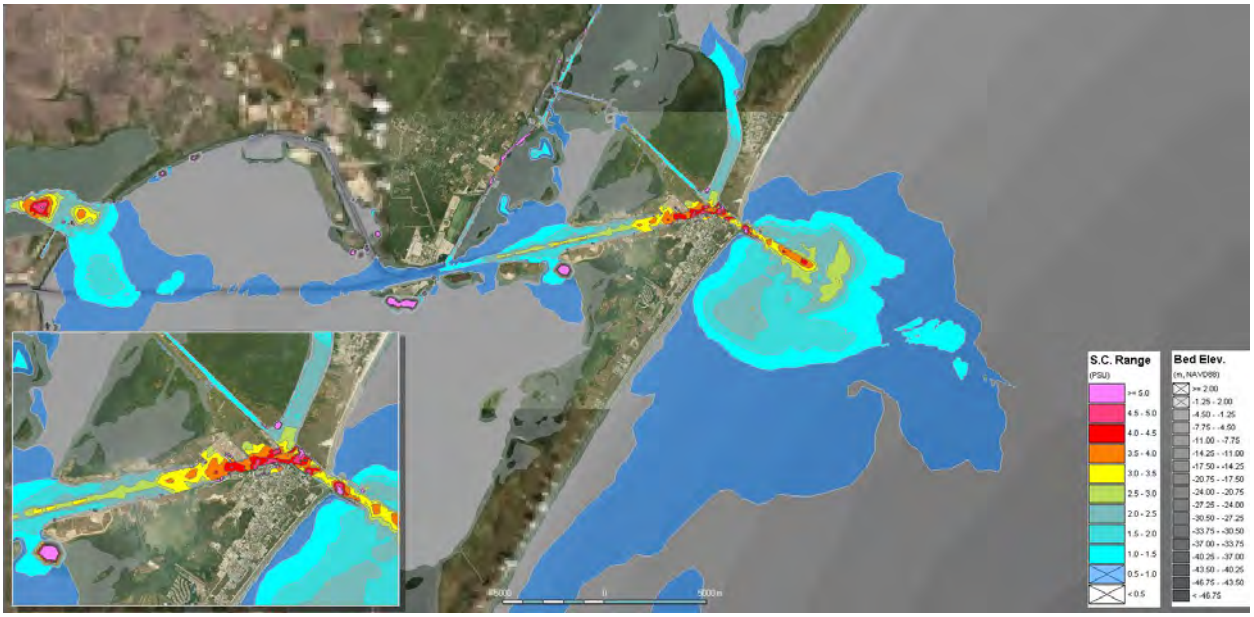

Figure B.40: Range of salinity change caused by FWP in Period 2

Figure B.41: Range of salinity change caused by FWP in Period 3

Appendix C

Impact of Future Without Project

C.1 Impacts on Water Level

C.1.1 Comparison of Tide Amplitudes between FWOP and EC

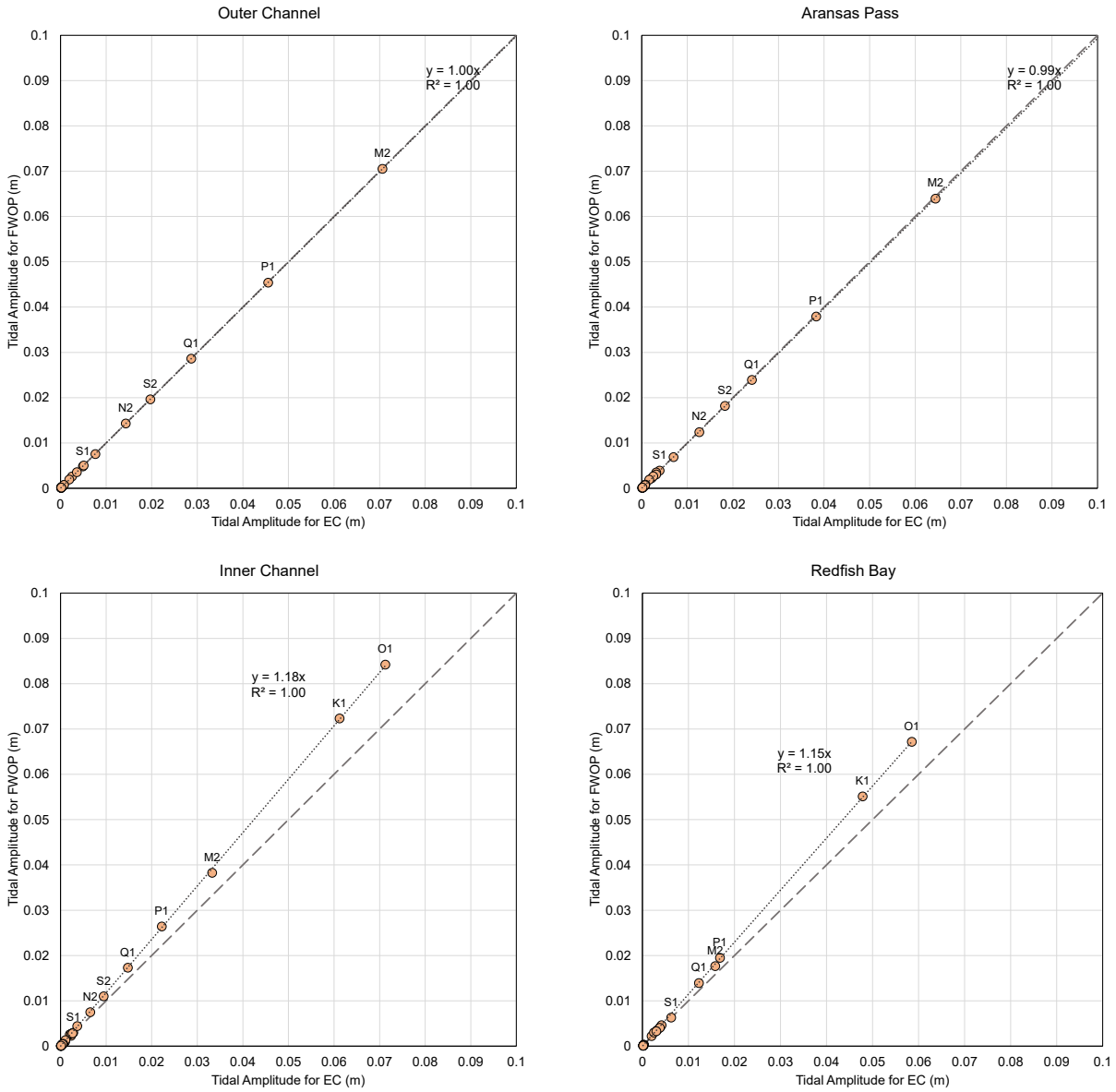

Figure C.1: Comparison of tide amplitudes FWOP with the existing condition from one-year run

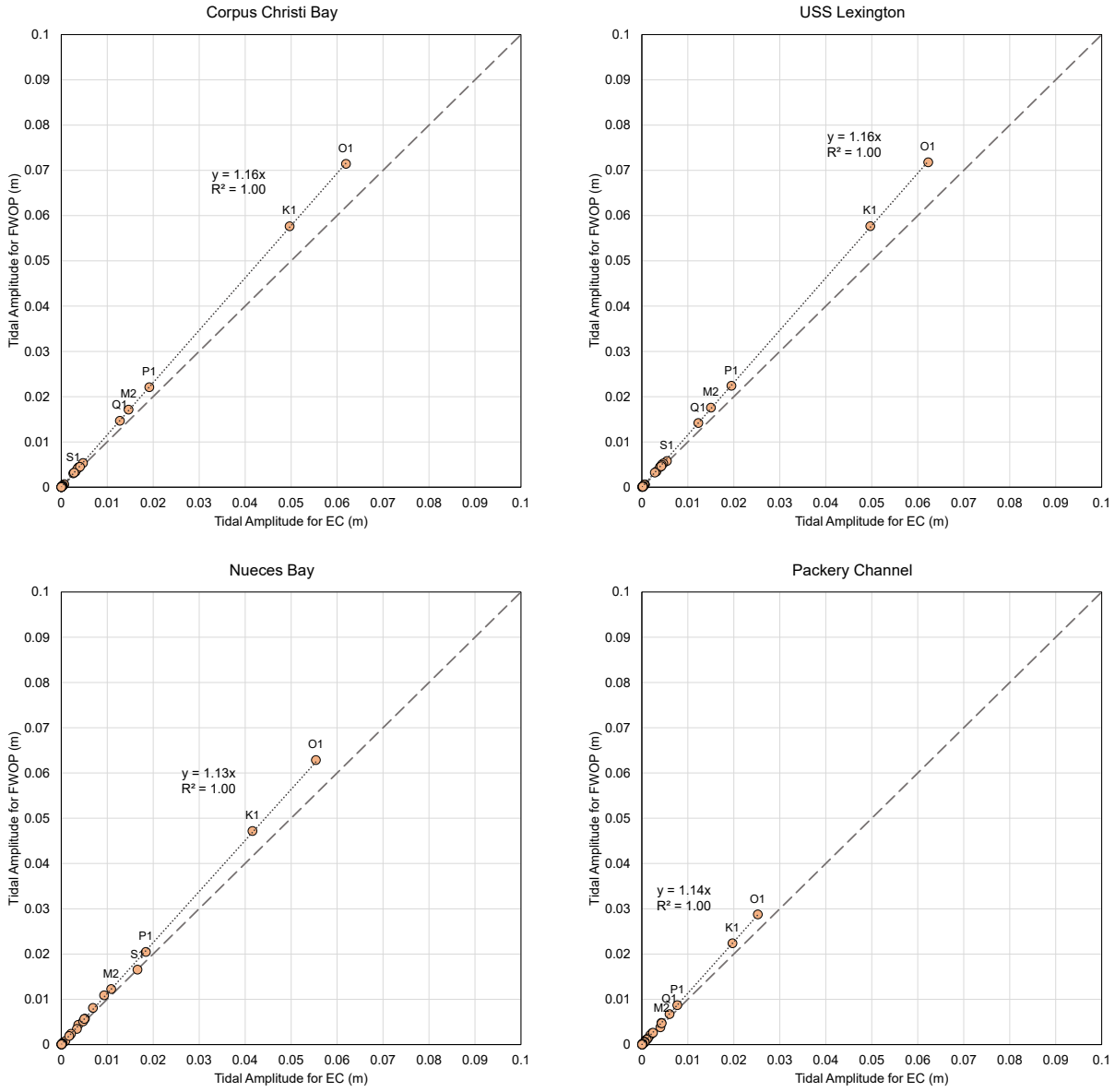

Figure C.2: Comparison of tide amplitudes FWOP with the existing condition from one-year run

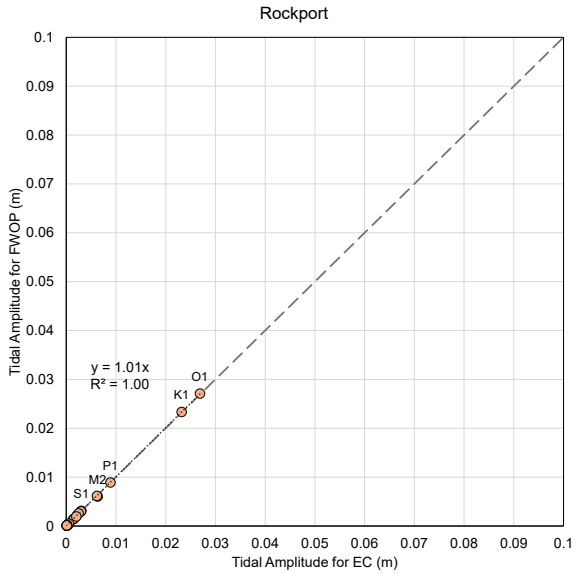

Figure C.3: Comparison of tide amplitudes FWOP with the existing condition from one-year run

Appendix D

Cumulative Impacts of Future With Project

D.1 Cumulative Impacts on Water Level

D.1.1 Comparison of Tide Amplitudes between FWP and EC

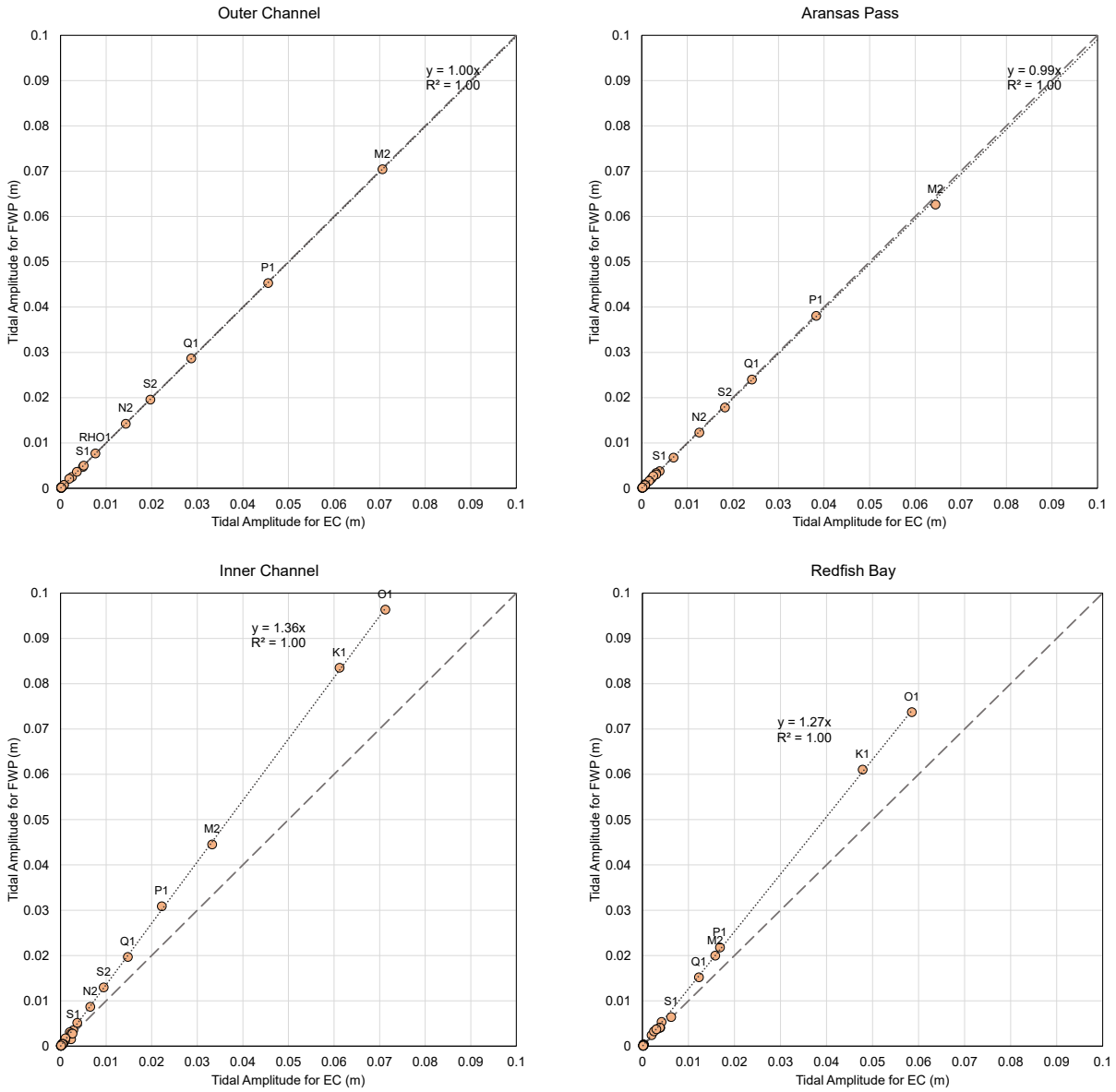

Figure D.1: Comparison of tide amplitudes FWP with the existing condition from one-year run

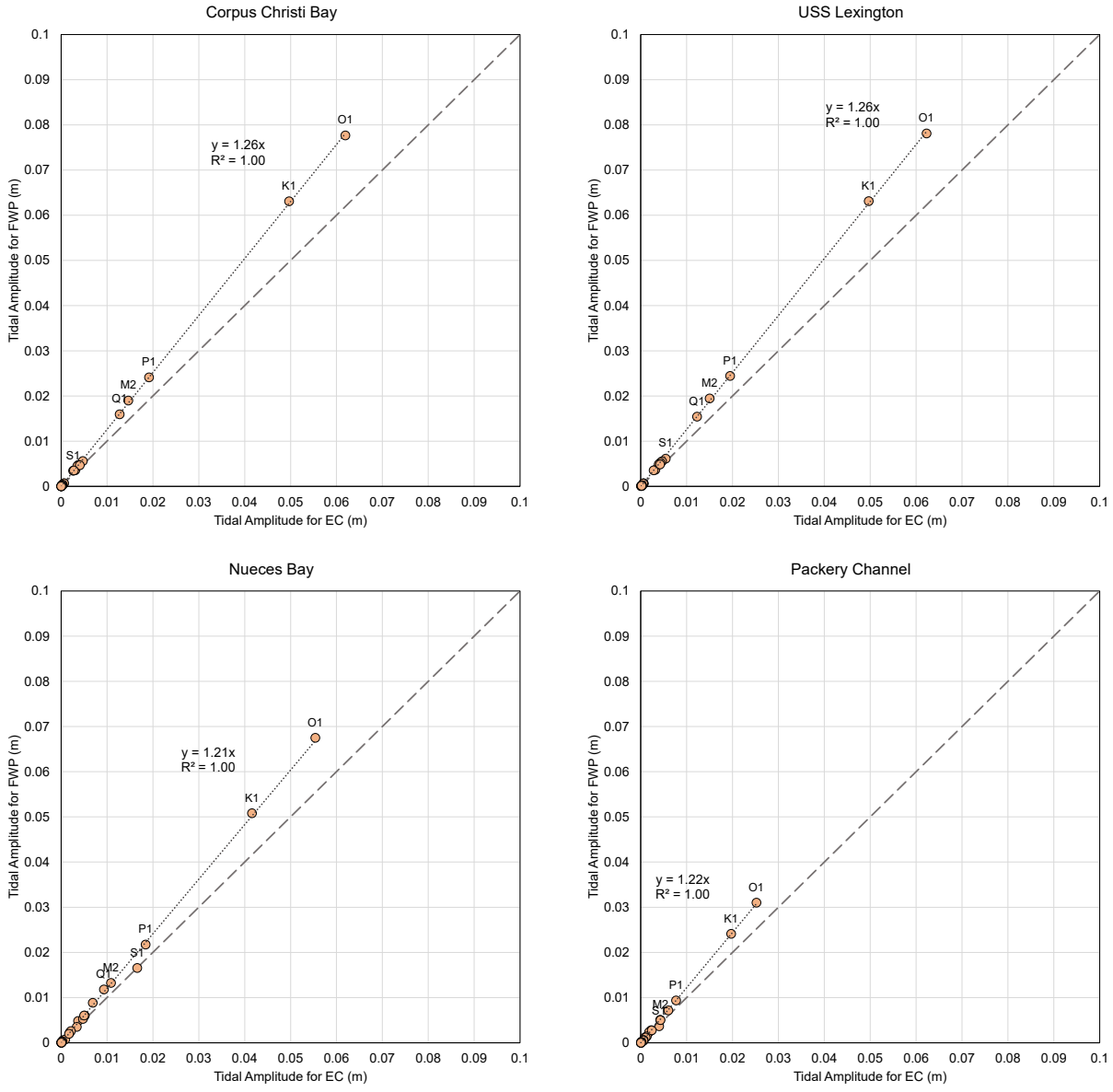

Figure D.2: Comparison of tide amplitudes FWP with the existing condition from one-year run

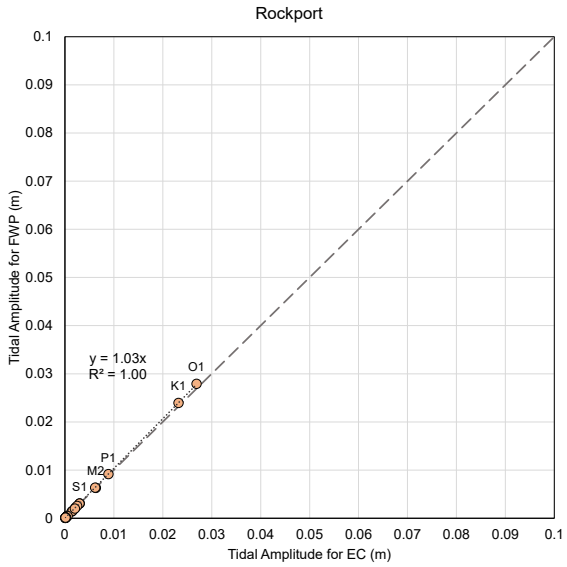

Figure D.3: Comparison of tide amplitudes FWP with the existing condition from one-year run